Genome mutation and physiology of *Synechocystis* sp. PCC 6803 wild types and pH-sensitive Photosystem II mutants

Jaz Nye Morris

A thesis submitted for the degree of

Doctor of Philosophy

University of Otago

Dunedin, New Zealand

September 2017

Abstract

The model cyanobacterium *Synechocystis* sp. PCC 6803 is widely used in studies of photosynthesis, environmental sensing, and stress-response. Its capacity for straightforward genetic engineering and the early publication of its genome sequence meant that substrains of this organism have been dispersed widely among laboratories, particularly for the purposes of investigating the function of the water-splitting enzyme of photosynthesis, Photosystem II (PS II). Recently, advances in genome sequencing technology have revealed genomic divergence among these substrains, with a largely unknown level of resultant phenotypic variation. In this study, the capacity for *Synechocystis* sp. PCC 6803 wild types to undergo genomic change was analysed by assembly of the genome sequence of the 'GT-O1' and 'GT-O2' substrains in use at the University of Otago. In the GT-O1 substrain, a possible instance of active genome transposition processes involving a Tc*1*/*mariner*-type transposase-encoding gene was observed, and in the GT-O2 substrain a mutation detected in *chlH* was associated with a reduction in chlorophyll biosynthesis. It is suggested that long-term culture conditions induce genomic changes with major functional consequences in some wild-type substrains, in spite of theoretically ideal laboratory growth conditions. However, phenotypic analysis suggested that the GT-O1 substrain is comparable to other substrains of *Synechocystis* sp. PCC 6803 held overseas. The capacity for genome mutation in response to gene deletions affecting PS II was also analysed. Some strains carrying mutations in the extrinsic proteins or domains of PS II display an enigmatic pH 7.5-sensitive phenotype, but pH 7.5-growth of a ΔPsbO:ΔPsbU strain could be rescued by genome mutations that apparently affect PS II-independent cellular processes. Assembly of the genome of a pH-insensitive ΔPsbO:ΔPsbU pseudorevertant identified a mutation in *pmgA* that appears to affect carbon uptake, and accordingly CO_2 enrichment rescued growth of some pH-sensitive PS II mutants, including the ΔPsbO:ΔPsbU strain. To further investigate the effect of external pH on the membrane-embedded PS II complex, analysis of a pH-sensitive strain lacking PsbV and carrying a mutation in Loop E of the PS II core antenna CP47 protein revealed that mutations in the vicinity of the redox-active tyrosine Y_D appear to alter PS II redox equilibria. In a CP47 E364Q:ΔPsbV mutant, the stability of $Y_D^+Q_A^-$ charge pairs in PS II and possibly the capacity of Y_D to maintain charge equilibrium with the PS II oxygen-evolving complex was altered, likely contributing to pH-sensitivity. This suggests that pH affects PS II directly and indirectly, due to a complex interplay of pH effects on electron transport, carbon uptake, pH homeostasis, and PS II redox equilibria.

Acknowledgements

This thesis is dedicated to the memory of the late Dr Pauline Mahalski, Associate Professor Ted Nye, and Adelheid Wassner – my sources of inspiration since childhood.

For their contribution to this work, I gratefully acknowledge the support of current and former members of the Bannister Lab, especially Dr Tim Crawford, and all my colleagues in the Department of Botany and Ecology Degree Program. Thanks also to the members past and present of the 308 Lab in the Department of Biochemistry, and Dr Simon Jackson and Jackie Daniels in particular. I am also indebted to Professor Imre Vass and Sándor Kovács of BRC, Szeged, Hungary, who were my very generous hosts on a research visit undertaking experiments towards this study.

Outside of the labs, my twin sanctuaries are the mountains and my family. Firstly, thanks must go to Dr Max Olsen and my friends in the Otago University Tramping Club and the New Zealand Alpine Team for distracting me from work at various stages of this study. Secondly, to Fiona Morris, Bruce Mahalski, Phoebe Morris, June & Michael Morris, and my wider family – this study would not have happened without your love and support.

Finally, and most importantly, to my supervisors. Dr Tina Summerfield – this study at all stages is indebted to your enthusiasm, your compassion and care for your lab, and your willingness to help. Professor Julian Eaton-Rye – throughout this study it was your attention to detail, rigour and insightful wit that kept me thinking, and inspires me to achieve the very best in science.

Table of Contents

List of Tables and Figures

Abbreviations

Δp	$\Delta pmgA$ (Gen^R) plasmid
ACMA	9-amino-6-chloro-2-methoxy acridine
ADP	adenosine diphosphate
ATP	adenosine triphosphate
AY	acridine yellow
CA	carbonic anhydrase
Cam^R	chloramphenicol resistance
CCM	carbon concentrating mechanism
CET	cyclic electron transport
Chl	chlorophyll
CLOG	co-occurring likely orthologous gene
CM-H$_2$DCFDA	5-chloromethyl-2',7'-dichlorodihydrofluorescein diacetate, chloromethyl derivative
Con	control
CRISPR	clustered regularly interspaced short palindrome repeats
CUP	carbon dioxide uptake
cyt	cytochrome
dNTP	dinucleotide triphosphate
DCBQ	2,5-dimethyl-1,4-benzoquinone
DCMU	3-(3,4-dichlorophenyl)-1,1-dimethylurea
EDTA	ethylenediaminetetraacetic acid
Ery^R	erythromycin resistance
F	fluorescence
Fd	ferredoxin
F_M	maximal chlorophyll fluorescence
F_0	dark state chlorophyll fluorescence
F_t	chlorophyll fluorescence at time t
F_V	variable chlorophyll fluorescence
Gen^R	gentamicin resistance
GT	glucose-tolerant
Gya	billion years ago
HEPES	4-(2-hydroxyethyl)-1-piperazineethanesulfonic acid
His$_D$	PS II reaction centre core protein D2 residue His189, coordinates Y_D
His$_Z$	PS II reaction centre core protein D1 residue His190, coordinates Y_Z
indel	insertion/deletion of DNA base pairs

Kan^R	kanamycin resistance
LB	lysogeny broth
LED	light-emitting diode
LEF	linear electron flow
LF	left flank
MW	molecular weight
NADPH	nicotinamide adenine dinucleotide phosphate
NDH	NADPH dehydrogenase
OCP	orange carotenoid protein
OD	optical density
OEC	oxygen evolving centre
OPP	oxidative pentose phosphate
ORF	open reading frame
PBS	phycobilisomes
PC	plastocyanin
pG93	*pmgA* Control (Ery^R) plasmid
pG93C	*pmgA* G93C (Ery^R) plasmid
PG	phosphatidylglycerol
Phe	pheophytin
PQ	plastoquinone
PQH$_2$	plastoquinol
PS I	Photosystem I
PS II	Photosystem II
RC47	CP43-less PS II reaction centre sub-complex
RF	right flank
ROS	reactive oxygen species
S2P	site-2 protease
SNP	single nucleotide polymorphism
Spec^R	spectinomycin resistance
TCA	tricarboxylic acid
TE	Tris-EDTA (solution)
Tris	tris(hydroxymethyl)aminomethane
$\mu E.m^{-2}.s^{-1}$	photon flux in micromoles of photons per square metre per second
Y$_D$	redox-active tyrosine-160 residue of PSII reaction centre core protein D2
Y$_Z$	redox-active tyrosine-161 residue of PSII reaction centre core protein D1

Chapter One: Introduction

1.1 General background

1.1.1 Photosynthesis and the origins of life on Earth

The advent of oxygenic photosynthesis over 2.35 Gya was the critical step in the formation of complex life on Earth (Fischer et al., 2016). In the original terraforming process, the photosynthetic ancestors of modern cyanobacteria gave rise to the Earth's oxygen-rich atmosphere, and, by producing carbon-based compounds with energy harvested from solar radiation, photosynthesis became the energetic basis of almost all food chains. The fundamental biochemical processes of oxygenic photosynthesis are believed to have changed little since its evolution, and, through processes of endosymbiosis and incorporation of cyanobacterial cell components into eukaryotic cells, photosynthesis has spread from cyanobacteria to algae and higher plants: phototrophic organisms are found in essentially all ecosystems exposed to solar radiation (Lyons et al., 2014; Soo et al., 2017).

In both cyanobacteria and higher plants, photosynthesis consists of two main processes. The light-dependent reactions take place on protein complexes of the thylakoid membrane, where light energy captured by tetrapyrrole pigment molecules is used to oxidise water; protons and electrons released by this process are directed towards generation of ATP and NADPH. These reducing compounds are then used in the light-independent reactions to energise the conversion of inorganic carbon into carbohydrates in the Calvin-Benson cycle. This store of chemical potential energy can be harnessed for later cellular metabolism, but consumption of part or all of the phototrophic organism by heterotrophs at the base of the food chain allows Earth to sustain an incredibly diverse and complex ecosystem of millions of species. As many higher trophic levels are therefore possible, almost all life is ultimately dependent on photosynthesis.

1.1.2 Cyanobacteria as model organisms for study

Cyanobacteria are an ancient lineage of photosynthetic, gram-negative prokaryotes with globally important roles in carbon and nitrogen cycling. They are the progenitors of modern plant chloroplasts and today thrive in an incredible range of habitats: from the oceans to geothermal springs, to freshwater rivers and lakes, and desert soil crusts (Whitton and Potts, 2012). Cyanobacteria were among the earliest life forms on Earth, with fossil evidence suggesting they arose as early as 3.5 Gya; although recent genomic evidence suggests that the

cyanobacterial common ancestor was not necessarily phototrophic. Oxygenic photosynthesis evolved more recently, circa 2.35-2.6 Gya, followed some 0.3-0.6 Gya later by the atmospheric 'great oxygenation event' (Schopf, 2012; Lyons et al., 2014; Fischer et al., 2016; Soo et al., 2017).

Cyanobacteria are the only oxygenic phototrophic prokaryotes; their photosynthetic apparatus, generally located on the thylakoid membrane, contains the water-plastoquinone oxidoreductase Photosystem II (PS II), an electron transport chain containing the cytochrome (cyt) b_6f complex, and the plastocyanin-ferredoxin oxidoreductase Photosystem I (PS I). Both PS II and PS I contain a special chlorophyll *a* cluster, P_{680} and P_{700} respectively, at their reaction centre (RC) core; energy is transferred to the RC core by light-harvesting antennae protein complexes called phycobilisomes (PBS) in cyanobacteria, and light-harvesting complexes in higher plants. Electrons donated to the RC by an oxygen evolving complex (OEC) are ultimately passed to $NADP^+$, and a proton motive force (PMF) across the thylakoid is used to generate ATP (photosynthesis is discussed in detail in subsequent sections). Alternative forms of RC exist in other autotrophic bacterial phyla. These include the quinone-type RCs (somewhat similar to PS II) found in purple bacteria and the filamentous anoxygenic phototrophs, and FeS-type RCs (somewhat similar to PS I) found in heliobacteria, green sulfur bacteria, and acidobacteria. Both quinone- and Fe-S-type RCs contain a chlorophyll *a* analogue, bacteriochlorophyll (derived from the chlorophyll biosynthesis pathway) at the charge-separating core, and light energy is used to drive the production of reducing equivalents such as NADPH and ATP (Hohmann-Marriott and Blankenship, 2011).

Among phototrophs, cyanobacteria are apparently the only group that has been recruited as endosymbiotic partners, having been incorporated into the rhodophytes, glaucophytes, and chlorophytes; the latter includes green algae and modern plants, which have lost the light-harvesting PBS and generally use chlorophyll *b* instead (Drews, 2011; Hohmann-Marriott and Blankenship, 2011; Nelson and Junge, 2015). The photosynthetic apparatus of cyanobacteria (excluding the thylakoid-less *Gloeobacter violaceus*) is housed on the thylakoid membrane, an intracytoplasmic membrane system that encloses a single, interconnected thylakoid lumen physically separated from the cytoplasm of the cell. The biogenesis of the thylakoid membrane is still unclear, but it may arise from so-called biogenesis centres connected to or near the plasma membrane (Liberton et al., 2006; van de Meene et al., 2006, 2012; Nevo et al., 2007; Rast et al., 2015). The thylakoids form a series of membrane layers that resemble the stacked

grana of green algae and higher plant chloroplasts. PS II, PS I, and electron transport components are in close proximity and take up much of the thylakoid membrane layer (Folea et al., 2008; Nelson and Junge, 2015); the phycobilisomes are membrane-anchored but project into the cytoplasm (Stanier and Cohen-Bazire, 1977; Mullineaux, 2008).

The similarity between cyanobacterial and higher plant photosynthesis makes cyanobacterial species attractive models for research. They have short generation times (hours/days) and small (1.4-11.6 Mb) genomes, many have the capacity for relatively straightforward genetic modification, and some can be grown heterotrophically (Eaton-Rye, 2011; Hess, 2011; Ruffing and Kallas, 2016; Mohanta et al., 2017). Cyanobacteria also possess other traits desirable for biotechnology, such as the ability to fix nitrogen and to produce secondary metabolites such as ethanol and butanol (see Wijffels et al., 2013), and cyanobacteria have subsequently have been described as the "green *[Escherichia] coli*" (Ruffing and Kallas, 2016). Model species include strains of the diazotrophic heterocyst-forming *Nostoc punctiforme*, the unicellular diazotroph *Cyanothece* sp. ATCC 51142, the food species *Arthrospira platensis* (marketed as 'Spirulina'), the ubiquitous marine genera *Synechococcus* spp., and the freshwater species *Synechocystis* sp. PCC 6803. Over 2700 species of cyanobacteria are known, and over 370 genomes are available as at July 2017 (Alvarenga et al., 2017; Dvořák et al., 2017; Fujisawa et al., 2017); the growing availability of genome sequences facilitates extensive phylogenetics and functional genomics studies in cyanobacteria.

1.1.3 The model cyanobacterium *Synechocystis* sp. PCC 6803

Among cyanobacteria, *Synechocystis* sp. PCC 6803 (hereafter *Synechocystis* 6803) is particularly widely studied, included in over 18,000 research articles available via a Google Scholar search in July 2017. A unicellular, spherical species (Figure 1.1), it was isolated from a freshwater lake in Oakland, California by R. Kunisawa at the University of California Berkeley (Stanier et al., 1971). Initially thought to be an *Aphanocapsa sp.*, it was deposited in the Pasteur Culture Collection (PCC 6803 strain) and the American Type Culture Collection (ATCC 27184 strain) (Rippka et al., 1979). This organism became widely used in photosynthesis research after it was found to be naturally transformable with exogenous DNA via double-homologous recombination (Grigorieva and Shestakov, 1982); worldwide laboratory 'wild-type' strains of *Synechocystis* 6803 are generally derived from a glucose-tolerant (GT) derivative of the ATCC 27184 strain (Williams, 1988; Ikeuchi and Tabata, 2001).

The ability to grow on glucose renders it particularly useful for functional genomics studies in photosynthesis; cells can survive despite the removal of PS II or PS I (Vermaas et al., 1990; Anderson and McIntosh, 1991; Eaton-Rye and Vermaas, 1991; Shen et al., 1993). It was also the first photosynthetic organism to have its entire genome sequenced, and only the third free-living organism overall (Kaneko et al., 1995, 1996, 2003).
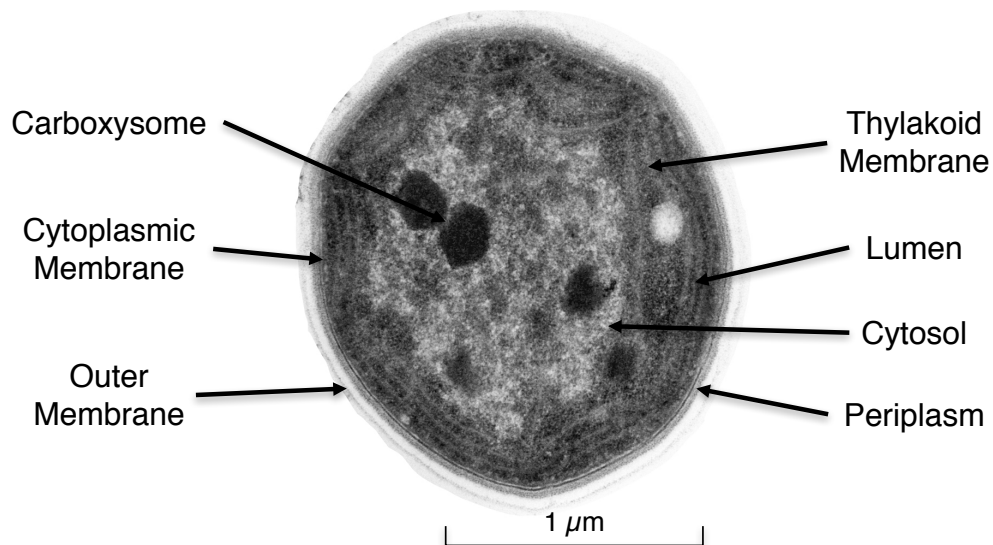
Figure 1.1. Transmission electron microscopy image of *Synechocystis* sp. PCC 6803 GT-O1 wild-type strain, showing major cellular structures such as the stacked thylakoid membranes separated by lumen, the polyhedral carboxysome, and cellular cytosol.

1.2 Photosystem II in cyanobacteria

1.2.1 Overview of PS II charge separation

The water-splitting reactions of photosynthesis take place in PS II, which is a thylakoid membrane-bound protein complex that functions as a water-plastoquinone oxidoreductase in oxygenic phototrophs (Vinyard et al., 2013). In cyanobacteria, energy is captured by PS II through absorption of photons in the phycobiliprotein-bound pigments of the membrane-extrinsic PBS antenna complex: phycobilin, phycoerythrobilin, and their respective isomers phycoviobilin and phycourobilin (Watanabe and Ikeuchi, 2013). Light energy is transferred to chlorophyll in CP47 and CP43, which contain 16 and 13 chlorophylls respectively, and then to the four-chlorophyll P_{680} RC bound to the D1 and D2 PS II core proteins.

Absorption of a photon excites one of the RC chlorophylls to P_{680}*, resulting in charge separation, whereupon an electron passes to the primary electron acceptor pheophytin (Phe), oxidising P_{680} (P_{680}^+). Phe reduces the bound primary plastoquinone (PQ) acceptor Q_A, which in turn reduces the secondary plastoquinone Q_B via a non-heme iron; Q_B binds to PS II from the thylakoid-mobile plastoquinone pool. Once Q_B has accepted two electrons from Q_A and two protons from the cytosol, it forms the mobile plastoquinol (PQH_2) species, which diffuses out of PS II. The electron transfer process from P_{680}* to PQH_2 is termed the PS II acceptor side. Oxidised P_{680}^+ is reduced by a nearby tyrosine residue, Y_Z (D1 Tyr161), which then oxidises the Mn_4CaO_5 cluster. Following four electron extractions from the Mn_4CaO_5 complex, two water molecules are split into four protons and one dioxygen molecule – hence, this complex is referred to as the OEC. The four-step reaction leading to oxygen evolution is termed the S-state cycle (S_0-S_4, also called the Kok cycle); oxygen is released in the transition of S_3-(S_4)-S_0, and although S_0 is the most reduced state, S_1 is the dark-stable state, due to reduction of S_0 by Y_D (D2 Tyr160), a cognate of Y_Z (Fig. 1.2). The electron transfer steps from water to P_{680}^+ are termed the PS II donor side (for review, see Shen, 2015; Barber, 2016; Vinyard and Brudvig, 2017).
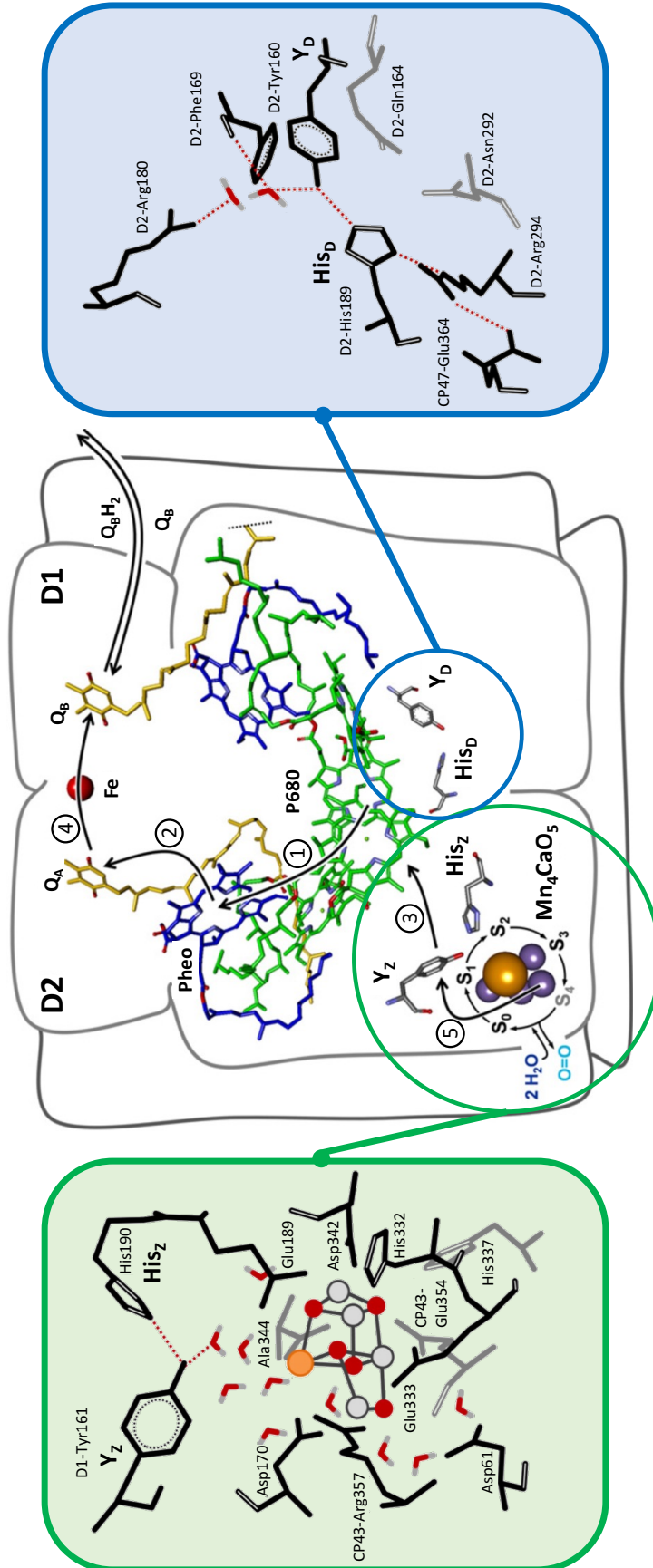
Overleaf: Figure 1.2. Electron transport steps and major redox-active components in PS II. A. Centre image: an electron is transported from the P_{680} RC to Phe (1) and then to Q_A (2). An electron from Y_Z (coordinated by His_Z) passes to P_{680}^+ (3) and the initially-extracted electron moves from Q_A to Q_B via a non-heme iron (4). Water oxidation by the Mn_4CaO_5 cluster in the S-state cycle replaces the electron at Y_Z (5); the S-state can also be advanced to S_1 by Y_D (coordinated by His_Z cognate His_D). Left, green box: coordination environment around Y_Z and the Mn_4CaO_5 cluster (residues not labelled are from D1, red/grey symbols are water molecules, red dotted line indicates H-bond). Right, blue box: coordination environment around Y_D (red dotted lines indicate H-bonds). Figure adapted from Styring et al. (2012), Figure 2, and Sjöholm et al. (2017), Scheme 1. Scheme 1 is reproduced and modified with permission from Elsevier.

1.2.2 Linear electron flow and generation of NADPH and ATP

Energy transfer in photosynthesis, described in the 'Z-scheme,' involves the light-induced increase in redox potential of the PS II and PS I RC by absorption of light energy, with electron transport between them mediated by electron carriers of intermediate redox potential. Linear electron flow (LEF) from PS II occurs when mobile plastoquinol is deprotonated and oxidised by the cyt b_6f complex. One electron is passed on plastocyanin (PC) or cyt c_6 on the lumenal side of the complex (called the high-potential chain), and the other electron is transferred to the cytoplasmic side of the membrane, whereupon it is used to regenerate plastoquinol (called the low-potential chain). The net result of this is that for two PQH_2 molecules from PS II oxidised by the cyt b_6f complex in the so-called Q-cycle, two PQ are released, two electrons are passed to PC or cyt c_6, four protons are released to the thylakoid lumen, and one plastoquinol is regenerated in the cytosol. In PS I, light-driven excitation of the reaction centre P_{700} to P_{700}^* supplies an electron to the primary and secondary acceptors, A0 (one or two chlorophyll molecules) and A1 (a phylloquinone pair) respectively, with the electron replaced at P_{700}^+ by one from PC or cyt c_6. Electrons are then passed to ferredoxin (Fd), the terminal electron acceptor of PS I (Fig. 1.3). Electrons from Fd can be used to generate NADPH in the cytosol in a reaction catalysed by ferredoxin NADPH reductase, or they can be passed back to the cyt b_6f complex in cyclic electron transport (CET). NADPH is used to energise a suite of cellular processes, in particular in the Calvin-Benson cycle and the function of NADPH dehydrogenase-1 (NDH-1) complexes. Both LEF and CET create a proton gradient used to

generate ATP; CET generates ATP independently of PS II electron transport at the expense of NADPH production (for reviews covering these topics, see Battchikova et al., 2011; Kallas, 2012; Lea-Smith et al., 2016; Yamori and Shikanai, 2016; Xu and Wang, 2017).

The build-up of protons in the lumen from PS II water-splitting contributes to the pH gradient (ΔpH) and membrane potential ($\Delta\psi$) across the thylakoid membrane, which creates a proton electrochemical potential (or PMF) that is used to drive the F_1F_0 ATP synthase-catalysed production of ATP. These add to the protons pumped into the lumen by NDH-1 complexes, and the cyt b_6f complex as part of LEF and CET. Additionally, respiratory electron transport transfers protons to the lumen, during a process where electrons from PS I are passed to respiratory terminal oxidases such as cyt *c* oxidase and succinate dehydrogenase (for review, see Kallas, 2012; Lea-Smith et al., 2016). As a consequence of proton-pumping across the thylakoid membrane from the cytosol, the cyanobacterial thylakoid lumen pH is acidified in the light, by around two pH units, relative to the cytosolic pH (Belkin et al., 1987; Belkin and Packer, 1988).
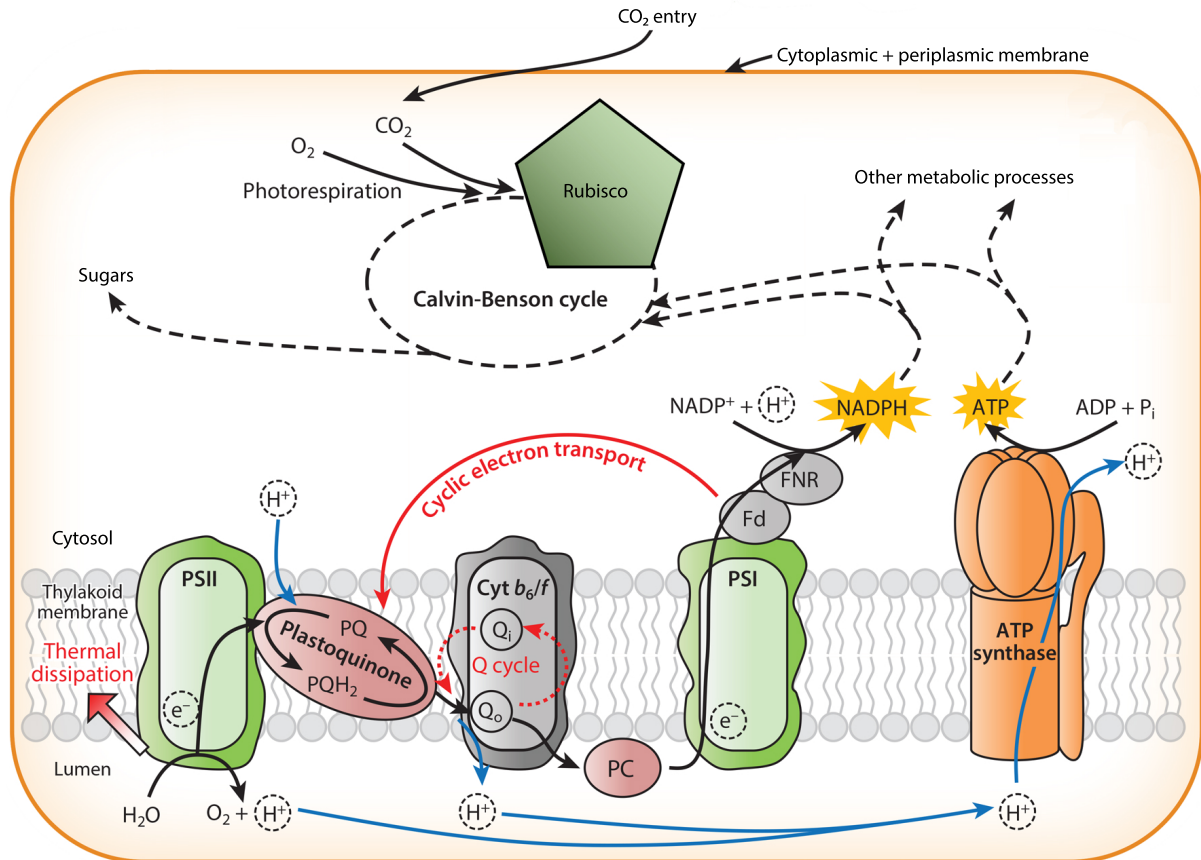
Figure 1.3. Energy transfer from cyanobacterial thylakoid membranes to the Calvin-Benson cycle. Electrons produced by PS II water splitting are transported via the plastoquinone pool to the cyt b_6f complex, then to PS I by PC or cyt c_6 (not shown) and used to generate NADPH. A proton gradient generated by PS II and cyt b_6f powers ATP synthase. ATP and NADPH energise the Calvin-Benson cycle and other metabolic processes. Figure adapted from Yamori and Shikanai (2016).

1.2.3 Structure and assembly of PS II

In cyanobacteria, the mature 350 kDa PS II monomer (Fig 1.4) contains at least seventeen membrane-spanning subunits, of which seven are essential for PS II function, as well as up to four extrinsic, thylakoid-lumen-associated subunits (PsbO, PsbU, PsbV, and possibly CyanoQ), which are necessary for maximal rates of oxygen evolution (Shen, 2015; Heinz et al., 2016; Roose et al., 2016). The PS II extrinsic proteins, along with the lumenal domains of the intrinsic RC-binding proteins D1 and D2, and the adjacent chlorophyll-binding core antenna proteins CP43 and CP47, form a protective environment around the site of the OEC,

in which a Mn_4CaO_5 cluster coordinated to D1 and CP43 catalyses the water-splitting reaction (Shen, 2015). In addition to CP47, CP43, D1 and D2, the α- and β- subunits of cyt b_{559} (encoded by PsbE and PsbF) form the experimentally-determined minimum subunit; these are also extremely conserved among all oxygenic phototrophs, in contrast to the low molecular weight (MW) and extrinsic subunits (Bricker et al., 2012; Barber, 2016).

Of the PS II intrinsic proteins, the D1 and D2 core proteins have five membrane-spanning helices each, CP47 and CP43 each have six, and the 13 low MW proteins (<10 kDa; PsbE-F, PsbH-M, PsbT, PsbX-Z and Psb30) have one, with the exception of the two helix PsbZ. In addition, a suite of cofactors and ligands is associated with the mature PS II monomer, including 35 chlorophylls, 11 β-carotenes, two Phe, two plastoquinones, one bicarbonate iron, which coordinates a non-heme iron, one *b*-type and one *c*-type cyt, >20 lipids, two chlorides, the Mn_4CaO_5 cluster and around 2,800 water molecules (Zouni et al., 2001; Umena et al., 2011; Shen, 2015; Suga et al., 2015).

Assembly of PS II (Fig 1.5) is dependent on the availability of chlorophyll, and is initiated with the formation of a D2-cyt b_{559} subcomplex, to which a dimer consisting of PsbI and pD1 (the precursor form of D1) is attached, concomitant with C-terminal processing of pD1 by C-terminal processing protease CtpA. This yields the so-called RC complex, consisting of the mature D1, D2, cyt b_{559} and PsbI subunits, which is attached to a further precursor sub-complex consisting of CP47 and several low MW subunits to form the RC47 complex, with Ycf48, Sll0933 and Psb28 acting as assembly factors. A CP43/PsbK/PsbZ/Psb30 sub-complex assembles to the RC47 complex, with Sll0933 and Psb27 acting as assembly factors. This PS II is able to provide ligands to the OEC, which is then assembled to PS II in light-dependent and light-independent steps, using energy from charge separation in a process termed photoactivation. Binding of the extrinsic proteins and the accessory light-harvesting PBS complex forms a mature PS II monomer, which then forms a dimer, with PsbL, PsbM and PsbT attributed a role in dimer stabilisation (Nickelsen and Rengstl, 2013; Mabbitt et al., 2014; Rühle and Leister, 2016). Although mature PS II is restricted to the thylakoid membranes, recent evidence has suggested that the biogenesis of some early PS II assembly intermediates originates on specialised membrane compartments that might connect the plasma membrane with the thylakoid, known as biogenesis centres or the 'PratA-defined membrane,' so-called for a protein which interacts with pD1 at this site. It is believed that the RC complex is assembled in these biogenesis centres, although as CP47 and CP43 cannot be detected in them,

later assembly steps are believed to be restricted to the true thylakoid membrane alone (Heinz et al., 2015; Rast et al., 2015).

The extrinsic proteins bind to the PS II monomer subsequent to assembly and photoactivation of the Mn_4CaO_5 cluster (Dasgupta et al., 2008; Nickelsen and Rengstl, 2013). Based on their locations in the X-ray-derived structure of PS II from *Thermosynechococcus vulcanus* (Umena et al., 2011; Suga et al., 2015), and extensive biochemical studies (Bricker et al., 2012; Ifuku, 2015; Ifuku and Noguchi, 2016; Roose et al., 2016), it seems likely that PsbO and PsbV bind first: PsbO binds via interactions with loop E of CP47, loop E of CP43 and the C-terminus of both D1 and D2. PsbV binds via loop E of CP43 and the C-terminus of both D1 and D2. Subsequently, PsbU binds via PsbO, PsbV, loop E of CP47, loop E of CP43 as well as the C-terminus of both D1 and D2; finally, CyanoQ is predicted to bind via associations with PsbO and loop E of CP47. Although none of the extrinsic proteins provide direct ligands to the Mn_4CaO_5 cluster, they protect this site from the reductive environment of the lumen, and increase the affinity for the co-factors Ca^{2+} and Cl^- (reviewed in Bricker et al., 2012; Roose et al., 2016). The X-ray-derived structures of PS II from *T. vulcanus* and *T. elongatus* have revealed that extensive hydrophilic regions and hydrogen bond networks in both extrinsic and intrinsic proteins in the vicinity of the OEC may allow water transport to and proton and molecular oxygen transport from the catalytic centre (Linke and Ho, 2014; Lorch et al., 2015; Vogt et al., 2015). For example, a protein channel in PsbU to water molecules H-bonded to the O4 of the Mn_4CaO_5 cluster, and a channel linking PsbV and PsbU to water molecules binding O1 of the Mn_4CaO_5 cluster allow access of the catalytic centre to the PS II lumenal surface in cyanobacteria, and these channels are apparently conserved in higher plants (Sakashita et al., 2017). PsbO is conserved across PS II, whereas PsbV and PsbU are absent from green algae and higher plants, and in their place PsbP, PsbQ, and possibly PsbR are present (Bricker et al., 2012). While CyanoQ is present in *Synechocystis* 6803 in stoichiometric amounts, the putative PsbP homolog CyanoP is substoichiometric and does not appear to contribute significantly to PS II function, and might instead be involved in assembly (Thornton et al., 2004; Summerfield et al., 2005b; Roose et al., 2016).
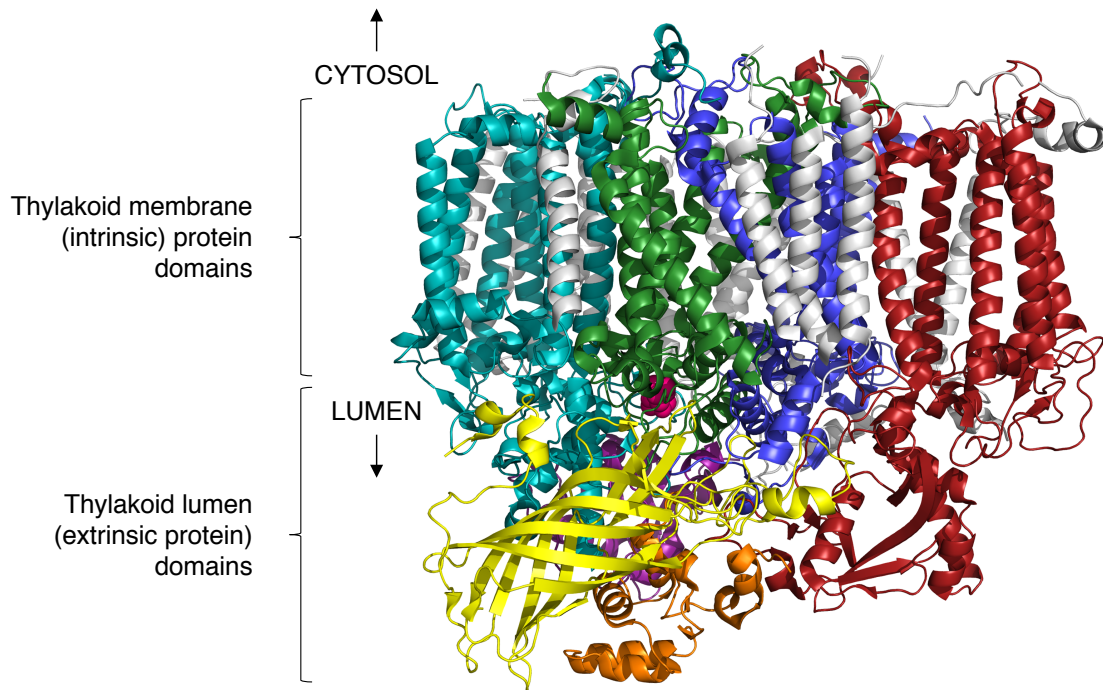
Figure 1.4. Crystal structure of PS II from *Thermosynechococcus vulcanus* at 1.95 Å. The major intrinsic proteins are arranged in the thylakoid membrane (not shown); from these, extrinsic domains project into the thylakoid lumen, where they interact with the extrinsic proteins. Intrinsic proteins: D1 – green; D2 – teal; CP43 – blue; CP47 – red). Other intrinsic subunits are shaded white. Extrinsic proteins: PsbO – yellow; PsbV – lilac; PsbU – orange. The OEC is depicted by red spheres. Image created with data obtained from Protein Data Bank accession 4UB6 (Suga et al., 2015).

1.2.4 PS II photoinhibition, repair, and energy recombination

PS II is susceptible to light-induced photoinhibition, in which oxygen-evolving and electron transport activity is lost due to photodamage of PS II overwhelming the capacity for PS II assembly and repair. This occurs primarily in high light conditions, and D1 is the primary target of photodamage. Additionally, in low carbon conditions, the efficiency of the Calvin-Benson cycle is reduced, and it becomes a less-effective sink for the electrons produced by PS II. Both high light and low carbon conditions can thus cause over-reduction of electron transport chain components and 'back-pressure' on PS II (Takahashi and Murata, 2005; Tyystjärvi, 2013).

Cyanobacteria possess a number of mechanisms for regulating the amount of light that reaches PS II to prevent excessive photodamage. These include the regulation of absolute PS II and PS I levels, and/or alteration of PS II:PS I stoichiometry, generally resulting in downregulation of PS I and CET in high light (Muramatsu and Hihara, 2012). So-called state transitions, in which altered coupling of PBS antennae to the photosystems regulates the light energy transferred to PS II and PS I (Mullineaux and Emlyn-Jones, 2005; Mullineaux, 2008), can be used to prevent photodamage. Additionally, excess energy from PS II can be diverted from Q_B via an as-yet uncharacterised system involving the *flv4-sll0218-flv2* operon (Zhang et al., 2009b; Bersanini et al., 2017); this system appears to be distinct from one involving the reduction of molecular oxygen (yielding water) by Flv1/Flv3 with excess electrons from PS I in a Mehler-type reaction (Allahverdiyeva et al., 2013). An additional, well-characterised photoprotective strategy involves the dissipation of excess energy as heat by light-activated orange carotenoid proteins embedded in the PBS antennae, termed non-photochemical quenching (for review, see Kirilovsky and Kerfeld, 2016).

Photodamage results in rapid turnover of D1 and regeneration of active PS II, termed the PS II repair cycle, which incorporates aspects of the *de novo* PS II assembly system (Fig 1.5). In repair, PS II is broken down to an RC47 complex containing the damaged D1, which is removed by the FtsH2/3 proteases and a pD1 is inserted in its place. After D1 processing by CtpA, the CP43 subcomplex is bound to the repaired RC47 complex and photoactivation and assembly of the final PS II monomer and dimer occurs (Mulo et al., 2012; Nickelsen and Rengstl, 2013). The precise mechanism of photodamage is a cause for debate, with damage to D1 attributed to reactive oxygen species (ROS), particularly singlet oxygen generated by charge recombination of the PS II donor and acceptor side (Cser and Vass, 2007; Vass, 2012), or alternatively by direct destruction of the Mn_4CaO_5 cluster and the inhibition of *psbA* expression by ROS, leading to reduced D1 synthesis and insufficient PS II repair (Murata et al., 2007; Takahashi and Badger, 2011). Both hypotheses have substantial experimental support and are in fact likely to be somewhat compatible – a unified theory suggests that damage to the Mn_4CaO_5 cluster by excess light energy prevents reduction of the primary electron donor, which increases charge recombination and ROS production, inhibiting PS II repair and potentially damaging nearby PS II as well (Tyystjärvi, 2013).
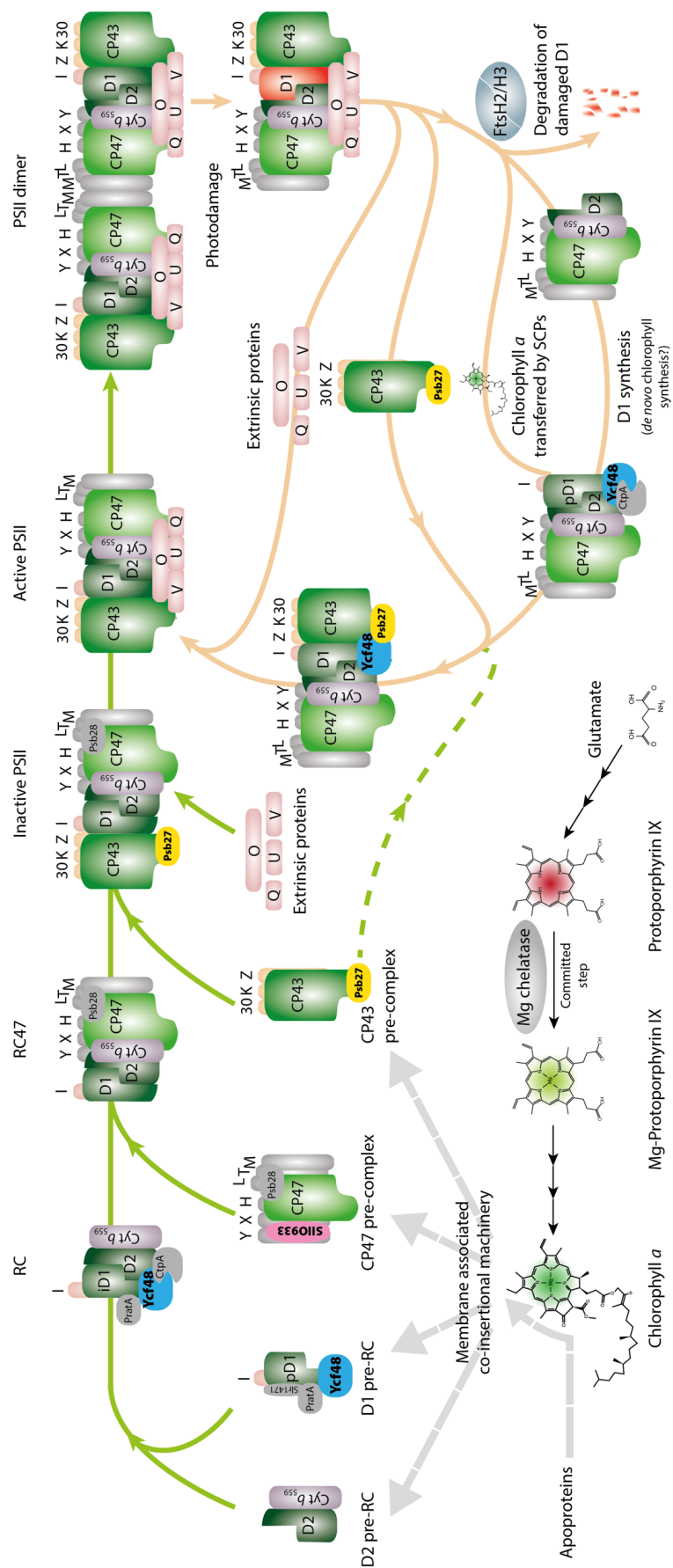
Overleaf: Figure 1.5. PS II assembly and repair cycle in *Synechocystis* 6803. Assembly: chlorophyll biosynthesis begins a process of *de novo* PS II assembly, wherein an RC complex is assembled into an RC47 complex with Ycf48 and Sll0933 acting as possible co-factors; the RC47 attaches to a CP43 pre-complex with Psb27 involved, and extrinsic proteins (possibly including CyanoQ) assemble to the mature monomer and then dimer. Repair: photodamaged D1 is excised from PS II by FtsH2/3 and replaced, incorporating steps of the assembly pathway. Figure: JJ Eaton-Rye and B Carlisle, unpublished.

1.2.5 Reactive oxygen species

Excessive light energy reaching PS II produces ROS, in particular singlet oxygen ($^1O_2$). $^1O_2$ is produced in PS II by the interaction of ground-state molecular oxygen ($^3O_2$) with excited P_{680}^* chlorophyll triplets formed by spontaneous conversion of singlet P_{680}^*, or by formation of $^3P_{680}^*$ from $^3[P_{680}^+Phe^-]$ via charge recombination when PS II is illuminated, either by single turnover flashes or by accumulation of $^3[P_{680}^+Phe^-]$ when forward electron transfer is blocked by singly- or doubly-reduced Q_A (Fig. 1.6) (Vass and Cser, 2009; Vass, 2012). Other charge recombination pathways yield fluorescence (radiative pathway, nanosecond time scale) or recombination with the OEC to yield $S_2Q_A^-$ or $S_2Q_B^-$ (stable for seconds-minutes) and do not produce ROS. $^1O_2$ is expected to be the most harmful form of ROS in PS II, and although the presence of carotenoids in the PS II RC is expected to quench short-lived $^1O_2$, its production by PS II can be detected by various methods including direct 1270 nm luminescence methods and histidine-trapping (Tomo et al., 2012; Rehman et al., 2013). As well as $^1O_2$ from charge recombination, other ROS species are produced in PS II, including superoxide (O_2^-) produced at the Phe and Q_A site, and hydroxyl ($HO^•$) radicals produced at the non-heme iron and at the Mn_4CaO_5 cluster; all can cause photoinhibition in PS II if their production exceeds the capacity of ROS scavengers (such as superoxide dismutase, carotenoids, and α-tocopherol) to quench them (Murata et al., 2012; Vass, 2012; Kale et al., 2017).
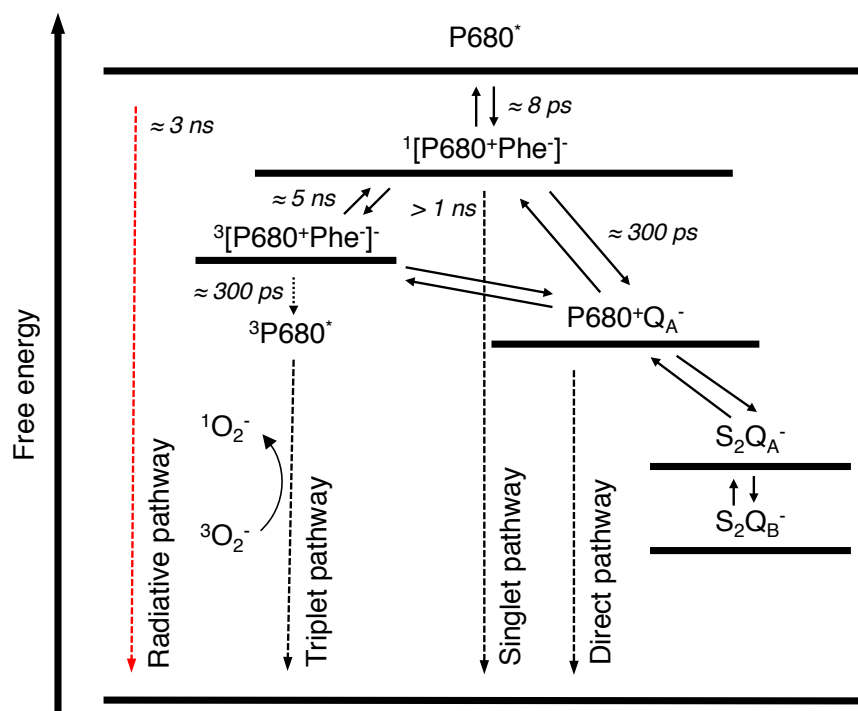
Figure 1.6. Charge separation and energy recombination pathways in PS II. Solid arrows indicate electron transport steps, dashed lines indicate charge recombination or energy dissipation pathways; processes are described in the text. Modified from Cser and Vass (2007).

1.3   Freshwater habitats and cellular homeostatic processes

1.3.1 Cyanobacterial habitats

Although cyanobacteria have one of the largest habitat ranges of any group of organisms, they are most abundant in marine and freshwater environments, where they adopt planktonic or benthic growth forms (Whitton and Potts, 2012). One characteristic feature of cyanobacterial freshwater habitats is a preference for pH >7.0 conditions, and cyanobacteria are generally partial or obligate alkaliphiles (Stal, 2012). Indeed, it was considered for decades that cyanobacteria were completely absent from habitats with a pH below ~4.0-5.0, whereupon eukaryotic algae are dominant (Brock, 1973). While reports identified *Oscillatoria/Limnothrix* and *Spirulina* spp. populations in acidic lakes (pH ~3.0) in mining regions of Germany (Steinberg et al., 1998), generally speaking the cyanobacteria are the major photosynthetic taxa in high pH environments; in extreme high pH habitats such as alkaline soda lakes, where pH in excess of 10.0 is common, cyanobacteria are the dominant prokaryotic taxa (Whitton and Potts, 2012).

1.3.2 pH and inorganic carbon in aquatic habitats

For organisms in aquatic environments, one of the most critical abiotic factors determining growth and survival is the pH ($-\log_{10}[H_3O^+]$). Whereas the pH of marine environments is a relatively constant pH ~8.1, the pH of freshwater lakes and rivers is generally variable: although freshwater pH is most commonly in the range of pH 6.0-8.0, extremes as low as pH ~2.0 and as high as pH ~12.0 are possible (Becking et al., 1960; Wetzel, 2001; Raven, 2012). Two major abiotic processes determine aquatic pH conditions: dissolution of atmospheric CO_2, and dissolution and oxidation of soil and bedrock minerals; their reactions in freshwater produce ionic species such as carbonates, sulfates and phosphates. Precipitation reactions of these ions in water can also occur, affecting the total ionic pool and $[H_3O^+]$.

In all aquatic environments, pH directly affects the chemical equilibria of biologically critical macronutrients such as nitrate, ammonia, phosphate, and the concentration of C_i, influencing the proportions of their respective dissolved species (Stumm and Morgan, 2012). Additionally, the micronutrient ions Cu^{2+}, Mg^{2+}, Mn^{2+}, Fe^{2+}, and Zn^{2+} are almost entirely soluble in freshwater at pH 6.0 but form substantially or entirely insoluble complexes at pH 9.0 (Turner et al., 1981). The solubility and hence bioavailability of macronutrients in solution is well

known to affect an organism's growth rate and general cellular processes (Turner et al., 1981; Stumm and Morgan, 2012).

C_i in freshwater habitats is largely dependent on equilibrium reactions of atmospheric CO_2 with water; CO_2 hydrates in water to form carbonic acid (H_2CO_3) (see Equation 1a), which then dissociates rapidly into bicarbonate (HCO_3^-) and protons (H^+, Equation 1b). Dissociation of HCO_3^- into carbonate CO_3^{2-} and further protons also occurs (Equation 1c).

Equation (Eq.) 1a. $\qquad$ $CO_{2\,(atmospheric)} \rightleftharpoons CO_{2\,(aqueous)} + H_2O \rightleftharpoons H_2CO_3$

Eq. 1b. $\qquad$ $H_2CO_3 \rightleftharpoons H^+ + HCO_3^-$

Eq. 1c. $\qquad$ $HCO_3^- \rightleftharpoons CO_3^{2-} + H^+$

Increased dissolution of CO_2 will therefore tend to reduce pH by shifting the equilibria of these reactions right, increasing H^+. However, dissolved HCO_3^- and CO_3^{2-} (e.g. from weathering of terrestrial limestone and chalk deposits) also react in equilibria (Eq. 2a, Eq. 2b), releasing hydroxyl ions (OH^-); inputs of terrestrial $HCO_3^- + CO_3^{2-}$ into freshwater increases OH^- and pH. Therefore, at a given atmospheric CO_2 concentration, relative abundance of C_i species is pH-dependent, and total C_i concentration increases with increasing pH. It is important to note that, as pH is a logarithmic scale, minor changes in pH can drastically alter the equilibria of carbon species in solution.

Eq. 2a. $\qquad$ $HCO_3^- + H_2O \rightleftharpoons H_2CO_3 + OH^-$

Eq. 2b. $\qquad$ $CO_3^{2-} + H_2O \rightleftharpoons HCO_3^- + OH^-$
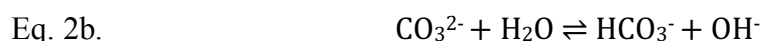
Atmospheric CO_2, (presently ~400 ppm and rising) and dissolved terrestrial carbonate deposits (e.g. from limestone, $CaCO_3$) are the two main sources of C_i in freshwater. As a result of terrestrial carbonate inputs, freshwater is generally super-saturated with respect to dissolved inorganic carbon (C_i), and pH is higher, compared to the levels expected based on dissolution of atmospheric CO_2 alone (Wetzel, 2001). In extremely productive environments, such as shallow lakes and microbial mats, biological activity can override the effects of chemical inputs by increasing and reducing environmental pH in diel cycles of 1-4 pH units (up to a maximum of ~pH 11.0) (Lopez-Archilla et al., 2004; Stal, 2012). In cyanobacterial mats, pH increases during the day due to photosynthetic uptake of inorganic carbon, and decreases at night due to

community respiration and carbon release (Jensen et al., 2011; Stal, 2012). Generally speaking, the tolerance of cyanobacteria to a broad pH range is astonishing; in contrast, a decline in mean oceanic pH due to anthropogenic CO_2 emissions and ocean acidification of around ~0.5 pH units is predicted to have major detrimental impacts on a wide range of other photosynthetic aquatic organisms, including macroalgae and various phytoplankton (Doney et al., 2009).

1.3.3 pH-dependence of inorganic carbon, and Rubisco

Within the typical environmental range of freshwater cyanobacteria (pH 7.0-8.0), the dominant form of C_i is HCO_3^- (Fig. 1.7) (Raven, 2012). At pH 7.0 there are only minor amounts of aqueous CO_2 (20.8% CO_2 : 79.2% HCO_3^-) and there is virtually none at pH 8.0 (<1% CO_2 : >97% HCO_3^-) or above (Wetzel, 2001; Raven, 2012). Thus, cyanobacteria grown at pH >8.0 are essentially wholly reliant on HCO_3^- transport to sustain Rubisco activity (Wetzel, 2001; Price, 2011; Raven, 2012). Crucially, for photosynthetic organisms, only the non-ionised species CO_2 is able to diffuse passively through lipid membranes into the cell; HCO_3^- requires active transport processes. Additionally, CO_2 is the only C_i form able to be utilised by Rubisco in the Calvin-Benson cycle, requiring further cellular processes to convert inwardly transported HCO_3^- into CO_2 at the site of Rubisco. The CO_3^{2-} species cannot readily be accumulated in the cell or converted into other C_i forms by cyanobacteria, and is essentially unavailable for photosynthesis (Raven, 2012).
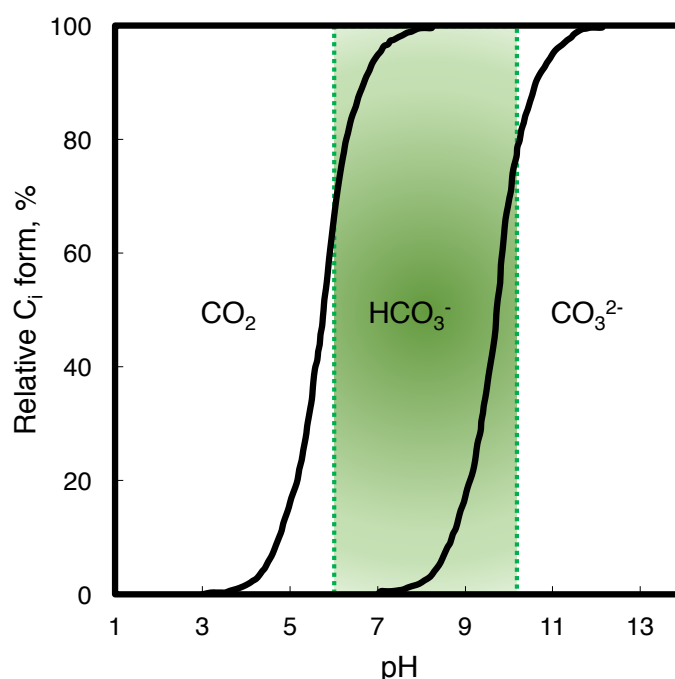
Figure 1.7. pH-dependence of the forms of inorganic carbon in solution; green shading indicates the approximate growth range of *Synechocystis* 6803. Created with reference to Kupriyanova et al. (2013) and Mangan et al. (2016).

1.3.4 pH and inorganic carbon in buffered culture media

Cyanobacteria are typically grown in laboratory media, the most common media being BG-11 or variants (Rippka et al., 1979). Strong buffers such as ~25 mM HEPES, TES and CAPS may be used to hold BG-11 at a desired pH for experiments (Eaton-Rye, 2011); this has the effect of 'fixing' the relative proportions of C_i species, although total C_i will vary depending on added CO_3^{2-} and the partial pressure of atmospheric CO_2 when cyanobacteria are cultured in a mixed open system (i.e. bubbled or stirred cultures). In an open system, if pH is buffered below pH ~8.0, and partial pressure of CO_2 in the atmosphere is lower than in the growth media, dissociation equilibria of carbon species dictate that C_i in excess (e.g. from added CO_3^{2-}) will be lost to the atmosphere as CO_2. Alternatively, many laboratories routinely use enriched levels of CO_2 to culture cyanobacteria such as *Synechocystis* 6803; it seems likely that these conditions might enhance growth in otherwise non-permissive conditions by counteracting the effects of low C_i, and the loss of photosynthetically available CO_2 and HCO_3^- carbon species at low pH and high pH, respectively.

1.4   Carbon uptake by cyanobacteria

1.4.1   Carbon concentrating mechanisms and the Calvin-Benson Cycle

One of the main sinks for NADPH produced by photosynthetic electron transport is the Calvin-Benson cycle, in which the enzyme ribulose-1,5-bisphosphate carboxylase/oxygenase (Rubisco) catalyses the main reaction of carbon fixation. In the carboxylase reaction, Rubisco catalyses the reaction of a ribulose-1,5-bisphosphate (RuBP) molecule with a CO_2 molecule to form two 3-phosphoglycerate (3PGA) molecules; reduction of 3PGA by NADPH and ATP forms glyceraldehyde-3-phosphate used for sugar metabolism and RuBP regeneration. Rubisco is also able to use O_2 as a substrate (oxygenase reaction), competing with carbon fixation and producing one 3PGA and one 2-phosphoglycolate (an inhibitor of other Calvin-Benson cycle enzymes). In order to favour the carboxylase reaction, CO_2 is concentrated in the vicinity of Rubisco by carbon concentrating mechanisms (CCMs). Cyanobacterial growth in broad pH conditions is facilitated by highly effective CCMs compared with those of green algae, which have a lower and narrower pH growth range (Kaplan and Reinhold 1999). Two CO_2 uptake (CUP) systems and three HCO_3^- transporters facilitate C_i uptake, and this topic has been reviewed extensively elsewhere (see Price et al., 2008; Price, 2011; Burnap et al., 2013, 2015; Raven and Beardall, 2016, and references therein). CCMs act to concentrate C_i in cellular carboxysomes, the protein-shelled cytosolic compartments that contain the Rubisco enzyme (Kerfeld et al., 2005; Rae et al., 2013).

The large flux of carbon required to maintain Calvin-Benson cycle activity far exceeds the passive rate of CO_2 diffusion and HCO_3^- entry (via porins) into the cell (Price, 2011). Thus, to concentrate CO_2 at the site of Rubisco, cyanobacteria possess a host of constitutive and inducible CO_2 and HCO_3^- uptake systems that are often interlinked with pH homeostatic mechanisms. Following illumination, CO_2 is the main substrate for around 30 s, and HCO_3^- uptake is activated after 20–60 s (Price et al., 2008). During initial CO_2 uptake, up to 20 mM C_i is transported into the cell, requiring the extrusion or neutralisation of an equivalent 20 mM protons as CO_2 is converted to HCO_3^- in the cell (Equation 1b); C_i flux results in considerable proton movement and requires tight control over pH homeostasis (Price et al., 2008).

As Rubisco can utilise only C_i in the form of CO_2, the more abundant HCO_3^- is actively transported into the cytosol and concentrated in carboxysomes, where it is converted to CO_2 by carbonic anhydrases. Although cyanobacterial Rubisco has a relatively low affinity for CO_2

(150 μM) compared with typical environmental C_i levels (~15 μM), CCM activity accumulates C_i in the carboxysomes to levels more than 1000-fold greater than in the external environment (Burnap et al., 2013). Internal C_i pools in cyanobacteria can exceed 30 mM, saturating Rubisco with respect to CO_2 and reducing energetically expensive photorespiration, whereby O_2 becomes the enzyme's substrate (Price, 2011). In alkaline pH, where aqueous CO_2 levels are negligible and HCO_3^- levels are high, HCO_3^- transporting CCM activity by cyanobacteria is extremely important for the maintenance of photosynthetic carbon uptake and cellular growth. Leakage of C_i from the cell cytoplasm back to the environment is possible, particularly with membrane-mobile CO_2/H_2CO_3, and it is proposed that internal pH homeostasis in cyanobacteria optimises the efficiency of inward C_i transport; based on modelling of chemical equilibria, CCM activity is predicted to be most efficient at an internal pH of ~8.0 (Raven et al., 2014; Mangan et al., 2016; Raven and Beardall, 2016).

1.4.2 Carbon dioxide uptake by cyanobacteria

Although CO_2 is able to move passively into cyanobacterial cells, diffusion alone is insufficient to support Calvin-Benson cycle activity in ambient conditions, and CUP systems are required for optimum growth, particularly at neutral pH (Price, 2011). CUP in cyanobacteria such as *Synechocystis* 6803 occurs via two modified NDH-1 complexes, which are similar to other bacterial type-I NAD(P)H dehydrogenases and mitochondrial complex I; they form membrane-bound protein complexes that pump protons across the membrane using energy from the oxidation of NAD(P)H. Cyanobacterial NDH-1 complexes are localised on the thylakoid membrane and participate in CET around PS I in the dark, respiration, and CO_2 uptake (Battchikova et al., 2011). Four NDH-1 complexes have been identified in *Synechocystis* 6803; NHD-1L and NHD-1L' complexes are involved in CET, and NDH-1MS and NHD-1MS' are required for inducible and constitutive CO_2 uptake, respectively (Klughammer et al., 1999; Shibata et al., 2001; Ma and Mi, 2008). The core NDH-1M complex contains 16 subunits encoded by the single-copy genes *ndhA-C*, *ndhE*, *ndhG-Q* and *ndhS* genes. The *ndhD* and *ndhF* genes are present in multiple copies (encoding NdhD1-6 and NdhF1-4). NDH-1M complexes containing NdhD1/F1 (L-subcomplex) and NdhD2/F2 (L'-subcomplex) subunits form the NDH-1L and L' complexes, respectively. NDH-1M complexes containing NdhD3/NdhF3/CupA/CupS (S-subcomplex) and NdhD4/NdhF4/CupB/ChpY (S'-subcomplex) form the NDH-1MS and MS' complexes, respectively. NDH-1 complexes utilise energy from NADPH to transport protons into the thylakoid lumen, increasing the trans-

thylakoid pH gradient and optimising photosynthesis and ATP production (Battchikova *et al.* 2011). The inducible, high affinity NDH-1MS complex and the constitutive, low-affinity NDH-1MS' complex are responsible for CUP in *Synechocystis* 6803 (Klughammer et al., 1999; Ohkawa et al., 2000a; Shibata et al., 2001).

Reverse-genetic studies have elucidated the function of and requirement for the different NDH-1 complexes in CUP when pH and C_i levels are modified. A ΔpH gradient across the thylakoid membrane generated by NDH-1 proton-pumping is likely to create an alkaline domain on the cytosolic face of the membrane, where the hydrophilic CupA/CupS and CupB/ChpY of the S or S' subcomplexes, respectively, act as carbonic anhydrases that convert $CO_{2(aq)}$ in the cytoplasm to HCO_3^-. Thus, they do not transport CO_2 directly but instead maintain an inward CO_2 gradient (Tchernov et al., 2001; Price et al., 2008; Battchikova et al., 2011). Genes encoding the S subcomplex are rapidly induced by C_i limitation, and various ΔS mutants in *Synechocystis* 6803 are impaired at pH 6.5 at low (50 ppm) CO_2 but like ΔNDH-1MS' mutants are able to grow at neutral to alkaline pH (pH 7.0-8.3) under high (3%) or ambient levels of CO_2 (Ohkawa et al., 1998, 2000a, 2000b; Shibata et al., 2001; Wang et al., 2004; Zhang et al., 2004). Double mutants ΔSΔS' (*ΔndhD3ΔndhD4* or other combinations of relevant genes) and the M55 mutant (lacking *ndhB* and hence all NDH-1 complexes) in *Synechocystis* 6803 are unable to grow in ambient CO_2 at neutral pH 7.0-7.5 (Shibata et al., 2001, 2002; Zhang et al., 2004). In moderately alkaline pH 8.3, where HCO_3^- uptake is induced, the M55 mutant and ΔSΔS' mutant are photoautotrophic, although they grow slowly compared to wild type (Zhang et al., 2004). At pH 9.0, where the only available C_i form is HCO_3^-, growth and HCO_3^- uptake of the single and double ΔS/ΔS' mutants was similar to wild type under ambient and 3% CO_2 (Shibata et al., 2001, 2002). These results lead to the conclusion that CUP systems are a requirement for growth in ambient CO_2 conditions, but are dependent on the presence of the CO_2 form of C_i (i.e. approximately neutral pH conditions, see Fig. 1); CUP becomes less important as pH increases.

1.4.3 Bicarbonate uptake by cyanobacteria

In the alkaline conditions favoured by many freshwater cyanobacteria, the major form of C_i is HCO_3^-, and CO_2 makes only a minor contribution. Active HCO_3^- uptake is essential and rapidly induced at high pH, and is facilitated by the high affinity ABC (ATP Binding Cassette)-type transporter protein complex Bct1 (encoded by the *cmpA-D* operon) (Omata et al., 1999), as

well as two Na^+-dependent uptake systems: the high affinity SbtA Na^+/HCO_3^- symporter (Shibata et al., 2002), and the low-affinity Na^+/HCO_3^- symporter BicA (Price et al., 2004). The role of BicA is less studied in *Synechocystis* 6803 and might play a minimal role, although it is able to support C_i uptake in the absence of other systems (Orf et al., 2015).

The SbtA transporter appears to make the dominant contribution to HCO_3^- uptake in *Synechocystis* 6803 in alkaline environments. SbtA, and an associated protein SbtB, were first identified by Shibata and colleagues in a *Synechocystis* 6803 mutant deficient in CO_2 uptake (ΔSΔS') and *cmpA-D* (ΔBct1), and SbtA appears to be dependent on an inward Na^+ gradient for HCO_3^- symport (Shibata et al., 2001, 2002). A ΔSΔS'ΔSbtA mutant was unable to grow under ambient CO_2, was impaired in growth at 3% CO_2 at pH 9.0, and HCO_3^- uptake rates were negligible in this mutant and in a ΔSΔS'ΔSbtAΔBct1 mutant (Shibata et al., 2002). SbtA and BicA activity, inferred from the HCO_3^- uptake of a ΔSΔS'ΔBct1 mutant, increases from pH 7.0-9.0 and with increasing HCO_3^- and Na^+ (Shibata et al., 2002). Na^+-dependent HCO_3^- uptake at pH 9.6 and low C_i (20 μM, ~1/10 ambient level) accounted for 88% of C_i uptake (So et al., 1998). Information obtained from the structure of CmpA (Bct1 complex) suggests that HCO_3^- transport via this protein requires Ca^{2+}, either as a co-factor, or that CmpA is a HCO_3^-/Ca^{2+} symporter (Koropatkin et al., 2007). Additionally, deletion of the Ca^{2+} transporter SynCAX (*slr1336*) significantly increased *cmpA-D*, *nhdF3* and *sbtA* gene expression as well as cytosolic pH (Jiang et al., 2013), indicating a possible interaction between Ca^{2+} transport, internal pH homeostasis and CCM regulation that remains to be elucidated.

No difference in growth or HCO_3^- uptake was found when Bct1 was deleted in the ΔSΔS' background at pH 9.0, implying a minimal role for this transporter in these conditions. HCO_3^- uptake occurred in a ΔBct1ΔSbtA strain at pH 9.0 (Shibata et al., 2002), but at the time of this study, BicA was not yet identified. Since apparent HCO_3^- uptake in this strain was dependent on HCO_3^- concentration, it could thus, to some extent, reflect spontaneous CO_2 production from equilibrium reactions in the growth media. *Synechocystis* 6803 ΔSΔS'ΔBct1ΔSbtAΔBicA strains lacking both CUP systems and all three HCO_3^- transporters are dependent on high levels of CO_2 (3%) to attain maximal growth rate (Xu et al., 2008). ΔSΔS'ΔSbtAΔBct1 cells in *Synechocystis* 6803 responded to a reduction in Ci supply from 5% to ambient CO_2 (at pH 7.0) by increasing the number of carboxysomes, but this response was insufficient to avoid photorespiration and oxidative stress in these cells (Orf et al., 2015).

1.4.4 Regulation of carbon concentrating mechanisms by pH

The regulation of CCM components to optimise C_i uptake in changing pH conditions appears to be so effective that the C_i concentration required to meet the half-maximum growth rate was statistically indistinguishable in *Synechocystis* 6803 grown at pH 7.5, pH 8.5, and pH 9.5 in one study (Nguyen and Rittmann, 2016). Essentially all CCM components show a degree of gene induction or repression when the environmental pH is modified, most likely reflecting perturbation in the ratio of different C_i species available for uptake (Fig. 1.7). However, many studies have investigated gene regulation in pH conditions at the limit of, or beyond the limit of growth, and results from such studies do not always provide a clear picture. Expression of the both CUP- and HCO_3^- uptake-system-encoding gene operons *ndhF3/ndhD3/cupA*, *cmpA-C*, and *sbtA-B* were rapidly and significantly repressed over 4 h upon a shift from pH 8.0 to highly acidic pH 3.0 using a gene microarray (Ohta et al., 2005). This study has led to several useful studies of possible pH-sensing genes and pH-response mechanisms (Uchiyama et al., 2012, 2014, 2015; Li et al., 2014; Matsuhashi et al., 2015; Tahara et al., 2015), but the extreme and rapidly lethal pH conditions in this study make it difficult to draw conclusions about CCM regulation under more moderate acid stress. In mild acid stress (pH 6.5 vs control pH 7.5), however, *Synechocystis* 6803 wild-type cells showed induction of the same genes (Zhang et al., 2012), which were also upregulated over 2-6 h following a shift from pH 10.0 to 7.5 and *vice versa* (Summerfield and Sherman, 2008). This latter result highlights the need to undergo reciprocal experiments when measuring gene expression, and raises the possibility that expression of CCM genes in these cases are responding to short-term disturbance rather than being under the strict control of pH. In proteomic experiments, however, analysis of cytoplasmic membrane proteins showed that levels of CmpA were similar at pH 6.0 and 7.5, and that these levels were ~3 fold higher compared to levels at acidic pH 5.5 and alkaline pH 9.0, in cells grown for several days (Kurian et al., 2006). CmpA was also reduced 1.9-fold in cells grown at alkaline pH 11.0 for 24 h compared to cells grown at pH 7.5 (Zhang et al., 2009a), but a further study found a 1.7-4.4-fold increase in Bct1 proteins, including CmpA, at pH 6.2 compared to pH 7.5 after 48 h (Ren et al., 2014). Relative to pH 7.5, pH 11.0 also increased cellular SbtB levels (Zhang et al., 2009a). One study found a small degree of induction of the constitutive CUP system *ndhD4/ndhF4/cupB* at pH 7.5 compared to 10.0 (Summerfield et al., 2013), and no induction of the BicA HCO_3^- transporter has been observed with changing pH; the importance of these constitutively expressed components in *Synechocystis* 6803 appears to be more limited than other CCM components, and their

regulation does not appear to reflect pH. Generally speaking, the variation in all these results reflects different experimental methodologies, particularly experimental duration and the scale of pH manipulation. Taken together, however, this range of studies gives some indication of the pH regulation of CCM components. Firstly, CCM component gene expression is rapidly induced or repressed by environmental changes. It is tempting to speculate that the CUP components are likely to be generally upregulated at ~neutral pH compared to acid or alkaline pH. However, microarray data are ambiguous, and no studies were found that investigated changes in synthesis of the thylakoid-embedded NDH-1MS and NDH-1MS' protein complexes in response to pH/C_i stress. However, there is some evidence for the induction of the cytoplasmic membrane bound SbtA at alkaline pH, in agreement with its increasing activity as pH increases (Shibata et al., 2002; Zhang et al., 2009a). Bct1/CmpA might be more important for HCO_3^- uptake at ~neutral pH (Kurian et al., 2006; Zhang et al., 2009a, Zhang et al., 2012; Ren et al., 2014), and accordingly this transporter accounted for minimal HCO_3^- uptake at pH ~9.0, where Na^+-dependent HCO_3^- uptake systems apparently make the dominant contribution (So et al., 1998; Shibata et al., 2001, 2002).

Expression of a number of CCM and pH homeostasis components is under the control of the LysR type transcription factor CcmR (NdhR), which was first identified as a major CCM regulator by Wang *et al.* (2004). The gene encoding CcmR is located upstream of *nhaS1* and negatively regulates the expression of this gene, as well as *sbtA/B*, genes encoding the NDH-1MS subcomplex, and the *mrp* operon (*ndhD5*, *ndhD6*) in C_i replete-conditions, and therefore contributes indirectly to pH homeostasis via modification of CCM and pH homeostasis systems in response to C_i. $NADP^+$ and α-ketoglutarate are co-repressors of CcmR, and high light and C_i affect the extent of gene induction by CcmR (McGinn et al., 2003; Daley et al., 2012; Burnap et al., 2013). Another Lys-R type regulator, CmpR, senses the Calvin-Benson cycle intermediates RuBP and 2-phosphoglycolate and increases transcription of the *cmpA-D* operon, presumably this is a strategy to reduce photorespiration caused by C_i limitation (Nishimura et al., 2008). C_i limitation in the ΔSΔS'ΔSbtAΔBct1 mutant involved changes in both NdhR and CmpR expression, but also posttranscriptional repression of genes involved in photosynthesis by PHOTOSYNTHESIS REGULATORY RNA1; the response to low C_i in this strain differed from that in ΔNdhR strains and the carboxysomes-less Δ*ccmM* mutant, and suggests a loss of C_i homeostasis in the ΔSΔS'ΔSbtAΔBct1 mutant (Orf et al., 2015).

1.5 pH homeostasis in cyanobacterial cells

1.5.1 Internal pH in cyanobacterial cells

In order to tolerate a highly variable external pH, (pH_{ext}), cyanobacteria maintain a relatively constant internal pH (pH_{int}) using a suite of homeostatic mechanisms, including cation/proton antiporters, proton pumps, and regulation of metabolic acid levels (Fig. 1.8) (Elanskaya et al., 2002; Wang et al., 2002; Krulwich et al., 2011; Price, 2011; Burnap et al., 2015; Mangan et al., 2016). Cyanobacterial pH homeostasis is complicated by a large proton flux due to PS II water-splitting activity, and dehydration of C_i species in the cytosol by CCM activity. Furthermore, pH_{int} is uniform in neither space nor time; cyanobacteria are known to differentially regulate the pH of the cytosol and thylakoid lumen, and the pH of these cellular compartments changes depending on light levels and subsequent PS II and carbon fixation activity (Teuber et al., 2001).

Internal and external pH vary because cellular membranes are barriers to free ionic movement; this create gradients of pH (ΔpH) and trans-membrane electrical potential ($\Delta\psi$) which establishes a PMF that is able to energise active transport and mechanical or synthetic processes (Padan et al., 2005; Krulwich et al., 2011). Across the cytoplasmic membrane, ΔpH and $\Delta\psi$ arise from proton extrusion from the lumen into the cytosol by thylakoid membrane-bound NDH-1 complexes, proton release in the cytosol resulting from the dehydration of C_i species by carbonic anhydrases, proton extrusion pumps across the cytoplasmic membrane, and cytoplasmic membrane bound proton/cation transporters. Across the thylakoid membrane, greater proton flux probably occurs; the splitting of water in the OEC of PS II releases protons to the thylakoid lumen via channels in the extrinsic domains of PS II, and LEF, CET and NDH-1 complexes also results in a build-up of protons in the lumen, generating a large ΔpH that is harnessed to drive ATP synthase (Checchetto et al., 2013; Mullineaux, 2014; Ifuku and Noguchi, 2016; Lea-Smith et al., 2016). Cyanobacteria generally display properties of alkaliphiles, which are a high external pH relative to internal pH, and a higher internal ψ relative to external ψ. The latter property renders alkaliphiles sensitive to toxic anions, such as Na^+, requiring Na^+ efflux systems to maintain pH homeostasis (Padan et al., 2005; Krulwich et al., 2011). Maintaining membrane stability is likely to be important for pH homeostasis in different cellular compartments. In *Synechocystis* 6803, deletion of the probable lipid transporter gene *slr1045* led to pH 6.0 sensitivity (compared to pH 8.0), apparently due to reduced phosphatidylglycerol (PG) lipid content in cellular membranes (Tahara et al., 2012).

Separately, in *Arabidopsis thaliana*, some experimental evidence suggests that a loss of PG affects energy transfer from the PS II antennae to the RC and increases photodamage (Kobayashi et al., 2016), however the antennae complex of higher plants and cyanobacteria vary significantly.

Internal pH is complex to measure in *Synechocystis* 6803 (and other cyanobacteria) as the small (~1 μm) cell size makes the use of micro-electrodes impractical. Measurement of pH_{int} is possible with the use of electron spin-resonance probes (Belkin et al., 1987; Belkin and Packer, 1988) and pH-sensitive fluorescent dyes, such as 5 (6)-carboxyfluorescein diacetate (CF-DA) (Jiang et al., 2013) and 2′,7′-bis(2-carboxyethyl)-5 (6)- carboxyfluorescein acetoxymethyl ester (Mangan et al., 2016). The cytosol-specific probe acridine yellow (AY) has become a commonly used tool to report changes in cytosolic pH (pH_{cyt}) as a result of cellular processes (for example, proton extrusion from the cytosol following illumination) (Teuber et al., 2001; Wang et al., 2002; Ryu et al., 2004; Berry et al., 2005). As light is applied to dark-adapted cells, an increase in AY fluorescence (ΔF) indicates alkalization of the cytosol as protons are extruded into the external medium. This process is attributed to dehydration of intracellular HCO_3^-; accordingly, when HCO_3^- is added to the external media during illumination, AY fluorescence drops, indicating carbon transport into the cell and cytosolic acidification (Berry et al., 2005). However, although ΔF of AY is used as an indicator of ΔpH_{cyt} (via ΔH^+) over time, it must be noted that relative fluorescence of this probe is partially concentration dependent; conversion of F to absolute measurements of ΔpH_{cyt} is therefore not possible (Teuber et al., 2001). A similar amine fluorescence method using 9-amino-6-chloro-2-methoxy acridine (ACMA) has also been applied to demonstrate lumen acidification and cytosol alkalization when light is applied to *Synechocystis* 6803 cells; chemicals such as the pesticide dimethoate can be used to disrupt this process, inferred by a lack of ACMA fluorescence (Mohapatra et al., 1996). Again, ΔpH_{cyt} and thylakoid lumen pH (pH_{thy}) cannot be inferred from this technique; absolute measurements of the pH in these internal compartments have been achieved in very few cyanobacterial species (e.g. Belkin et al., 1987; Belkin and Packer, 1988; Belkin and Boussiba, 1991).

Data on the internal pH in *Synechocystis* 6803 are limited, but some general statements are possible: as in other cyanobacteria, pH_{int} is neutral to slightly alkaline in the pH_{ext} range of 6.5-10.0. Katoh et al. (1996b) reported a pH_{int} of 6.5 in dark-adapted cells and pH_{int} 7.5 in the light (pH_{ext} 6.5) in *Synechocystis* 6803. In another study, the pH_{int} of dark-adapted cells was 6.8 at

pH$_{ext}$ 8.0, and 7.2 at pH$_{ext}$ 10.0 (Jiang et al., 2013); this is the first apparent report relating change in pH$_{ext}$ to pH$_{int}$ in *Synechocystis* 6803. Both these studies appear to have used pH buffering in the growth media, which might alter pH$_{int}$ in turn; Mangan et al. (2016) recently reported a somewhat higher pH$_{int}$ of 7.3 in the dark and 8.4 in the light in *Synechococcus elongatus* PCC 7942 in the absence of pH buffering. No data are available on the pH$_{thy}$ in *Synechocystis* 6803; other cyanobacteria maintain a pH$_{thy}$ in the light approximately two units lower than the pH$_{cyt}$ (Belkin et al., 1987; Belkin and Packer, 1988; Belkin and Boussiba, 1991) due to proton pumping across the thylakoid and proton release from PS II water splitting. In other cyanobacterial species at pH$_{ext}$ ~8.0, illumination results in an increase in pH$_{cyt}$ of 0.5 units, and a reciprocal decrease in pH$_{thy}$ (Belkin et al., 1987). The proteinaceous shells of cyanobacterial carboxysomes are believed to be proton-permeable and to thus reflect the pH$_{cyt}$ (Menon et al., 2010). However, it has been recently suggested that a ΔpH across the carboxysome shell, in which the carboxysome is acidified relative to the cytosol, would increase the efficiency of Rubisco, whilst also allowing optimum CCM function (Mangan et al., 2016); although the authors acknowledge that testing this hypothesis would be extremely challenging. In summary, available information on the internal pH in *Synechocystis* 6803 is extremely limited, although advances in molecular probe technologies and their detection tools may in future provide insight into the pH of micro-compartments in *Synechocystis* 6803 as it metabolises and photosynthesises.

1.5.2 Primary mechanisms of internal pH homeostasis

The primary effectors of internal pH homeostasis in *Synechocystis* 6803 are membrane-bound proteins or protein complexes, which regulate the pH of cellular micro-compartments by pumping protons and other ions across cellular membranes; they may be energised by ATP, NADPH or by electrochemical gradients that permit cation/proton antiport (Fig. 1.8). Coupled to pH homeostasis is control over cellular osmolarity, particularly Na$^+$ flux (Krulwich et al., 2011). In *Synechocystis* 6803, known pH-regulatory mechanisms are the sodium/proton (Na$^+$/H$^+$) antiporters encoded by five genes (*nha1-5*) (Elanskaya et al., 2002; Wang et al., 2002); four NADPH-dehydrogenase (NDH-1) complexes (Battchikova et al., 2011); and the proton extrusion pump encoded by *pxcA* (Katoh et al., 1996a, 1996b). Other ancillary components of pH homeostasis include the multi-component Na$^+$ pump encoded by the *mrp* operon (Blanco-Rivero et al., 2005); the Ca^{2+}/H$^+$ antiporter SynCAX encoded by *slr1336* (Waditee et al., 2004); the H$_2$O/CO$_2$ porin AqpZ (Akai et al., 2011); and the K$^+$ uptake KtrABE

system (Matsuda et al., 2004). In other bacteria, production of organic acids and other metabolites to modify internal or external pH is a common strategy (Krulwich et al., 2011), and appears to exist in *Synechocystis* 6803 as well (Maestri and Joset, 2000).

Na^+/H^+ antiporters play an essential role in pH and Na^+ homeostasis, are ubiquitous in cellular membranes, and are particularly important for adaptation to alkaline pH in bacteria (Padan et al., 2005; Krulwich et al., 2011). The *nhaA* gene was first identified in *E. coli*, whereupon it plays an essential role when cells are grown in the presence of Na^+ or at alkaline pH (Krulwich et al., 2011). The *nha* genes are highly conserved in many bacteria; *Synechocystis* 6803 *nhaS1* and *nhaS3* genes have been found to functionally complement Na^+/H^+ activity in a $\Delta nhaA$ *Escherichia coli* TO114 strain grown at pH 5.0-9.0 (Hamada et al., 2001; Inaba et al., 2001; Tsunekawa et al., 2009). In the same *E. coli* strain, introduction of *nhaS4* suggested a role for this gene in K^+ uptake (Inaba et al., 2001). Whereas *nhaS3* was functional in the *E. coli* TO114, *nhaA* could not complement a loss of *nhaS3* in *Synechocystis* 6803; the gene product NhaS3 is localised to the thylakoid membrane, potentially due to a unique, putatively thylakoid-targeting N-terminal sequence missing from NhaA (Tsunekawa et al., 2009). Reverse genetic studies show that some *Synechocystis* 6803 mutants deficient in single or multiple Na^+/H^+ antiporters exhibit altered pH- and Na^+-sensitive phenotypes (Hagemann, 2011). The gene *nhaS3* is essential for cell growth, and a partial gene knockout strain shows growth sensitivity to high Na^+/pH 9.0 compared to high Na^+/pH 7.0 (Elanskaya et al., 2002; Wang et al., 2002). It has been speculated that *nhaS3*, by regulating Na^+ influx/H^+ efflux in the thylakoid lumen, might act to reduce the trans-thylakoid pH gradient and prevent over-reduction of the photosynthetic electron transport chain (and production of ROS) when Na^+ levels reach cytotoxicity or when extracellular/intracellular pH is too high (Tsunekawa et al., 2009). Interestingly, $\Delta nhaS2$ cells are unable to grow at pH 9.0, whereas growth of $\Delta nhaS4$ cells is comparable to wild-type cells at pH 9.0, but impaired at pH 6.4 in standard Na^+ conditions (Wang et al., 2002). This might mean that NhaS2 is responsible for high pH Na^+ efflux, and NhaS4 is a Na^+ importer functional at low pH (Fig. 1.8). While no significant induction of any *nha* gene was observed at pH 7.0, 8.0, or 9.0 in the wild type, or in single or multiple knockouts of other *nha* genes, *nhaS3* is induced by high Na^+ and moderately high pH (gene expression: pH 7.0 < 8.0 > 9.0) (Elanskaya et al., 2002). Expression of *Synechocystis* 6803 *nhaS3* introduced into *E. coli* TO114 was similar across a pH 6.5-9.0 range (Tsunekawa et al., 2009). At pH 10.0, however, *nhaS3* expression was induced in *Synechocystis* 6803 (Summerfield and Sherman, 2008). Increased expression of the remaining *nhaS* genes in double or triple gene knockouts of *Synechocystis*

6803 generally suggests that different NhaS forms (with the exception of the essential NhaS3) can functionally replace each other (Elanskaya et al., 2002). However, the roles of the *nhaS1-5* genes in pH and Na^+ homeostasis in *Synechocystis* 6803 have been addressed in only a few studies and this topic, especially the stoichiometry of Na^+:H^+ exchange, is still not well understood (Waditee et al., 2006; Hagemann, 2011). Na^+ homeostasis also has roles in carbon uptake and proton extrusion; Na^+ is essential for growth below pH 7.2, and both nitrate and HCO_3^- uptake are impaired at pH 6.0 compared to pH 8.0 in low-Na^+ media (Katoh et al., 1996b; Sonoda et al., 1998).

During CO_2 uptake and conversion into HCO_3^-, protons are generated in the cytoplasm, and the gene product of *pxcA* is essential to H^+ extrusion and CO_2 uptake at low pH (Katoh et al., 1996a, 1996b). PxcA-dependent activity requires Na^+ and results in H^+ extrusion and acidification of pH_{ext} during the initial CO_2 uptake that follows the illumination of cells. CO_2 uptake is impaired in a $\Delta pxcA$ mutant at acidic pH, and *pxcA* deletion also reduced nitrate uptake at low Na^+ conditions in neutral and alkaline pH (Katoh et al., 1996a; Ohkawa et al., 1998; Sonoda et al., 1998). PxcA is widespread in cyanobacteria, but it is unclear how H^+ extrusion is energised; PxcA lacks an ATP-binding motif, is dependent on PS II electron transport but not PSI (and is therefore unlikely to be energised by NADPH), and may instead be a regulator of an alternative H^+ extrusion pump (Sonoda et al., 1998; Price et al., 2011).

1.5.3 Other mechanisms of internal pH homeostasis

A number of ancillary components of pH homeostasis show pH-dependent growth responses. Na^+ extrusion is essential to maintain pH homeostasis at alkaline pH, but inward Na^+ movement is essential for HCO_3^- uptake and cell growth in these conditions. At alkaline pH, the PMF and NhaS4 activity might be insufficient for the required flux of Na^+, raising the possibility that a primary ion pump might be required to maintain appropriate Na^+ balance. The *mrp* operon was first identified in *Anabaena* sp. PCC 7120, and is a multi-subunit protein that pumps Na^+ out of the cytoplasm using energy supplied by NADPH (Blanco-Rivero et al., 2005, 2009). Its homolog in *Synechocystis* 6803, the seven-gene *mrpA-G* operon encodes two components that belong to the NDH-1 subunit NdhD family (designated NdhD6 and NdhD7). All genes in the cluster are up-regulated following a shift from neutral to alkaline pH, in accordance with their putative role (Summerfield and Sherman, 2008). Additionally, it was found that expression of this operon is under the control of the carbon concentrating mechanism regulator CcmR (Wang

et al., 2004). Although the *mrp* gene family has not been investigated in detail in this species, it is believed to play an important role in establishing an inward Na^+ gradient (or possibly an outward H^+ gradient) that permits Na^+/HCO_3^- symport (Burnap et al., 2013).

The cytoplasmic membrane H_2O/CO_2 porin AqpZ (*slr2057*) is likely to affect internal pH indirectly, as it provides a porin for CO_2 entry, and CO_2 is then converted to HCO_3^- and H^+ (Akai et al., 2011). Expression of this gene was induced by a shift from pH 7.5 to 10.0 (Summerfield and Sherman, 2008), and *aqpZ* is essential to photomixotrophic growth at moderately alkaline pH (pH 7.5-8.5) but not pH 7.0 or pH 9.0-10.0 (Akai et al., 2011).

The sole Ca^{2+}/H^+ antiporter in *Synechocystis* 6803 SynCAX (encoded by *slr1336*) also appears to have a role in pH and Na^+ homeostasis at alkaline pH. Although growth rate was similar between wild-type and $\Delta slr1336$ strains in unbuffered media, as well as pH 7.5- and pH 8.8-buffered media, both chlorophyll and accessory pigment levels were lower in $\Delta slr1336$ at alkaline pH, and sensitivity to salt was higher (Waditee et al., 2004; Jiang et al., 2013). Accordingly, intracellular Na^+ was higher in the $\Delta slr1336$ mutant at alkaline pH, and pH_{int} was on average ~0.4 units higher in the $\Delta slr1336$ mutant when grown at pH 10.0 compared to the wild type, with no difference in pH_{int} between mutant and wild-type strains grown at pH 8.0 (Jiang et al., 2013). The SynCAX protein is therefore probably localised to the cytoplasmic membrane and is responsible for Ca^{2+} efflux/H^+ influx (stoichiometry $Ca^{2+}:H^+ >1:2$) from the cytosol to the periplasm, especially in alkaline pH (Waditee et al., 2004; Jiang et al., 2013). Levels of the SynCAX protein in the cytoplasmic membrane are significantly higher under alkaline pH conditions than neutral pH conditions (Kurian et al., 2006).

A well-known response to hyperosmotic conditions (e.g. high Na^+) in cells, including cyanobacteria, is the preferential accumulation and exchange of K^+ for cytotoxic Na^+ ions, increasing cellular osmolarity and counteracting plasmolysis (Hagemann, 2011). In *Synechocystis* 6803, the Na^+ dependent, K^+ uptake KtrABE system utilises the PMF generated by Na^+/H^+ antiport to energise K^+ uptake (Matsuda et al., 2004). This three-gene system was originally identified in a $\Delta ktrB$ mutant, which was unable to transport HCO_3^- via SbtA at alkaline pH 9.0 in the absence of CO_2 uptake. The KtrABE system is functional in *E. coli* at roughly neutral to alkaline pH (6.5 - 8.5), but not at acidic pH 5.5 (Matsuda et al., 2004). In *Synechocystis* 6803, Na^+-requiring HCO_3^- uptake is highest in alkaline pH levels (Shibata et

al., 2001, 2002), Na$^+$ toxicity is exacerbated at high pH (Wang et al., 2002), and therefore KtrABE activity is likely to be adapted to counteracting Na$^+$ effects at alkaline pH.
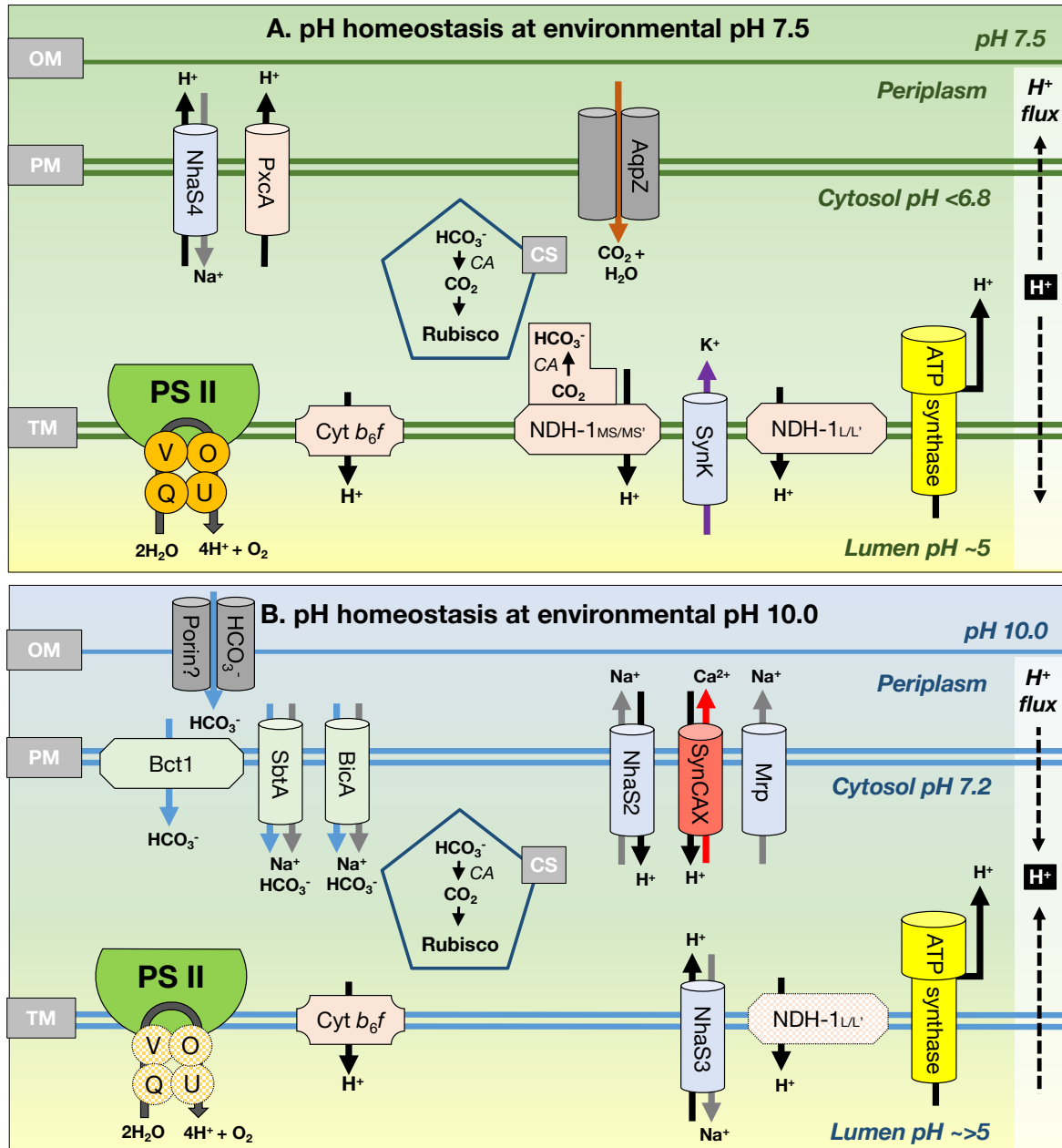
Figure 1.8. Proposed model of pH homeostasis components that affect PS II at neutral external pH 7.5 and alkaline external pH 10.0 in *Synechocystis* 6803. A. Neutral pH model: at pH 7.5, transport of protons from the OEC of PS II to the lumen is critical to generation of a ΔpH across the thylakoid membrane that is used to drive the thylakoid-bound ATP synthase. Protons are transported to the lumen via PS II with an active OEC protected by PS II extrinsic proteins (possibly including CyanoQ), cyt b_6f, and NDH-1 complexes involved in respiration and CET

(NDH-1L/L'). Uptake of carbon is driven by CAs coupled to via NDH-1MS/MS' complexes, which also pump protons to the lumen. K^+ transport by SynK is necessary for maintenance of $\Delta\psi$, export of excess protons in the cytosol by PxcA and NhaS4 enhances the ΔpH, and the resulting PMF drives ATP synthase. B. Alkaline pH model: at pH 10.0, ΔpH is naturally higher, delivery of protons to the lumen by PS II is less critical. At high pH, the cellular reliance on HCO_3^- for carbon uptake via SbtA and BicA involves the symport of Na^+ ions; in these conditions, proper maintenance of cytosolic Na^+ and pH is needed to maintain cellular activity. Ca^{2+} is exported by SynCAX in favour of H^+ to the periplasm where it is used as a co-factor for Bct1/CmpA mediated HCO_3^- uptake. Where Na^+ levels are too high, it is transported out of the cytosol by Mrp or NhaS2, or to the thylakoid by NhaS3. Membrane bound proteins or protein complexes that play a role in cation/proton transport, carbon uptake, ATP production and photosynthetic oxygen evolution by PS II are depicted on the thylakoid membrane (TM), plasma membrane (PM) and outer membrane (OM). Additionally, the protein-shelled carboxysome (CS), the site of CO_2 fixation by Rubisco, is shown, as well as the CO_2 porin AqpZ and a hypothetical HCO_3^- porin. Inter-conversion of carbon species CO_2 and HCO_3^- for Rubisco is maintained by CAs. Internal pH measurements are predicted based on Belkin et al. (1987) and Jiang et al. (2013) *Colours:* rose – proton pump; blue – monovalent cation transporter; green – HCO_3^- transporter; red – divalent cation transporter; green – PS II, orange – PS II extrinsic proteins; yellow – ATPase; grey – porin. Cross-hatched components with dotted boxes are believed be less important for pH homeostasis at that pH level. *References:* for PS II, cyt b_6f and ATP synthase (Kallas, 2012; Vinyard et al., 2013); carbon uptake and carboxysomes (Espie and Kimber, 2011; Price, 2011; Burnap et al., 2013; Rae et al., 2013; Orf et al., 2015); NDH-1 complexes (Battchikova et al., 2011); Nha2-4 (Elanskaya et al., 2002; Wang et al., 2002; Billini et al., 2008; Tsunekawa et al., 2009); K^+ homeostasis (Checchetto et al., 2012); AqpZ (Akai et al., 2011; Ding et al., 2013); PxcA (Katoh et al., 1996b; Sonoda et al., 1998); Mrp (Blanco-Rivero et al., 2005, 2009); SynCAX (Waditee et al., 2004; Jiang et al., 2013).

1.6   pH effects on the physiology of cyanobacteria

1.6.1   pH-sensing and gene regulation

The gene induction study by Ohta et al. (2005) has led to an interest in possible candidates for acid-sensing genes. The genes *slr0967* and *sll0939* are of unknown function but were found to be upregulated under acid stress (Ohta et al., 2005) and downregulated under neutral pH compared to alkaline pH (Summerfield et al., 2013). Both genes are under the control of the SphS-SphR two-component system, and a Δ*sphR* strain was sensitive to pH 6.0 and did not induce *slr0967* and *sll0939* expression compared to the wild type (Uchiyama et al., 2012). Expression of *sll0939* is induced by *slr0967*, and over-expression of either gene increased tolerance to acid stress (Uchiyama et al., 2014). Another mechanism of pH-sensing in *Synechocystis* involves Slr0643, a site-2-protease (S2P) homolog that is essential for growth below pH 7.0 (Zhang et al., 2012). Growth at pH 6.5 induced expression of the transcriptional regulator SigH in the wild type but not in a Δ*slr0643* mutant, leading the authors to speculate that low pH-sensing might occur via an S2P/anti-sigma factor/sigma factor mechanism (Zhang et al., 2012). Ren et al. (2014) identified three hypothetical proteins (Slr1259-Slr1261) downregulated in Δ*slr1909* at pH 6.2 compared to the wild type, which may be encoded by an acid-responsive operon that is presently uncharacterised.

Gene regulation by RNA polymerase sigma (σ) factors is a common response to stress in many bacteria including *Synechocystis* 6803 (Castielli et al., 2009; Gunnelius et al., 2010; Tyystjärvi et al., 2013). *Synechocystis* 6803 possesses 9 σ factors (Kaneko et al., 1996), of which three group 2 σ factors (SigB, SigC and SigD) and the group three σ factor SigH has been implicated in pH stress responses (Ohta et al., 2005). Li et al. (2014) adopted a bioinformatic approach based on predicted protein interactions and available gene expression data from *Synechocystis* 6803 and other species to construct a gene regulatory network for the acid stress response of this organism. Although lacking in experimental support, their model predicts a wide range of cellular responses based on signal transduction from SigB and SigD (which are homologs of the *E. coli* response regulator σ^{38}, encoded by *rpoS*) to response regulators such as histidine kinases, to H^+ extrusion mechanisms, systems for DNA replication and repair, and production of metabolites that modify intracellular pH.

1.6.2 Growth of *Synechocystis* 6803 across a broad pH range

Like many cyanobacteria, *Synechocystis* 6803 is capable of growth in a broad range of neutral to alkaline pH. Carbon uptake, respiration and other metabolic activity in cell cultures alters the external pH, which increases during exponential cell growth. The reported rate of photoautotrophic growth of *Synechocystis* 6803 in buffered BG-11 media is similar between pH 7.5-10.0 and between common media buffers TES, HEPES, CAPS, MES and bis-Tris (Maestri and Joset, 2000; Eaton-Rye et al., 2003; Kurian et al., 2006; Zhang et al., 2012; Summerfield et al., 2013). During growth over several days in standard conditions, *Synechocystis* 6803 cell cultures raise the pH of non-buffered BG-11 growth media to pH ~11.0 from a typical starting point of pH ~8.0; cells even in strongly buffered media (e.g. 50 mM HEPES-NaOH pH 8.0) are capable of raising pH by around one pH unit over several days (Maestri and Joset, 2000). In non-buffered media, it was found that onset of stationary growth phase occurs at the pH 11.0 maximum and thereafter declines, following a pattern that reflects the induction of acetolactate synthase; this protein is involved in pH regulation by production of organic acid compounds, and this response may be a direct strategy by *Synechocystis* 6803 to reduce pH below alkaline toxicity (Maestri and Joset, 2000).

1.6.3 Nutrient uptake

Many nutrients (e.g. Fe, Cu, Zn ions, or other ionic species such as phosphates) are insoluble at alkaline pH in the oxidizing conditions typical of freshwater environments (Turner et al., 1981). Considering the direct effects of pH on nutrient ion speciation and availability, there has been somewhat limited consideration in *Synechocystis* 6803 and other cyanobacteria of the effects of pH on nutrient uptake (excluding carbon uptake). One study found similar levels of phosphate uptake at pH conditions permissive to growth in *Synechocystis* 6803 (pH 7.0-10.0) but little uptake above or below this range (Burut-Archanai et al., 2011). This result contrasts with an increase in phosphate transporting Pst1 and SphX proteins at pH 11.0 compared to pH 7.5 (Zhang et al., 2009a), and suggests that alkaline pH impairs phosphate uptake, despite increased production of these cellular transporters. Additionally, a host of other nutrient transporters were upregulated at pH 11.0, including the Fe^{2+} transporter FutA, nitrate transporter NrtA, and urea-binding protein UrtA, and cells were impaired in growth at pH 11.0 compared to pH 7.5 (Zhang et al., 2009a). Adaptation of nutrient uptake systems in *Synechocystis* 6803 is likely to occur regardless of whether the pH stress is acidic or alkaline,

but few studies have addressed this issue; as a result, it is impossible to generalise whether highly alkaline pH is lethal because nutrient uptake is impaired, or *vice versa*.

1.6.4 pH and photomixotrophic growth

One of the main virtues of *Synechocystis* 6803 as a model organism is that the major lab substrains worldwide are generally glucose-tolerant (Williams 1988), and cells are capable of light-driven photomixotrophic growth even when PSII activity is eliminated (Anderson and McIntosh, 1991; Shen et al., 1993). Recently, a number of studies have emerged demonstrating a clear but poorly understood link between photomixotrophic growth and pH. Photomixotrophic conditions in certain pH ranges are lethal for *Synechocystis* 6803 mutants lacking the glucose-sensing duplicated *hik31* operon (Kahlon et al., 2006; Nagarajan et al., 2014), the H_2O/CO_2 porin AqpZ (Akai et al., 2011) and also putative regulatory genes *slr1736* and *pmgA* (Sakuragi, 2006).

The glucose/H^+ symporter GlcP (*sll0771*) transports exogenous glucose into the cytoplasm whereupon it is catabolised for the production of NADPH and ATP via respiratory electron transport. The H^+ symport associated with glucose uptake via GlcP does not seem to reduce cytosolic pH in *Synechocystis* 6803; in fact, introduction of 10 mM glucose increased cytosolic pH as a result of respiratory electron transport; Ryu et al. (2004) used AY fluorescence to determine that glucose addition in the dark caused around half the cytosolic alkalinisation of saturating light (therefore, a pH_{cyt} increase of ~0.25 pH units). Cytosolic alkalinisation in the presence of glucose disappeared in the absence of GlcP or the presence of electron transport uncouplers, and it was found that cytosolic alkalinisation, rather than changes to cellular redox state (from altered ATP/NADPH levels), was responsible for the induction of a number of carotenoid genes (Ryu et al., 2004).

Two proteins involved in a suite of cellular processes in *Synechocystis* 6803, Slr1736 (encoded by *slr1736*, essential for α-tocopherol metabolism and possibly high-light adaptation) and PmgA (*sll1968*, involved in regulating PS I:PS II stoichiometry in high light conditions, CCM regulation and photomixotrophic growth) are required for glucose metabolism at neutral pH 7.0, but not pH 8.0 (Hihara and Ikeuchi, 1997; Hihara et al., 1998; Hihara, 2001; Sakuragi, 2006; Haimovich-Dayan et al., 2011). The lethal, light-independent response of the α-tocopherol ΔSlr1736 mutant to glucose suggests a non-antioxidant role of α-tocopherol in

Synechocystis 6803 that is essential for photomixotrophic growth at neutral or low pH; a similar response was found in the ΔPmgA mutant, and PmgA is apparently essential for photomixotrophic growth (Hihara and Ikeuchi, 1997; Sakuragi, 2006). Intriguingly, both PmgA and Slr1736 appear to have a role in regulating the expression of CCM component-encoding genes *ndhF3* and *sbtA* in photomixotrophic conditions (Sakuragi, 2006; Haimovich-Dayan et al., 2011); these similarities raise the possibility of a shared signal transduction pathway that regulates growth in response to glucose, carbon, and pH. PmgA has structural homology with RbsW in *Bacillus subtilis*, a Ser-Thr kinase that regulates the σ factor SigB (Sakuragi, 2006). SigB is involved in pH-sensing in that species, as is its homolog in *Synechocystis* 6803 (*sll0306*) and also *E. coli* (*rpoS*, σ^{38}) (Price, 2000; Ohta et al., 2005; Li et al., 2014). Whole genome re-sequencing of 13 pseudorevertant cultures from a ΔPmgA strain grown on glucose revealed that 11 carried mutations in NDH-1 complexes; eight mutations affected and likely prevented functional expression of *nhdF3* (Nishijima et al., 2015). Clearly, NdhF3/NDH-1MS activity and PmgA expression are incompatible in the presence of glucose, even though CUP is ordinarily downregulated in photomixotrophic conditions, in order to maintain an appropriate balance of sugar catabolism and anabolism (Takahashi et al., 2008). It has been suggested that PmgA might act as a regulator of carbon partitioning between Calvin-Benson cycle and the oxidative pentose phosphate (OPP) pathway, and accordingly the mutant appears to maintain higher Calvin-Benson cycle activity than the wild-type in the presence of glucose, leading to a ten-fold greater accumulation of the tricarboxylic acid cycle (TCA cycle) intermediate isocitrate (Takahashi et al., 2008). The interplay between pH and photomixotrophic growth is therefore likely to relate to the overall redox state of the cell, with pH fluctuations that affect the carbon uptake rate requiring appropriate regulation of the OPP pathway and Calvin-Benson cycle supply to the TCA cycle. Over-reduction of the cellular electron transport chain might cause upstream issues with photosynthetic activity, such as the accumulation of ROS; this would suggest that photoinhibition and cellular death can arise when regulation of carbon flux in the cell is impaired (Takahashi and Murata, 2005, 2008).

1.6.5 Upper and lower pH limits for growth of *Synechocystis* 6803

No data on the natural pH environment of the original wild-type strain of *Synechocystis* 6803 is available, and it appears that the precise Oakland location from where the strain originated is not reported in the literature. However, cultures of this strain were originally isolated in neutral (pH ~7.0) BG-11 media (Stanier et al., 1971), and photoautotrophic growth of

Synechocystis 6803 laboratory strains over multiple generations is possible from pH 6.0 to pH <11.0 (Kurian et al., 2006; Zhang et al., 2009a, 2012; Uchiyama et al., 2012).

The main effect of variable pH in freshwater on cyanobacteria is presumably that it affects the availability of carbon to the organism. However, the precise factors that determine the upper and lower pH limit of cyanobacterial growth are not known. Low pH may have direct effects on membrane stability (Tahara et al., 2012). Additionally, it is possible that in acidic conditions, a reduction in internal pH reduces the trans-thylakoid pH gradient that drives ATP synthesis. In high pH ecosystems, on the other hand, the comprehensive CCMs of cyanobacteria, which allow saturation of Rubisco with CO_2 regardless of whether the C_i source is CO_2 or HCO_3^-, are the likely reason why cyanobacteria are dominant in high pH ecosystems. It is likely in the case of alkaline environments that the upper pH limit on growth is determined by pH homeostasis, which relies on Na^+/H^+ antiporters; these are dependent on a pool of external protons to prevent Na^+ cytotoxicity and subsequent reduction in cellular processes, including photosynthetic activity (Tsunekawa et al., 2009).

1.7 pH-sensitive PS II mutants of *Synechocystis* 6803

1.7.1 pH-sensitive PS II mutants of *Synechocystis* 6803 lacking extrinsic proteins

The loss of extrinsic proteins, or mutation in lumenal domains of the intrinsic proteins, has multiple effects on PS II (Bricker et al., 2012). By destabilizing the binding of Ca^{2+} and Cl^- in the OEC, function of the Mn_4CaO_5 catalytic site might be directly affected (Ifuku and Noguchi, 2016). In addition, the extrinsic domains of PS II include channels that allow the access of substrate water to the catalytic site, and egress of oxygen and protons. The absence of either of the extrinsic PS II proteins PsbO and PsbV reduced growth and oxygen evolution compared to the *Synechocystis* 6803 wild type (Burnap and Sherman, 1991; Shen et al., 1995), but did not affect pH tolerance (Eaton-Rye et al., 2003). Deletion of PsbO or PsbV resulted in decreased oxygen-evolution compared to deletion of PsbU or CyanoQ, consistent with the partial dependency of PsbU and CyanoQ binding on the presence of PsbO or PsbV (Shen et al., 1998; Bricker et al., 2012; Roose et al., 2016). Deletion of PsbU or CyanoQ in ΔPsbO or ΔPsbV backgrounds, respectively, revealed an enigmatic pH-sensitive phenotype; ΔPsbO:ΔPsbU and ΔPsbV:ΔCyanoQ strains do not grow autotrophically at pH 7.5, whereas growth at pH 10.0 is possible (Eaton-Rye et al., 2003; Summerfield et al., 2005a). Another extrinsic PS II protein, CyanoP, was also putatively assigned a role in the PS II dimer (Thornton et al., 2004; Nickelsen and Rengstl, 2013), but evidence suggests it may be a PS II assembly factor rather than a stoichiometric OEC subunit (Cormann et al., 2014; Jackson and Eaton-Rye, 2015; Roose et al., 2016). Deletion of CyanoP from other extrinsic protein mutants did not affect pH-sensitivity (Summerfield et al., 2005b).

1.7.2 pH-sensitive PS II mutants of *Synechocystis* 6803 with mutations in CP47

Mutations in the large, lumenal loop E of the PS II intrinsic protein CP47 (loop E: residues ~260-~450) also resulted in a loss of photoautotrophic growth and reduction in PS II centre assembly at pH 7.5, in some strains also lacking PsbV. Alkaline pH 10.0 restored autotrophic growth (compared to pH 7.5) in ΔPsbV mutants carrying a CP47 Glu364 to Gln substitution, or a deletion between Arg384 and Val392; however, ΔPsbV strains with either Phe363 of CP47 changed to Arg, or a deletion between Gly429 and Thr436, could not grow autotrophically at either pH (Morgan et al., 1998; Clarke and Eaton-Rye, 1999; Eaton-Rye et al., 2003).

Mutations in loop E of CP47 are likely to contribute to a loss of growth in *Synechocystis* 6803 ΔPsbV strains by affecting assembly of the further extrinsic proteins to PSII. The C-terminal half of loop E of CP47 crosslinks with amino acids in the N-terminal region of PsbO, and interacts with PsbU and possibly CyanoQ (Bricker et al., 2012; Roose et al., 2016). Analysis of analogous amino acid residues from the *T. vulcanus* PS II crystal structure (Protein Data Base accession 4UB6, Suga et al. 2015) using MacPyMOL software (see Chapter Two, Section 2.5.1) show that the Arg384 to Val392 (Arg385-Val393 in *T. vulcanus*) region is within 4 Å of *T. vulcanus* PsbO Leu164-Gly167, and PsbU Asn11-Gly18; a CP47 Δ(R384-V392):ΔPsbV mutant could not grow photoautotrophically at pH 7.5, possibly due to perturbation of PsbO and PsbU assembly to PS II. However, as noted above, the deletion of Gly429 to Thr436 in the ΔPsbV mutant resulted in a strain unable to grow at pH 7.5 or pH 10.0. This more severe phenotype might result from impaired CyanoQ binding in addition to perturbed PsbO binding. The Gly429-Thr436 (Gly427-Thr434 in *T. vulcanus*) residues are in close proximity (~5.8 Å) to CP47 Asp440, and within 4 Å of *T. vulcanus* PsbO Lys178. CP47 Asp440 and PsbO Lys178 in *T. vulcanus* correspond to CP47 Asp440 and PsbO Lys180 in *Synechocystis* 6803, which were suggested to be important crosslinking sites for CyanoQ (Liu et al., 2014). Consistent with the hypothesis that impaired CyanoQ binding caused the loss of all photoautotrophic growth in the CP47 Δ(G429-T436):ΔPsbV strain, deletion of CyanoQ in the CP47 Δ(R384-V392):ΔPsbV background resulted in a strain that could not be rescued by pH 10.0. In the CP47 Δ(R384-V392) mutant, loss of PsbO did not cause pH-sensitivity, potentially these cells were already impaired in PsbO binding; therefore, deletion of PsbV in this strain might have resulted in a phenotype similar to the obligate photoheterotrophic ΔPsbO:ΔPsbV mutant (Shen et al., 1995).

1.7.3 Hypotheses explaining the pH-sensitivity of PS II mutants

Although the pH microenvironment in the vicinity of PS II would be expected to be independent of environmental pH, changes in environmental pH do affect PS II. A number of mutants in the model strain *Synechocystis* 6803, which are deficient in extrinsic proteins that stabilise the OEC, are obligate photoheterotrophs or photomixotrophs in pH 7.5-buffered growth media, but were observed to grow photoautotrophically at pH 10.0 (Eaton-Rye et al., 2003; Summerfield et al., 2005a).

Introduction

During photosynthesis, a ΔpH across the thylakoid membrane drives ATP synthase. Lumenal pH is low relative to the cytosol, and ΔpH is enhanced by proton release from light-driven oxidation of water by PS II. In PS II mutants, a reduction in assembled PS II centres, or a perturbation of water, oxygen and proton channels in the OEC, would be likely to result in reduced proton delivery to the lumen. In cyanobacteria, ΔpH between the lumen and cytosol is as much as 2-3 pH units, and ΔpH increases with increasing environmental pH (Belkin et al., 1987). Therefore, reduced proton egress from PS II might be more harmful at pH 7.5 than pH 10.0, since ΔpH would already be reduced at lower environmental pH, potentially leading to ATP levels insufficient for cellular requirements. While this theory is inconsistent with data on the pH-optimum for oxygen-evolving activity in extrinsic-protein deficient PS II centres isolated from higher plants (e.g. Commet et al., 2012), the function of isolated PS II in experimental conditions would be independent of cellular ATP and NADPH requirements. PS II mutants can grow in the presence of glucose at pH 7.5; respiration of added glucose could permit growth in these mutants by favouring CET, allowing generation of ATP independently of PS II function. In *Synechococcus* Y-7c-s, a reduction in total cellular ATP, and the ATP:(ATP+ADP) ratio, was observed when external pH was reduced from pH 8.0 to growth-limiting pH 6.0 (Kallas and Castenholz, 1982). However, overall internal pH (the average of cytosol and thylakoid pH) across the same external pH range was only somewhat affected, suggesting that the observed limitation of energy supply might not be due to ΔpH alone. In support of the hypothesis that ATP supply might limit growth as pH is reduced, two strains of *Synechocystis* 6803 cells acclimated to pH 5.5 growth over three months independently acquired mutations in genes encoding F_1-F_0 ATP-synthase components (Uchiyama et al., 2015), although these mutations are, as yet, functionally uncharacterised. Furthermore, experimental investigation of this hypothesis would require greater investigation of internal pH changes within the cell during photosynthesis and respiration, which to date has proven difficult (Berry et al., 2005).

As highlighted earlier, channels that surround the PS II OEC are likely to be severely perturbed by the loss of extrinsic proteins. Mutants with Phe363 to Arg (hereafter F363R) and Glu364 to Gln (hereafter E364Q) substitutions in loop E of CP47 might also harbour impaired channels to the OEC. The *T. vulcanus* PS II crystal structure (*T. vulcanus* numbering is used throughout this paragraph) shows that CP47 Phe363 and Glu364 are adjacent to PsbO and D2 in a probable channel that might allow substrate water access to the OEC active site (Bricker et al., 2015). Additionally, Phe363 is implicated in the formation of a hydrophobic region around Y_D (D2

Tyr160), with the side-chain carboxyl group on Glu364 contributing to an H-bond network with Y_D via D2 Arg294 (Glu364-Arg294 distance: 2.8 Å) (Ferreira et al., 2004; Saito et al., 2013; Suga et al., 2015). Compounding the absence of PsbV, a perturbed hydrophobic pocket in the obligate photoheterotrophic F363R double mutant might affect Y_D oxidation, altering the dark redox-state of Mn_4CaO_5 and resulting in a more deleterious phenotype than in the pH 7.5-sensitive E364Q mutant, where the carboxyl group on the substituted Gln might be able to partially contribute to H-bonding with D2 Arg294 (Fig. 1.2). Such speculation is only possible because of advances in the resolution of the PS II structure; experimental manipulation of putative channels in PS II in variable pH conditions has not been investigated as yet.

The number of PS II centres was generally reduced by the loss of extrinsic proteins, particularly at pH 7.5. The extrinsic proteins stabilise the OEC and PS II dimer (Bricker et al., 2012), therefore, reduced PS II levels could be a result of altered PS II assembly processes. Alternatively, or additionally, they might be a consequence of the production of ROS by an impaired OEC; ROS cause photoinhibition by affecting PS II repair following photodamage, as well as by targeting PS II directly (see Murata et al., 2007; Nixon et al., 2010; Vass, 2012). However, PS II centres lacking all, or specific combinations of extrinsic proteins are probably natural assembly and repair intermediates in the cyanobacterial cell. Assuming that PsbO and PsbV attach to PS II first, centres lacking PsbO and PsbU but retaining PsbV and CyanoQ (or retaining PsbV and CyanoQ, but lacking PsbO and PsbU) might not ordinarily occur, and could result in excess ROS leading to photoinhibition and a loss of photoautotrophic growth at low pH. Some lines of evidence support this theory. Firstly, although ΔPsbO:ΔPsbU cells, for example, cannot grow autotrophically at pH 7.5, cells supplemented with 5 mM glucose can grow and evolve oxygen from PS II, when assayed with actinic light at 2.0 mE m^{-2} s^{-1} (Summerfield et al., 2005a). However, when 6.5 mE m^{-2} s^{-1} light is applied, rapid and total inactivation of oxygen evolution occurs in the same strains (Eaton-Rye et al., 2003). This implies that light dosage, as well as pH, causes the loss of PS II activity in these mutants. Secondly, cyanobacteria appear to be more sensitive to ROS at low pH; photomixotrophic growth of both the *Synechocystis* 6803 wild type and PS II mutants showed increased sensitivity to the $^1O_2$ ROS generator Rose Bengal at pH 7.5 compared to pH 10.0 (Summerfield et al., 2013). ΔPsbO:ΔPsbU and ΔPsbV:ΔCyanoQ cells were also more sensitive to the ROS generator methyl viologen than wild-type cells at either pH. At pH 10.0, cells may be able to better resist oxidative damage; a suite of general oxidative stress-responsive genes were downregulated in ΔPsbO:ΔPsbU cells at pH 7.5 compared to pH 10.0, or compared to wild-

type cells at either pH (Summerfield et al., 2013). Interestingly, a similar set of stress-responsive genes was upregulated in a ΔPsbO:ΔPsbU pseudorevertant capable of pH 7.5 growth (Summerfield et al., 2007), implying that antioxidant defence is involved in pH 7.5 recovery. Considering that total PS II levels are already reduced in these mutants, any photoinhibition by ROS at pH 7.5 might further reduce the number of effective PS II centres to levels that cannot sustain sufficient oxygen evolution and growth, especially in high light conditions. However, it must be considered that the relative level of PS II in these mutants does not correlate well with the capacity for photoautotrophic growth or oxygen evolution (Eaton-Rye et al., 2003; Summerfield et al., 2005a), indicating that more factors underpin the pH-sensitive phenotype than the capacity for PS II assembly alone.

1.8   Cyanobacterial genomes

1.8.1   Cyanobacterial genome structure and diversity

As at July 2017, over 370 cyanobacterial genomes have complete or draft genome sequences available in online databases such as CyanoBase, representing over 20 years of progress since the first publication of the *Synechocystis* 6803 genome (Kaneko et al., 1995, 1996; Fujisawa et al., 2017). Genome sizes in cyanobacteria studied to date range from 1.4 to 11.6 Mb, with ~1200-10000 genes per species (Hess, 2011; Mohanta et al., 2017; Zhu et al., 2017). Based on analyses of the cyanobacterial phylum to date, a core genome encoding around 500-1000 co-occurring likely orthologous genes (CLOGs) is predicted, with all species sharing a large number (>80) of highly conserved genes involved in oxygenic photosynthesis; other genes are characteristic of growth habit, including 3 CLOGs in thermophiles and 57 CLOGs found throughout heterocyst-forming cyanobacteria (Mulkidjanian et al., 2006; Simm et al., 2015; Beck et al., 2017). Most cyanobacterial genomes consist of one circular chromosome and several plasmids that can be several hundred kb in size, although plasmid-less species, multi-chromosome species and species with linear DNA elements are known (Hess, 2011). Some species are oligoploid, including *Synechocystis* 6803, which has around 10-12 chromosome copies per cell (Labarre et al., 1989). Most species have 3-10 chromosome copies, although many marine picocyanobacteria are monoploid or diploid (Mitschke et al., 2011). Genome size appears to increase with apparent complexity of growth habit, with larger genomes in heterocyst-forming diazotrophic species such as *N. punctiforme* (~9 Mb), and smaller genomes in marine picocyanobacteria such as those of the genus *Prochlorococcus* (~1.6-2.6 Mb) (Hess, 2011). Unsurprisingly, the number of genes encoding histidine kinase domains (from two-component sensor/regulatory systems) matches this trend, with 132 in *N. punctiforme* and 7-15 per genome throughout *Prochlorococcus* (Hess, 2011). Advances in genome sequencing technology in the past decade have greatly increased the rate of genome publication, but there is some suggestion that there is a substantial sequencing bias towards axenic cultures currently held in the Pasteur Culture Collection (Paris, France), and techniques for genome sequencing of non-axenic cultures have been recently suggested (Alvarenga et al., 2017).

1.8.2   Genome of *Synechocystis* 6803

The publication of the genome sequence of the *Synechocystis* 6803 chromosome in the mid-1990s by Kaneko et al. (1995, 1996) represented a major leap for the field of genetics, cyanobacterial studies, and photosynthesis research. The genome was only the third published

from a free-living organism worldwide, and was double the length of the *Haemophilus influenzae* Rd genome published slightly earlier (Fleischmann et al., 1995). The availability of the complete genome sequence facilitated functional genetics studies in the species, in particular in the field of photosynthesis. The sequence of three small plasmids pCA2.4, pCB2.4, and pCC5.2 (~10 kb in total) was reported separately (Yang and McFadden, 1993, 1994; Xu and McFadden, 1997). At the time of chromosome sequencing, the four large plasmids of *Synechocystis* 6803, pSYSA, pSYSG, pSYSM, and pSYSX (~370 kb in total) had either not yet been identified, or only their existence was reported (e.g. Kotani et al., 1994), and their sequence was published later (Kaneko et al., 2003). A total of 3168 genes were reported for the *Synechocystis* 6803 chromosome (3.57 Mb), with 397 on the large plasmids, 12 on the small plasmids, and a total genome size of 3.96 Mb (Kaneko and Tabata, 1997; Kaneko et al., 2003).

Notable characteristics of the *Synechocystis* 6803 genome include a large number of transposable elements, with around 134 open reading frames (ORFs) with significant homology to transposase-encoding genes from 11 transposase gene families, in contrast to 32 genes from six families found in the closely related *Synechocystis* sp. PCC 6714, which was isolated from the same freshwater lake in Oakland as *Synechocystis* 6803 (Kopf et al., 2014a). Strangely, a large number of these transposase homologs apparently have ORFs interrupted by frameshift and deletion, and apparent variation in the number of insertion sequences (IS) between substrains of *Synechocystis* 6803 (see Section 1.8.3) suggests that transposase activity and genome rearrangement in this strain is common (Kaneko et al., 1996; Urasaki et al., 2002). Around 90 genes, representing 45 histidine kinase two-component sensor systems have been described in *Synechocystis* 6803, with important roles in responses stressors such as salt stress, low temperature, and osmotic stress (Mizuno et al., 1996; Murata and Suzuki, 2006). One important histidine kinase-response regulator system, encoded by *hik31/rre34* is apparently duplicated, found on both the chromosome and on pSYSX, and several other genes found on plasmids encoding cation transporters and glycosyltransferases might be critical to cellular function (Kaneko et al., 2003); but there have been proportionately fewer mutagenesis studies establishing the function of genes on the plasmids compared to the genes located on the chromosome. For example, pSYSA contains the only *Synechocystis* 6803 CRISPR-Cas (Clustered Regularly Interspaced Short Palindrome Repeats – CRISPR associated proteins) systems CRISPR1-3, which are associated with immunity to phages and other genetic elements (Scholz et al., 2013). Investigations of CRISPR-Cas type genome editing in *Synechocystis* 6803

have been limited to date (Yao et al., 2016), in spite of growing interest in CRISPR-Cas in other fields.

1.8.3 Divergence in *Synechocystis* 6803 wild-types

As described earlier, the ability of *Synechocystis* 6803 to be transformed with exogenous DNA and grow on glucose led to its wide dispersal around the world as a model species, particularly in photosynthesis studies. As one of the model cyanobacterial species, *Synechocystis* 6803 has been distributed to multiple labs, with ensuing genetic and phenotypic divergence in 'wild-type' substrains (Ikeuchi and Tabata, 2001). Genome re-sequencing has revealed numerous genetic differences between these substrains held in laboratories around the world, with strains designated either PCC- (Pasteur Culture Collection) or GT- (Glucose Tolerant), depending on their lineage. PCC-substrains, originally from the collection of RY Stanier held at the Pasteur Culture Collection, are generally motile, and a glucose tolerant substrain from the lab of S Shestakov (Moscow State University) known as PCC-Moscow, is an important representative of this lineage (Rippka et al., 1979; Grigorieva and Shestakov, 1982; Trautmann et al., 2012). GT-strains were obtained from a glucose tolerant derivative of the ATCC 27184 substrain (GT-Williams strain) by JGK Williams at DuPont (Williams, 1988; Ikeuchi and Tabata, 2001), whereupon it passed to other researchers including Prof WFJ Vermaas (Arizona State University), who passed it to Prof JJ Eaton-Rye, who brought it to Otago University in the early 1990s. The original Otago substrain has been dubbed 'GT-O1.' A single representative clone of a GT-Williams-derived substrain, known as GT-Kazusa, was used for the genome sequencing project of Kaneko et al. (1995, 1996, 2003), at the Kazusa DNA Research Institute, Japan. A basic strain history has been proposed for this organism (Ikeuchi and Tabata, 2001), with variation in substrains apparent even in the first few years following the publication of the genome. Since 2011, when the first 'resequencing' project of Tajima et al. (2011) published the sequence of the GT-S substrain, at least ten other strains have had their genome sequenced. From this information, around 20 errors of the original sequence have been identified, and a family tree of the *Synechocystis* 6803 wild types can be determined (see Chapter Six, Fig. 6.1).

All substrains sequenced to date possess unique genetic mutations that cause residue changes in encoded proteins, and unsurprisingly there is phenotypic variation between substrains. The GT-lineage has lost motility due to a single nucleotide polymorphism (SNP) in the gene *spkA* (Kamei et al., 2001) and the GT-Kazusa substrain is non-competent for transformation due to

a frameshift in the pilin gene *pilC* (Bhaya et al., 2000); it is believed that pili facilitate ingress of exogenous DNA into the cell. Other mutations cause substrain-specific variation in traits such as phototaxis (Kanesaki et al., 2012), chlorophyll biosynthesis (Crawford et al., 2016; Tichý et al., 2016), and growth rate in photomixotrophic or high light conditions (Hihara and Ikeuchi, 1997; Hihara et al., 1998). The number of IS sequences appears to vary, with a greater number of ISY*203*-type transposase sequences apparently found in the GT-Kazusa substrain.

1.8.4 "Cyanobacterial genome instability – the elephant in the room?" (Jones, 2014)

The divergence of *Synechocystis* 6803 wild-types, in terms of substrain genomic and phenotypic variation, points to an active process of genetic mutation and selection in this organism, in spite of theoretically ideal laboratory growth conditions in terms of light, nutrients, and temperature. Culturing practices, including maintenance of *Synechocystis* 6803 as freezer stocks, should in theory reduce the effective time available for divergence and hence genetic distance between substrains, but this does not seem to have been the case. Certainly, selection for growth on glucose could be expected to result in a few fundamental differences between GT- and PCC- substrains. However, even within lineages, mutation processes are active, for example, with the insertion of four ISY*203* transposase genes in GT-Kazusa relative to other GT-strains (Trautmann et al., 2012), and the acquisition of a mutation in the gene *pmgA* in a culture of the GT-I wild-type, which led to that culture being dominated by the faster growing mutant within days (Hihara and Ikeuchi, 1997). The appearance of pseudorevertants derived from deliberately mutated strains is common in the literature (see Jones, 2014), but selection to avoid deleterious phenotypes is unsurprising. Repeated reports of genome mutation in permissive conditions that led one researcher to propose that cyanobacteria such as *Synechocystis* 6803 display a degree of genomic instability that could be considered an "elephant in the room" (Jones, 2014). That is, high inherent mutation rates might compromise the use of cyanobacteria mutants, both for production of biofuels (for example), and for reliable experimental conclusions when cyanobacterial substrains and mutants are compared; these could be affected by unforeseen genetic variation in the bacterial substrains used.

Although bacterial genomes are considered relatively stable from one generation to another, short generation times, the actions of mobile DNA elements, and horizontal gene transfer increases the apparent rate of mutation in human time scales (for review, see Darmon and

Leach, 2014). In *E. coli*, rates of mutation appear to be attenuated by the loss of a gene, *recA*, encoding an enzyme involved in DNA recombination, but the deletion of *recA* was not possible in *Synechocystis* 6803 in standard growth conditions; low light, and hence low rates of UV-induced DNA damage were essential to segregation of the ΔRecA mutant (Minda et al., 2005). Jones (2014) interprets this result to suggest that prospects for engineering genome stability in cyanobacteria will not be straightforward. Although the report of Jones (2014) discusses these reports predominantly in the context of cyanobacterial growth for industry (e.g. in bioreactors, with mutants developed for secondary metabolite production), genetic instability also affects other studies in cyanobacteria where differing background strains (e.g. *Synechocystis* 6803 wild-types) might be used to investigate the effect of deliberate gene mutations, such as studies of PS II. For example, CP47, chlorophyll, and PS I biosynthesis was inhibited in a Psb28 deletion strain (Dobakova et al., 2008), but this phenotype was later attributed to the GT-W wild-type background strain used, which had undergone spontaneous mutation, wherein a large area of its chromosome was duplicated (Tichý et al., 2016). Prior to the advent of relatively inexpensive, so-called 'high-throughput' or 'next-generation' sequencing platforms such as those of the Illumina and Roche corporations, there was no straightforward way to detect such instances of mutation, and recent resequencing studies are addressing this question.

1.9   Aims of the current study

The first aim of this study was to investigate instances of genome mutation in *Synechocystis* 6803 in wild-type substrains grown in standard laboratory conditions, and also in pH-sensitive mutants lacking PS II extrinsic proteins, which are incapable of photoautotrophic growth at low pH 7.5 but are photoautotrophic at pH 10. These model systems theoretically represent ideal and highly stressful growth conditions respectively, and accordingly the study aimed to provide evidence in general terms of the prevalence and effect of genomic mutation in this species. The second aim of this research was to investigate the effect of pH on PS II mutants of *Synechocystis* 6803 known to be pH-sensitive, and identify factors that can contribute to low pH-sensitivity or low-pH tolerance in these cells; the strains used included those lacking PsbO & PsbU, PsbV & CyanoQ, and strains carrying mutations in loop E of CP47 and deletion of PsbV (Morgan et al., 1998; Clarke and Eaton-Rye, 1999; Eaton-Rye et al., 2003). It was hypothesised that factors dependent on PS II, such as production of reactive oxygen and PS II redox state, as well as factors independent of PS II activity, such as carbon supply, are explanatory factors in low-pH-sensitivity. These hypotheses were published as a perspective article in *Frontiers in Plant Science* (Morris et al., 2016).

The first part of this study involved the assembly of the genome sequence of two wild-type substrains of *Synechocystis* 6803, GT-O1 and GT-O2, to investigate the hypothesis that aberrant growth and chlorophyll biosynthesis observed in GT-O2 prior to this study might have arisen from genomic mutation. Additionally, a long-term culturing experiment was used to trace the fate of a novel genomic mutation in GT-O1 that arose during this study. Further, the broader topic of genome mutation in *Synechocystis* 6803, and its functional relevance, was addressed by investigating genome mutations and physiology of the GT-O1 substrain in comparison to the internationally studied PCC-Moscow GT-Kazusa substrains. The findings of these investigations were published in two publications in the *New Zealand Journal of Botany* (Morris et al., 2014, 2017).

The second part of this study investigated genomic and physiological differences between a Control:ΔPsbO:ΔPsbU mutant and a derived Control:ΔPsbO:ΔPsbU pseudorevertant mutant of *Synechocystis* 6803 (first described in Summerfield et al., 2007), in which the genomic basis of pH 7.5-growth of the pseudorevertant was sought. Additionally, aspects of low pH growth in these two strains were studied in terms of ROS production by PS II, low-pH acclimation of

PS II, and the effect of C_i supply. In addition, the effect of C_i on low pH-growth was investigated in growth experiments in a number of other pH-sensitive PS II mutants, including a ΔPsbV:ΔCyanoQ strain lacking the important CUP component-encoding *ndhF3* gene.

The final part of this study addressed the possibility that perturbations in the redox state of PS II arise from mutations in the vicinity of Y_D, and that these perturbations might be enhanced by low pH growth. Using a strain carrying a conservative Glu364 to Gln substitution in loop E of CP47 (adjacent to the Y_D pocket) in the presence and absence of PsbV, the function of PS II was investigated in depth in photoautotrophic conditions at pH 7.5, pH 10.0 and in photomixotrophic conditions at pH 7.5. Multiple aspects of photosynthesis, such as PS II thermoluminescence, room-temperature and low temperature fluorescence, flash-oxygen yield and PS I P_{700} oxidation state in the E364Q and E364Q:ΔPsbV strains were investigated and compared with the pH-sensitive ΔPsbV:ΔCyanoQ strain, and the non-pH-sensitive and nearly PS II-less CP47 F363R and F363R:ΔPsbV strains.

Chapter Two: Materials and Methods

2.1 General methods

Standard sterile microbiological techniques were used throughout this study, such as the use of a laminar flow hood during culturing procedures, autoclaving of equipment (15 psi, 20 min), and the use of reagent-grade chemicals and deionised ultrapure water with maximum resistivity of 18.2 MΩ (at 25°C).

Significant contributions of others to this work are noted in the methods, table captions, and figure legends, where applicable. These are summarised for reference in the Appendices, Section A.1.

2.2 Culturing

2.2.1 *Synechocystis* 6803

Wild-types: The wild-type 'GT-O1' substrain of *Synechocystis* 6803 used throughout this study is derived from a GT-Williams substrain held by Prof. WFJ Vermaas (University of Arizona); this substrain is referred to as GT-Vermaas. Two derived substrains were used either for whole genome sequencing (GT-O2) or for a long-term growth experiment (GT-O3). The GT-O2 substrain was isolated in the mid-2000s as a spontaneous mutant from GT-O1 cells, which were believed to have been maintained continuously on photoheterotrophic BG-11 plates (see Section 2.2.1) over a period of several months (JJ Eaton-Rye, *pers. comm.*). The GT-O3 substrain was isolated during this study from GT-O1 cells maintained continuously on photoheterotrophic BG-11 plates over the course of a year, with 25 re-streaks on BG-11 agar every 1-4 weeks. The PCC-Moscow and GT-Kazusa cells were a kind gift from Prof. A Wilde (University of Freiburg).

PS II mutant strains: PS II mutant strains produced prior to this study originated in the laboratory of JJ Eaton Rye, and are credited below.
GT-O1 background:
ΔPsbO:ΔPsbU**, ΔPsbV, ΔPsbV:ΔCyanoQ, F363R, F363R:ΔPsbV, E364Q, E364Q:ΔPsbV – (Morgan et al., 1998; Clarke and Eaton-Rye, 1999; Eaton-Rye et al., 2003; Summerfield et al., 2005a)
PsbB Control strain* background:

Control:ΔPsbO:ΔPsbV, Control:ΔPsbO:ΔPsbU**, Control:ΔPsbO:ΔPsbU pseudorevertant – (Eaton-Rye et al., 2003; Summerfield et al., 2007).

*Hereafter shortened to 'Con' when naming mutants, e.g. 'Con:ΔPsbO:ΔPsbU strain.' The Control strain is a GT-Vermaas wild type-derived strain with a null phenotype associated with a kanamycin resistance (Kan^R) cassette inserted downstream of *psbB* (Eaton-Rye and Vermaas, 1991).

**Two ΔPsbO:ΔPsbU strains, with an apparently identical growth and PS-II function phenotype were used throughout this study. Generally, the Con:ΔPsbO:ΔPsbU strain was used, but as it already possesses a spectinomycin antibiotic resistance (Spec^R) cassette, the GT-O1-derived ΔPsbO:ΔPsbU strain was used for transformations requiring Spec^R insertions.

The genetic background of the strains was determined by PCR and Sanger sequencing as described in Sections 2.3.3-2.3.5. All other mutant strains described in this study were made in the GT-O1 background, or in the background of existing strains described above.

2.2.1.1   Growth media and culture conditions

Synechocystis 6803 cultures were grown in BG-11 liquid media (Rippka et al., 1979), or on solid BG-11 agar plates (BG-11 supplemented with 1.5% agar, 10 mM TES-NaOH pH 8.2, and 0.3% sodium thiosulfate). Unless stated otherwise, solid BG-11 plate cultures were grown in the presence of 20 µM atrazine to inhibit PS II function, and 5 mM glucose to sustain photoheterotrophic growth (see Eaton-Rye, 2011). Where appropriate, the following antibiotics were added to plates or liquid cultures: chloramphenicol – 15 µg.mL^{-1}, erythromycin – 25 µg.mL^{-1}, gentamicin – 2 µg.mL^{-1}, kanamycin – 25 µg.mL^{-1}, spectinomycin – 25 µg.mL^{-1}.

Cultures were kept at 30°C under constant ~40 µE.m^{-2}.s^{-1} warm, white illumination provided by fluorescent lamps in a dedicated growth room (hereafter referred to as standard conditions); cultures were occasionally grown in analogous light and temperature conditions in a smaller growth cabinet. Liquid cultures were grown in modified Erlenmeyer conical flasks with continuous humidified aeration provided by an aquarium pump which bubbled air into the culture flask through sterile water and a Millex FG50 air filter (Millex, USA). All media, culture vessels, and the filter apparatus were autoclaved prior to use. BG-11 plate cultures were re-streaked onto fresh plates every 2-3 weeks. For long term storage, 50 mL of liquid BG-11-

grown cells were harvested by centrifugation (5 min, ~2500 x g), re-suspended in 2 mL BG-11/15% glycerol, and kept in a -80°C freezer in sterile microfuge tubes. Every 2-3 months (~4-5 plate re-streaks), BG-11 plate cultures were discarded and new plate cultures were initiated from these freezer stocks, to minimise genetic drift.

Prior to experiments, a starter culture of cells was produced by inoculation of cells scraped from a 2-week-old BG-11 plate into either 150 mL or 250 mL of liquid BG-11 supplemented with 5 mM glucose and antibiotics as appropriate. The starter culture was incubated for 8-12 hours in standard conditions prior to the initiation of aeration, as described above.

For physiological experiments, as well as for transformation and growth experiments, starter cultures were grown to mid-exponential growth phase (OD $_{730\ nm}$ 0.6-1.0) and harvested by centrifugation at ~2760 x g for 10 min. Cells were washed by gentle re-suspension with pipetting or with a clean cotton swab in ~5 mL of fresh BG-11, which was topped up to ~50 mL and centrifuged again. Cells were washed by re-suspension again, and the OD $_{730\ nm}$ or chlorophyll concentration of the suspension was spectrophotometrically determined. Cells were then inoculated to a target OD $_{730\ nm}$ or chlorophyll concentration in BG-11 and supplemented as appropriate with 5 mM glucose, 25 mM HEPES-NaOH pH 7.5, 25 mM CAPS-NaOH pH 10, 25 mM TAPS-NaOH pH 7.7, or 25 mM TAPS-NaOH pH 9.0. Growth experiments and transformations were initiated immediately, but for physiological experiments, cells were generally allowed to acclimate in standard conditions for a pre-determined period of time. Cells were acclimated in 50 or 100 mL Erlenmeyer conical flasks on an orbital shaker at ~100 rpm, generally at 10 $\mu g.mL^{-1}$ chlorophyll concentration, prior to the initiation of physiological measurements. Antibiotics were omitted from physiological and growth experiments. Where applicable, following physiological experiments the chlorophyll concentration was re-determined and measurements were subsequently calibrated using this value.

Cells treated as above are hereafter referred to as prepared cells throughout the Methods.

2.2.1.2   **Transformation of *Synechocystis* 6803**

Cells were prepared as described as in Section 2.2.1.1, except that OD $_{730\ nm}$ at the point of harvest was generally 0.4-0.6 (early exponential growth phase). Cells were re-suspended at OD

$_{730\ nm}$ 2.5 in 500 μL aliquots in sterile microfuge tubes in the presence of ~1-5 μg of transforming plasmid DNA and incubated for 6 h under standard conditions; 200 μL of transformed cells were then spread on sterile Whatman Nucleopore 0.22 μm track-etch filters (Sigma-Aldrich/Merck, USA) or Pall Supor 0.2 μm filters (Pall Corporation, USA). Filters were incubated overnight on BG-11 plates in the presence of 5 mM glucose, 20 μM atrazine, and the absence of antibiotics, before being transferred to fresh BG-11 plates supplemented with selective antibiotics, glucose, and atrazine. Colonies of transformants were seen after 2-4 weeks; single colonies were picked and successively streaked out on fresh BG-11 plates until segregation of the inserted mutation into all chromosome copies could be verified using colony PCR as described in Section 2.3.3.

2.2.1.3 Other methods for culturing of *Synechocystis* 6803

For high CO_2 incubation experiments (Chapter Four), cells were grown in liquid BG-11 supplemented with 25 mM HEPES-NaOH pH 7.5, which was aerated with a mix of 3% CO_2 in air, with the flow rate and gas mix controlled by low pressure flow regulators. CO_2 aeration reduced pH in the BG-11 to ~pH 7.1 but did not affect culture temperature (data not shown). Adjacent cultures aerated with ambient air showed no alteration in pH (data not shown) due to nearby CO_2 enhancement, and no CO_2-induced phenotype, indicating that any slight increase in ambient CO_2 in the growth room did not affect cultures not directly aerated by the 3% CO_2 in air mix.

For high-light photoautotrophic growth experiments (Chapter Four), prepared cells were grown in standard temperature and photoperiod conditions in a growth cabinet; light levels were 200 $μE.m^{-2}.s^{-1}$.

In a 24-hour incubation experiment in cells grown at pH 7.7/pH 9.0 (Chapter Four), two cell preparation stages occurred. Prepared cells were standardised to OD $_{730\ nm}$ 0.4 and grown overnight in BG-11 supplemented with 25 mM CAPS-NaOH pH 10 (in the absence of glucose or antibiotics), then harvested, prepared again, and inoculated at 5 $μg.ml^{-1}$ chlorophyll in BG-11 supplemented with 25 mM TAPS-NaOH pH 7.7 or 25 mM TAPS-NaOH pH 9.0 for 24 hours (in the absence of glucose or antibiotics), with physiological measurements made at 2 h and/or 24 h. The purpose of this strategy was to exclude any buffer effects (TAPS-NaOH was used at both pH levels) on a fluorescence-based ROS assay (Section 2.4.14), and also observe

physiological effects of the transition from permissive growth conditions in alkaline pH to near-neutral pH in photoautotrophic conditions, to exclude any effects of physiological adaptation from photomixotrophic to photoautotrophic growth during the 24 h acclimation. The pH after 24 h was pH 7.8 ± 0.1 and pH 8.9 ± 0.3 in pH 7.7- and pH 9.0-buffered cultures respectively.

A portion of the experiments of this work (in Chapter Four-Five) was carried out by the author (with assistance noted where appropriate) in the laboratory of Prof. I Vass, Molekuláris Stressz és Fotobiológiai Csoport (Photobiology Lab), Biological Research Centre, Hungarian Academy of Sciences, Szeged, Hungary (BRC Szeged). Experimental conditions varied slightly to those outlined earlier but were deliberately kept as similar as practicable. Liquid BG-11 cultures grown for experiments carried out at BRC Szeged were not aerated, but were instead shaken on an orbital mixer in standard 50 mL, 100 mL, or 250 mL Erlenmeyer conical flasks. Liquid starter cultures were supplemented with 25 mM HEPES-NaOH pH 7.5 in the presence of 5 mM glucose, appropriate antibiotics, and 3% CO_2 in air, and grown to late exponential or stationary growth phase. Around 16 h prior to physiological experiments, a portion of starter culture was transferred to a fresh 200 mL BG-11 flask containing glucose and kept at ambient CO_2. Cells were then prepared as described in Section 2.2.1.1; physiological experiments were carried out in ambient CO_2 conditions, with glucose or pH-buffering conditions as appropriate to the experiment. The light level, light spectrum, temperature, and cell harvesting strategy was analogous to that described earlier, except that chlorophyll concentrations of 5 µg.ml^{-1} were used during measurements of thermoluminescence, room-temperature fluorescence, $^1O_2$ production, and P_{700} oxidation. The experiments conducted at BRC Szeged with ΔPsbO:ΔPsbU and ΔNdhF3 mutants (Chapter Four) and PsbB/ΔPsbV mutants in photomixotrophic conditions (Chapter Five) were carried out at BRC Szeged by the author with technical assistance from Prof. I Vass and S Kovács. Upon the author's return to New Zealand, S Kovács kindly carried out 2-3 additional experimental replications at BRC Szeged. These were, specifically, experiments on the effect of pH/autotrophic growth on P_{700} oxidation, thermoluminescence, and room-temperature fluorescence of PsbB/ΔPsbV mutants (Chapter Five). In these instances, experimental design was provided the author, and at least one experimental replication or substantially similar pilot experiment had been carried out on-site by the author.

2.2.2 *E. coli*

The competent DH5α strain of *E. coli* was used throughout this study (Sigma-Aldrich/Merck, USA).

2.2.2.1   Growth media and culture conditions

E. coli was maintained in standard Lysogeny Broth (LB) medium or Super Optimal broth with Catabolite repression (SOC) medium (LB: 1% bactotryptone, 0.5% yeast extract, 0.1% NaCl; 1.5% agar was added to form LB-agar; SOC: 2% bactotryptone, 0.5% yeast extract, 10 mM NaCl, 2.5 mM KCl, 10 mM $MgCl_2$, 10 mM $MgSO_4$ and 20 mM glucose). Where appropriate, the following antibiotics were added to plates or liquid cultures: ampicillin – 50 $\mu g.mL^{-1}$, erythromycin – 50 $\mu g.mL^{-1}$, gentamicin – 10 $\mu g.mL^{-1}$, kanamycin – 50 $\mu g.mL^{-1}$, spectinomycin – 50 $\mu g.mL^{-1}$.

2.2.2.2   Preparation and transformation of *E. coli*

Competent DH5α cells were prepared for the heat-shock method (Hanahan, 1983; adapted by Inoue et al., 1990), frozen immediately in $N_{2\ (l)}$, and stored at -80°C until used for transformation. Transformations were carried out in chilled 1.5mL microfuge tubes with 100 μL of cells and ~10 μL of transforming DNA suspension. Cells were incubated on ice for 20 min in the presence of the transforming DNA, heat shocked at 42°C for 1 min, placed on ice for 3 min before addition of 800 μL sterile SOC media. Cells were then incubated at 37°C for 45 min. Transformed cells (200 μL) were then plated onto LB-agar plates containing appropriate antibiotics and grown overnight at 37°C in a Ratek OM11 incubator (Ratek Instruments, Australia).

2.3 Molecular biology techniques

2.3.1 DNA extraction from *Synechocystis* 6803

Genomic DNA for PCR was extracted from ~200 mg of cells scraped from the surface of a BG-11 agar plate, or from ~200 μL of cell pellet subsequent to centrifugation (~2500 x g) of ~50 mL of culture (OD $_{730 nm}$ >1.0); cells were disrupted using 0.1 mm glass beads (DNature, NZ) by vortexing for 5-10 min; DNA was extracted using a DNeasy Mini Kit (Qiagen, Netherlands).

Genomic DNA from GT-O3 was extracted using a protocol provided by Prof. J Meeks (University of California, Davis). DNA was isolated from 50 mL liquid culture of *Synechocystis* 6803 grown to late exponential/early stationary phase (OD $_{730 nm}$ >1.0), harvested by centrifugation (~>2500 x g), washed twice with 5M NaCl to remove extracellular polysaccharides, suspended in TE buffer (TE: 10 mM TRIS-HCl, 1 mM disodium EDTA, pH 8.0), and incubated for 1 h at 37°C in the presence of 10 mg.mL^{-1} lysozyme (Sigma-Aldrich/Merck, USA) to break down cell walls. Following addition of 50 mM EDTA, proteins were degraded by incubation of the cell lysate with 0.5 mg.mL^{-1} proteinase K (Roche, Germany) and 0.5% sodium dodecyl sulfate at 37°C for 1 h, followed by addition of 1/6 volume 5M NaCl. A 1/8 volume of freshly prepared 0.7 M NaCl/10% cetyltrimethylammonium bromide solution was then added to remove lipids and polysaccharides in a 10 min incubation at 65°C. To remove cellular debris, the lysates were centrifuged at 10,000 x g for 10 min and the supernatant transferred to a new tube. Nucleic acids were extracted by gentle inversion on a wheel in a 1:1 sample:chloroform wash for 30 min, followed by a 5 min, 5,000 x g centrifugation step, and the aqueous phase was transferred to a new tube. DNA was precipitated with ice-cold 95% ethanol and pelleted at 10,000 x g for 5 min. To remove contaminating RNA, pellets were re-suspended in TE buffer and incubated at 37°C for 30 min in the presence of 40 μg.mL^{-1} RNase A (Qiagen, Netherlands) followed by a series of 3-5 extractions in 1:1 phenol:chloroform. The sample was then inverted continuously for 5 min prior to 5 min centrifugation at 10,000 x g; the aqueous upper phase was retained and the inversion/centrifugation process was repeated until the phase interface was clear. DNA was precipitated by addition of 2/1 volume 95% ethanol and 1/10 volume 3 M sodium acetate pH 5.2 at -20°C for >1 h. Genomic DNA was pelleted at 12,000 x g and 4°C for 10 min, followed by a wash with -20°C 70% ethanol and dried on a 37°C heat block for 10 min before final re-suspension in 200 μL TE buffer.

Genomic DNA from GT-O1, GT-O2, Con:ΔPsbO:ΔPsbU, Con:ΔPsbO:ΔPsbU pseudorevertant, and other strains used for whole genome sequencing (Section 2.3.6) was isolated prior to the commencement of this study by JA Daniels (University of Otago), using the method described above.

2.3.2 DNA visualisation, purification, and quantification

Isolated genomic DNA, plasmid DNA, and DNA amplified by PCR was visualised by gel electrophoresis using an integrated UV trans-illuminator, camera, and imaging software set-up (Kodak, USA); DNA fragment size was compared with 1 kb Plus DNA Ladder (Invitrogen/Thermo Fisher Scientific, USA) or KAPA Universal Ladder (KAPA Biosystems, USA). Gels contained 1% agarose and 0.25 μg.mL^{-1} ethidium bromide in TAE buffer (TAE: 40 mM Tris, 20 mM acetic acid, 1 mM EDTA). Electrophoresis was carried out using empirically determined settings (generally 90 V, 50 min); typically, 5 μL of DNA was loaded to the gel with 1 μL of 6x loading buffer (DNA loading buffer: 1.5% bromophenol blue, 1.5% xylene cyanol FF, 30% glycerol).

PCR products were purified using a PureLink PCR Purification Kit (Life Technologies/Thermo Fisher Scientific, USA) according to the manufacturer's instructions. GT-O3 genomic DNA, and genomic DNA used for whole genome sequencing (Section 2.3.6), was purified using a Genomic DNA Clean and Concentrator kit (Zymo Research, USA) according to the manufacturer's instructions.

DNA was quantified using a NanoDrop 2000c spectrophotometer (Thermo Fisher Scientific, USA).

2.3.3 Polymerase chain reaction

Routine PCR: Standard PCR amplification reactions were performed, following the manufacturer's instructions, in 25 μL or 50 μL reaction volumes using KAPA2G Robust HotStart DNA Polymerase (KAPA Biosystems, USA) or Platinum Taq Polymerase (Invitrogen/Thermo Fisher Scientific, USA), and the respective buffers and dNTPs. Template genomic DNA or plasmid DNA quantities to attain a final reaction concentration of ~200-1000 pg.μL^{-1} were used. All PCR reactions were carried out using an MasterCycler Gradient thermal

cycler (Eppendorf, Germany), with 30-35 cycles of amplification performed using empirically determined annealing and extension parameters; the denaturation temperature was 95 ℃ and the extension temperature was 72 ℃, with an initial denaturation step of 5 min and a final extension time of 5 min.

High-fidelity PCR: For amplification of DNA fragments intended for cloning or template construction, PCR was carried out as above in 50 μL reaction volumes using the KAPA Hifi HotStart DNA Polymerase (KAPA Biosystems, USA) or Platinum Taq DNA Polymerase High Fidelity (Invitrogen/Thermo Fisher Scientific, USA).

Colony PCR: Colony PCR to verify segregation of *Synechocystis* 6803 mutants was carried out as above in 50 μL reaction volumes with the KAPA3G Plant PCR Kit (KAPA Biosystems, USA). The templates used were: *Synechocystis* 6803 liquid culture – 1 μL of culture diluted with ultrapure water to an empirically determined 'faint green' concentration; *Synechocystis* 6803 grown on agar – cells picked from a plate using a sterile pipette tip were suspended in ultrapure water to 'faint green' concentration, and 1 μL of this suspension was used. PCR reactions employed a 'touchdown' PCR protocol with an increased initial denaturation step and 40 cycles as follows: initial denaturation, 95 ℃, 10 min; (13 x denaturation, 95 ℃, 20 s; annealing, 60 ℃, 15 s; extension, 72 ℃, 2 min); (13 x 95 ℃, 20 s; 56 ℃, 15 s; 72 ℃, 2 min); (14 x 95 ℃, 20 s; 52 ℃, 15 s; 72 ℃, 2 min); final extension, 72 ℃, 5 min. In some cases, stepwise increases or decreases of ~2 ℃ in primer annealing temperature were used. This protocol, or a variation upon it (with 5 min initial denaturation and ~35 cycles in total), was occasionally employed for problematic amplifications using genomic DNA for routine PCR applications.

2.3.4 Oligonucleotides

Oligonucleotide primers were designed by eye and synthesised to order by Sigma-Aldrich (Singapore) or Integrated DNA Technologies (Singapore).

Table 2.1. Oligonucleotides used for PCR reactions in this study.

Gene target or primer name	Forward Primer (5' – 3')	Reverse Primer (5' – 3')
Verification of GT-O1/GT-O2 SNPs		
slr1609	AGTGCCTACATTGACCAGA	TATTTACCCCACCGCCTT
slr1055	GAAACCACCGCATCCACA	ACATTAACCGTACCAACTCCA
slr1204	CTGTCATACTCGTCCCCT	TTACTGTCACTTCATCGGC
sll1428	AGAAGATTGAGCGTTACAG	TTGATTATGTTTGGCATGGG
sll0154	AGGTAAACGGGATGGGAA	AAATTGTCGTAGTGGGGG
sll0750	GGGACTGCGTAAATCGTG	AGGAGGAGAAGGGTTAATG
sll0550	CATTGGTTACTTGGCTGT	GTGGTTTTCTATGTGGCT
ssr6089	GCCCGGAGATTTAACTATAACC	CAATCGGCCACATCTACT
Verification of GT-O1/PCC-Moscow/GT-Kazusa Indels		
slr1084	CGTATTCTTGCTCCTTTGT	CCTGATCAAATGCATAACC
slr1753**	GAGCCAGGCAATGTATTC	AGGAAAGTTGCCATTCAG
ISY203b	AGTAGAAGCGGATGATTG	TTTGACGAGGAGTATCGG
ISY203e	TTTGACTTCTTGCCTGTTCT	GTGATTGCCAAGATGATAG
ISY203g	ATAGACCGCACTAACCTTTC	TGGAATCCTACAGCAGAACG
ISY203j	GCCCTTTCCATCATATGC	GCCCTTTCCATCATATGC
CRISPR1	GGACTGAAACGATATATGGC	AATTGTGCCAGTGACTGC
CRISPR2	AACCTCGTAAGCTAGGCAACGG	CACAGGTGGCGATTAGACAGG
Amplification of *slr0856* transposase		
slr0856	CATGGGGTGTACAAGATGAACAGGT	CTGGTGTTTAACTGGATGGGGATGG
Verification of Con:ΔPsbO:ΔPsbU/pseudorevertant SNPs, and photoautotrophic selection assay		
pmgA	TAAACAATGAACTGACCAGCC	TTTACTCCTTGATCCTCCC

ssr1558	AAGGTTGTCTTAGAAGGG	GGTGTATGTGGAATATGG
cheA	CTGGAGTGGGAAGAGGTT	CAGGGATATGGCTAGTAAGTTT
petH-prk	AAACCCTCAATAACCACCA	GTCCTACCACCCTAACAAA
rre2	CGTTTAGCAATATCCACCA	CTACCCAACAACCTACAAT

Construction of Δ*pmgA*/gentamicin resistance plasmid (Δp/Gen^R) by overlap-extension PCR

Δp_LF	GCTATTCACCTACTTGGC	CGAGTCCGGTAAACCTAGTGGTAGCAGAATTTC
Δp_Gen^R	CTACCACTAGGTTTACCGAGCTCGAATTGGC	TCAATGGTTAATACCGAGCTCGAATTGACAAAGC
Δp_RF	CGAGCTCGGTATTAACCATTGACCGCTTTGAG	CTGGAGCCTCTATTACAG
Δp_Internal	CCTGGCAGAATTTTACCAAGC	CTGTGCAGGATGATCGC

Construction of *pmgA* Control/erythromycin resistance plasmid (pG93/Ery^R) and *pmgA* G93C/Ery^R plasmid (pG93C/Ery^R) by overlap-extension PCR

pG93_LF/ pG93C_LF	GCTATTCACCTACTTGGC	GATAAGCTTGCAACCTAGTGGTAGCAGAATTTC
pG93_Ery^R/ pG93C_Ery^R	CCACTAGGTTGCAAGCTTATCGATTCACAA	GAGTTTGTAGGCCCTTTCGTCTTCAAGAAT
pG93_RF/ pG93C_RF	ACGAAAGGGCCTACAAACTCAGCAAACGGTAAC	TTGCTGATCTGAGCTTTAGCC
pG93_Internal/ pG93C_Internal	CCTGGCAGAATTTTACCAAGC	AGCTACTGTTAACCAGCG

Construction of a *pmgA* neutral-site (pΔ*slr0168*) Control plasmid (Spec^R) by ligation into a pΔ*slr0168* plasmid produced by TS Crawford (synthetic HindIII site underlined)

pmgA-HindIII	CGGTCC<u>AAGCTT</u>TCTGCTACCACTAGGTTCTAC	AATGTG<u>AAGCTT</u>TTGGCTGGTACCGTAGAGAC
slr0168	TTTAATTGAAGAAATGGC	GGATCTAGCACTGCACCG

Other PCR primers, used to confirm the presence of mutations, including segregation of the pΔ*ndhF3*/Kan^R plasmid, or confirm desired ligation of DNA into a plasmid vector

psbO	GTTCAGCTCGTCAAAGTAAC	TGAGATTGACTTAAGCGAGG
*psbU**	CCCAAAATCGGATCCGTCGGCATAATTTTC	AAAGGGTACGCAATGGAATTCGGTTAGCAG
*psbV**	CCAATGCCGTGGAGTTAACC	CTTCACCGTCATAACTCTTG
*cyanoQ**	TAATGTCCTGCAAACGGGTG	GGGCATTGGGAGATTCGTAA
psbB	AATAAAAATTAAAACGTCTTTAAGACAC	TCCCAAGACTTAGAACCTGTTTGTAAAG

Δ*cheA*	AACAGAGGAAGAATGAAGC	CAATATTGGCACCAACTAGC
ndhF3	AACAGATTGCATTTCATCGGC	TCCTAGCACCGAGTAAGCCG
M13*	CCCAGTCACGACGTTGTAAAACG	AGCGGATAACAATTTCACACAGG

*these primers were not designed in this study but were obtained from laboratory stocks.

**while this primer successfully amplified the genomic target, variable band sizes or double bands were observed, depending on PCR conditions.

2.3.5 Sanger sequencing

Sanger sequencing of plasmid DNA and purified PCR products was carried out by the Genetic Analysis Service (http://gas.otago.ac.nz), Dunedin, NZ.

2.3.6 Whole genome sequencing

Sequencing of the GT-O1, GT-O2, Con:ΔPsbO:ΔPsbU and Con:ΔPsbO:ΔPsbU pseudorevertant strains was carried out prior to the commencement of this study by A Jeffs and others (NZ Genomics Limited, NZ). Sequencing libraries were prepared using the Illumina TruSeq DNA Sample Preparation v2 kit (Illumina, USA). 1 μg of each genomic DNA was sheared to approximately 350 base pair (bp) size using a Covaris S220 focused-ultrasonicator (Covaris, USA). Gel size selection and library enrichment resulted in final libraries of approximately 500 bp average fragment length. The libraries were validated by using an Agilent 2100 Bioanalyzer High Sensitivity DNA assay (Aligent, USA), and quantified by using a Qubit v2.0 Fluorimeter and Qubit dsDNA HS assay (Life Technologies/Thermo Fisher Scientific, USA). 100 bp paired-end sequencing was performed on an Illumina HiSeq 2000 system and de-multiplexed using the Illumina CASAVA application, version 1.8.2 (Illumina, USA).

2.3.7 Restriction digest

Restriction enzymes were obtained from New England Biolabs (USA) and digestion reactions performed according to the manufacturer's instructions; visualisation of the digested DNA, along with a non-digested control, was carried out by gel electrophoresis as described in Section 2.3.2.

2.3.8 Ligation

For preparation of plasmids for transformation, DNA constructs were ligated into the pGEM-T Easy plasmid according to the manufacturer's instructions; >150 ng of insert DNA was ligated into 50 ng of vector with 3 units of T4 DNA Ligase provided with the plasmid (Promega, USA).

Blunt-ended PCR products created by overlap-extension PCR were 'A-tailed' by incubation of the DNA for 20 min at 72 ºC in a standard PCR reaction mixture (Section 2.3.3) containing only dATPs and no primer.

2.3.9 Plasmid miniprep

Plasmid DNA was isolated from DH5α *E. coli* transformed as in Section 2.2.2.2 using the alkaline lysis method (Birnboim and Doly, 1979); single colonies of transformed cells were used to inoculate 3 mL aliquots of LB containing appropriate antibiotics. These were grown overnight at 37°C and ~180 rpm on a Ratek OM11 shaker-incubator (Ratek Instruments, Australia). Cell lysates generated by alkaline lysis were treated for >30 min at 37°C in the presence of 40 µg.mL^{-1} RNase A (Qiagen, Netherlands) following extraction of plasmid DNA in 1:1 phenol:chloroform.

2.3.10 Overlap-extension PCR and generation of mutagenesis plasmids

For preparation of Δ*pmgA*/Gen^R (Δp), *pmgA* Control/Ery^R (pG93), and *pmgA* G93C/Ery^R (pG93C) plasmid constructs, an overlap extension PCR protocol was employed (Ho et al., 1989). For each construct, primers were designed to amplify three components by high fidelity PCR as described in Section 2.3.3: a left flank and right flank of the *Synechocystis* 6803 genome and an antibiotic resistance cassette from laboratory stocks of pUC19 vector were produced. These were designed with overlapping complementary ends between the 3' end of the left flank and 5' end of the antibiotic cassette, and the 3' end of the antibiotic cassette and the 5' end of the right flank. Around 20 ng each of purified left flank, cassette, and right flank PCR products were assembled in a further high-fidelity PCR that used interaction of the overlaps at the interface of the components, and the use of internal primers nested within the 5' end of each strand, to give a single PCR product. This single PCR product for each construct was purified, A-tailed, ligated into pGEM-T Easy, and transformed into *E. coli*; plasmid DNA was isolated by miniprep, as described above.

For preparation of a ligation of a *pmgA* neutral-site (Δ*slr0168*) Control plasmid (Spec^R) a high-fidelity PCR product generated by *pmgA*-HindIII primers was purified and HindIII-digested prior to ligation (as described) into a HindIII-digested Δ*slr0168* (Spec^R) plasmid produced in the laboratory by TS Crawford (Crawford et al., 2016). Construction of this plasmid, and those described above, is discussed in greater detail in Chapter Four.

The pΔ*pmgA* (Spec^R) and pΔ*ndhF3* (Kan^R) plasmids were a kind gift from Prof. Y Hihara (Saitama University), and originate from the studies of Hihara et al. (1997) and Ohkawa et al. (2000b), respectively.

2.4 Physiological analyses in *Synechocystis 6803*

2.4.1 Determination of growth rate

Prepared cells (as in Section 2.2.1.1) were inoculated into 150 mL BG-11 cultures (supplemented as appropriate) at OD $_{730\,nm}$ 0.05. OD $_{730\,nm}$ was determined using an Ultrospec 3000 spectrophotometer (Pharmacia Biotech, USA) or a Thermo Scientific Evolution 201 UV/Visible spectrophotometer (Thermo Fisher Scientific, USA) and monitored every 12-24 hours for ~100 hours.

2.4.2 Electron microscopy

GT-O1, PCC Moscow and GT-Kazusa cells were prepared as described above, and transmission electron microscopy was carried out by the Otago Centre for Electron Microscopy (http://ocem.otago.ac.nz/), Dunedin, NZ.

2.4.3 Photoautotrophic growth selection assay

Two photoautotrophic growth selection assay strategies were employed in this study, using BG-11 plates in the absence of antibiotics, atrazine, and glucose. In a 'top-agar' experiment, 1 mL of prepared cells of the non-pH 7.5-photoautotrophic Con:ΔPsbO:ΔPsbU *Synechocystis* 6803 strain at OD $_{730\,nm}$ 1.0 were suspended in 3 mL 0.8% BG-11 agar at ~40°C, and the mixture was rapidly spread atop a 25 mL BG-11 agar plate buffered with 25 mM TES-NaOH pH 7.5. Approximately 1 μg of transforming DNA (>10 μL) was spotted on to the agar, and DNA spots producing colonies of transformed, photoautotrophic cells were observed after ~3 weeks in standard conditions.

In a second experiment, the effect of pH and CO_2 on the growth of *Synechocystis* 6803 strains was determined by production of BG-11 plates produced without glucose, atrazine or antibiotics buffered with 25 mM TES-NaOH pH 7.5, 25 mM TES-NaOH pH 8.0, 25 mM TAPS-NaOH pH 8.5, or 25 mM TAPS-NaOH pH 9.0. Spots of 2 μL of prepared cells were applied directly onto the agar at OD $_{730\,nm}$ 1.0, 0.01, and 0.01. Using this technique, the growth of multiple strains could be assessed on a single BG-11 plate. Plates were incubated in standard conditions inside clear plastic containers aerated with air (ambient, 0.04% CO_2) or with 3% CO_2 in air (enriched CO_2). Growth of cell spots was observed after 4 days. Ambient CO_2 cultures were duplicated and grown at 50 $\mu E.m^{-2}.s^{-1}$ and 20 $\mu E.m^{-2}.s^{-1}$.

2.4.4 Chlorophyll analysis

To quantify cellular chlorophyll levels, 50 µL of cells suspended in 950 µL methanol were vortexed and centrifuged at >12,000 x g for 10 min, and measurement of A $_{663\,nm}$ of the supernatant was made using an Ultrospec 3000 UV/Vis spectrophotometer (Pharmacia Biotech, USA) or a Thermo Scientific Evolution 201 UV/Vis spectrophotometer (Thermo Fisher Scientific, USA). Chlorophyll concentrations expressed in µg.mL^{-1} were calculated from A $_{663\,nm}$ as previously described (MacKinney, 1941).

2.4.5 Flow cytometry

Cell counts and light forward scattering properties (an indicator of cell size) of prepared cells from wild-type substrains were determined using an Accuri C6 flow cytometer (BD, USA). Aliquots of 10 µL of cells standardised to OD $_{730\,nm}$ 0.25 were counted using a 10 µm pore size and 10 µL.min^{-1} flow rate. A standard curve showed that the relationship between cell count and OD $_{730\,nm}$ with these instrument settings was linear between OD $_{730\,nm}$ 0.01-0.50 (r^2=0.99, data not shown).

2.4.6 Whole cell absorption spectra

Whole cell absorption spectra (A $_{400-800\,nm}$) of prepared cells standardised to OD $_{730\,nm}$ 1.0 were analysed using a ThermoScientific Evolution 201 UV/Vis spectrophotometer (Thermo Fisher Scientific, USA), using empirically determined scan settings against a reference of cell-free BG-11 medium, and data were normalized to the ~685 nm chlorophyll absorption maxima.

2.4.7 Cellular motility assay

Motility of prepared cells from wild-type substrains was assessed by spotting 50 µL of cells standardised to OD $_{730\,nm}$ 1.0 on 0.8% agar BG-11 plates supplemented with 5 mM glucose. Plates were kept in a tight-fitting black-lined box open on only one side, which was exposed to light supplied by a broad-spectrum LED array. Movement of cells was observed after 7 days.

2.4.8 Oxygen evolution

Oxygen evolution measurements in were made using a Clarke-type electrode (Hansatech, UK) maintained at 30°C. Illumination of 1 mL of prepared cells standardised to 10 µg.mL^{-1} chlorophyll was provided by an FLS1 light source (Hansatech, UK) equipped with a 580 nm

band-pass filter (Melles Griot, USA), which provides red light illumination of 5 mE.m^{-2}.s^{-1}. Oxygen evolution was supported by the artificial quinone 2,5-dimethyl-1,4-benzoquinone (DCBQ) in the presence of 1 μM $K_3Fe(CN)_6$, or by $NaHCO_3$ (15 mM) as PS II-specific and whole electron transport chain electron acceptors respectively. Measurements were made for 60 s in the dark, followed by 180 s illumination. Instrument control and oxygen concentrations were measured using custom made software (Dr SA Jackson, University of Otago). The voltage of oxygen-saturated water was calculated by equilibration with atmospheric oxygen following ~30 min electrode stabilisation, and the voltage of oxygen-free water was determined by the addition of ~mg quantities of sodium dithionite, to yield a calibration voltage (cal.volt). Rates of oxygen evolution, or total oxygen yield, were determined on a chlorophyll basis and calculated by use of the following equation:

$$\mu mol\ O_2.(mg\ chlorophyll)^{-1}.h^{-1} = slope\ (first\ 60\ sec\ illumination) * \left(\frac{0.235 * t(sec) * vol(mL)}{cal.volt(V) * ([chlorophyll](mg)} \right)$$

2.4.9 Determination of relative flash oxygen yield

Flash oxygen yield was determined using a Joliot-type electrode (Joliot and Joliot, 1968) custom-built by Dr SA Jackson and others in the laboratory of JJ Eaton-Rye (see Jackson and Eaton-Rye, 2015); generally speaking the design was analogous to that described previously (e.g. Renger and Hanssum, 2009). Briefly, cells in direct contact with a bare platinum cathode were illuminated via a quartz tube with saturating single-turnover flash light pulses provided by a 617 nm LED array (25 flashes at 4 Hz were used, flash width 4-8 μs). Measurements were made in the presence of a ~750 mV polarising current between the silver anode and the cathode, mediated by a running buffer (10 mM $CaCl_2$, 50 mM NaCl); an ion-permeable dialysis membrane physically separated the cells and the cathode from the anode, and from dilution by the running buffer. Voltage changes associated with oxygen release by the cells were measured via an analog-to-digital converter connected to a laptop with a custom-made software program, which collected measurements in V and permitted control of the instrument. Prior to measurements, 1 mL of prepared cells standardised to 10 μg.mL^{-1} chlorophyll were centrifuged at 10,000 x *g* for 30 s, the pellet was resuspended in 10 μL running buffer and 2.5 μL of the cell suspension was applied directly to the cathode (~2.5 μg chlorophyll); cells were dark adapted for 5 min prior to polarisation of the electrode, a 30 s electrode stabilisation period, and ~ 6 s measurement time.

2.4.10 Room-temperature chlorophyll fluorescence induction and decay

Cells for room-temperature chlorophyll fluorescence induction and decay measurements were grown at BRC Szeged and prepared as described. Cells were standardised to 5 μg.mL^{-1} chlorophyll and dark-adapted for 5 min prior to measurements. Measurements were made using an FL-3000 double-modulation fluorimeter (Photon Systems Instruments, Czech Republic), which is equipped with an LED array providing 639 nm actinic illumination and a weak measuring flash (8 μs, 620 nm) to determine fluorescence using parameters previously described (Deák et al., 2014). Briefly, chlorophyll fluorescence decay from PS II from a single-turnover 20 μs actinic flash was recorded by measuring flashes every 200 μs from 200 μs-15 s after the flash (logarithmic time scale). Baseline fluorescence (F_0) was determined as the average of measuring flash yields prior to the actinic flash, maximum fluorescence (F_{max}) was the value at ~1300 μs; prior measurements following the flash were discarded to exclude flash-induced measurement artefacts. Measurements were made in the presence and absence of 20 μM DCMU added in the dark adaptation period.

Chlorophyll fluorescence induction measurements (to analyse the so-called 'OJIP' transient) were made using the same apparatus, with 60s continuous red (639 nm) actinic illumination and measuring flashes on the μs scale from 0-2000 μs, the ms scale from 2000 μs-2 s, and the s scale from 2-60 s. Baseline fluorescence (F_0) was determined as the average of measuring flash yields prior to initiation of actinic light, maximum fluorescence (F_{max}) was the maximum value at ~1 s.

2.4.11 Measurement of low temperature chlorophyll fluorescence

Low temperature (77 K) chlorophyll fluorescence emission spectra measurements were made using a modified MPF-3L fluorimeter (Perkin-Elmer, USA), with 1 mL of prepared cells (standardised to 5 μg.mL^{-1} chlorophyll) assayed in glass tubes (inner diameter 4 mm, outer diameter 6 mm) in a custom-built, silver-lined liquid nitrogen Dewar (Jackson, 2012). Fluorescence was determined using 440 nm and 580 nm chlorophyll and PBS excitation wavelengths, respectively; fluorescence emission data were baseline corrected using calculations originally provided to the laboratory by Dr MF Hohmann-Marriott (Norwegian University of Science and Technology), in which approximate emissions maxima are based on Gaussian curves. Corrected data were normalised to the ~725 nm PS I emission maxima.

2.4.12 Quantification of photosynthetic thermoluminescence

Measurement of thermoluminescence was carried out using a custom-built machine (Vass et al., 1981; Ducruet and Vass, 2009) at BRC Szeged. For determination of thermoluminescence, 6 mL of cells at 5 μg.mL^{-1} chlorophyll (30 μg chlorophyll in total) were applied to a glass fibre filter by vacuum, and placed on a copper sample well connected to a N$_{2 (l)}$ tank and computer-controlled Peltier heater. After 30 s of 250 μE.m^{-2}.s^{-1} illumination at 20 °C and 3 min dark adaptation at 20 °C, the sample well was cooled to -20 °C, and a single-turnover saturating light flash was provided by a flash bulb. 100 μL of BG-11 was added to the filter disc in the dark, prior to cooling, to ensure thermal contact between the sample well and the filter, and for measurements in the presence of the Q$_B$ pocket-binding PS II inhibitor 3-3,4-dichlorophenyl)-1,1-dimethylurea (DCMU), 94 μL BG-11 and 6 μL 10 mM DCMU (pre-mixed) were applied to the filter. The sample is rapidly cooled (~100 °C.min^{-1}) to -40 °C, and a photon-counting photomultiplier tube is positioned above the sample well. Following temperature stabilisation and baseline determination, the sample is warmed to 80 °C at 20 °C.min^{-1} and photon yield for thermoluminescence is measured. A custom-made program (L Sass, BRC Szeged) designed for a MS DOS/Norton Commander computer was used for machine control and data collection.

2.4.13 Estimation of PS I oxidation state

PS I oxidation state can be determined by detection of absorbance changes induced by redox changes of the PS I RC P$_{700}$. P$_{700}$-dependent absorbance changes induced by illumination with 635 nm actinic light (~1000 μE.m^{-2}.s^{-1}) in 1 mL of prepared cells (standardised to 5 μg.mL^{-1} chlorophyll) were detected by a Dual-PAM-100 measuring system (Walz, Germany). Cells were dark-adapted for 5 min prior to measurements. P$_{700}$ oxidation was determined by absorbance change in the near-infrared (A $_{875 nm}$-A $_{830 nm}$). As P$_{700}$ is oxidised to P$_{700}^+$ immediately following illumination, the instrument signal (absorbance difference) increases, but the signal is quenched as LEF from PS II and CET from cyt b_6f reaches PS I and reduces P$_{700}^+$ (Klughammer and Schreiber, 1994). Shortly thereafter, electron flow becomes rate-limiting, and the absorbance difference approaches its maximum value again. Operation of the instrument was done by S. Kovacs; experimental design and data processing was done by the author. Data were baseline-corrected and normalised to the P$_{700}^+$ oxidation state maxima (maximum instrument signal immediately following illumination).

2.4.14 Reactive oxygen species assays

Histidine trapping assay: Estimation of singlet oxygen $^1O_2$ production by PS II was carried out at BRC Szeged using to the histidine-trapping method developed by Prof. I Vass and colleagues (see Rehman et al., 2013). The presence of 5 mM histidine (His) acts as chemical trap for $^1O_2$, with a reduction in voltage measured with a Clark-type electrode (Hansatech, UK) used to infer oxygen decline due to $^1O_2$-trapping. Relative production of $^1O_2$ during PS II oxygen evolution activity can therefore be inferred from an apparent reduction in oxygen evolution rate in the presence of 5 mM His compared to oxygen evolution rate in the absence of His. An instrument set-up very similar to that described in Section 2.4.8 was used (3 $mE.m^{-2}.s^{-1}$ broad-spectrum illumination), with custom software for data collection (L Sass), and manual instrument operation. Calibration voltage determination was as described, except that oxygen-free voltage was determined by N_2 gas bubbling. In some measurements, 1 μM DCMU was added as a PS II inhibitor, as $^1O_2$ production would be expected to be independent of overall oxygen evolving activity, and reduced oxygen yield overall should increase the ease of $^1O_2$ detection. In some measurements, 10 mM of the $^1O_2$ quencher sodium azide was added. Validation of the method by measurements of the effect of His, DCMU and NaN_3 in cell-free BG-11, in the presence and absence of 1 μM of the light-induced $^1O_2$-generator Rose Bengal, is provided in Appendix Figure A.1. It must be noted that, based on these data, 25 mM HEPES-NaOH pH 7.5-buffered BG-11 might possess a slightly enhanced capacity to trap $^1O_2$ compared to 25 mM CAPS-NaOH pH 10-buffered BG-11 (indicated by a reduced $^1O_2$ signal in cell-free media), potentially complicating the interpretation of between-pH $^1O_2$ measurements.

For measurement of $^1O_2$ production by *Synechocystis* 6803 substrains, oxygen evolution from 2 mL of prepared cells (standardised to 5 $μg.mL^{-1}$ chlorophyll) was assayed by measurement of voltage for 60 s in the dark, followed by 60 s illumination in the presence and absence of His as appropriate. A standardised respiration rate and oxygen evolution rate was determined based on the equations described in Section 2.4.8. Maximum respiration rate (determined from the slope of 20-60 s measurement) was used to correct the maximum oxygen evolution rate (from 70-110 s), and differences in the oxygen evolution rate due to His, expressed as oxygen consumption, were determined and used to indicate relative $^1O_2$ production.

Fluorescence assay: an alternative ROS assay employed the cell-permeable fluorescent probe 5-chloromethyl-2',7'-dichlorodihydrofluorescein diacetate, chloromethyl derivative (CM-

H$_2$DCFDA) (Life Technologies/Thermo Fisher, USA), which fluoresces at 520 nm due to the cleavage of acetate groups on the molecule by cellular esterases, in a manner that reflects the relative level of cellular ROS. Application of this technique in *Synechocystis* 6803 has been described previously (e.g. Havaux et al., 2005). 500 µL of cells (standardised to 10 µg.mL^{-1} chlorophyll) were prepared following a 24 h incubation experiment (Section 2.2.1.3), placed in a 24-well plate, and incubated for 30 min in standard conditions in the presence of 10 µM of the CM-H$_2$DCFDA probe. Measurements were made by extraction of duplicate 200 µL aliquots from each well, which were placed in a black CELLSTAR 96-well plate (Grenier Bio-One, Austria). Fluorescence *in vivo* was quantified using 490 nm excitation and 520 nm emission detection using a POLARstar II microplate reader (BMG LabTech, Germany).

2.5 Software and analyses

2.5.1 General software and statistical analyses

Data manipulation and curation was carried out using Microsoft Excel (Microsoft, USA), except for statistical analyses, which were performed using R - *https://www.r-project.org/foundation/* (post-2013 versions).

Construct design, routine sequence analysis and primer design was carried out using Geneious version 6 and above (Biomatters, NZ), and primer characteristics were checked using digital PCR using Amplify 3 (Bill Engels, University of Washington, USA).

Genetic regions with sequence variants, gene products and affected protein domains were checked using the following online services: Basic Local Alignment Search Tool (BLAST) – *https://blast.ncbi.nlm.nih.gov/Blast.cgi* (Altschul et al., 1990),
Constraint-based multiple Alignment Tool (COBALT) –
https://www.ncbi.nlm.nih.gov/tools/cobalt/re_cobalt.cgi,
InterPro – *http://www.ebi.ac.uk/interpro/*,
GenBank – *https://www.ncbi.nlm.nih.gov/genbank/*,
and Cyanobase – *https://genome.microbedb.jp/cyanobase/* (Fujisawa et al., 2017).

Visualisation of the PS-II crystal structure and measurements of residue distances were performed using MacPyMOL (version 1.8.6.0) - *https://www.pymol.org/* - using the PS II crystal structure data of Suga et al. (2015) (Protein Data Bank accession: 4UB6).

2.5.2 Assembly of genome sequencing data

The GT-Kazusa chromosome (Kaneko et al. 1995, 1996) and major plasmid sequences (Kaneko et al. 2003) were used as reference templates for assembly of genome data (GenBank accession: Chromosome – BA000022; pSYSA – AP004311; pSYSG – AP004312; pSYSM – AP004310, and pSYSX – AP006585).

Two approaches were used to construct genomic sequences for the GT-O1, GT-O2, Con:ΔPsbO:ΔPsbU, and Con:ΔPsbO:ΔPsbU pseudorevertant substrains, to identify SNPs and indels. Firstly, paired reads were mapped to the reference sequences using the software BWA (Li and Durbin, 2009) and variants detected using SAMtools (Li et al., 2009) by Dr PA

Stockwell (University of Otago/NZ Genomics Ltd), using the default program settings. Secondly, reads were mapped to the reference sequences using CLC Genomics Workbench (version 6.02) - *https://www.qiagenbioinformatics.com/products/clc-genomics-workbench/* in conjunction with CLC Genomics Server (version 5.02) (hereafter collectively referred to as 'CLC') - *https://www.qiagenbioinformatics.com/products/clc-genomics-server/* - by the author, using the software's default settings. In the case of the Con:ΔPsbO:ΔPsbU and Con:ΔPsbO:ΔPsbU pseudorevertant sequences, a manually altered version of BA000022, containing approximations of the relevant antibiotic resistance cassette insertions at their appropriate genome insertion site, was used as a chromosome reference.

In both cases, detected variants were manually curated by the author, based on a threshold of >70% frequency in mapped reads, >0.25 forward and reverse read balance, and quality score (>25 for CLC and >150 for SAMtools); quality thresholds between CLC and SAMtools vary as they are based on proprietary criteria. All novel variants not previously reported in the literature, and large indels known to be poorly detected by genome assembly software (e.g. known IS*Y203*-type transposase insertions), were verified by PCR and Sanger sequencing, as described in Section 2.3.3 and 2.3.5.

2.5.3 Determination of fluorescence decay kinetics

The kinetics of room-temperature chlorophyll fluorescence decay from PS II following a single-turnover flash were calculated according the equations of Vass et al. (1999), updated in Deák et al. (2014), which fits two exponential phases and one hyperbolic phase:

$$F(t) - F_0 = A_1 \exp(-t/T_1) + A_2 \exp(-t/T_2) + A_3/(1+t/T_3) + A_0$$

Where $F(t)$ represents variable fluorescence yield, F_0 is the yield before the flash, $A_{1\text{-}3}$ are percentage amplitudes, $T_{1\text{-}3}$ are the constants from which half-lifetimes can be calculated; $t_{1/2} = \ln(2)/T_n$ for the exponentials, $t_{1/2} = T$ for the hyperbolic component, and A_0 is an offset that reflects the fact that F may not return to F_0 following the flash. In this model, the first exponential ('fast') phase represents fluorescence decay due to rapid electron transfer from Q_A^- to Q_B, the second exponential ('middle') phase represents fluorescence decay due to the binding of a plastoquinone molecule to empty Q_B sites and electron transfer to the newly bound Q_B, and the hyperbolic ('slow') component represents fluorescence decay due to charge

recombination of Q_A^- with the S_2 state of the OEC. In experiments in the presence of 1 µM DCMU, forward electron transfer from Q_A^- is blocked, and fluorescence decay primarily occurs through charge recombination of Q_A^- with S_2 in the slow phase, and minor fast phase decay from $Y_Z^+(P_{680}^+)Q_A^-$ recombination (Vass et al., 1999; Fufezan et al., 2007). These decay kinetics can be modelled with one exponential and one hyperbolic phase with a similar equation to that above:

$$F(t) - F_0 = A_1 \exp(-t/T_1) + A_2/(1+t/T_2) + A_0$$

The kinetic analyses and calculations were performed using the software Origin (2017 version) - *http://www.originlab.com/.*

2.5.4 Analysis of thermoluminescence profile

A custom-made program (L Sass) was used to baseline correct and fit thermoluminescence curves and determine thermoluminescence peak temperatures (T_{max}) and peak amplitudes. This program, originally designed for Windows DOS/Norton Commander could be emulated on a modern personal computer using DOS Box (version 0.74) - *https://www.dosbox.com/* - for convenience. Peak T_{max} and amplitude are approximated manually by the user, and the program removes signal noise and runs a series of automated curve-fits. On occasion, automated curve-fitting of thermoluminescence peaks with high noise and/or low yield failed, and basic manual fits were used, or else measurements were excluded. For validation of the curve-fitting algorithm, a comparison of example baseline-corrected and raw thermoluminescence traces is provided in Appendix Fig. A.2.

Chapter Three: Wild type genomic and phenotypic analysis

3.1. Divergence in genomes of *Synechocystis* 6803 wild types

3.1.1. Genome assembly of University of Otago-based wild-type substrains of *Synechocystis* 6803

As one of the model cyanobacterium, *Synechocystis* 6803 has been distributed to multiple labs, with ensuing genetic and phenotypic divergence in 'wild-type' substrains (Ikeuchi and Tabata, 2001). Genome re-sequencing has revealed numerous genetic differences between these substrains held in laboratories around the world, with strains designated either PCC- or GT-, depending on their lineage (see Chapter One, Section 1.8). The acquisition of unique mutations in wild-type substrains is in spite of theoretically ideal growth conditions, and the possibility of resulting phenotypic differences highlights the need to know the genomic background of the parent strain when using *Synechocystis* 6803 for mutagenesis studies. In this study, the genome sequence for two glucose-tolerant laboratory wild-type strains, GT-O1 and GT-O2, in use at the University of Otago, was determined. Using high-throughput genome sequencing techniques and subsequent Sanger sequencing of detected variants, nine *de novo* mutations in the two substrains were detected, of which six are unique to GT-O2 cells.

Table 3.1. Number of SNPs and indels called in GT-O1 and GT-O2 compared to GT-Kazusa by two independent genome mapping methods.

SNPs and indel homology	Variants detected by mapping programs				
	Both programs	CLC	BWA/ SAMtools	Neither program	*Total*
Kazusa database errors	11	10	1	0	*22*
Previously reported mutations shared by GT-O1 and GT-O2	1	1	3	2[a]	*7*
Novel mutations shared by GT-O1 and GT- O2	2	1[b]	0	0	*3*
Mutations unique to GT-O1	0	0	0	1[d]	*1*
Mutations unique to GT-O2	4	2[c]	0	0	*6*
Total	*18*	*14*	*4*	*3*	*39*

[a]ISY*203j* deletion and *CRISPR2* deletion. [b, c]The indel in the plasmid pSYSA (Table 3.3, #8) and an SNP in pSYSX (Table 3.3, #9), respectively, could not confirmed by Sanger sequencing as PCR products did not amplify. [d]*slr0856* heterozygous insertion. Sequence data was obtained prior to this study, genome assembly using CLC was carried out by the author, and genome assembly using BWA/SAMtools was carried out by P Stockwell.

Table 3.2. List of SNPs, indels, database errors, and their effects on gene products in GT-O1 and GT-O2 substrains compared to the GT-Kazusa reference sequence identified by genome assembly and PCR, excluding novel variants detected in GT-O1 and GT-O2 (Table 3.3).

Mutation					Gene affected				Comment
#	*Region*	*Type*	*Nucleotide change*	*Amino acid change*	*Gene annotation*	*Gene name*	*Product*		*Comment*
Chromosome									
1	386410-386411 (386406)	Ins	102 bp insertion	34 additional AAs	***slr1084***		**Hypothetical protein**		Identified by CLC and BWA/SAMtools as SNP at loci in parentheses. Deletion is GT-Kazusa and GT-S specific* [b, c, d]
2	943495	SNP	G→A	V604I	*slr1834*	*psaA*	P$_{700}$ apoprotein subunit I		Previously observed [a, b, c, d]
3	1012958	SNP	G→T	-	IGR *ssl3177-sll1633*				Previously observed [a, b, c, d]
4	1200143-1201488 (1200309 +1201473)	Del	1.2 kb deletion	Loss *ISY203b*	***sll1780***	**ISY*203b***	**Transposase ISY*203b***		Identified by BWA/SAMtools as SNP at loci in parentheses, not found by CLC. ISY*203b* insertion is GT-Kazusa specific.* Previously observed [a, b, c, d]
5	1364187	SNP	A→G	116 Silent	*sll0838*	*pyrF*	Orotidine 5' monophosphate decarboxylase		Previously observed [a, b, c, d]
6	1819782	SNP	A→G	72 Silent	*sll1867*	*psbA3*	Photosystem II D1 protein		Not found by BWA/SAMtools [a, d]
7	1819788	SNP	A→G	70 Silent	*sll1867*	*psbA3*	Photosystem II D1 protein		Not found by BWA/SAMtools [a, d]
8	2048341-2049583 (2048409 +2049586)	Del	1.2 kb deletion	Loss *ISY203e*	***slr1635***	**ISY*203e***	**Transposase ISY*203e***		Called by BWA/SAMtools as SNP at loci in parentheses, not found by CLC. ISY*203e*

								insertion is GT-Kazusa and GT-S specific.* Previously observed [a, b, c, d]
9	2092571	SNP	A→T	L313*	*sll0422*		Asparaginase	Previously observed [a, b, c, d]
10	2198893	SNP	T→C	689 Silent	*sll0142*		Probable cation efflux system protein	Previously observed [a, b, c, d]
11	2204584	Del	G→	Frameshift	*slr0162*	*pilC/gspF*	PilC, required for twitching motility	Not found by BWA/SAMtools. Insertion GT-Kazusa specific. Previously observed [a, b, c, d]
12	2301721	SNP	A→G	K403E	*slr0168*		Hypothetical protein	Previously observed [a, b, c, d]
13	2350285-2350286	Ins	→A		IGR *sml0001-slr0363*			Not found by BWA/SAMtools [a, b, c, d]
14	2360245-2360246	Ins	→C	Frameshift	*slr0364*		Hypothetical protein	Not found by BWA/SAMtools [a, b, c, d]
15	2409244	Del	C→	Frameshift	*sll0762*		Hypothetical protein	Not found by BWA/SAMtools [a, b, c, d]
16	2419399	Del	T→	Frameshift	*sll0751 + sll0752*	*ycf +* unnamed	Hypothetical proteins	Not found by BWA/SAMtools [a, b, c, d]
17	2544044-2544045	Ins	→C	Frameshift	*ssl0787*		Hypothetical protein	Previously observed [a, b, c, d]
18	2602717	SNP	C→A	H82Q	*slr0468*		Hypothetical protein	Previously observed [a, b, c, d]
19	2602734	SNP	T→A	I88N	*slr0468*		Hypothetical protein	Previously observed [a, b, c, d]
20	2748897	SNP	C→T		IGR *slr0210-ssr0332*			Previously observed [a, b, c, d]
21	3096187	SNP	T→C	I47T	*ssr1175*	ISY*100v1*	Transposase ISY*100v1*	Not found by CLC [a, b, d]
22	3110189	SNP	G→A		IGR *slr0666-slr0665*			Not found by BWA/SAMtools [a, c, d]

	Region							
23	3110343	SNP	G→T	P73Q	*sll0665*	ISY*523r*	Transposase ISY*523r*	Previously observed [a, d]
24	3142651	SNP	A→G	75 Silent	*sll0045*	*spsA*	Sucrose phosphate synthase	Previously observed [a, b, c, d]
25	3260096	Del	C→		IGR *sll0529-sll0528*			Previously observed [a, b, c, d]
26	3400322-3401506 (3400331)	Del	1.2 kb deletion	Loss ISY*203g*	**slr1474**	**ISY*203g***	**Transposase ISY*203g***	Identified by BWA/SAMtools as 3 bp indel at loci in parentheses, not found by CLC. Insertion of ISY*203g* is GT-Kazusa specific.* Previously observed [a, b, c, d]
Plasmid pSYSA								
27	71558-71596	Ins	159 bp insertion	New CRISPR2 spacer	**CRISPR2**	**CRISPR2**	**CRISPR2**	Not found by BWA/SAMtools or CLC. Deletion of *CRISPR1* spacer is GT-Kazusa specific.* Previously observed [c]
Plasmid pSYSM								
28	117269-118451	Del	1.2 kb deletion	Loss ISY*203j*	**ssl7018-ssl7020**	**ISY*203j***	**Transposase ISY*203j***	Not found by BWA/SAMtools or CLC. ISY*203j* insertion is GT-Kazusa specific.* Previously observed [c, d]
Plasmid pSYSX								
29	82405	SNP	A→G	N37S	*ssr6089*		Hypothetical protein	Not found by BWA/SAMtools, [c, d]

Errors previously reported in the Kazusa database are shaded in grey; large indels investigated by PCR are in bold. 'Region' refers to the base position in the original GT-Kazusa sequence, accession references are: Chromosome, BA000022; pSYSM, AP004310; pSYSX, AP006585; pSYSA, AP004311; pSYSG, AP004312; pCC5.2, CP003272; pCA2.4, CP003270 and pCB2.4, CP003271. Abbreviations: Chr – chromosome; SNP – single nucleotide polymorphism; Ins – insertion; Del – deletion; IGR – intergenic region. *Was not identified, or failed quality criteria in CLC and/or BWA/SAMtools but was investigated by PCR. [a] Tajima et al. (2011) [b] Kanesaki et al. (2012) [c] Trautmann et al. (2012) [d] Ding et al. (2015). Sequence data was obtained prior to this study, but genome assembly using CLC was carried out by the author.

Table 3.3. List of novel mutations and their effects on gene products in the GT-O1 and GT-O2 substrains.

Mutation				Effect	Gene affected			Comment
#	*Location*	*Region*	*Type*	*Nucl. change*	*AA Change*	*Gene annotation*	*Gene name*	*Gene product*	*Comment*
1	Chr	489211	SNP	G→A	R642Q	*slr1609*	*fadD*	Long-chain-fatty-acid CoA ligase	GT-O2 specific
2	Chr	509098	SNP	G→A	G195E	*slr1055*	*chlH*	Magnesium protoporphyrin IX chelatase subunit H	GT-O2 specific
3	Chr	886384	Del	G→	Frameshift	*slr1204*	*htrA*	Serine protease	GT-O2 specific. Not found by BWA/ SAMtools
4	Chr	1581467	SNP	G→A	Q115L	*sll1428*		Probable sodium-dependent transporter	
5	Chr	2337531	SNP	G→A	S307F	*sll0154*	*sll0154*	Hypothetical protein	GT-O2 specific
6	Chr	2422495	SNP	G→A	R65C	*sll0750*	*hik8/sasA*	Part of two-component sensor histidine kinase	GT-O2 specific
7	Chr	2807666	SNP	C→T	A423T	*sll0550*	*flv3*	Flavoprotein	
8	pSYSA	18520-18521	Ins	→G		IGR *ssl7019-ssl7020*[b]			GT-O2 specific. Not found by BWA/ SAMtools[a]
9	pSYSX	3282	SNP	C→T		IGR *slr6001-slr6002*			Not found by CLC[a]

'Region' refers to the base position in the original GT-Kazusa sequence. Abbreviations: AA – amino acid; Chr – chromosome; SNP – single nucleotide polymorphism; Ins – insertion; Del – deletion; IGR – intergenic region. [a]Not verified by Sanger sequencing. [b]The existence of these hypothetical genes is disputed by Trautmann et al. (2012) and Sholz et al. (2013) who identified the Clustered Regularly Interspaced Short Palindrome Repeats (CRISPR)-associated-protein, CRISPR1, at this site. However, this region is the site of a large deletion in the PCC-M strain used in those studies; therefore, in the absence of PCR confirmation, the nature of this region in GT-O1/GT-O2 is unclear. Sequence data was obtained prior to this study, but genome assembly using CLC was carried out by the author.
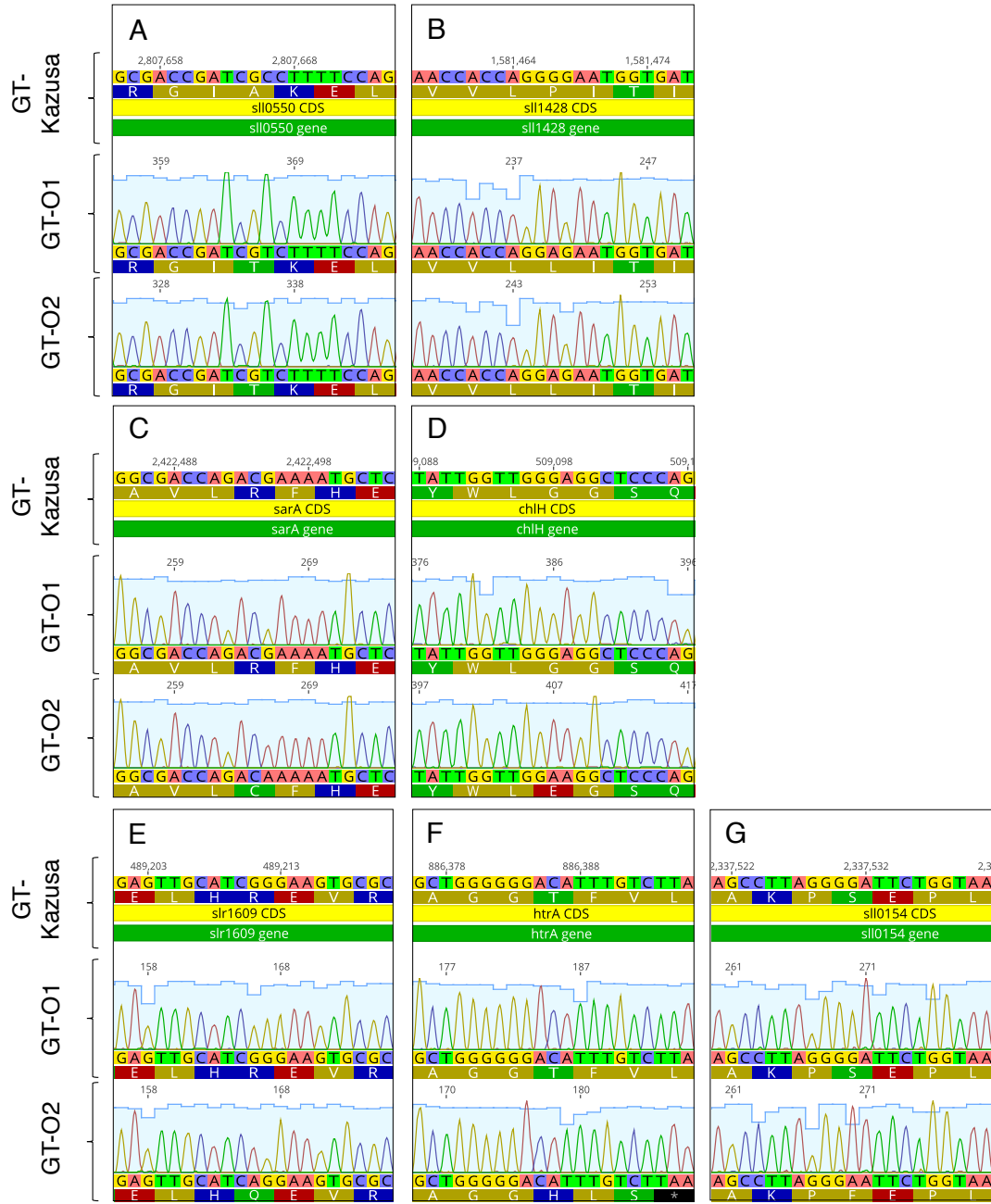
Figure 3.1. Sanger sequencing data depicting genetic mutations in the Otago-based wild-types of *Synechocystis* 6803 GT-O1 and GT-O2, compared to the GT-Kazusa reference sequence. A-B: Mutation events that occurred prior to the isolation of GT-O1; A – *sll0550* (encoding Flv3 protein), B – *sll1428* (encoding hypothetical protein Sll1428). C-D: Mutation events subsequent to the isolation of GT-O1 but prior to GT-O2; C – *sll0750/sarA* (encoding Hik8), D – *slr1055* (encoding ChlH). E-G: GT-O2-specific mutations; E – *slr1609* (encoding FadD/Aas); F – *slr1204/htrA* (encoding HtrA); G – *sll0154* (encoding hypothetical protein Sll0154).

3.1.2. Comparing the GT-O1 and GT-O2 substrain genomes to other substrains

Genomic DNA from GT-O1 and GT-O2 cells was sequenced for comparison with the database sequence from GT-Kazusa, which is used as a reference worldwide. More than 11 million short (100 bp) paired reads were obtained from genomic DNA sequencing with an Illumina HiSeq 2000 system, equating to 2700 and 2200 Mb in total for the GT-O1 and GT-O2 strains, respectively. This represents more than 500-fold coverage of the 3.9 Mb *Synechocystis* 6803 genome. Using CLC Genomics Workbench and BWA/SAMtools software, genomic sequences were constructed and putative variants detected by mapping reads to the GT-Kazusa reference sequences (Kaneko et al., 1995, 1996, 2003). A total of 38 single nucleotide polymorphisms (SNPs) and insertion/deletions (indels) were found (Table 3.1) compared with GT-Kazusa, scattered primarily throughout the 3.5 Mb *Synechocystis* 6803 chromosome (Appendix Fig. A.3). A further mutation, a heterozygous insertion in the gene *slr0856* not detected by genome sequencing, will be discussed in Section 3.2. Of the 38 mutations found, 32 were found in both the GT-O1 and GT-O2 sequences, and six are unique to GT-O2 (Fig. 3.1, Table 3.2-3.3). Of these, 29 have been reported in the literature, including 22 identified as errors of the GT-Kazusa database (Table 3.2, shaded grey) (Tajima et al., 2011; Kanesaki et al., 2012; Trautmann et al., 2012; Morris et al., 2014; Ding et al., 2015). This included two putative errors found variably in other studies. For example, the mutation found in *ssr1175* (transposase *ISY100v1*) in both GT-O1 and GT-O2 was initially reported in the GT-Kazusa and GT-S sequences by Tajima et al. (2011), suggesting that this SNP is likely to be a further error of the GT-Kazusa sequence and is common to all strains. However, in a subsequent paper from the same group, this SNP was detected only in PCC-N and PCC-P strains, but was absent from both GT-Kazusa and GT-S strains (Kanesaki et al., 2012). Trautmann et al. (2012) did not detect this SNP in the PCC-M strain, but it was present in GT-G (Ding et al., 2015). The findings of this study presented the first report of the presence of a SNP in *ssr6089* in both the GT-O1 and GT-O2 strains (Morris et al., 2014), but its subsequent identification in the substrain GT-G (Ding et al., 2015) suggests that this mutation is also an error of the original GT-Kazusa database. Other substrains are expected to possess the variation in *ssr6089* from the database sequence as well. The nature of a further reported error of the Kazusa sequence, a 600 bp deletion in *slr1753* found in the GT-Kazusa, PCC-M and GT-V sequences (Trautmann et al., 2012) was not clarified in this study, and was not detected in the genome of GT-G (Ding et al., 2015); repeated PCR attempts yielded either the predicted or 600 bp deletion band size (or both) in GT-O1 and GT-O2, with

no consistency in results (data not shown). These findings highlight the variability of variant detection tools and raise the possibility that further mutations may exist in the GT-O1 and GT-O2 strains. In particular, mapping software has been shown to incorrectly call large indels as SNPs, or (especially where these occur in regions of direct repeats) fail to detect them altogether, such as in *slr1084* (Tajima et al., 2011, Kanesaki et al., 2012, Trautmann et al., 2012).

This study investigated several large indels reported to vary between GT-Kazusa and other strains (Fig. 3.2); these were found in *slr1084*, *sll1780* (ISY*203b*), *sll1635* (ISY*203e*) and *sll1474* (ISY*203g*) (Okamoto et al., 1999; Tajima et al., 2011; Kanesaki et al., 2012; Trautmann et al., 2012). In this study, as in cases reported previously, mapping failed to detect large indels, but instead reported SNPs at the target genomic loci. An SNP was located in GT-O1 and GT-O2 sequences in *slr1084* of the chromosome that failed the mapping software's frequency and/or quality criteria. Nevertheless, because this site matched that of a previously reported 102 bp insertion in the gene *slr1084* in the GT-I, PCC-P, PCC-N (Kanesaki et al., 2012) and PCC-M strains (Trautmann et al., 2012), this region was investigated using PCR and the presence of a 102 bp indel was confirmed; this was also mistakenly called an SNP by the mapping software used by Kanesaki et al. (2012). It appears that this represents a deletion specific to the GT-Kazusa and GT-S strains (Kanesaki et al., 2012; Trautmann et al., 2012). In addition, SNPs detected by BWA/SAMtools at loci matching putative transposase insertion sites in regions of poor read coverage (suggesting a large deletion) suggested that GT-O1 and GT-O2 lack the near-identical 1.2 kb transposases *sll1780* (ISY*203b*), *sll1635* (ISY*203e*) and *sll1474* (ISY*203g*) in other GT-substrains. PCR amplification of regions flanking the *sll1635* (ISY*203e*) insertion site resulted in a 1.3 kb amplicon, rather than the 2.5 kb PCR product expected if the 1.2 kb GT-Kazusa- and GT-S-specific insertion of ISY*203e* (Tajima et al. 2011) were present in the GT-O1 and GT-O2 strains. Similarly, amplification using primers flanking the GT-Kazusa-specific *sll1780* (ISY*203b*) and *sll1474* (ISY*203g*) transposase insertion sites resulted in PCR products 1.2 kb smaller than that anticipated if these transposases were present (Tajima et al., 2011; Kanesaki et al., 2012; Trautmann et al., 2012, Ding et al., 2015).
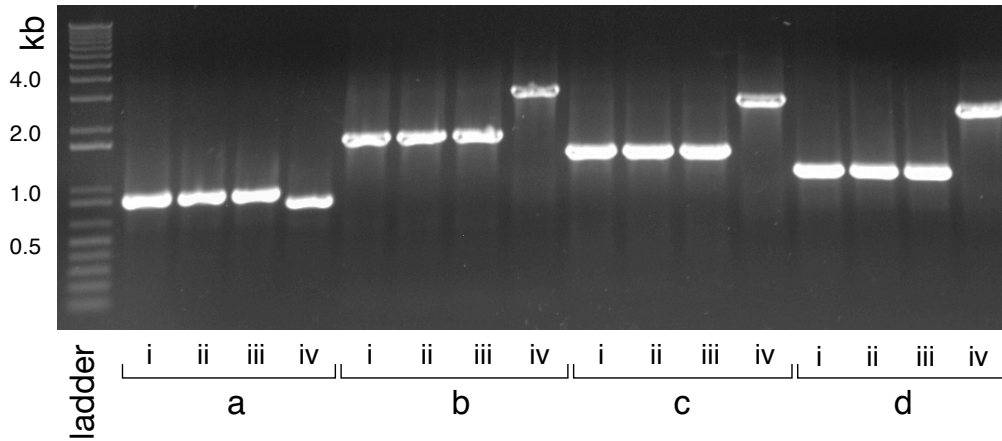
Figure 3.2. PCR amplification of large indels specific to the GT-Kazusa lineage of *Synechocystis* 6803 that were not identified during genome assembly of GT-O1 and GT-O2. Regions amplified by PCR: (a) 102 bp deletion in GT-Kazusa *slr0184*; (b-d) insertion of *ISY203b*, *ISY203g*, and *ISY203e* transposases in GT-Kazusa. GT-O1 substrain (i); GT-O2 (ii); PCC-Moscow (iii); GT-Kazusa (iv).

Indels in ISY*203j*, *CRISPR1* and *CRISPR2* were identified by Trautmann et al. (2012) as differences in the PCC-M substrain genome relative to GT-Kazusa, but were not detected by other studies (with the exception of the identified loss of ISY*203j* in GT-G) (Tajima et al., 2011; Kanesaki et al., 2012; Ding et al., 2015). PCR analysis (Fig. 3.3) of GT-O1, PCC-Moscow, and GT-Kazusa revealed that two indels in plasmids, insertion of the 1.2 kb transposase *ISY203j* into pSYSM, and a 159 bp deletion in *CRISPR2* in pSYSA, happened in the GT-lineage subsequent to the divergence of GT-O1, and might be GT-Kazusa specific. In contrast, a 2.4 kb deletion in *CRISPR1* (in pSYSA) was found to be PCC-Moscow specific. Previously, it was unclear whether these mutations were unique to specific substrains, or found throughout either the GT- or PCC- lineages. Based on this study, the large *CRISPR1* deletion in PCC-M might be specific to the PCC-lineage, whereas the *CRISPR2* mutation appears to be a GT-Kazusa insertion, rather than a PCC-Moscow deletion as previously reported (Trautmann et al., 2012). Although these data suggest that the ISY*203j* and *CRISPR2* insertions occurred in the GT-lineage subsequent to the divergence of GT-O1, whether these variations exist in the other sequenced GT substrains GT-S and GT-I is unknown (Tajima et al., 2011; Kanesaki et al., 2012). The strain GT-G appears to possess a more ancestral genetic sequence compared to the GT-O1 strain (Ding et al., 2015), and also lacks the ISY*203j* insertion. These data form the

basis of the most recently reported *Synechocystis* 6803 wild-type family tree (see Chapter Six, Fig. 6.1, and Morris et al., 2017), and highlight the advantage of using more than one computerised genome mapping method, as well as complementing genome mapping with PCR amplification of indels found by other researchers, if it is suspected these may also be in the target substrain. Additionally, the fact that the PCC- and GT-lineages of *Synechocystis* 6803 differ in *CRISPR1* and, in the case of GT-Kazusa, *CRISPR2* as well, may have implications for the use of CRISPR-Cas technology in genetic modification of this species (see Scholz et al., 2013; Yao et al., 2016).
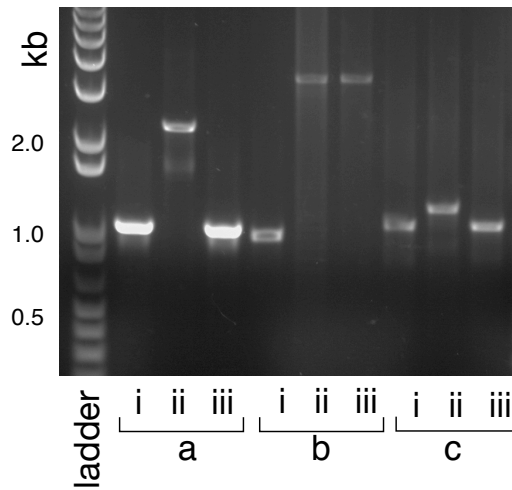
Figure 3.3. PCR amplification of other indels in *Synechocystis* 6803 wild-type substrains reveals the GT-Kazusa specific 1.3 kb insertion of *ISY203* (a), the PCC-Moscow specific 2.4 kb deletion in *CRISPR1* (b), and the Moscow substrain (i); GT-Kazu

3.1.3. Novel mutations in GT-O1 and GT-O2

Nine novel variants in the GT-O1 and GT-O2 strains, of which six are unique to the latter, were identified, and seven of these variants were verified using Sanger sequencing of PCR amplicons (Table 3.3; Fig. 3.1). No false-positive variants were found. Two variants located in the plasmids pSYSA and pSYSX, could not be verified by Sanger sequencing due to poor PCR amplification despite multiple PCR using different primer pairs (data not shown).

Of the nine GT-O1 and GT-O2 mutations identified, seven are SNPs, two are indels, and seven of these mutations are in open reading frames (ORFs) (Table 3.3). Surprisingly, all of the ORF mutations cause an amino acid change or frame-shift in the gene product; in both strains, two common mutations were located affecting ORFs, an Ala423Thr change in the Sll0550 hypothetical protein at the start of a coding region for a predicted flavin mononucleotide-binding site, and a mutation causing a Gln115Leu amino acid change in a predicted membrane-spanning region of the probable sodium-ion-transporter Sll1428. In the GT-O2 strain, gene mutations result in an Arg642Gln substitution in Slr1609 (FadD, long-chain-fatty-acid CoA ligase); a G195E residue change in Slr1055 (ChlH, magnesium-protoporphyrin IX chelatase subunit H); a deletion in in *slr1204* (causing a frame-shift mutation in the serine protease protein HtrA); a Ser307Phe change in Sll0154 (CruE); GT-O2 also displays an Arg65Cys mutation in a predicted Kai-B-interacting domain of the two-component sensor Sll0750 (Hik8/SasA). A further GT-O2 variant in the plasmid pSYSA, which could not be confirmed by Sanger sequencing, occurred in a region encoding a Clustered Regularly Interspaced Short Palindrome Repeats-associated-protein 1 (CRISPR1), (Trautmann et al., 2012; Scholz et al., 2013). This region was also the site of a 2399 bp deletion in the PCC-M strain (see Section 3.1.2) (Trautmann et al. 2012), and as such may be an active site for genomic mutations. In particular, the gene encoding Slr1609 appears to be particularly mutable – the YF, PCC-M, GT-O2, GT-W, and GT-P strains all carry unique mutations in *slr1609* (Aoki et al., 2012; Trautmann et al., 2012; Tichý et al., 2016), whose gene product functions in the reuse of fatty acids released after the action of lipases, but whose deletion did not result in any reported growth or photosynthetic deficiencies (Kaczmarzyk and Fulda, 2010; Tichý et al., 2016).

3.1.4. Resequencing in other University of Otago *Synechocystis* 6803 strains

Assembly of genome sequencing data using CLC Genomics software was also carried out for four other *Synechocystis* 6803 substrains carrying deliberate mutations. The strains were a

ΔPsbMΔPsb27 strain; a PsbB H469Q pseudorevertant strain, a Con:ΔPsbO:ΔPsbU strain; and an associated Con:ΔPsbO:ΔPsbU pseudorevertant strain. The genome assembly of the Con:ΔPsbO:ΔPsbU and Con:ΔPsbO:ΔPsbU pseudorevertant strains is discussed in detail in Chapter Four. Genome assembly methodology for all four strains was identical to that used for GT-O1 and GT-O2, but as the ΔPsbM:ΔPsb27 and PsbB H469Q pseudorevertant strains were not otherwise investigated in this study, technical details, e.g. read count, database errors, etc., are omitted here. Based only on the presence and absence of mutations identified during genome assembly, it was possible to construct a simple family tree of Otago-lab-based strains whose genomes were either assembled using CLC Genomics (Fig 3.4, black boxes), or which were otherwise used in this study, and whose position on the family tree was clarified by sequencing candidate mutations as required (Fig 3.4, no boxes; Sanger sequencing data to confirm mutations is not shown except for Con:ΔPsbO:ΔPsbU and ΔPsbO:ΔPsbU pseudorevertant, shown in Chapter Four). The data obtained reveal that ΔPsbM:ΔPsb27 was obtained from a GT-O1-GT-O2 intermediate strain (the *slr1055* and *sll0750* mutations were present in ΔPsbM:ΔPsb27), and that the Control and PsbB mutant strains used in this study derive from a wild-type strain predating GT-O1 (they lack the *sll1428* SNP), here dubbed GT-Vermaas (from Professor WFJ Vermaas, University of Arizona, whose lab was the proximal source of Otago-based *Synechocystis* 6803 strains). The *sll0550* mutation was ubiquitous – this SNP may be diagnostic for GT-Vermaas derived strains, in contrast to those derived from GT-Williams.
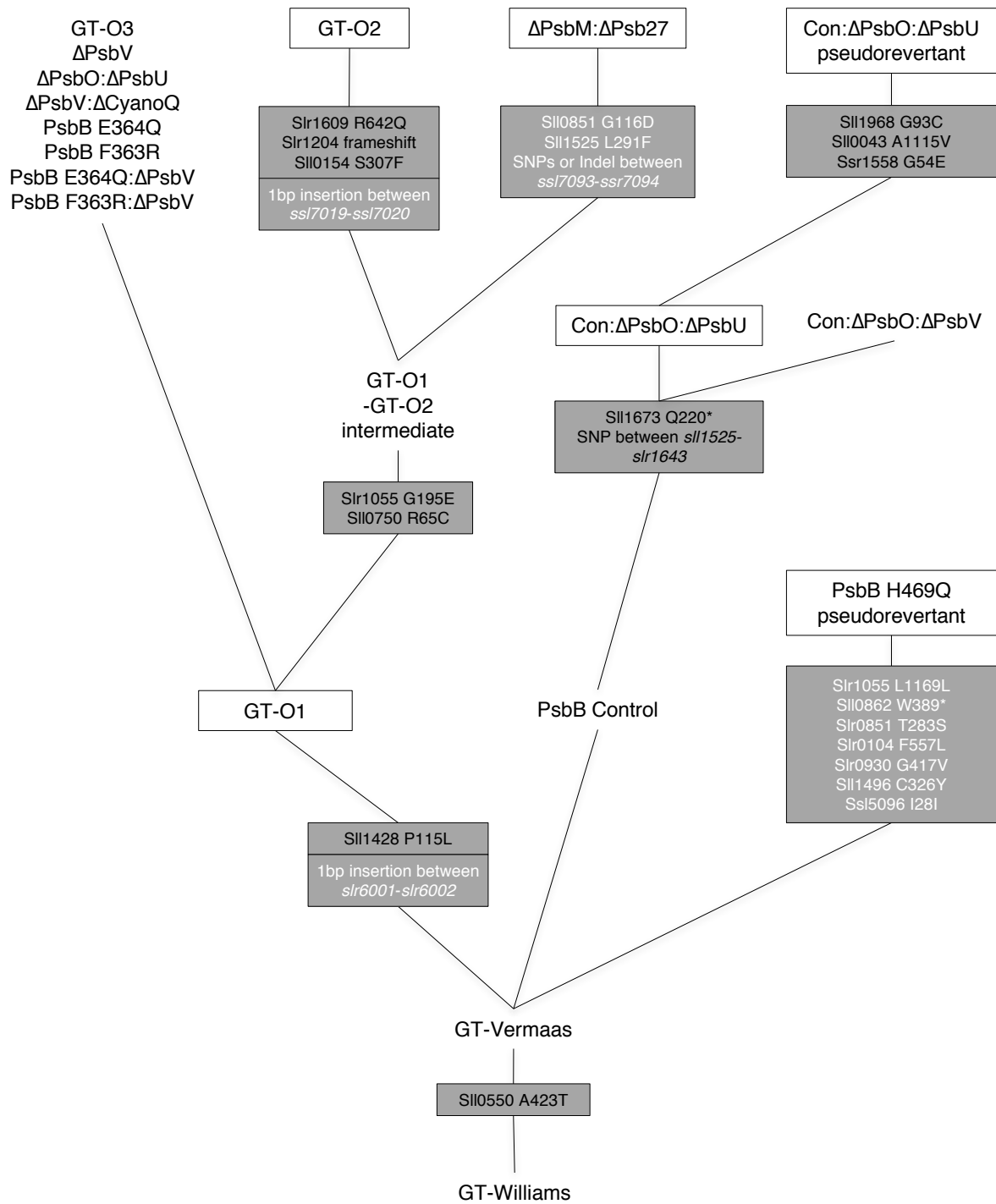
Figure 3.4. Graphical representation of the divergence of some *Synechocystis* 6803 substrains in use at the University of Otago. Sequenced substrains (white boxes) underwent whole-genome resequencing during this study and are located on branches with respect to their unique mutations (shaded boxes) that cause amino acid substitutions in encoded proteins or changes in inter-genetic regions of the *Synechocystis* 6803 chromosome. Other strains used in this study, or ancestral strains, are also depicted (no box). Black text: mutations confirmed via Sanger sequencing; white text: mutations identified using genome assembly but not

independently verified. The position of the Control strain, along with any strains whose genetic background was unclear in lab records (e.g. ΔPsbV:ΔCyanoQ) was confirmed via Sanger sequencing (data not shown). The mutation affecting Sll0550 happened prior to isolation of all known Otago strains, but its position prior to the isolation of the GT-Vermaas substrain (for Prof. WFJ Vermaas) is speculative.

3.1.5. Origin and phenotype of GT-O2

In routine culturing of *Synechocystis* 6803 on BG-11 agar, re-streaks every fortnight or so are recommended, along with the maintenance of freezer stocks; from these, new culture lines should be obtained every few months, and older working cultures discarded (Eaton-Rye, 2011). The GT-O2 substrain appears to have arisen from an excessively long period of continuous culturing (>6 months) of GT-O1 cells on photoheterotrophic BG-11 agar with insufficiently regular re-streaks (JJ Eaton-Rye and JA Daniels, *pers. comm.*). An intermediate GT-O1 and GT-O2 strain was used as a mutation background for the ΔPsbMΔPsb27 strain (Fig. 3.4); an unexpectedly severe growth phenotype associated with this strain (JJ Eaton-Rye & colleagues, unpublished data), along with a GT-O2:ΔYcf48 strain, prompted the decision to resequence ΔPsbMΔPsb27 and GT-O2.

The phenotype of the GT-O2 substrain has been discussed in other studies (Crawford, 2015; Crawford et al., 2016). Briefly, the mutation in *slr1055*, which causes a Gly195 to Glu substitution in a catalytic subunit of ChlH (magnesium protoporphyrin IX chelatase), appears to affect this enzyme's role in the first committed step of chlorophyll *a* (hereafter chlorophyll) biosynthesis (Jensen et al., 1996). In GT-O2, and in a non-photoautotrophic ChlH G195E:ΔYcf48, strain the production of chlorophyll is inhibited, and subsequent assembly and function of PS II is impaired, although a ChlH G195G:ΔYcf48 strain is photoautotrophic (Crawford et al., 2016). The Gly65 to Cys mutation in Hik8 is also likely to have an effect on growth of the GT-O2 substrain; preliminary data suggests that GT-O2 cells are impaired in short-day photomixotrophic growth (K Hanning and TC Summerfield, unpublished data), similar to a ΔHik8 mutant (Singh and Sherman, 2005). Prior to these studies, the growth rate of GT-O2 cells was compared to that of GT-O1 cells as part of this work; the photoautotrophic growth and photomixotrophic growth of GT-O2 cells was consistently reduced compared to in GT-O1 cells (Fig. 3.5), although the initial growth rate of the GT-O2 substrain in

photomixotrophic conditions is slightly higher. Mean doubling times ($\pm$ SEM, $n = 3\text{-}5$) of GT-O1 and GT-O2 substrains in photoautotrophic conditions (11.33 ± 0.92 h and 15.41 ± 0.82 h respectively) were significantly different ($P = <0.05$), but did not vary significantly in photomixotrophic conditions (10.18 ± 0.50 h and 9.64 ± 0.49 h respectively) ($P = >0.05$) (Table 3.4).
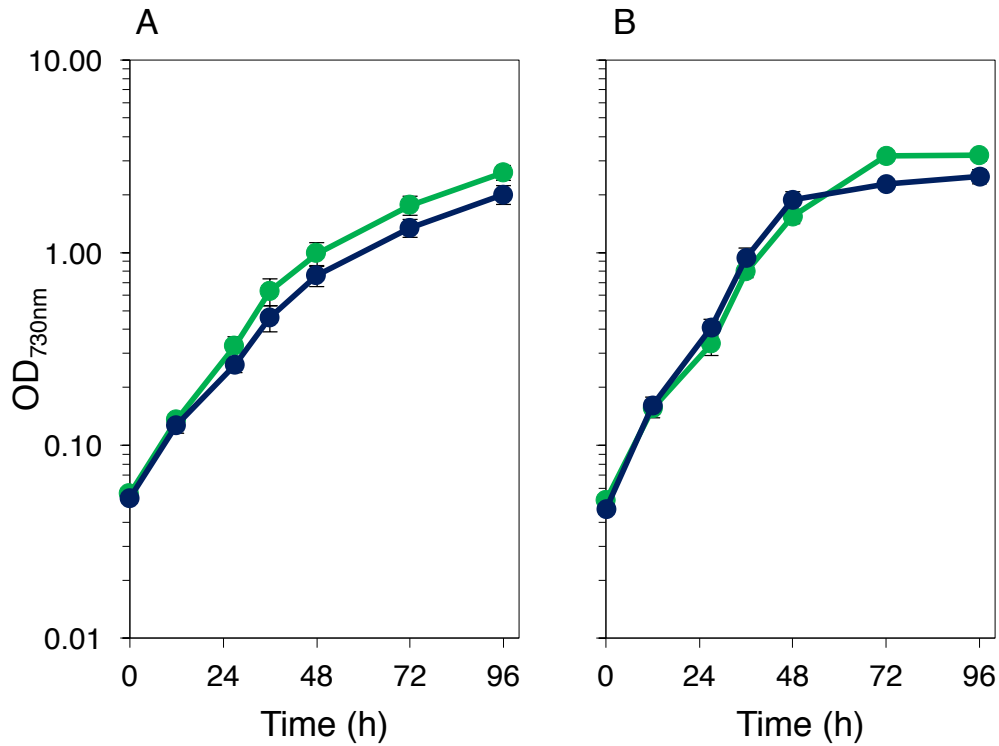
Figure 3.5. Growth of Otago-based *Synechocystis* 6803 wild types. A: photoautotrophic growth ($n = 7$ independent biological replicates), and B: photomixotrophic growth ($n = 5$ independent biological replicates), of the substrains GT-O1 (green) and GT-O2 (blue). Error bars ($\pm$ SEM) not visible are smaller than the symbols.

3.2. Observing the acquisition of a novel mutation in GT-O1

Divergence in the genomes of *Synechocystis* 6803 wild-types appears to be an active process in spite of theoretically ideal growth conditions. This study was able to trace the emergence and subsequent disappearance of a novel mutation that was not identified during genome assembly. Routine screening of a ΔPsbC mutant of *Synechocystis* 6803 by a colleague revealed the presence of an indel in the gene *slr0856* (LE Nicol, 2014, unpublished data), located upstream of *psbC*, and further investigation revealed that this mutation was present in the putative GT-O1 background strain. The homozygous 'A' insertion in this substrain (Fig. 3.6) causes a frameshift in Slr0856 that extends its ORF, creating a hybrid ORF with the 3' end of the downstream *slr0857* gene. Analysis of other wild-type strains showed that the '2014' GT-O1 strain used as the ΔPsbC genomic background was the only substrain available possessing this homozygous insertion. Screening of *slr0856* from genomic DNA isolated from the PCC-M, GT-Kazusa, and GT-O2 cells, and from the oldest available stocks of Otago wild-type genomic DNA (two samples, isolated in 1992 by JJ Eaton-Rye and in the mid-late 1990s by JA Daniels) lack this insertion, and display the split ORFs encoding a separate Slr0856 and Slr0857. However, in Sanger sequencing of *slr0856* 'double peaks' observed in the electropherogram subsequent to the putative insertion site revealed that the GT-O1 cells used in genome sequencing and throughout this study are heterozygous for the insertion; *Synechocystis* 6803 carries ~10 copies of the chromosome per cell. The source of the homozygous LE Nicol GT-O1 substrain was presumably this heterozygous substrain. Subsequently, in order to investigate whether lab culture conditions might have selected for the complete segregation of this mutation, the heterozygous GT-O1 strain was subjected to continuous culturing over an extended period of time (~1 year) with re-streaks haphazardly every 1-4 weeks on BG-11 agar in photoheterotrophic conditions (similar to the predicted conditions that gave rise to the GT-O2 strain). In GT-O1 cells after 5, 10 and 15 re-streaks on BG-11 agar, the heterozygous *slr0856* gene remained, although by 25 re-streaks the gene became homozygous for the 'normal' (i.e. database sequence) *slr0856*, the opposite to what occurred in the LE Nicol substrain. The GT-O1 strain grown over 25-restreaks is hereafter referred to as GT-O3.

Synechocystis 6803 is notable for having a very large number of transposase genes encoded in its genome, with at least 134, compared to only 32 in the very closely related *Synechocystis* 6714 (Kopf et al., 2014a). The *slr0856* and *slr0857* genes (495 and 379 bp respectively)

together represent one of 21 members of a large family of ISY*100*-type transposases in *Synechocystis* 6803. Around half the members of this family, including *slr0856/slr0857*, have two short ORFs due to a region of 9 consecutive adenine residues, rather than the stretch of 10 seen in single-ORF ISY*100*s in this species. The frameshifted gene copy in the LA Nicol GT-O1 strain possesses this distinctive 10-A sequence and forms a single ORF with >97% similarity to the ten ISY*100*-type transposases in *Synechocystis* 6803 encoded by a single 949 bp ORF. ISY*100* belongs to the IS*630* family of transposable elements with elements similar to the eukaryotic Tc*1*/*mariner* superfamily; in *Synechocystis* 6803 ISY*100* transposase expression, and the formation of linear Tc*1* and Tc*3* molecules allows DNA transposition to new genetic sites in a 'cut and paste' system that recognises TA target sequences (Urasaki et al., 2002). The single-ORF *Synechocystis* 6803 ISY*100* is transposable in *E. coli* in the absence of any host factors (Urasaki et al., 2002), is likely to be mobile in the *Synechocystis* 6803 genome, and has been described as being "highly active" both *in vitro* and *in vivo* (Cassier-Chauvat et al., 1997; Feng and Colloms, 2007).

Whether the LE Nicol GT-O1 substrain *slr0856* represents an additional functional (i.e. complete) transposase in this substrain is unclear; since the two-ORF type might be functional anyway (Urasaki et al., 2002). Non-canonical gene transcription/translation ('recoding') of transposable elements of prokaryotic genomes, involving 'programmed ribosomal frameshifting,' or 'programmed transcriptional realignment,' is common, although which of these recoding mechanisms (if any) might allow transposase expression in two-ORF transposases in bacteria is unknown (Siguier et al., 2014). Such translational frameshifting in the 9-A sequence might render both types of ISY*100* functional (Urasaki et al., 2002); this would imply no phenotypic outcome of the LE Nicol GT-O1 strain mutation. Alternative theories as to the function of insertion sequences such as ISY*100* in bacterial genomes also makes it difficult to speculate about the relevance of this mutation; the ability of transposases to rearrange genomes and increase variation is likely to allow adaptation to new or stressful environments; on the other hand, transposition might actually be associated with a loss of stress (such as in the transition from free-living to endosymbiont growth strategies), where it acts to remove now-unnecessary genes and 'streamline' genome size (Siguier et al., 2014); the role of transposable DNA elements in natural selection has always been somewhat enigmatic (see Doolittle and Sapienza, 1980; Darmon and Leach, 2014; Vandecraen et al., 2017). It is certainly difficult to conclude that the divergence observed in the heterozygous GT-O1 substrain *slr0856* to 10-A on the one hand (LE Nicol culture) and 9-A on the other (in GT-O3 cells) represents

the result of any strong selection pressure, since both cultures were grown under the same conditions (despite presumable handling differences between researchers). Nevertheless, the fact both substrains eventually became homozygous does tempt us to speculate that the cultures experienced some unknown selection pressure towards (or away from) transposase activity. One thing is clear: based on this observation, and the frequency of transposase insertions in the GT-Kazusa substrain (see Section 3.1.2), the mechanisms of DNA transposition are active in *Synechocystis* 6803 wild types in laboratory conditions. Such activity reduces genetic stability and promotes phenotypic diversity in cyanobacteria (Lin et al., 2011); the loss of the photoreceptor encoded by *hik32* in the GT-Kazusa substrain (due to ISY*203g* interruption of *hik32*) is a good example of this phenomenon. It is frustrating, then, that accurate genome sequencing around sites of transposase insertion/deletion in *Synechocystis* 6803 wild-types through the genome resequencing techniques described in this study appears to be problematic, and any new transposase activity in the LE Nicol GT-O1 substrain might be hard to detect.
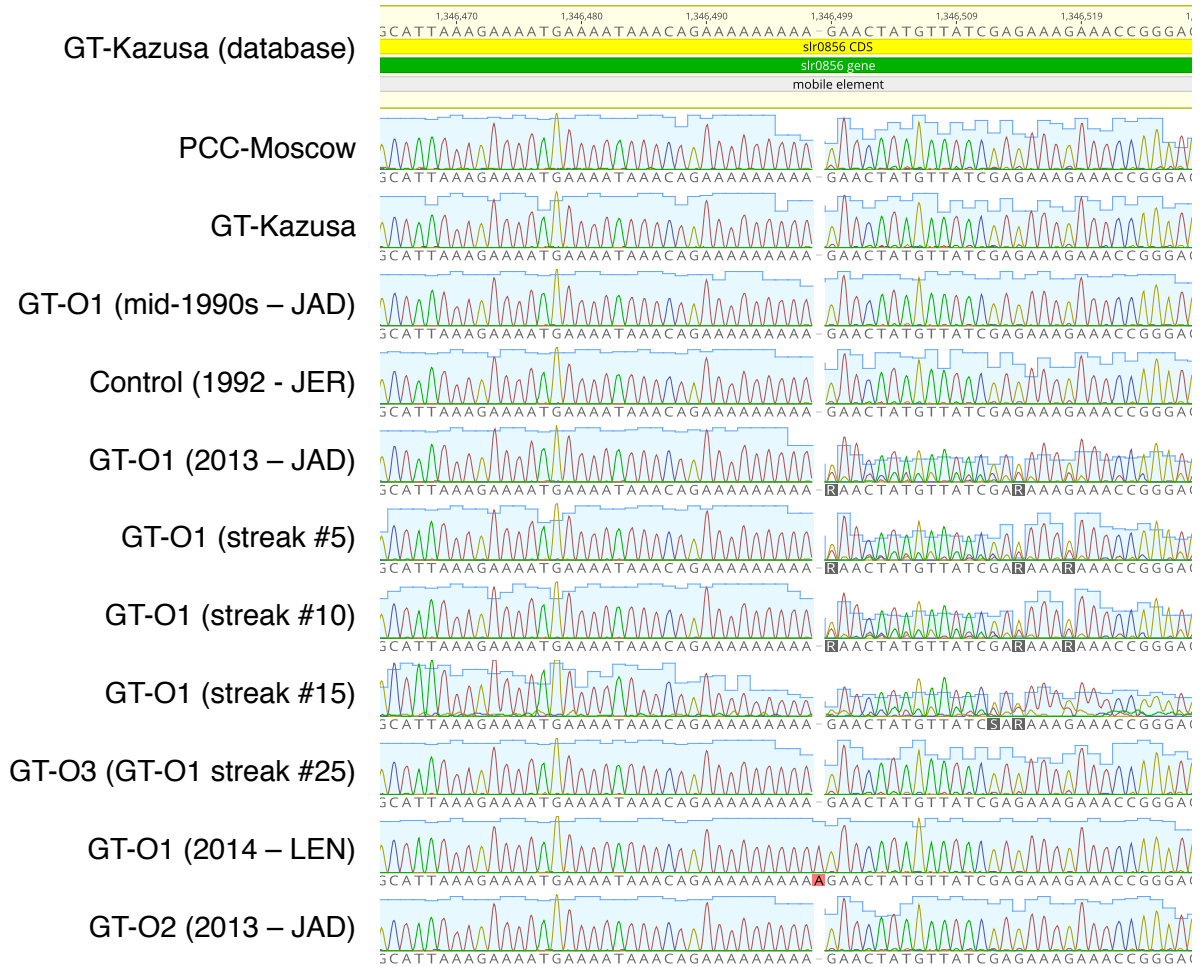
Figure 3.6. Sanger sequencing data from the gene *slr0856* (encoding a putative transposase) in strains of *Synechocystis* 6803. Whereas *slr0856* from the PCC-Moscow strain, the GT-Kazusa strain, a mid-1990s GT-O1 strain, the Control strain, and the GT-O2 strain is identical to the database sequence, the GT-O1 strain used in this study ('GT-O1 2013-JAD') displays a heterozygous inserted 'A' at chromosome position 1,346,498, which appears as double-peaks in the electropherogram. This heterozygous insertion persisted during 15 re-streaks of this strain on photoheterotrophic BG-11 petri dishes over 7 months. After 25 re-streaks (~1 year in culture), however, the mutation disappeared in the strain since dubbed GT-O3. In contrast, a GT-O1 strain held by LE Nicol ('2014 – LEN'; also derived from 'GT-O1 2013-JAD') was homozygous for the insertion. Letters refer to the researcher who held the strain and/or isolated its DNA: JAD – JA Daniels; JER – JJ Eaton-Rye; LEN – LE Nicol. Strains not attributed to a researcher were obtained and/or had their genomic DNA isolated during in this study.

3.3. Phenotypic variation in wild-type substrains of *Synechocystis* 6803

3.3.1. General differences between substrains

Although major differences between substrains (e.g. the lack of motility in GT-substrains, and the positive and negative phototaxis of PCC-P and PCC-N substrains, respectively) are well known (Yoshihara et al., 2000; Kamei et al., 2001), less obvious phenotypic variation between substrains, including photosynthetic rates and morphology, has not been documented. Interestingly, each branch of the *Synechocystis* 6803 family tree is associated with 2-8 unique genetic variations, almost all of which encode amino acid changes in the respective proteins, raising the possibility of functional change, phenotypic variation and genetic adaptation. For example, environmental stress tolerance in the PCC-M substrain might be affected by mutations in *sigF* and *slr0534_as3* (a *hik10* antisense RNA) (Trautmann et al., 2012). Loss of genetic competence in GT-Kazusa cells likely arises from an insertion in *pilC* (Bhaya et al., 2000; Yoshihara et al., 2001), but changes associated with several large ISY*203*-type transposase insertions are unclear. This study therefore investigated phenotypic variation between two wild-type substrains of *Synechocystis* 6803, the PCC-Moscow and GT-Kazusa substrains, and the Otago substrain GT-O1, grown in routine laboratory conditions.
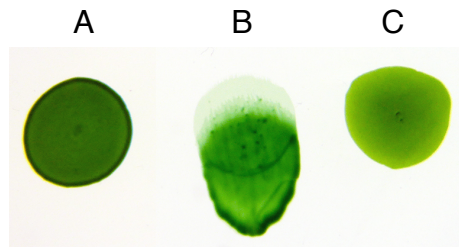
Figure 3.7. Motility of *Synechocystis* 6803 wild-type substrains. Cells from the substrains GT-O1 (A), PCC-Moscow (B), and GT-Kazusa (C) were applied to 0.8% agar and exposed to a directional light source (from below the field of view) over seven days; PCC-Moscow cells

3.3.2. Variation in growth and cell size of PCC-Moscow, GT-Kazusa, and GT-O1 wild types

The original isolate of *Synechocystis* 6803 was described as motile, and possesses type-IV pili that facilitate motility (Stanier et al., 1971; Rippka et al., 1979; Ikeuchi and Tabata, 2001; Kamei et al., 2001). However, the GT-lineage is non-motile, due to a mutation in SpkA (Kamei et al., 2001). Therefore, unsurprisingly, wild-type substrains from the GT-lineage analysed in this study were non-motile, in contrast to PCC-Moscow (Fig. 3.7).

The simplest way to compare substrains of *Synechocystis* 6803 is through measurement of photoautotrophic growth rate, since this theoretically represents the net result of any changes with respect to photosynthetic rate, genome, and gene regulation. Photoautotrophic growth rate (measured by OD $_{730nm}$) of wild-type substrains was very similar (Fig. 3.8). Mean doubling times (± SEM, n = 4-5) of GT-O1, PCC-Moscow and GT-Kazusa cells in photoautotrophic conditions (11.33 ± 0.92 h, 11.00 ± 1.39 h, and 11.15 ± 0.72 h respectively) did not vary significantly (P = >0.05) (Table 3.4). However, the observed similarity in growth rate and doubling is in spite of striking differences in cell size and cell density between strains. Transmission electron microscopy (TEM) analysis showed that mean GT-O1 cell size (1385 ± 30 nm) was ~80-90% of the mean cell size of PCC Moscow (1555 ± 42 nm) and GT-Kazusa (1769 ± 37.41 nm) cells respectively; cell sizes between all strains were significantly different (P = <0.001) (Fig. 3.9; Table 3.4). Cells from the GT-O2 substrain were similar in terms of size to GT-O1 cells (data not shown). No significant variation in total chlorophyll on an OD $_{730nm}$ basis was detected between substrains (Fig 3.10A, solid bars; Table 3.4), although GT-O2 cells showed reduced chlorophyll, as reported previously (data not shown) (Crawford et al., 2016). Accordingly, given the similarity in apparent growth rate and discrepancy in cell size, there was a significant difference in cell density (P=<0.001) between GT-O1, PCC-Moscow and GT-Kazusa substrains measured using flow cytometry (Fig. 3.10A, empty bars; Table 3.4). There was no significant variation in cell density between PCC-Moscow and GT-Kazusa substrains, whereas the cell density in GT-O1 cultures was significantly different compared to both PCC-Moscow (37% the number of cells mL^{-1} OD $_{730\ nm}$$^{-1}$ compared to GT-O1) and GT-Kazusa (49% compared to GT-O1) cultures, in a Tukey's HSD test (P = <0.01). GT-O2 cultures had similar cell density to GT-O1 cultures (data not shown). There appears to be some discrepancy between cell size and cell count in respect of the magnitude of GT-O1 variation,

and differences between PCC-Moscow and GT-Kazusa substrains; this might reflect that stationary phase cells were measured for TEM rather than log-phase grown cells for flow cytometer analysis, or the several orders-of-magnitude lower number of cells analysed by TEM compared to flow cytometry. Forward scatter (Fig 3.10B), a proxy for cell size also measured by flow cytometry, also indicated a significantly smaller GT-O1 cell size; while PCC-Moscow and GT-Kazusa cell sizes did not vary significantly, both were significantly greater than size of GT-O1 cells ($P = <0.01$; Tukey's HSD). Thus, two lines of evidence support the general observation that GT-O1 cells are smaller, although the detection of significant differences between PCC-Moscow and GT-Kazusa cells varied between measuring technique.
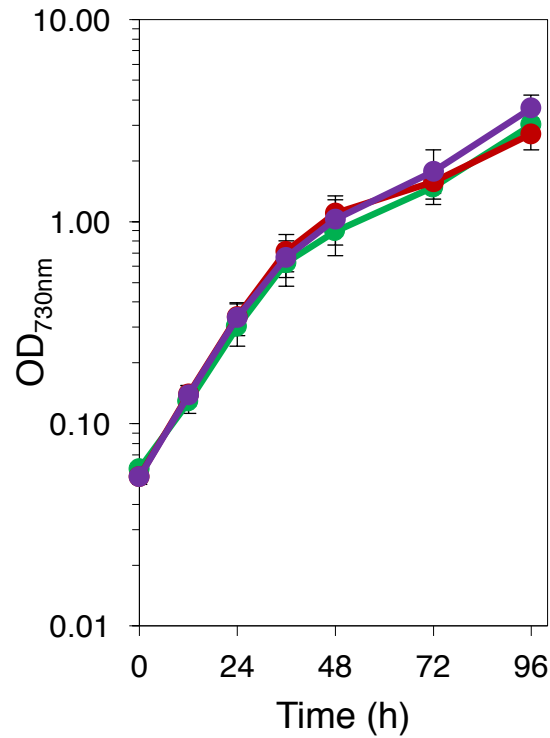
Figure 3.8. Photoautotrophic growth of *Synechocystis* 6803 wild-type substrains GT-O1 (green), compared to the PCC-Moscow strain (red), and GT-Kazusa strain (purple) (*n* = 7). Error bars (± SEM) not visible are smaller than the symbols.
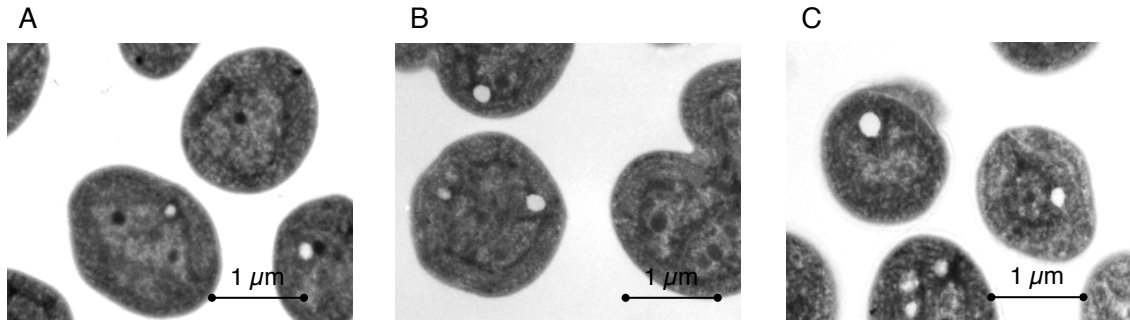
A   B   C

Variable	df	Mean square	*F*-value	*P*-value
Chlorophyll *a* concentration	2	0.65	2.327	0.126
Cell density	2	2.804×10^{16}	15.68	<0.001 ***
Forward scatter	2	2.372×10^{11}	11.54	0.0016 **
Cell size	2	6.46×10^{5}	25.44	<0.001 ***
Doubling time	2	0.1	0.026	0.974
Oxygen evolution rate	2	4000	1.747	0.224
GT-O1/GT-O2 photoautotrophic doubling time	1	31.2	9.007	0.024 *
GT-O1/GT-O2 photomixotrophic doubling time	1	0.7	0.611	0.457

3.3.3. Other phenotypic variation between PCC-Moscow, GT-Kazusa, and GT-O1 wild types

Photosynthetic oxygen evolution as a measure of PS II activity was assessed between substrains using a Clark-type electrode, with HCO_3^- as an artificial electron acceptor. In contrast to PS II-specific artificial electron acceptors such as DCBQ, HCO_3^- theoretically acts as an acceptor downstream of PS I; therefore, oxygen yield in this case represents the net result of the entire photosynthetic electron transport chain. In cultures of GT-O1, PCC-Moscow, and GT-Kazusa, oxygen yield was similar when normalised to chlorophyll concentration (Fig. 3.10C). One representative measurement is displayed; oxygen evolution rate (GT-O1 279 ± 24.3, PCC-Moscow 261 ± 22.9, GT-Kazusa 322 ± 19.9 µmol O_2.(mg chlorophyll)$^{-1}$.h^{-1}, mean $\pm$ SEM, $n = 4$-5) did not vary significantly ($P = >0.05$) between substrains.

Measurement of whole-cell absorption spectra in *Synechocystis* 6803 reveals the characteristic dual-absorption peaks associated with chlorophyll (~440 nm and ~685 nm), as well as absorbance peaks of carotenoids (~500 nm, visible as a shoulder on the 440 nm chlorophyll absorbance maxima) and the accessory light-harvesting phycobilin pigments (~620 nm). Variation in whole cell absorption spectra was observed between GT-O1, PCC-Moscow and GT-Kazusa cells when traces were normalised to chlorophyll absorption at 685 nm (Fig. 3.10D). The GT-O1 substrain showed elevated carotenoid pigments by around 15% relative to other substrains, and the PCC-Moscow substrain showed somewhat reduced phycobilin pigments.

Underlying measurements of photosynthetic oxygen evolution is an assumption that because the majority of chlorophyll is associated with PS I, and PS II:PS I ratios between cultures assayed are similar, oxygen yield between cultures reflects the average PS II centre in the respective culture. However, variation in PS II:PS I ratios would undermine this assumption. Low temperature fluorescence allows precise measurement of this ratio by determination of fluorescence maxima when chlorophyll is specifically excited at a 440 nm wavelength. The 685 nm and 695 nm peaks are associated with PS II, whereas the 725 nm peak is associated with PS I (Murata and Satoh, 1986). No major differences in fluorescence emission were observed between wild-type strains (Fig. 3.10E), suggesting that photosystem stoichiometry was similar. Additionally, the relative contribution of the PS II 685 nm and 695 nm emission

peaks (associated particularly with CP43 and CP47 respectively, Eaton-Rye and Vermaas 1991) to overall fluorescence yield did not vary between strains, indicating that PS II assembly was similar; a relative loss of one peak might indicate reduced expression or assembly of a particular PS II component (Eaton-Rye and Vermaas, 1991; Emlyn-Jones et al., 1999; Joshua and Mullineaux, 2005).

Low temperature fluorescence can also be used to determine the extent of PBS pigment coupling to PS II and PS I, by excitation of PBS at 580 nm. In these conditions, fluorescence emission peaks arise from C-phycocyanin and allophycocyanin (650 and 667 nm, respectively), the PBS terminal emitter ApcE associated with PS II (at ~685 nm), and PBS bound to PS I (~725 nm); emission can arise from PBS completely coupled to PS II and PS I, but also uncoupled PBS (Fork and Mohanty, 1986; Shen et al., 1993; Emlyn-Jones et al., 1999). In *Synechocystis* 6803 wild types, the relative fluorescence of the 685 nm ApcE peak was similar between substrains (Fig. 3.10F), whereas, fluorescence peaks associated with C-phycocyanin and allophycocyanin were reduced by around 30% in the PCC-Moscow substrain compared to GT-Kazusa and GT-O1. This might be a result of the slight reduction in total phycobilins observed in whole-cell absorption spectra (Fig. 3.10D). Alternatively, this result might arise from altered coupling of PBS pigments, whereby energy transfer from the antenna complex to PS II is more efficient in the PCC-Moscow substrain.
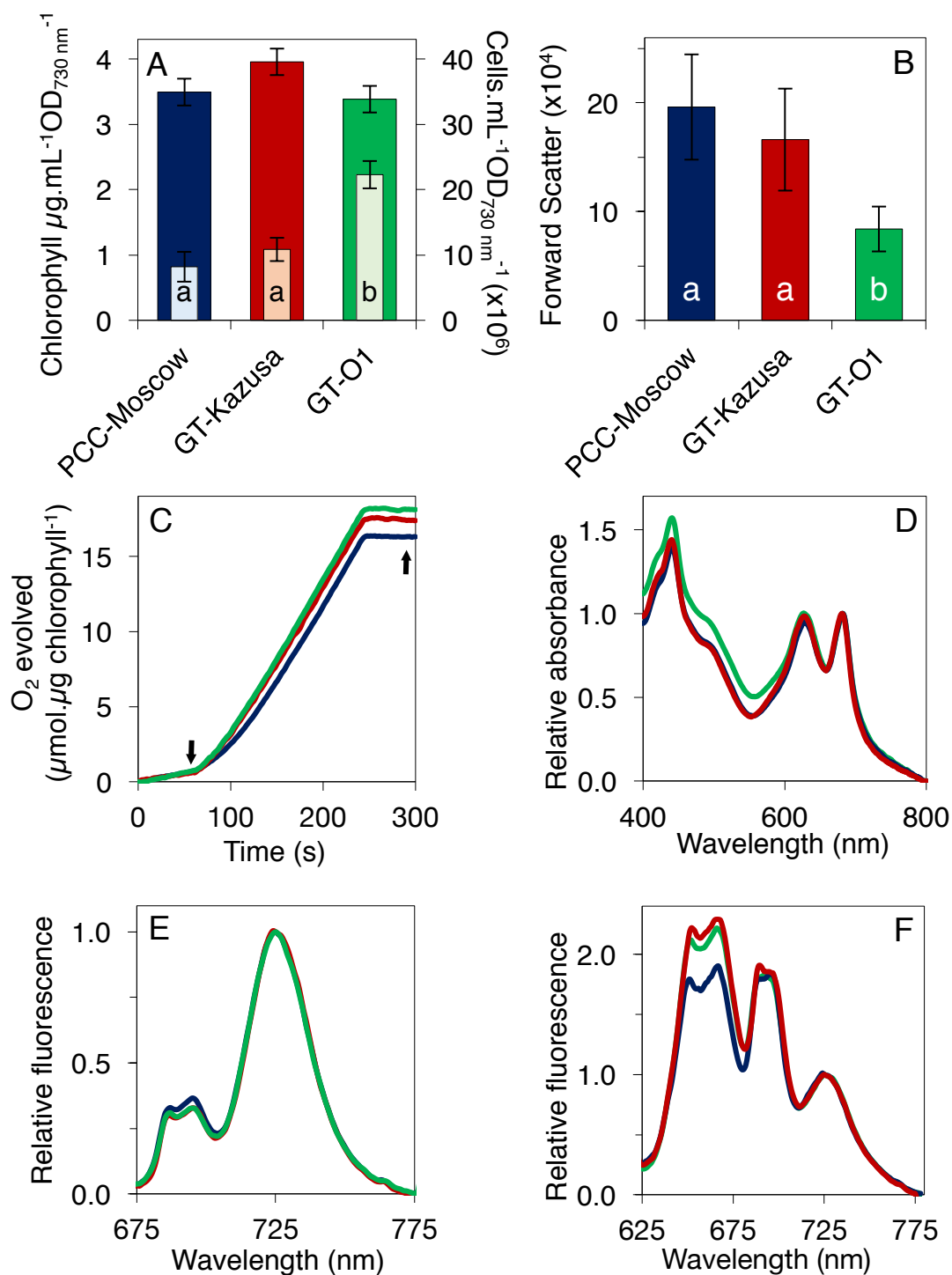
Figure 3.10. Characterisation of *Synechocystis* 6803 wild-type substrains. A-B: cellular properties of *Synechocystis* 6803 wild-type substrains; A: mean chlorophyll concentration (n = 7), solid bars, and mean cell concentration of PCC-Moscow, GT-Kazusa and GT-O1 cells, normalised per mL, per unit of OD $_{730\ nm}$ ($n = 5$), shaded bars. B: forward scatter, a proxy for cell size, of PCC-Moscow, GT- Kazusa and GT-O1 cells ($n = 5$). Letters represent the results

of a Tukey's HSD post-hoc test following one-way ANOVA; A – GT-O1 cell concentration was significantly different from that of PCC-Moscow and GT-Kazusa ($P \leq 0.01$); B: GT-O1 forward scatter was significantly different from that of PCC-Moscow and GT-Kazusa ($P \leq 0.01$). C: HCO_3^- -supported photosynthetic oxygen evolution; light was applied at 60 s and turned off at 240 s (indicated by arrows), data are representative traces of oxygen evolution of cells re-suspended to 5 μg.mL^{-1} chlorophyll. D: mean whole-cell absorption spectra ($n = 6$–8), normalised to the chlorophyll absorption maxima at 685 nm. E-F; 77 K fluorescence of substrains; D: fluorescence emission following excitation at 440 nm, targeting chlorophyll; E: fluorescence emission following excitation at 580 nm, targeting excitation of the phycobilins. Traces in E-F are baseline-corrected, normalised to the PS I emission peak at 725 nm and represent the mean of five independent measurements. Colours in C-F: PCC-Moscow (blue line); GT-Kazusa (red line); GT-O1 (green line).

3.4. Discussion

This study has identified a significant number of novel mutations in the genomes of the *Synechocystis* 6803 wild types GT-O1 and GT-O2, some of which are likely to affect gene function, which have arisen during routine laboratory culture conditions. *De novo* mutations found in these substrains indicate that these have diverged from the lineage that led to the GT-Kazusa strain and that both are unique to the Otago laboratories of JJ Eaton-Rye and TC Summerfield. Further mutations detected in the GT-O1 and GT-O2 sequences are in agreement with previously published sequences of lab strains of *Synechocystis* 6803, and the apparent lack of false-positive variants found in two completely independent genome mapping methods demonstrate the effectiveness both of modern high-throughput sequencing techniques and recent advances in genome mapping software. However, particular care is needed to address the difficulty of detecting large indels, such as transposase insertions. PCR analysis, in complement to genome assembly, presents a straightforward and cheap strategy to confirm the presence or absence of previously detected indels, but additional strategies are required to detect novel indels. In the future, whole genome re-sequencing of laboratory strains of *Synechocystis* 6803 will probably become routine, and multiple studies now address this matter (Tajima et al., 2011; Kanesaki et al., 2012; Trautmann et al., 2012; Morris et al., 2014; Ding et al., 2015). The data presented in this study provide further evidence for lineage- and substrain-specific mutations that can be used to identify the divergence of *Synechocystis* 6803 in labs worldwide. A ΔPsbMΔPsb27 strain and a ΔYcf48 strain in the GT-O2 genomic background both presented unexpected phenotypic traits due to impaired assembly of PS II arising from reduced chlorophyll supply (Crawford et al., 2016; JJ Eaton-Rye and colleagues, unpublished data), making the choice of an appropriate wild-type strain critical to mutagenesis studies. It is imperative that researchers maintain viable freezer-stocks of an appropriate *Synechocystis* 6803 wild-type from which working cultures are routinely revived and disposed of after a few (<6) months, to avoid the divergence of GT-O2-like strains.

The mutations in the GT-O2 substrain point to a process of genetic selection based on the conditions experienced during long-term culturing. Photoheterotrophic growth on agar would diminish cellular reliance on photosynthesis for carbon fixation, and 24 h light conditions would render a day/night response such as the one involving Hik8 unnecessary; the principle of resource allocation (Cody, 1965) would suggest that resources diverted from chlorophyll biosynthesis or day/night detection would favour optimal growth in GT-O2. Accordingly, the

somewhat higher initial growth rate of GT-O2 cells in the presence of glucose compared to GT-O1 might represent an optimisation of growth strategy, and the lower final culture density seen in GT-O2 cells might reflect the exhaustion of the glucose supply. The GT-O2 substrain therefore represents a useful strain for studies in PS II assembly (Crawford et al., 2016), but is certainly not comparable to other *Synechocystis* 6803 wild-types. Interestingly, the substrain GT-W acquired a ~110 kb duplication of a region of the chromosome containing the genes encoding PsbA1 (PS II D1 protein), Psb28, Mg-protoporphyrin IX monomethyl ester cyclase, and >90 other genes; this strain was impaired in growth, chlorophyll biosynthesis, and PS II assembly compared to the GT-P wild-type (Tichý et al., 2016). Supporting the hypothesis that such mutations represent a selection response that might indicate resource allocation, the GT-W culture grown in photoautotrophic conditions over six months lost the genome duplication and returned to a GT-P phenotype (Tichý et al., 2016).

In the course of this study, a culture of GT-O1 cells obtained a homozygous insertion in *slr0856*, which apparently arose from a heterozygous mutation in the sequenced GT-O1 substrain. To further investigate the inheritance of mutations in long-term culturing, the fate of this mutation was traced, particularly as it might give rise to a new, functional ISY*100*-type transposase ORF; over 25 re-streaks on BG-11 agar this mutation apparently reverted to the wild-type sequence. The genome sequence for this strain, dubbed 'GT-O3,' is presently unavailable; phenotypic analysis has also not been carried out. As discussed in Section 3.2, it is unclear what phenotypic result the *slr0856* mutation might cause, but it certainly demonstrates an active process of genome mutation in *Synechocystis* 6803. It is noteworthy that the large genome duplication site in the GT-W wild type was flanked by ISY*100*-type transposase genes, raising the possibility that this genome duplication arose from ISY*100* transposition (Tichý et al., 2016).

The data presented here reveal small differences in physiological traits between the PCC-Moscow and GT-Kazusa substrains compared to the GT-O1 substrain. Whereas growth rate was similar, cells from the GT-O1 substrain are smaller than PCC-Moscow and GT-Kazusa cells. The overall similarities in most respects between PCC-Moscow and GT-Kazusa cells revealed by this study imply that the reduced cell size is a GT-O-specific phenotype. It is not clear which of the two genome changes in GT-O substrains that cause amino-acid substitutions might cause this phenotype. One candidate might be a Gln115Leu mutation in the predicted

plasma membrane transporter Sll1428 (Morris et al., 2014). However, the *sll1428* gene has below-detection threshold expression levels in standard conditions in the PCC-Moscow strain (Kopf et al. 2014), and the function of this gene has not been characterized as yet.

Further differences in wild-types observed in this study include an elevated level of carotenoid pigments, revealed by whole-cell absorption spectra, in GT-O1 cells. In the PCC-Moscow substrain, a decrease in PBS emission detected by low temperature fluorescence emission might reflect the finding that phycobilin pigments were reduced in this substrain compared to GT-Kazusa and GT-O1 cells. Although no immediately obvious mutations in photosynthetic or phycobilisome genes that could explain these results are known in the PCC-Moscow/GT-O1 substrains, the former does possess a number of SNPs that affect environmental sensor or transcriptional regulator genes that could have an indirect effect on light harvesting. SNPs in PCC-Moscow relative to the GT-lineage of *Synechocystis* 6803 affect *hik25*, *rre22*, *slr0534_as3* (*hik10* antisense RNA) and *sigF* (Trautmann et al., 2012); what functional consequence these mutations have, however, is unknown. It should also be noted that the *hik25* and *rre22* 'mutations' are found throughout the PCC-lineage, and might represent the ancestral form of these genes, considering that a number of mutations, such as a 1 bp insertion in *spkA* (causing a loss of motility) in the GT-lineage suggest the PCC-group is the more ancestral *Synechocystis* 6803 lineage (Trautmann et al., 2012).

Considering that each substrain of *Synechocystis* 6803 to have been sequenced thus far displays several unique genome mutations (resulting in amino acid changes in the encoded proteins), it is unsuprising that some phenotypic variation between these substrains exists. In fact, leaving cell motility and cell size aside, these data suggest a high level of similarity between GT-O1, PCC-Moscow, and GT-Kazusa cells, considering that they have presumably been isolated for many years or decades. Overall, despite the difference in cell size, this study demonstrates that the GT-O1 substrain is sufficiently similar to the PCC-Moscow and GT-Kazusa substrain to be a useful *Synechocystis* 6803 wild-type for analysis, especially in terms of PS II function. Possibly, the response to stressors may vary between substrains, but this was not investigated in this work. Genome instability, and instances where populations of cells become rapidly dominated within only a few generations by a genetic mutant, as a stress response to the deliberate introduction of deleterious mutations by researchers, has been well documented in *Synechocystis* 6803 and other bacterial species (Darmon and Leach, 2014; Jones, 2014). In one study, a spontaneous mutation in the gene *pmgA* apparently improved growth of the

Synechocystis 6803 GT-I wild type (Hihara and Ikeuchi, 1997; Kanesaki et al., 2012). Genetic variation between *Synechocystis* 6803 wild types is less likely to be a stress response, considering that cells are grown in nutrient-replete media in theoretically optimal light and temperature conditions. Long-term culturing in conditions that are subtly different between labs may promote 'fine-tuning' of the genome to favour optimal growth in *Synechocystis* 6803, and excessive time in culture can lead to pronounced genetic change, as seen in GT-O2. So, although the genetic instability of cyanobacteria has been highlighted (Jones, 2014), baseline comparisons between wild-type substrains of *Synechocystis* 6803 in this study showed little variation. Nevertheless, there is the potential for genotypic and phenotypic variation between substrains of this species, as spontaneous mutation events in wild types during long-term culturing are known to occur (e.g. Hihara & Ikeuchi 1997).

Chapter Four: Exploring aspects of pH-sensitivity and genome mutation in mutants lacking specific combinations of PS II extrinsic subunits

4.1 pH-sensitivity in *Synechocystis* 6803

4.1.1 pH range of *Synechocystis* 6803

Like many cyanobacteria, *Synechocystis* 6803 is capable of growth in a broad range of neutral to alkaline pH conditions. Adaptation to pH involves the regulation of CCM component and pH homeostasis genes in particular, with RNA polymerase σ factors playing a major role (see Chapter One). Review of the literature suggests that although growth of *Synechocystis* 6803 is possible from pH ~6.0 to pH ~11.0, the optimal growth range is probably around pH ~7.5 to pH ~10.0 (Maestri and Joset, 2000; Eaton-Rye et al., 2003; Kurian et al., 2006; Zhang et al., 2009a, 2012; Summerfield et al., 2013). A number of *Synechocystis* 6803 mutants appear to be pH-sensitive, which is here used to mean substantially or completely impaired in growth at a given pH level. In several mutants, gene deletions associated with heterotrophy cause pH-sensitivity in mixotrophic conditions, such as deletion of *hik31* (Kahlon et al., 2006; Nagarajan et al., 2014), *slr1736,* and *pmgA* (Sakuragi, 2006). In addition, a number of PS II mutants are incapable of autotrophic growth at pH 7.5, but are autotrophic at pH 10.0. In these mutants, addition of 5 mM glucose permits growth at either pH level, suggesting that the cause of pH-sensitivity is impaired transduction of cellular energy from PS II-dependent processes at pH 7.5, rather than a direct effect of pH 7.5.

4.1.2 pH-sensitivity of PS II extrinsic protein mutants

A number of PS II mutants are pH-sensitive, and among the best characterised of these is the ΔPsbO:ΔPsbU mutant, which is incapable of pH 7.5 autotrophy, but is capable of pH 10.0-growth, and a pseudorevertant has been isolated that is capable of growth at both pH 7.5 and pH 10.0 (Eaton-Rye et al., 2003; Summerfield et al., 2007). Microarray data show that, compared to the GT-O1 wild-type, a Con:ΔPsbO:ΔPsbU strain and a ΔPsbV:ΔCyanoQ strain have increased expression of *rre34* (of the *hik31* operon) and a suite of oxidative stress-response genes at pH 10.0 compared to pH 7.5 (Summerfield et al., 2013). Both Con:ΔPsbO:ΔPsbU cells and the Con:ΔPsbO:ΔPsbU pseudorevertant have increased expression of *hik31* itself, *hik34,* and *sigB* at pH 10.0; the Con:ΔPsbO:ΔPsbU pseudorevertant

alone shows induction of *sigD* and, in particular, *ocp* at pH 7.5 (encoding orange carotenoid protein, involved in quenching excess light energy) (Summerfield et al., 2007, 2013). Generally speaking, it appears that at a genetic level, some oxidative stress responses are enhanced at pH 10.0 in these PS II mutants, and accordingly the resistance of the Con:ΔPsbO:ΔPsbU strain and ΔPsbV:ΔCyanoQ cells to the $^1O_2$-sensitiser Rose Bengal was enhanced at pH 10.0 compared to pH 7.5 (Summerfield et al., 2013). Despite these observations, the functional basis of the pH-sensitivity of these PS II extrinsic protein deletion mutants remains enigmatic. The advent of affordable and practical whole-genome resequencing technology provided a novel opportunity to attempt to address this matter further in this study. Additionally, comparing variation between the genome of the Con:ΔPsbO:ΔPsbU strain and the Con:ΔPsbO:ΔPsbU pseudorevertant genome might provide evidence of an adaptation at the genomic level to extreme stress (i.e., non-permissive growth conditions), and as such provide a complement to the studies of wild-type genome divergence in theoretical no-stress conditions outlined in Chapter Three.

4.2 Genomic differences between the Con:ΔPsbO:ΔPsbU mutant and the Con:ΔPsbO:ΔPsbU pseudorevertant

4.2.1 Assembly of the Con:ΔPsbO:ΔPsbU and Con:ΔPsbO:ΔPsbU pseudorevertant genome

Genomic DNA from Con:ΔPsbO:ΔPsbU and Con:ΔPsbO:ΔPsbU pseudorevertant (hereafter pseudorevertant) cells was sequenced for comparison with a manually curated version of the database sequence from GT-Kazusa (Kaneko et al., 1995, 1996, 2003), which contained approximations of the antibiotic-resistance cassette insertions in these mutant strains, as follows. The Control strain, which was used as a genomic background for the Con:ΔPsbO:ΔPsbU strain, and hence the pseudorevertant as well, possesses a 1.2 kb Kan^R cassette inserted at a NcoI site 396 bp downstream of *psbB* (Eaton-Rye and Vermaas, 1991). To interrupt *psbO*, a 2.0 kb spectinomycin resistance (Spec^R) cassette was inserted at a unique intragenic BamHI site 558 bp downstream of the start codon (Morgan et al., 1998), and *psbU* was interrupted with a chloramphenicol resistance (Cam^R) cassette 160 bp downstream of the start codon at a SwaI site (Eaton-Rye et al., 2003).

More than 13 million short (100 bp) paired reads per strain were obtained from genomic DNA sequencing with an Illumina HiSeq 2000 system, equating to 2600 and 3000 Mb in total for the Con:ΔPsbO:ΔPsbU and pseudorevertant strains, respectively. This represents more than 650-fold coverage of the 3.9 Mb *Synechocystis* 6803 genome. Using CLC software, genomic sequences were constructed and putative variants detected by mapping reads to the GT-Kazusa reference sequences (Appendix Fig. A.4, Table 4.1). In both strains, database errors also found in GT-O1 were identified, along with the *sll0550* mutation, which is presumably characteristic of all University of Otago-based *Synechocystis* strains, or alternatively the GT-Vermaas strain (see Chapter Three, Section 3.1, and Figure 3.4). However, the GT-O1 *sll1428* mutation, and all GT-O2 mutations, were not identified in Con:ΔPsbO:ΔPsbU and pseudorevertant genome, in accordance with the earlier isolation of these strains compared to the GT-O1 strain; these results were confirmed by Sanger sequencing (not shown). PCR and Sanger sequencing of the earliest available genomic DNA sample from the Control strain (circa 1992, results not shown) showed the same results, confirming the presence of the *sll0550* mutation and absence of the *sll1428* mutation in this strain.

Table 4.1. List of novel mutations and their effects on gene products in the Con:ΔPsbO:ΔPsbU and pseudorevertant substrains, compared to the GT-O1 wild type.

Region	Gene affected					Comment
Region	*Nucl. change*	*AA change*	*Gene annotation*	*Gene name*	*Gene product*	*Comment*
252249	G→A	Q220*	*sll1673*	*rre2*	Two-component response regulator	
909348	C→A	G93C	*sll1968*	*pmgA*	Photomixotrophic growth protein A	Pseudorevertant-specific
1581467	A→G	Q115L	*sll1428*		Probable sodium-dependent transporter	These substrains lack the GT-O1 mutation and instead have the database (GT-Kazusa) *sll1428* sequence
2067053	C→T	IGR				Between *prk* and *petH*, adjacent to *ncl1020*
3145078	G→A	A1115V	*sll0043*	*cheA/hik18*	Positive phototaxis protein	Pseudorevertant-specific
3233062	G→A	G54E	*slr1558*		Hypothetical protein	Pseudorevertant-specific

'Region' refers to the base position in the original GT-Kazusa sequence, but comparisons are made to the GT-O1 strain. Genetic differences associated with the deliberate mutations in these strains, i.e. those in *psbB* (Kan^R cassette inserted downstream), and the *psbO* and *psbU* deletions are omitted. Abbreviations: AA – amino acid; Nucl. – nucleotide; IGR – intergenic region. Sequence data was obtained prior to this study, but genome assembly using CLC was carried out by the author.

Two mutations common to the Con:ΔPsbO:ΔPsbU and pseudorevertant strains were identified and confirmed by Sanger sequencing; a SNP causing a premature stop codon in the gene product of *rre2*, and a mutation in an intergenic region between *prk* and *petH*, adjacent to the non-coding RNA (ncRNA) *ncl1020*. Three SNP mutations specific to the pseudorevertant strain were found, resulting in a Gly93 to Cys change in PmgA, an Ala1115 to Val mutation in Chemotaxis protein A (CheA/Hik18), and a Arg54 to Glu mutation in the hypothetical protein Ssr1558 (Figure 4.1, Table 4.1). All mutations result in changes to what appear to be either extremely conserved (PmgA, Ssr1558) or highly conserved (CheA) residues of proteins found in many cyanobacteria (Fig. 4.2); PmgA and CheA homologs are found in other bacterial lineages as well.
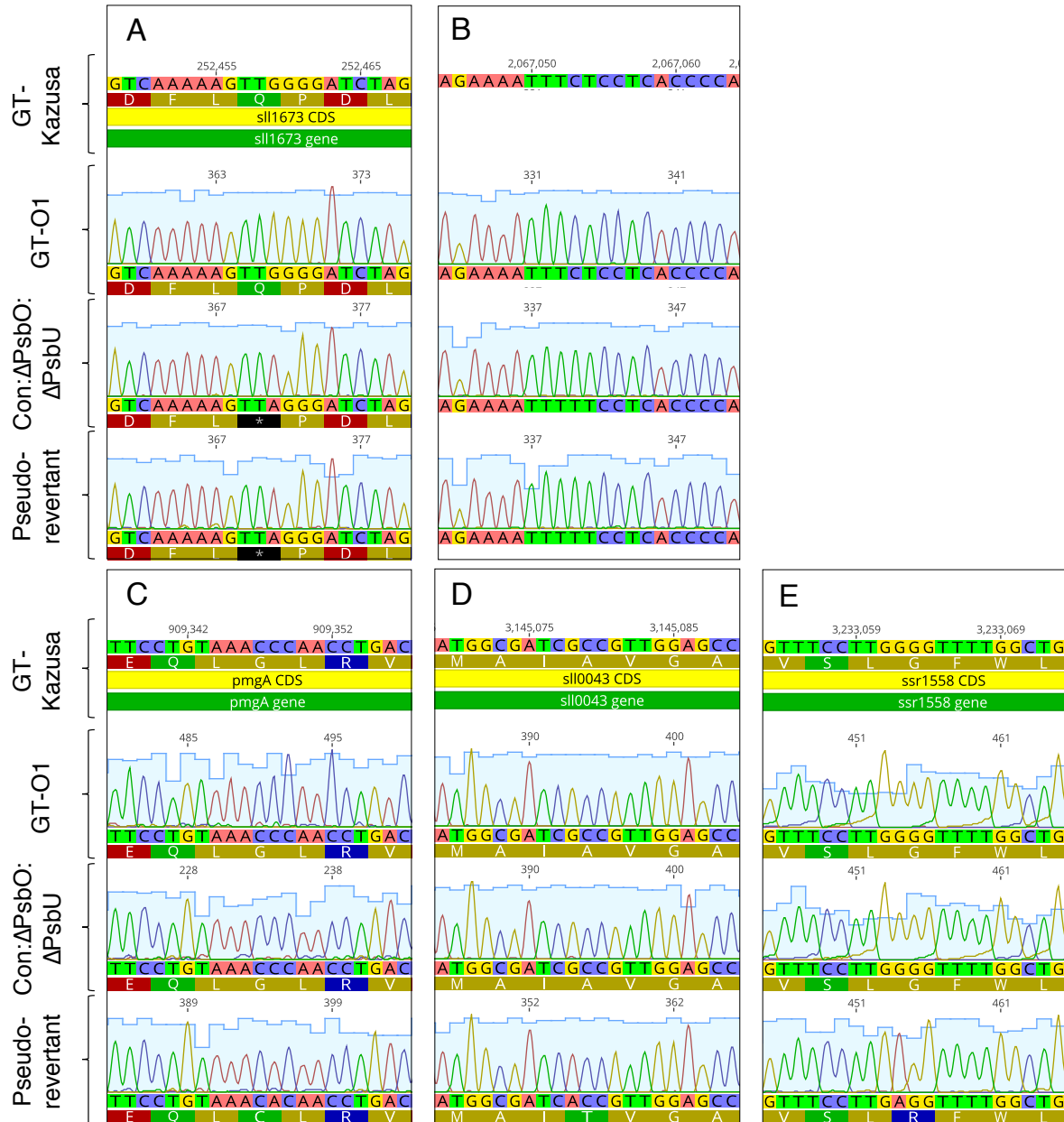
Figure 4.1. Sanger sequencing data depicting genetic mutations in the Con:ΔPsbO:ΔPsbU and pseudorevertant mutants of *Synechocystis* 6803, compared to the GT-O1 sequence. A-B: mutation events that occurred prior to the isolation of the pseudorevertant; A: *sll1673* (encoding Rre2 protein), B: intergenic region between *petH* and *prk*. C-E: mutation events unique to the pseudorevertant; C: *sll1968/pmgA* (encoding PmgA), D: *sll0043/cheA* (encoding CheA/Hik18), E: *ssr1558* (encoding a hypothetical protein). The GT-O1 *sll1428* mutation and those associated with antibiotic-resistance cassettes in these substrains are omitted.

In PmgA, the Gly93 to Cys pseudorevertant mutation seems likely to alter the conformation of the protein at that site, potentially resulting in additional disulfide interactions from the introduced cysteine residue and affecting the start of an ATPase region predicted by InterPro analysis. Although *pmgA* mutants are the subject of diverse studies in *Synechocystis* 6803 (e.g. Hihara and Ikeuchi, 1997; Haimovich-Dayan et al., 2011; Nishijima et al., 2015; De Porcellinis et al., 2016), no protein structure is available for PmgA, despite apparently extensive attempts by other researchers to isolate the protein by His-tagging or overexpressing the protein in *E. coli*, for crystallography purposes (Y Hihara, University of Saitama, *pers. comm.*). As discussed earlier (see Chapter One, Section 1.6.4), PmgA appears to have a role in regulating the expression of CCM component-encoding genes *ndhF3* and *sbtA* in photomixotrophic conditions (Haimovich-Dayan et al., 2011), and PmgA has structural homology with a *Bacillis subtilis* Ser-Thr kinase that regulates SigB (Sakuragi, 2006). SigB is involved in pH-sensing in that species, as is its homolog in *Synechocystis* 6803 (*sll0306*) and *E. coli* (*rpoS*, σ^{38}) (Price, 2000; Ohta et al., 2005; Li et al., 2014).

The CheA Ala1115 to Val mutation in theory would be a much more conservative residue change, although it too affects a predicted functional protein domain. CheA in *Synechocystis* 6803 is a hybrid sensor kinase with phosphodonor and phosphoacceptor sites (Shin et al., 2008); InterPro analysis suggests that Ala1115 is in a domain with predicted homology to CheW, which mediates signal transduction to the CheA kinase in many bacteria, such as *Thermatoga marina* (Bilwes et al., 1999). Mutagenesis experiments in *Synechocystis* 6803 show that *sll0043* deletion caused negative phototaxis in a positively phototactic motile wild-type background, apparently by supressing pilin and twitching motility proteins (Shin et al., 2008). However, what functional relevance the pseudorevertant mutation might have is unclear, given that the proximal GT-Vermaas, Control, and Con:ΔPsbO:ΔPsbU parent strains are non-motile. Additionally, an Δ*sll0043* mutant grew similarly to the wild type under photoautotrophic and photoheterotrophic conditions (Shin et al., 2008).

A PmgA

Accession	Consensus alignment	Description [species]
BAA20429.1	LNSVPKPLHNEVRLGLQEALVNAATHGNA	pmgA [Synechocystis sp. PCC 6803]
WP_028946959.1	LNSVPEPLHNEVRLGLQEALVNAATHGNA	PmgA protein [Synechocystis sp. PCC 6714]
WP_009630361.1	LAEVPEKWHAELRLGLQEALVNAAKHGNK	serine/threonine protein kinase [Synechocystis sp. PCC 7509]
WP_006530647.1	LINIPSQLQGDIRLGLQEALVNAAKHGNK	serine/threonine protein kinase [Gloeocapsa sp. PCC 73106]
WP_015083047.1	LTDIPAKLQSELRLGLQEALVNAAKHGNN	anti-sigma regulatory factor [Anabaena sp. 90]
AFY71767.1	LSEVPSIWHAELRLGLQEALVNAVRHGNK	putative anti-sigma regulatory factor, [Pseudanabaena sp. PCC 7367]
WP_015951442.1	LAEVPAKLQAELRLGLQEALVNAAKHGNN	serine/threonine protein kinase [Anabaena sp. PCC 7108]
WP_015217483.1	LADVPTKLQAELRLGLQEALVNAAKHGNN	serine/threonine protein kinase [Anabaena cylindrica]
WP_015130967.1	LAEIPVKLQAELRLGLQEALVNAAKHGNN	anti-sigma regulatory factor [Calothrix sp. PCC 7507]
WP_015325175.1	LANIPKQLQPEIRLGLQEALVNAAKHGNK	serine/threonine protein kinase [Cyanothece sp. PCC 7822]

B CheA

Accession	Consensus alignment	Description [species]
WP_010874009.1	CLVGQNQ--GAPTAIAIPSDSVAELMVPTAT-	chemotaxis protein CheA [Synechocystis sp. PCC 6803]
WP_028946378.1	CSVGQDN--TALTAIAIPSDSVAELMVPRAD	chemotaxis protein CheA [Synechocystis sp. PCC 6714]
ACK71190.1	CLMNAKTHdGGVGAIALPSDSIEEIIIPEPQ	CheA signal transduction histidine kinase [Cyanothece sp. PCC 7424]
WP_013321240.1	CLINTKNLeGGVSAIALPSDSIEEIIIPEPE	chemotaxis protein CheA [Cyanothece sp. PCC 7822]
WP_015144017.1	CLMNQEVT-GQATAVALPSDSIEEIIIPTGE	chemotaxis protein [Pleurocapsa minor]
WP_035798735.1	CLIQQHNY-HQGSAIALPSDSIEEIIMPEPE	chemotaxis protein CheA [Cyanothece sp. CCY0110]
ACB53538.1	CLIQQDNS-HQGSAIALPSDSIEEIIMPEPE	CheA-like two-component hybrid sensor and regulator [Cyanothece sp. ATCC 51142]
WP_015187881.1	CFVG-------TNAYALPSDSIAEILIPEAN	signal transduction histidine kinase [Gloeocapsa sp. PCC 7428]
WP_015181308.1	CLIG-------PTAIALPSDSVEEIVVPKSD	chemotaxis protein [Microcoleus sp. PCC 7113]
WP_009554092.1	CLAD-------IATLALPTDGIEEIITPPAG	chemotaxis protein [Oscillatoriales cyanobacterium JSC-12]

C Ssr1558

Accession	Consensus alignment	Description [species]
WP_010874077.1	'FGSVTALILASFLGVLAGGSLAQFLPTF	hypothetical protein [Synechocystis sp. PCC 6803]
WP_028947301.1	'FGSVTALILASFLGVLAGGSLAQFLPTF	hypothetical protein [Synechocystis sp. PCC 6714]
WP_013323140.1	'VGSITALILASFLGVIAGGSMAQLLPTF	hypothetical protein [Cyanothece sp. PCC 7822]
WP_007306145.1	'FGSITALILASFLGVIAGGTIAQFLPTF	hypothetical protein [Crocosphaera watsonii]
WP_006510709.1	'LGSTVALVLASFLGVIAGGGVAQFLPEF	membrane protein [Xenococcus sp. PCC 7305]
WP_015145330.1	'FGSITALILASSLGVIAGGGVAQLLPEF	hypothetical protein [Pleurocapsa minor]
WP_002764179.1	'FGSITALILTSFLGVLAGGSMAQLFPAF	hypothetical protein [Microcystis aeruginosa]
WP_015201231.1	'FGSITALILTSFLGVLAGGSMAQLFPAF	hypothetical protein [Crinalium epipsammum]
WP_036481041.1	'FGSVTALLLASFLGVLAGGQMATLLPAF	hypothetical protein [Myxosarcina sp. GI1]
WP_019506978.1	'LGSTVALILASFLGVIAGGSVAQILPEF	hypothetical protein [Pleurocapsa sp. PCC 7319]

Figure 4.2. Consensus alignment and protein domains from PmgA, CheA, and hypothetical protein Ssr1558. Amino acid sequences were compared to other cyanobacterial species using COBALT. Red arrows indicate the site of the pseudorevertant mutation in the amino acid sequence, and patterned areas in the protein cartoon represent the location of predicted or

known protein domains. PmgA contains a histidine kinase (HK)-like ATPase region; CheA contains three HK phosphotransfer domains (indicated by '*'), a HK core domain, a CheW domain, and a CheY domain (indicated by '**'). No predicted domains could be assigned to Ssr1558.

The hypothetical protein Ssr1558 does not appear to have any predicted function in cyanobacteria, but a Arg54 to Glu mutation would likely result in conformational change in the vicinity of this residue. InterPro analysis suggests that the protein has homology to the Gtd1 protein family in higher plants, which has recently been suggested to include CCHA1/Pam71, a chloroplast membrane-bound Ca^{2+} (and possibly Mn^{2+})/H^+ antiporter which apparently directs Ca^{2+} and/or Mn^{2+} into the lumen, and regulates pH homeostasis. In *Arabidopsis thaliana*, deletion of CCHA1/Pam71 resulted in reduced PS II protein biosynthesis and oxygen evolution (Schneider et al., 2016; Wang et al., 2016). However, *ssr1558* encodes a protein around ¼ the size of CCHA1/Pam71, and Ssr1558 must presumably interact with other unidentified proteins in *Synechocystis* 6803 if it carries out a similar role; it seems therefore unlikely that Ssr1558 is a functional, independent transporter. Only one other Ca^{2+}/H^+ antiporter, SynCAX, has been identified in *Synechocystis* 6803 to date; its deletion results in altered pH_{int} homeostasis and altered carbon uptake via CmpA (Waditee et al., 2004; Jiang et al., 2013).

4.2.2 The *pmgA* mutation is the candidate for restoring growth in the pseudorevertant

Although all three pseudorevertant mutations are intriguing *prima facie* candidates for alteration of cellular processes that might permit pH 7.5 growth, a photoautotrophic growth selection assay suggested that the PmgA mutation alone was the candidate for growth restoration. When *pmgA*, *cheA*, and *ssr1558* were amplified by PCR from the pseudorevertant and applied to Con:ΔPsbO:ΔPsbU cells in a top-agar buffered at pH 7.5 (Figure 4.3), the *pmgA* PCR product (either alone, or in combination with *cheA*, and/or *ssr1558*; no dosage effect was evident when combinations were used: not shown) resulted in a cluster of cell growth after four weeks similar to that arising from application of wild-type *psbO*, GT-O1 genomic DNA, or pseudorevertant genomic DNA (not shown). Unfortunately, attempts to culture colonies from the *pmgA*-transformed top-agar were unsuccessful (due to rapid culture bleaching), and a

subsequent mutagenesis strategy was employed to further investigate if the *pmgA* mutation is indeed responsible for pH 7.5 growth.
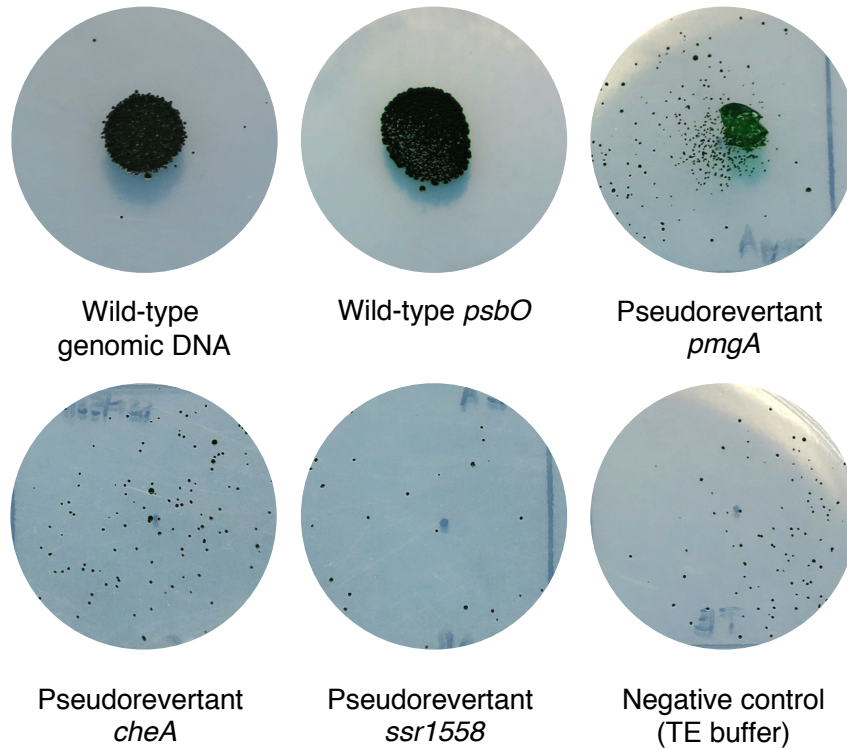
Figure 4.3. Photoautotrophic growth selection assay. A top-agar of Con:ΔPsbO:ΔPsbU cells buffered at pH 7.5 was spotted with ~1 µg of DNA to screen for pH 7.5 growth in this strain, seen as a cluster of colonies of cells growing after four weeks in the vicinity of the DNA spotting area (centre of each image). Wild-type GT-O1 genomic DNA, as well as purified PCR products from amplification of GT-O1 *psbO*, and pseudorevertant *pmgA*, *cheA/hik18* and *ssr1558*, were used to transform cells.

4.3 Attempts to replicate the Gly93 to Cys mutation in PmgA in GT-O1 and ΔPsbO:ΔPsbU substrains

4.3.1 Mutagenesis strategies

4.3.1.1 Deletion of *pmgA* from GT-O1, Con:ΔPsbO:ΔPsbU, and pseudorevertant cells

To conclusively establish that the Gly93 to Cys mutation alone is responsible for pH 7.5 growth, it was desirable to produce a Con:ΔPsbO:ΔPsbU strain possessing the pseudorevertant mutation, or produce a pseudorevertant strain with wild-type *pmgA*, these strains would therefore be expected to display pH 7.5 growth and pH 7.5-sensitivity respectively. A strategy was devised to delete the native *pmgA* and replace it with either the wild-type or Gly93 to Cys (G93C)-encoding *pmgA* copy (Figs. 4.4-4.7).

For deletion of *pmgA*, a plasmid construct was created using overlap-extension PCR that replaced almost the entire *pmgA* ORF with a Gen^R cassette flanked by ~500 bp regions of upstream *sll1967* and downstream *sll1969* for double homologous recombination (Δp plasmid, Fig. 4.4). This plasmid was introduced into the wild-type GT-O1, Con:ΔPsbO:ΔPsbU and pseudorevertant cells (Fig. 4.7). Since *Synechocystis* 6803 has ~10 copies of the genome per cell, it is possible for the cell to express both the wild-type gene and the antibiotic resistance cassette following transformation. Ordinarily, a transformant would fully segregate (have the introduced DNA incorporated into all chromosome copies) after 8-12 weeks. Fully segregated GT-O1:Δ*pmgA* cells were obtained following introduction of the Δp plasmid, but Con:ΔPsbO:ΔPsbU:Δ*pmgA* cells remained heterozygous (contained native *pmgA,* and the gene deletion and antibiotic resistance) over >19 weeks in heterotrophic conditions. No colonies were obtained for transformed pseudorevertant cells. Subsequent transformations of Con:ΔPsbO:ΔPsbU with the same plasmid employing double-strength gentamicin, or growth in lower light conditions (~20 μE.m^{-2}.s^{-1}), had the same result (not shown), implying that *pmgA* is essential to the Con:ΔPsbO:ΔPsbU mutant in the conditions tested. Growth of both GT-O1:Δ*pmgA* and heterozygous Con:ΔPsbO:ΔPsbU:Δ*pmgA* cells was problematic, with sporadic culture bleaching on BG-11 plates, and variable success in producing viable BG-11 liquid cultures.

Figure 4.4. Construction of a Δ*pmgA* plasmid by overlap-extension PCR for introduction into *Synechocystis* 6803. A: depiction of the genomic region of *pmgA*, with the location of the left flank (LF) and right flank (RF) regions used to generate the PCR construct shown in blue. B: PCR amplification of overlap-extension PCR components; i – left flank (amplified from GT-O1), ii – Gen^R cassette (amplified from lab plasmid stocks), iii – right flank (from GT-O1). C: single PCR product for Δ*pmgA* plasmid insert generated by amplification of PCR products (from B) with internal primers. D: map of final Δ*pmgA*/Gen^R (Δp/Gen^R) plasmid generated by ligation of PCR product (from B) into the pGEM-T Easy plasmid, which was transformed into *E. coli* and mini-prepped. E: EcoRV/HindIII digestion of plasmid DNA from Δp, confirming appropriate insert size. F: depiction of the *pmgA* genomic region of *Synechocystis* 6803 following transformation with the Δp plasmid. (B, C, E: L = 1 kb^+ DNA ladder, used to estimate amplicon sizes).

4.3.1.2 *pmgA* complementation into GT-O1 and Con:ΔPsbO:ΔPsbU cells

GT-O1 and Con:ΔPsbO:ΔPsbU cells carrying complete or partial *pmgA* deletions were transformed in order to introduce the wild-type or G93C-encoding gene copy. Two plasmids were constructed by overlap-extension PCR, which were designed to reintroduce either wild-type (*pmgA* Control plasmid, pG93) or G93C (pG93C plasmid) *pmgA* into its native site, displacing the Gen^R cassette (in previously constructed Δ*pmgA* strains) and inserting an Ery^R cassette downstream of *pmgA* in the very small (7 bp) *pmgA-sl1969* intergenic region (Fig. 4.5). Unfortunately, transformation of the GT-O1:Δ*pmgA* strain with the pG93 or pG93C plasmid did not yield colonies of transformants when the plasmid was introduced into 2-3 independent cultures of GT-O1:Δ*pmgA* cells. While transformation of the heterozygous Con:ΔPsbO:ΔPsbU:Δ*pmgA* strain with both plasmids did yield colonies, which eventually segregated completely (Fig. 4.7), the wild-type *pmgA* gene copy was retained in all cases. This transformation was repeated, with cells exposed to an initial 4-week period of pH 7.5 autotrophic selection on BG-11 plates in the presence of erythromycin following transformation. Due to extremely slow growth rates under these conditions, cultures were subsequently grown on photoheterotrophic BG-11 plates for complete segregation of the mutation before screening *pmgA* by PCR and Sanger sequencing; surprisingly, the wild-type *pmgA* was retained in these cases as well.

GT-O1, Con:ΔPsbO:ΔPsbU and pseudorevertant cells were also transformed directly with the pG93 or pG93C plasmids, without an initial *pmgA* deletion. Segregated cells were obtained for GT-O1 and Con:ΔPsbO:ΔPsbU cells transformed with both plasmids, but Sanger sequencing showed that the wild-type *pmgA* gene copy was retained. No transformed colonies were obtained from the pseudorevertant.

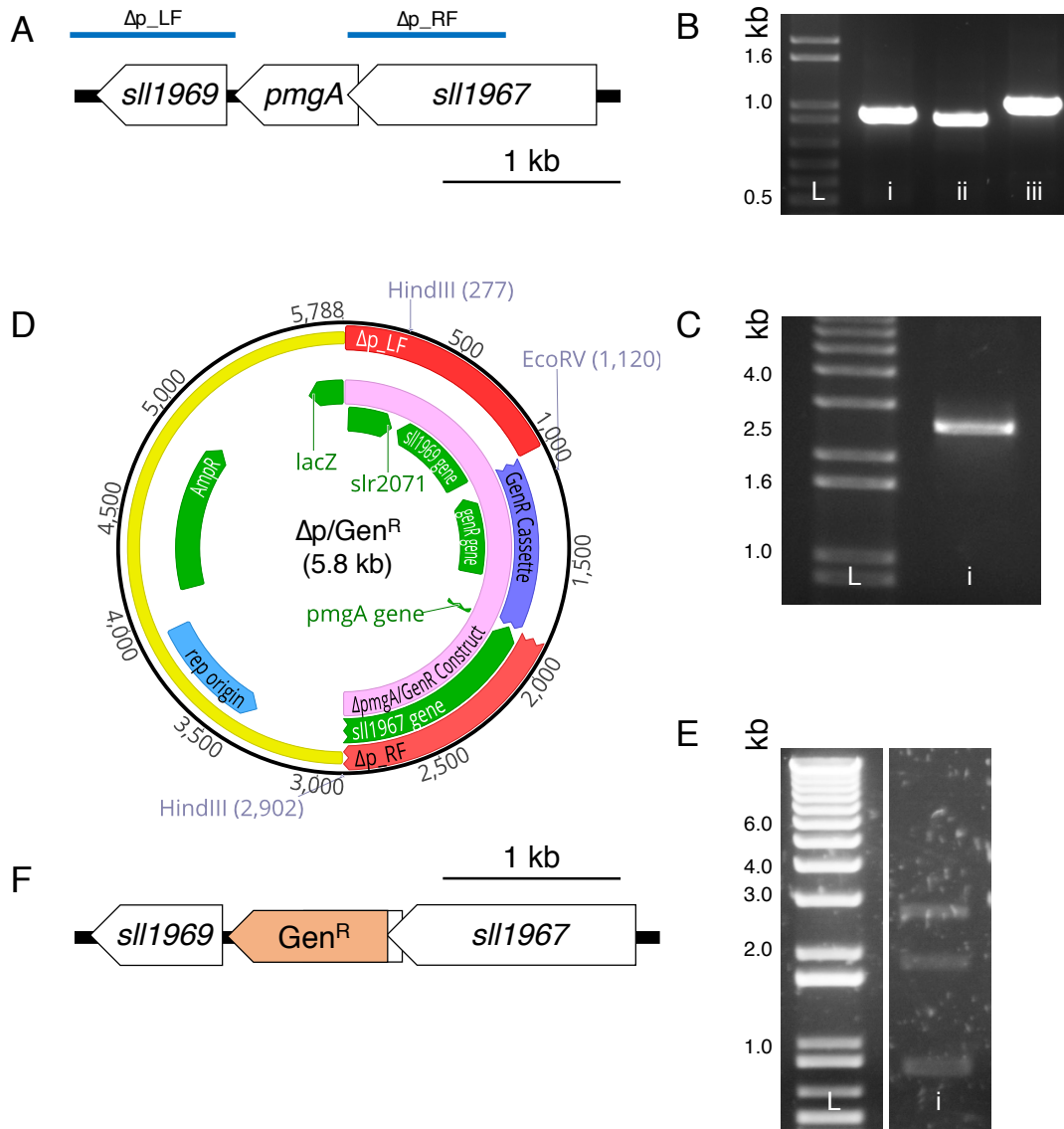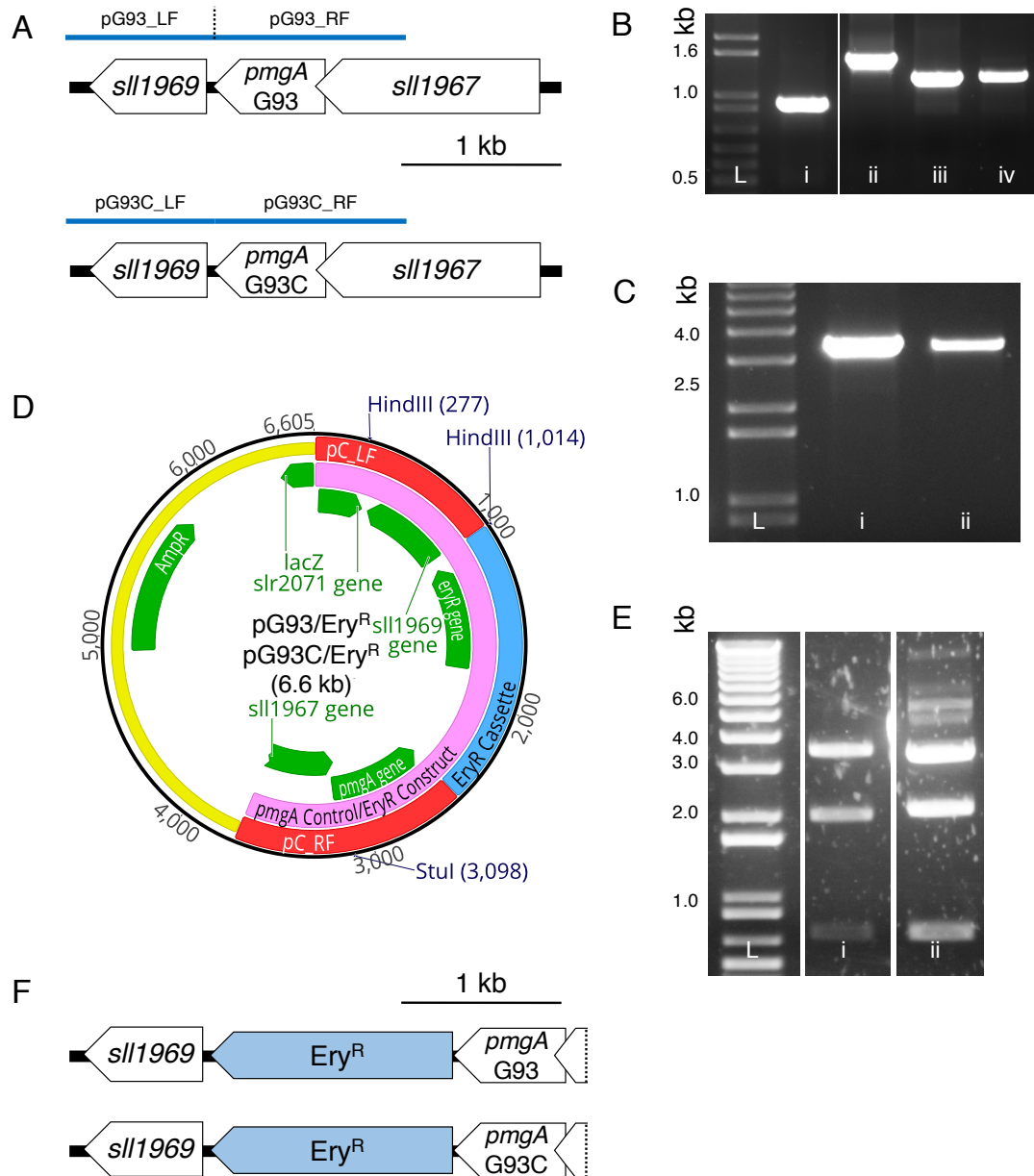Figure 4.5. Construction of a *pmgA* control plasmid and a *pmgA* G93C plasmid by overlap-extension PCR for introduction into *Synechocystis* 6803. A: depiction of the genomic region of *pmgA* in the GT-O1 wild-type, and the G93C encoding copy from the pseudorevertant, with the location of the left flank (LF) and right flank (RF) regions used to generate the PCR construct shown in blue. B: PCR amplification of overlap-extension PCR components; i – left flank (amplified from GT-O1), ii – Ery^R cassette (amplified from lab plasmid stocks), iii – pG93 right flank (from GT-O1), iv – pG93C right flank (from the pseudorevertant). C: single PCR product for pG93 and pG93C insert generated by amplification of PCR products (from B, pG93 = i + ii + iii, pG93C = i + ii + iv) with internal primers. D: map of *pmgA* Control/Ery^R (pG93/Ery^R) plasmid and *pmgA* G93C/Ery^R (pG93C/ Ery^R) plasmid generated by ligation of

PCR product (from B) into the pGEM-T Easy plasmid, which was transformed into *E. coli* and mini-prepped. E: HindIII/StuI digestion of plasmid DNA from pG93 (i) and pG93C (ii), confirming appropriate insert size. F: depiction of the *pmgA* genomic region of *Synechocystis* 6803 following transformation with the pG93 or pG93C plasmid. (B, C, E: L = 1 kb$^+$ DNA ladder, used to estimate amplicon sizes).

4.3.1.3   Other strategies to introduce the pseudorevertant mutation into the ΔPsbO:ΔPsbU mutant

Since the strategies described above were unsuccessful in obtaining the desired mutants, other strategies were employed. It is important to note that *pmgA* mutagenesis strategies to attempt to alter pH-sensitivity in the Con:ΔPsbO:ΔPsbU and pseudorevertant strains were restricted by antibiotic resistance genes already inserted into these strains during prior mutant construction. Although Gen^R and Ery^R cassettes appear to be less widely-used in mutagenesis of *Synechocystis* 6803, and did not result in the desired transformants, few options were available for transformation of these Kan^R, Spec^R, and Cam^R strains. While other ΔPsbO:ΔPsbU strains were available (for example, those created with 'markerless' deletions), which might have permitted use of other antibiotic-resistance cassettes, the *pmgA* candidate mutation occurred in the Con:ΔPsbO:ΔPsbU background, with its associated (and uncharacterised) background mutations (SNPs in *rre2*, intergenic region *petH-prk*), which could in theory complement the *pmgA* mutation's ability to restore pH 7.5 growth.

In order to address the broader question of whether a PmgA G93C change is sufficient to restore pH 7.5 growth in any ΔPsbO:ΔPsbU strain, additional mutagenesis strategies employing a ΔPsbO:ΔPsbU (Kan^R & Cam^R) strain, produced in the GT-O1 background and obtained from lab freezer stocks, were used (the GT-O1 background was confirmed by Sanger sequencing, not shown). Introduction of a pΔ*pmgA* deletion plasmid provided by Y Hihara into this strain produced a non-segregated partial deletion strain (Fig. 4.7), similar to the Con:ΔPsbO:ΔPsbU:Δp transformant, supporting the theory that *pmgA* might be essential to this strain. While the pΔ*pmgA* plasmid has produced successful Δ*pmgA* strains when transformed in the GT-I wild-type background, and possibly other GT- backgrounds (e.g. Hihara and Ikeuchi, 1997; De Porcellinis et al., 2016), oddly, it did not yield segregated colonies in the GT-O1 background (Fig. 4.7). When the ΔPsbO:ΔPsbU:pΔ*pmgA* partial deletion strain was

transformed with the pG93 or pG93C plasmid, segregated colonies were obtained, but Sanger sequencing (not shown) revealed that the wild-type *pmgA* copy was retained in all cases, including in four independently segregated cultures of the ΔPsbO:ΔPsbU:pΔ*pmgA* strain transformed with the pG93C plasmid.

Since *pmgA* deletion in ΔPsbO:ΔPsbU backgrounds was problematic, a final strategy was employed. This attempted to introduce either native or G93C-encoding *pmgA* to a neutral site in the *Synechocystis* 6803 genome, allowing subsequent deletion of the gene in its native site and sole expression of the remaining, desired gene copy. PCR primers were designed to amplify *pmgA* from both GT-O1 and the pseudorevertant with synthetic HindIII sites at the 5' and 3' end of the PCR product. These PCR products were HindIII digested and ligated separately into HindIII-digested pΔ*slr0168*/Spec^R plasmids (Crawford et al., 2016) that contain a unique HindIII site adjacent to the Spec^R cassette. DNA from *pmgA* was amplified from the GT-O1 wild type and successfully ligated into this plasmid, which was then used to transform competent *E. coli* cells. Plasmid DNA isolated by miniprep from these cells was introduced into GT-O1 cells, yielding a segregated mutant containing the *pmgA* complementation at the *slr0168* site (Appendix Fig. A5). However, ligation of the G93C copy into the pΔ*slr0168*/Spec^R plasmid was unsuccessful, and this strategy was not pursued further.
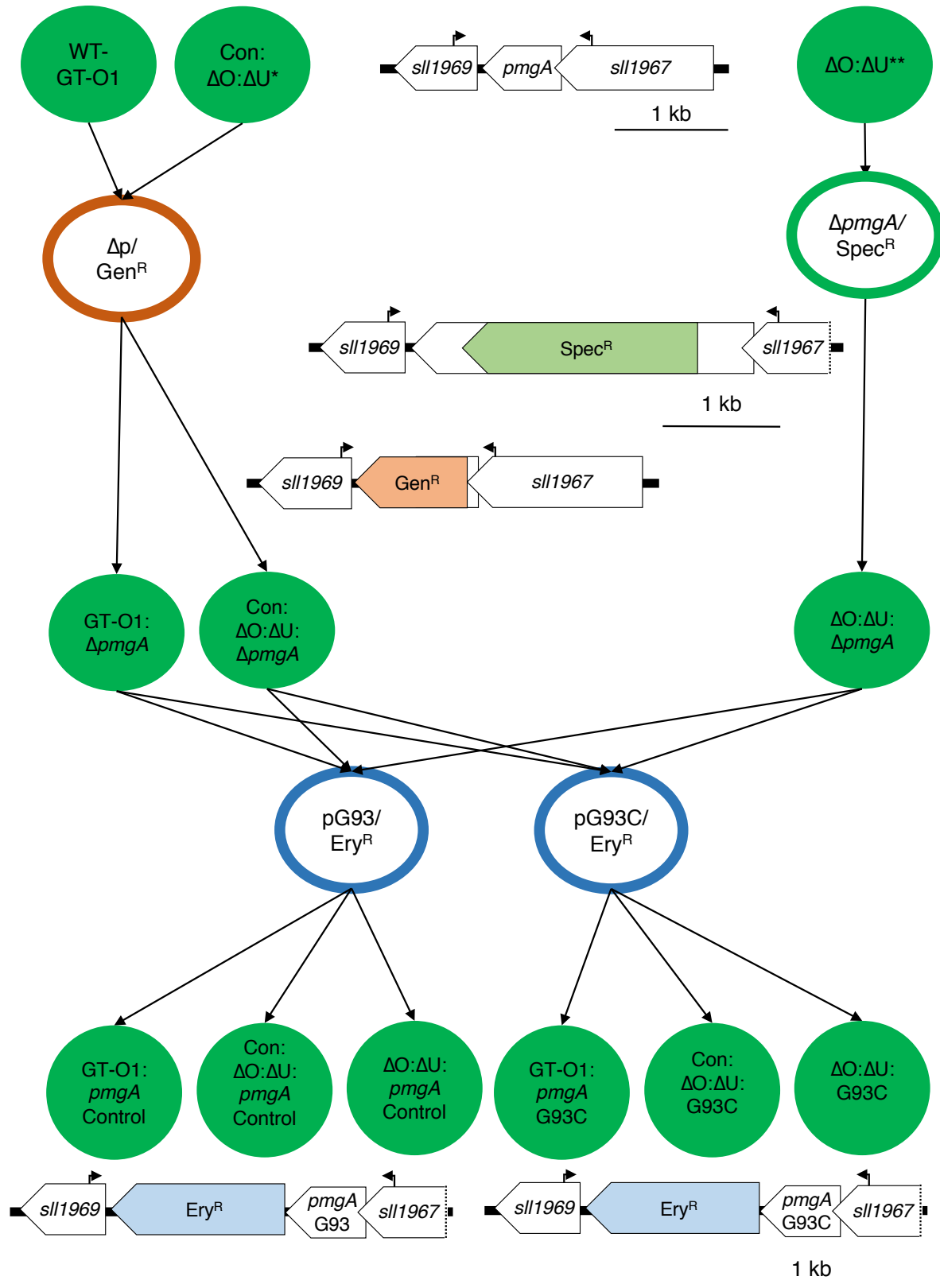
Figure 4.6. Summary of two attempted *Synechocystis* 6803 mutation strategies to insert the pseudorevertant *pmgA* gene copy into the GT-O1, Con:ΔPsbO:ΔPsbU (Con:ΔO:ΔU), and ΔPsbO:ΔPsbU (ΔO:ΔU) strains. Differing antibiotic resistance in the otherwise analogous Con:ΔPsbO:ΔPsbU and ΔPsbO:ΔPsbU strains presented the opportunity to use two *pmgA*

deletion strategies. The *pmgA* gene region is depicted top centre. In a first mutation step, GT-O1 and Con:ΔPsbO:ΔPsbU were transformed using the Δp plasmid, and the ΔPsbO:ΔPsbU strain was transformed by a pΔ*pmgA* plasmid provided by Y Hihara. Subsequently, mutated strains were transformed with pG93 or pG93C plasmids, to re-insert either the native or pseudorevertant (G93C) gene copy respectively into the native *pmgA* site, displacing the original mutation and Gen[R] cassette insertion. Arrows represent the binding site for primers used for mutant sequencing (see Fig. 4.7).

Not shown in this figure: GT-O1, Con:ΔPsbO:ΔPsbU, and ΔPsbO:ΔPsbU cells were also transformed directly with the pG93 and pG93C plasmid, and GT-O1 was also transformed using the pΔ*pmgA*/Spec[R] plasmid. Attempts to transform the pseudorevertant with the Δp, pC, and pG93C plasmid did not yield cell colonies, and this strain may be non-competent for transformation. Sanger sequencing revealed that no mutagenesis strategy used in this study yielded any strain showing the G93C *pmgA* copy.
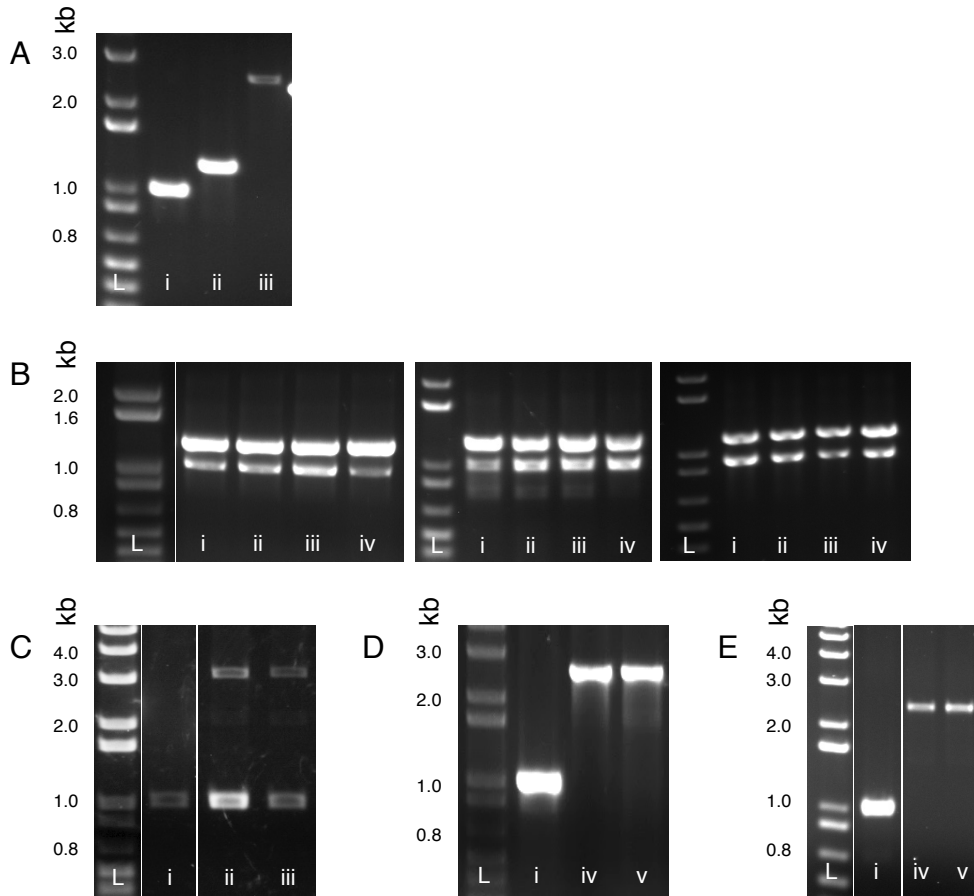
Figure 4.7. PCR analysis of *Synechocystis* 6803 strains transformed with Δp, pG93, pG93C and pΔ*pmgA*/Spec^R plasmids. A: Confirmation of Δ*pmgA* and *pmgA* Control strains by amplification of *pmgA* from the GT-O1 wild-type (i), GT-O1:Δp (ii) and GT-O1: pG93 (iii) strains. B: Incomplete segregation of Con:ΔPsbO:ΔPsbU:Δp mutants; PCR amplification of *pmgA* from independent mutant cultures (i-iv), showed GT-O1 (~1 kb) and plasmid insert (~1.2 kb) bands following 9, 11 and 17 weeks of culture growth and re-streaking. C: Incomplete segregation of GT-O1:pΔ*pmgA*/Spec^R (ii) and ΔPsbO:ΔPsbU:pΔ*pmgA*/Spec^R (ii) mutants revealed by PCR amplification of *pmgA* from GT-O1 (i) and mutant cultures (ii-iii), showing GT-O1 (~1 kb) and plasmid insert (~3.1 kb) bands in mutants following ~20 weeks of culture growth and re-streaking. D: Confirmation of Con:ΔPsbO:ΔPsbU:Δ*pmgA:pmgA* Control and apparent Con:ΔPsbO:ΔPsbU:Δ*pmgA:pmgA* G93C* strains, following PCR amplification of *pmgA* from GT-O1 (i), Con:ΔPsbO:ΔPsbU:Δp:pG93 cells (ii), and Con:ΔPsbO:ΔPsbU:Δp:pG93C* cells (iii). E: PCR amplification of *pmgA* from GT-O1 (i), ΔPsbO:ΔPsbU:pΔ*pmgA*/Spec^R:pC cells (ii), and ΔPsbO:ΔPsbU:pΔ*pmgA*/Spec^R:pG93C* cells (iii). L – 1 kb$^+$ DNA ladder, used to estimate amplicon sizes. *Sanger sequencing (not shown) revealed that the wild-type *pmgA* copy was retained in these mutants, rather than insertion of the G93C copy, despite repeated, independent transformation attempts.

4.3.2 Characterisation of *pmgA* mutants

Although neither Con:ΔPsbO:ΔPsbU cells transformed with the pG93C plasmid strain, nor a pseudorevertant strain transformed with a pG93 plasmid strain were successfully obtained in this study, several *pmgA* mutants were briefly characterised in order to assess their growth. GT-O1 cells transformed with the pG93 plasmid (*pmgA* Control strain) and the Δp plasmid (Δ*pmgA* strain) grew similarly to GT-O1 cells in photoautotrophic conditions at pH 7.5 and pH 10.0 (Fig. 4.8). In a high light (~200 μE.m^{-2}.s^{-1}) experiment, the three strains grew similarly in unbuffered BG-11 media, although GT-O1 cells initially grew faster.

A Con:ΔPsbO:ΔPsbU:*pmgA* Control strain was obtained when the pG93 plasmid was introduced into the partially-segregated Con:ΔPsbO:ΔPsbU:Δ*pmgA* strain. This strain grew similarly to Con:ΔPsbO:ΔPsbU cells (Fig. 4.9), and thus was non-autotrophic at pH 7.5 and autotrophic at pH 10.0; pseudorevertant cells were autotrophic at both pH levels.
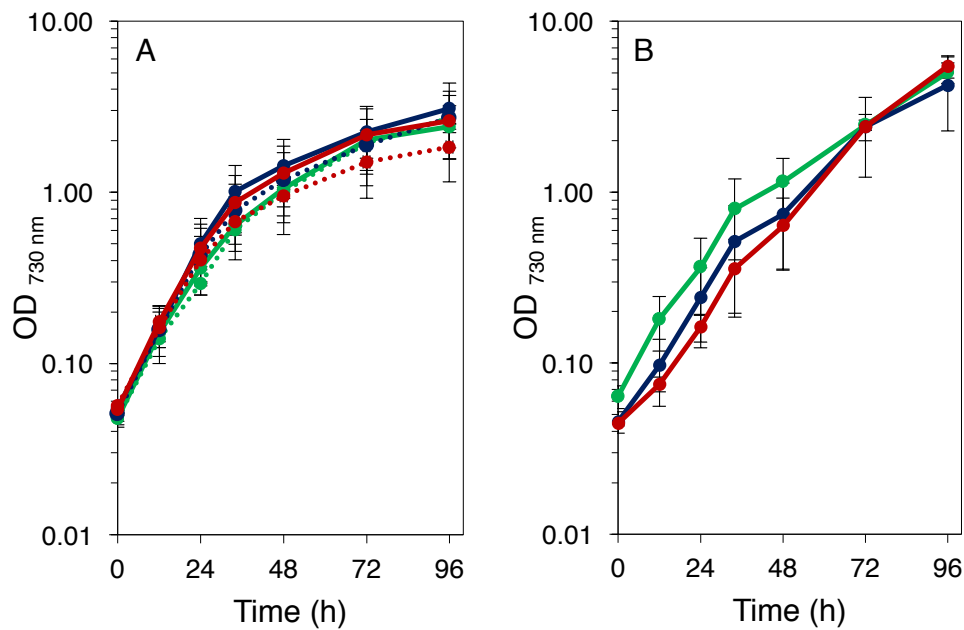
Figure 4.8. Photoautotrophic growth of Δ*pmgA* and *pmgA* Control mutant substrains in standard and high light conditions. GT-O1 wild type (green), Δ*pmgA* (blue), and *pmgA* Control (red) cells were grown in standard (A, ~40 μE.m^{-2}.s^{-1}) and high-light (B, ~200 μE.m^{-2}.s^{-1}) conditions. Dotted lines in A represent cultures grown in pH 7.5-buffered BG-11 media, solid lines in A and B represent cultures in unbuffered media, *n* = 2-3, error bars represent SEM.
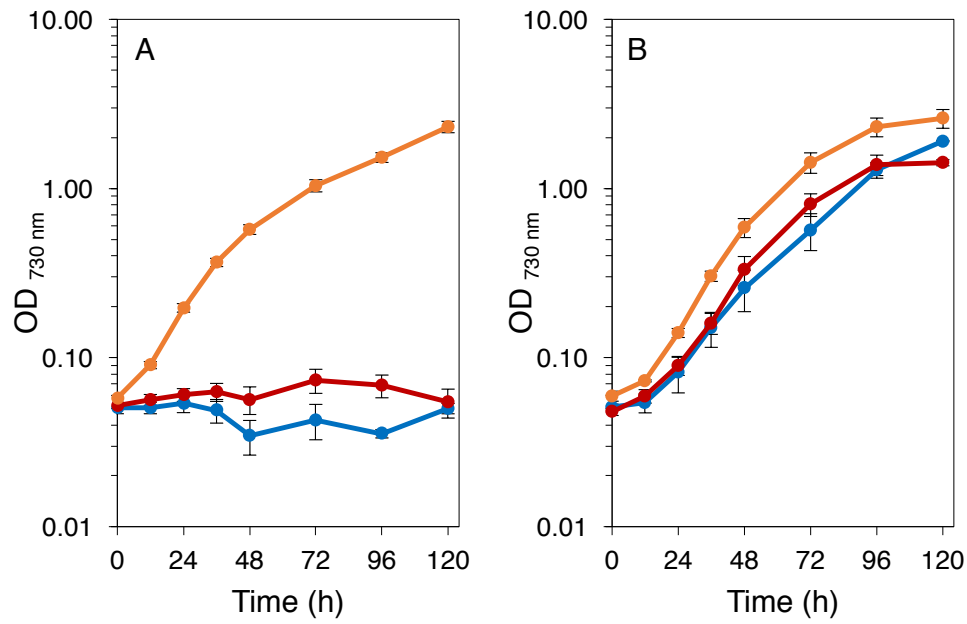
Figure 4.9. Photoautotrophic growth of mutant substrains at different pH levels. Con:ΔPsbO:ΔPsbU (blue), pseudorevertant (orange), and Con:ΔPsbO:ΔPsbU:*pmgA* Control (red) cells were grown in pH 7.5-buffered BG-11 media (A) and pH 10.0-buffered media (B), *n* = 3-4, error bars represent SEM. The Con:ΔPsbO:ΔPsbU:*pmgA* Control strain was obtained when the pG93 plasmid was introduced into the partially-segregated Con:ΔPsbO:ΔPsbU:Δ*pmgA* strain, but a Con:ΔPsbO:ΔPsbU:*pmgA* G93C strain was unable to be obtained.

4.4 Ci enrichment allows low pH growth of PS II mutants

4.4.1 Ci enrichment allows low pH growth of Con:ΔPsbO:ΔPsbU cells

The inability to conclusively establish that the *pmgA* mutation in the pseudorevertant was the mutation allowing pH 7.5 growth prompted investigation of indirect evidence for this hypothesis. It was noted that PmgA has a role in induction of the CUP component NdhF3, and two studies have shown that PmgA deletion frequently leads to the occurrence of mutations in *ndhF3*, and expression of this gene is impaired (Haimovich-Dayan et al., 2011; Nishijima et al., 2015). If the Gly93 to Cys PmgA mutation results in gain-of-function or loss-of-function of the protein, then induction or repression of carbon uptake might occur. This would be more relevant at pH 7.5, when CUP is more important than at pH 10.0 where HCO_3^- uptake occurs. For example, if PmgA is an anti-sigma factor as suggested (Sakuragi, 2006), an alteration in its conformation and loss-of-function might cause de-repression of gene expression in a downstream target, such as NdhF3. Subsequently, the photoautotrophic growth of GT-O1, Con:ΔPsbO:ΔPsbU, and pseudorevertant cells at pH ~7.5 in ambient (~0.04%) and enriched (3%) CO_2 was determined (Fig. 4.10). GT-O1 and pseudorevertant cells were insensitive to the CO_2 enhancement, and grew similarly to each other in ambient and enriched CO_2. Con:ΔPsbO:ΔPsbU cells were found to be photoautotrophic in 3% CO_2, despite the reduction of the pH to ~7.1, although the growth rate was reduced compared to the pseudorevertant.

In a photoautotrophic growth selection assay, GT-O1, Con:ΔPsbO:ΔPsbU and pseudorevertant cells were spotted at OD $_{730\ nm}$ 1.0, 0.1, and 0.01 onto pH 7.5, 8.0, 8.5 and 9.0 BG-11 plates and grown over 4 days in ambient and enriched CO_2 (as above); ambient CO_2 plates were duplicated and incubated at ambient light (50 $\mu E.m^{-2}.s^{-1}$) or low light (20 $\mu E.m^{-2}.s^{-1}$) to investigate the effect of light and pH (Fig 4.11). GT-O1 and pseudorevertant cells were photoautotrophic in all conditions, although growth rate was enhanced by increased pH (8.5-9.0) in pseudorevertant cells in low light. Con:ΔPsbO:ΔPsbU cells were photoautotrophic only in enriched CO_2 or in ambient CO_2 at pH 8.5 or 9.0. Growth was reduced compared to the pseudorevertant in ambient CO_2, but was similar in enriched CO_2. These results put the pH-cut-off for autotrophic growth of the Con:ΔPsbO:ΔPsbU strain at pH 8.0-8.5, roughly the pH at which CUP is limited by near zero equilibrium concentrations of CO_2/H_2CO_3 (see Chapter One, Fig. 1.7).
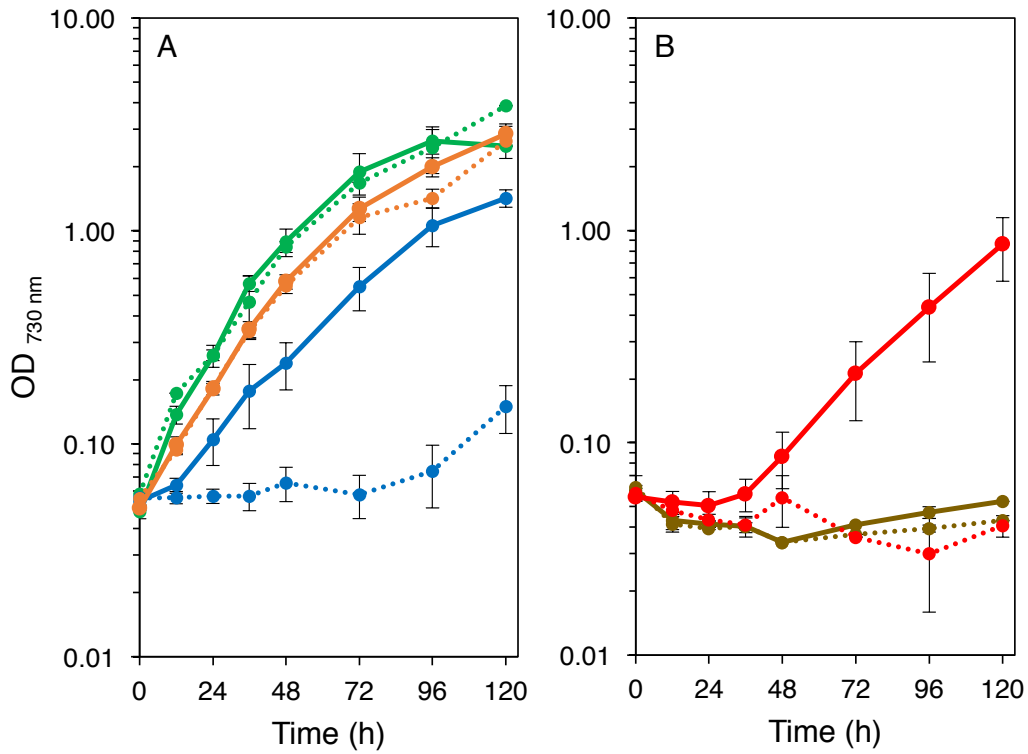
Figure 4.10. Photoautotrophic growth at pH ~7.5 of *Synechocystis* 6803 strains in enriched CO_2 (3%, solid lines) and ambient CO_2 (~0.04%, dotted lines). A: growth of GT-O1 (green), Con:ΔPsbO:ΔPsbU (blue) and pseudorevertant (orange) cells. B: growth of Con:ΔPsbO:ΔPsbV cells (brown) and ΔPsbV:ΔCyanoQ cells (red). Error bars represent SEM (A: *n* = 6-8, B: *n* = 2-4).
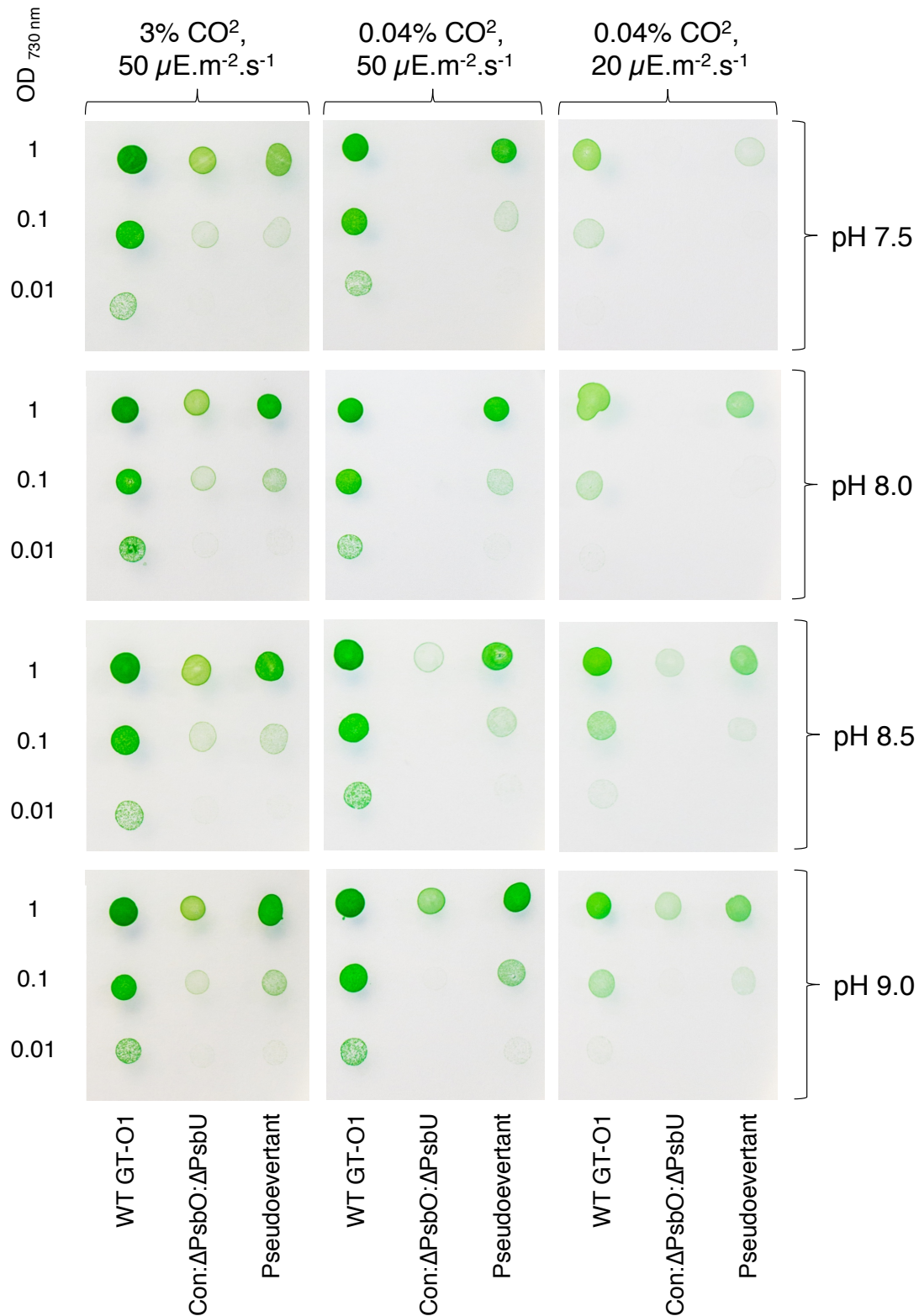
Figure 4.11. Photoautotrophic growth on BG-11 agar at pH 7.5-9.0 of the *Synechocystis* 6803 GT-O1 wild-type, and Con:ΔPsbO:ΔPsbU and pseudorevertant mutants, in enriched CO_2 (3%) and ambient CO_2 (~0.04%) at ~50 µE.m^{-2}.s^{-1} light, and ambient CO_2 conditions at ~20 µE.m^{-2}.s^{-1} light. Cells were inoculated onto the BG-11 plate at an OD $_{730 nm}$ of 1.0, 0.1, or 0.01 and incubated for four days.

4.4.2 Ci enrichment allows low pH growth of other pH-sensitive PS II mutants

It was also found that enriched CO_2 (as above) permitted pH ~7.5 growth in ΔPsbV:ΔCyanoQ cells (Fig 4.10), which like Con:ΔPsbO:ΔPsbU, display the pH-sensitive phenotype in ambient CO_2 (Summerfield et al., 2005a). Growth was reduced compared to Con:ΔPsbO:ΔPsbU cells, and followed a ~48 h growth lag; however, this result was reproducible. Growth of the non-pH-sensitive, non-autotrophic Con:ΔPsbO:ΔPsbV strain was unaffected by CO_2, with no growth in ambient or enriched CO_2 conditions.

Although 3% CO_2 appears to be sufficient to support cells lacking CUP (Zhang et al., 2004), the possibility that a reduction in CUP components might reverse the effect of enriched CO_2 was tested in a ΔPsbV:ΔCyanoQ mutant (the GT-O1 background of this strain was confirmed by Sanger sequencing, not shown) and a ΔPsbV:ΔCyanoQ strain transformed with a pΔ*ndhF3* plasmid (Ohkawa et al., 2000a) gifted by Y Hihara (Fig. 4.12). Mutant strains were grown in a photoautotrophic growth selection assay (as described above, Fig 4.13), along with GT-O1 and GT-O1:Δ*ndhF3* cells (GT-O1:Δ*ndhF3*, hereafter ΔNdhF3; this strain was also produced in this study using the same plasmid). Growth of the ΔNdhF3 strain was identical to wild-type GT-O1 in all conditions tested. Neither the ΔPsbV:ΔCyanoQ strain, nor ΔPsbV:ΔCyanoQ:ΔNdhF3 were autotrophic in ambient CO_2 at any pH level, with the exception of limited growth in ΔPsbV:ΔCyanoQ cells at pH 9.0 in low light. This result is in line with substantial prior evidence that increased light reduces growth of PS II mutants (see Bricker et al., 2012), further supporting the hypothesis that photoinhibition due to ROS might play a role in pH-sensitivity.

Unlike Con:ΔPsbO:ΔPsbU cells, which grew similarly in enriched CO_2 at all pH levels tested, ΔPsbV:ΔCyanoQ cell growth was reduced at pH 9.0, but was similar at pH 7.5-8.5. The ΔPsbV:ΔCyanoQ:ΔNdhF3 mutant was capable of limited growth at pH 7.5-8.5, but was impaired in growth compared to the ΔPsbV:ΔCyanoQ strain and was unable to grow at pH 9.0 at 3% CO_2.
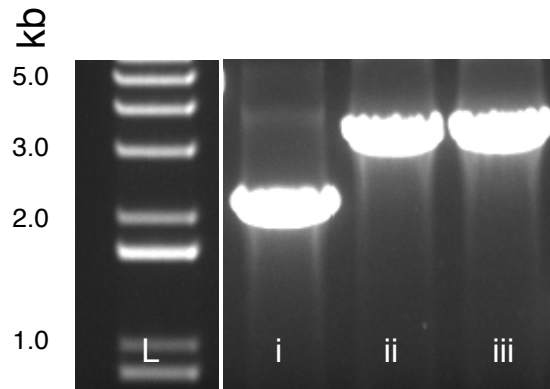
Figure 4.12. PCR amplification of the *ndhF3* gene region of *Synechocystis* 6803 from GT-O1 (i), ΔNdhF3 (ii), and ΔPsbV:ΔCyanoQ:ΔNdhF3 (iii) substrain DNA; the latter two substrains were transformed with a pΔ*ndhF3* plasmid, and segregation of the mutants is evident from the sole presence of the insert (3.2 kb) band, with no trace of the wild-type (2.0 kb) band. L = 1 kb$^+$ DNA ladder.
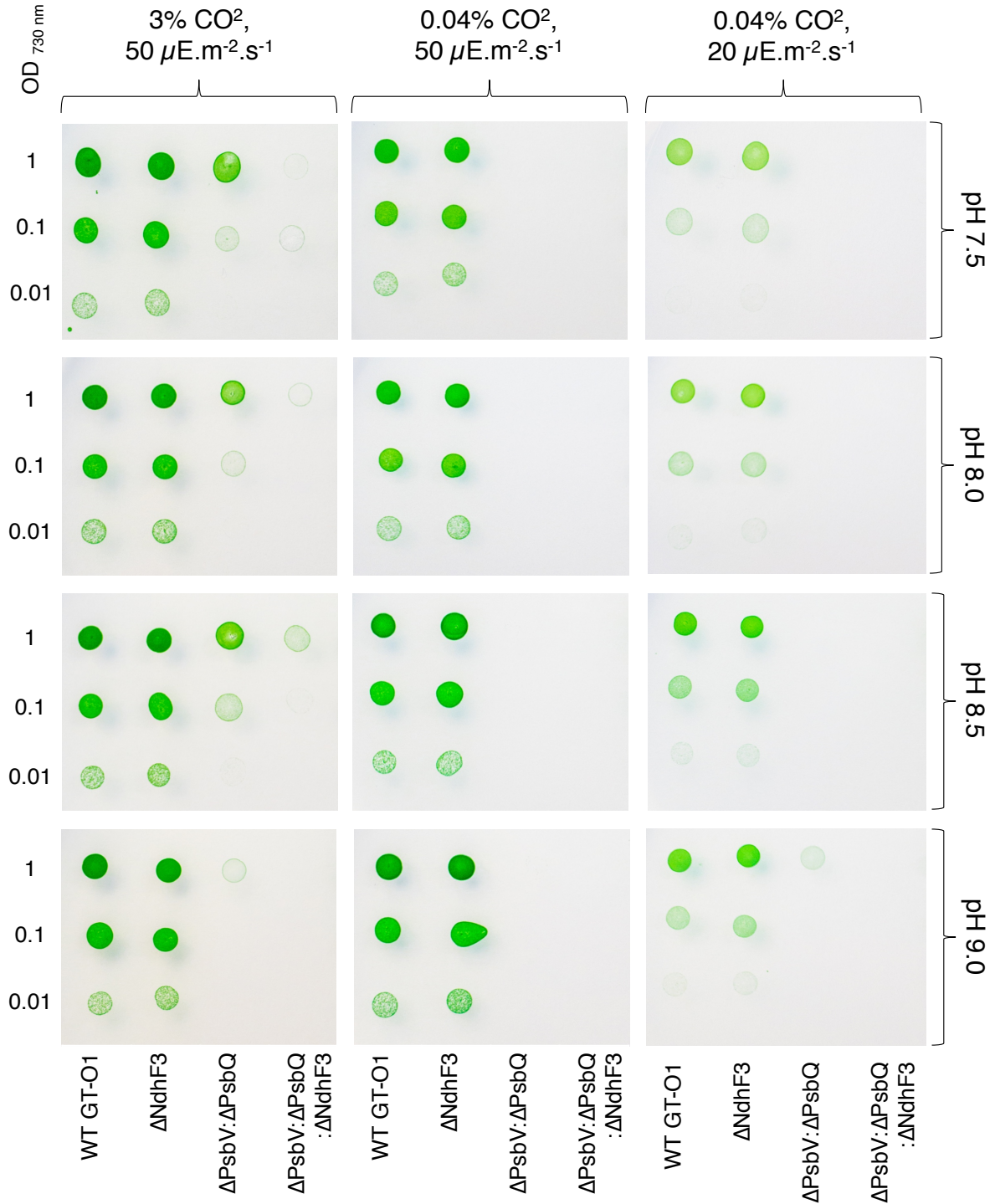
Figure 4.13. Photoautotrophic growth on BG-11 agar at pH 7.5-9.0 of the *Synechocystis* 6803 GT-O1 wild type, and ΔNdhF3, ΔPsbV:ΔCyanoQ, and ΔPsbV:ΔCyanoQ:ΔNdhF3 mutants, in enriched CO_2 (3%) and ambient CO_2 (~0.04%) at ~50 $\mu E.m^{-2}.s^{-1}$ light, and ambient CO_2 conditions at ~20 $\mu E.m^{-2}.s^{-1}$ light. Cells were inoculated onto the BG-11 plate at an OD $_{730\ nm}$ of 1.0, 0.1, or 0.01 and incubated for four days.

4.5 Investigating differences between the Con:ΔPsbO:ΔPsbU and pseudorevertant strains

4.5.1 General responses of Con:ΔPsbO:ΔPsbU and pseudorevertant cells to pH

Several aspects of the pH 7.5/pH 10.0 response of Con:ΔPsbO:ΔPsbU and pseudorevertant cells have been previously published. Eaton-Rye et al. (2003) showed increased PS II assembly and steady-state oxygen evolution in Con:ΔPsbO:ΔPsbU cells grown in heterotrophic conditions at pH 10.0 compared to pH 7.5, in line with photoautotrophic growth rate. Summerfield et al. (2007) established that the PS II level and the PS II-dependent steady-state oxygen evolution rate between Con:ΔPsbO:ΔPsbU and pseudorevertant cells are similar between strains at pH 7.5 (~1/2 of wild-type GT-O1). That study also investigated transcript-level gene regulation changes in Con:ΔPsbO:ΔPsbU and pseudorevertant cells grown initially in autotrophic conditions at pH 10.0, then subjected to 2 h growth at pH 7.5. A subsequent study investigated several aspects of pH 7.5 and pH 10.0 growth between strains in photoheterotrophic conditions (Summerfield et al., 2013), which revealed a range of differences between the strains. Low-temperature fluorescence of the Con:ΔPsbO:ΔPsbU and pseudorevertant strains suggested improved PBS coupling at pH 10.0 compared to pH 7.5 in both mutants, and improved PBS coupling overall in the pseudorevertant. Whereas growth of the Con:ΔPsbO:ΔPsbU strain was minimally affected by the presence of the $^1O_2$ sensitiser Rose Bengal at pH 10.0, and growth at pH 7.5 was not possible, the pseudorevertant was sensitive to Rose Bengal at both pH 7.5 and 10.0. These findings primarily investigated either the short-term (~2 h) effect of pH 7.5 autotrophic growth, or mid-long-term (~24 h) effects of pH 7.5 heterotrophic/mixotrophic growth in cells initially raised in pH 7.5/mixotrophic conditions, where acclimation to pH and/or trophic condition might be expected. Subsequently, this study aimed to investigate mid-long-term (24 h) responses in autotrophic conditions in cells already raised in pH 10.0/autotrophic conditions, to eliminate trophic acclimation and look exclusively at pH-related changes. In addition, measurements of photosynthetic $^1O_2$ production and PS I P_{700} oxidation kinetics were made following a short (2 h) incubation at pH 7.5 and 10.0.
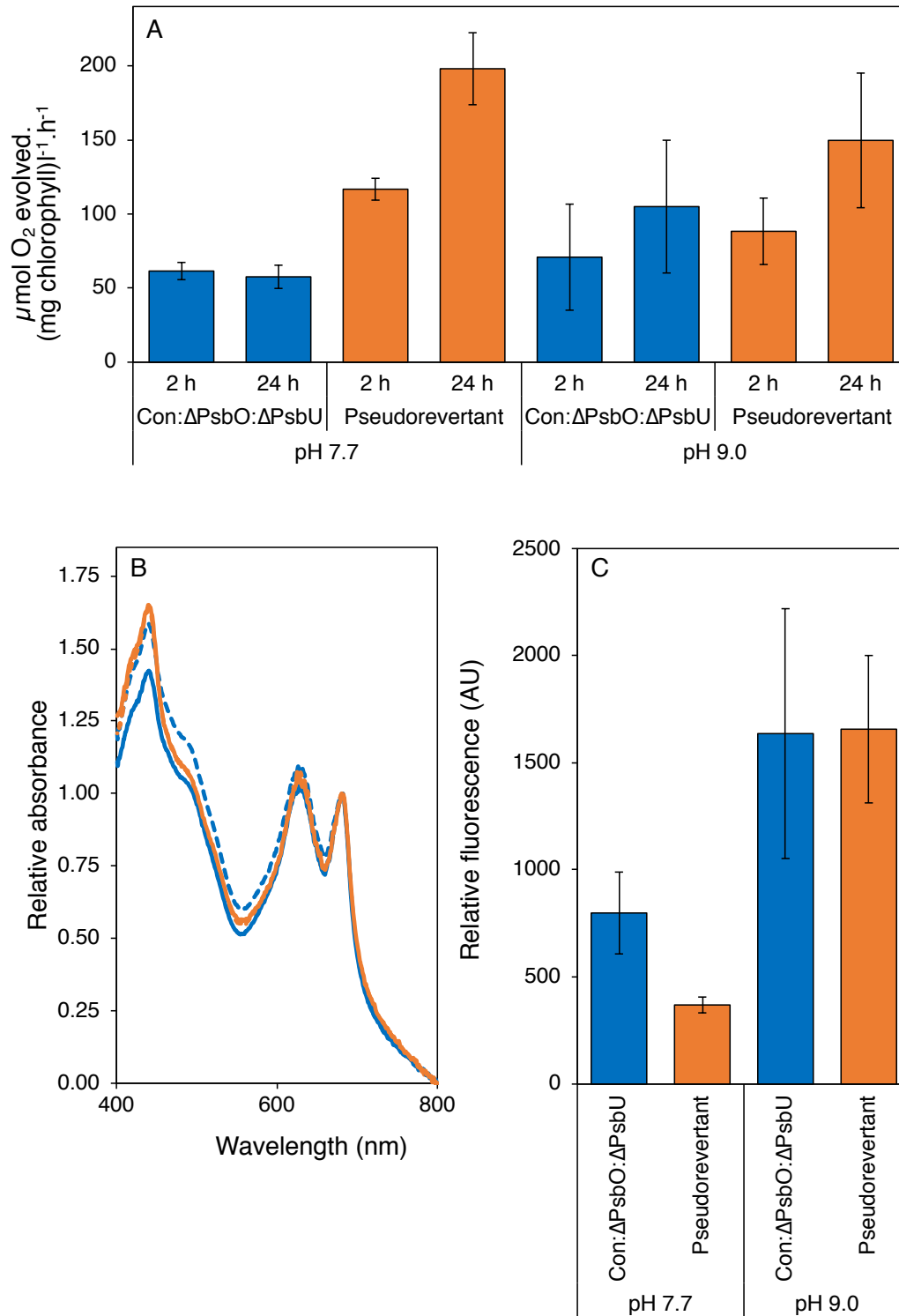
Figure 4.14. Physiological analyses of the Con:ΔPsbO:ΔPsbU and pseudorevertant mutants incubated for 24 h in photoautotrophic conditions in pH 7.7- or pH 9.0-buffered BG-11 media (Con:ΔPsbO:ΔPsbU: blue, pseudorevertant: orange). A: Maximum oxygen evolution rate after 2 h and 24 h in cells measured in the presence of the electron acceptor DMBQ (mean ± SEM, n = 2-4). B: whole-cell absorption spectra following pH 7.7 (dotted lines) or pH 9.0 (solid lines)

incubation. Traces represent the mean of 3-4 independent measurements and are normalised to the chlorophyll absorption maxima at 685 nm. C: fluorescence of the ROS probe CM-H_2DCFDA in cells following 24 h incubation and 30 min incubation in the presence of the probe (mean ± SEM, *n* = 3-5).

4.5.2 Responses of Con:ΔPsbO:ΔPsbU and pseudorevertant cells to 24 h pH 7.7 incubation

In a pH incubation experiment, Con:ΔPsbO:ΔPsbU and pseudorevertant cells were grown in pH 7.7- and pH 9.0-buffered BG-11 without glucose in standard conditions for 24 h. Use of the same 25 mM TAPS-NaOH buffer at both pH levels was intended to minimise any possible between-buffer effects, which was considered particularly important for a fluorescence-based ROS-assay. In a preliminary experiment, the standard BG-11 pH buffers (25 mM HEPES-NaOH pH 7.5 and 25 mM CAPS-NaOH pH 10.0) displayed altered fluorescence emission in the absence of cells and presence of the ROS probe (data not shown). BG-11 buffered with TAPS-NaOH also displayed a somewhat variable pH-dependent fluorescence that could not be explained (in the absence of cells and presence of the probe, data not shown). Subsequently, it seems reasonable to make ROS comparisons between *Synechocystis* 6803 substrains using this probe, but between-pH comparisons might be problematic.

PS II-dependent oxygen evolution in the presence of the artificial electron acceptor DMBQ was increased at 24 h compared to 2 h, at both pH 7.7 and 9.0, except in the Con:ΔPsbO:ΔPsbU strain at pH 7.7 (Fig. 4.14A). Pseudorevertant cells displayed a higher oxygen evolution rate at pH 7.7 than Con:ΔPsbO:ΔPsbU cells at 2 h (256.5 ± 144.3 vs 94.7 ± 29.4 µmol O_2.[mg chlorophyll]$^{-1}$.h^{-1}), but were similar at pH 9.0 (Con:ΔPsbO:ΔPsbU: 126.6 ± 73.1, pseudorevertant: 193.5 ± 95.8 µmol O_2.[mg chlorophyll]$^{-1}$.h^{-1}). By 24 h, pseudorevertant oxygen evolution was higher at pH 7.7 and pH 9.0 (pH 7.7: 241.9 ± 57.5, pH 9.0: 200.2 ± 29.4 µmol O_2.[mg chlorophyll]$^{-1}$.h^{-1}) compared to Con:ΔPsbO:ΔPsbU cells (pH 7.7: 77.0 ± 6.8, pH 9.0: 157.2 ± 8.3 µmol O_2.[mg chlorophyll]$^{-1}$.h^{-1}).

Cellular pigment levels at 24 h, measured by spectrophotometric determination of whole cell absorption, showed that the chlorophyll, carotenoid, and PBS pigments in the pseudorevertant were not affected by pH (Fig. 4.14B). Levels of PBS pigments did not appear to vary

substantially between pH or strain. However, the Con:ΔPsbO:ΔPsbU strain appears to have increased carotenoid levels at pH 7.7, indicated by an increase in the absorbance shoulder at ~500 nm.

Fluorescence from the non-specific ROS probe CM-H$_2$DCFDA was generally increased at pH 9.0 compared to pH 7.7, and was similar in both strains, at pH 9.0 (Fig. 4.14C). As discussed earlier, interpretation of between-pH results might be problematic. However, the pseudorevertant showed a clearly reduced fluorescence signal at pH 7.7, indicating a reduction in ROS production in these cells compared to Con:ΔPsbO:ΔPsbU cells.

Low-temperature fluorescence emission analysis revealed similar results to those reported in mixotrophic conditions (Summerfield et al., 2013), in which reduced fluorescence emission overall broadly indicates improved energy transfer in pseudorevertant PS II compared to Con:ΔPsbO:ΔPsbU PS II. When cells were assayed with a 440 nm excitation wavelength (targeting chlorophyll), PS II fluorescence emission generally dropped from the PS II CP43 and CP47 emitters (685 and 695 nm peaks, normalised to the 725 nm PS I emission peak) from 2 h to 24 h at pH 7.7 and 9.0 in both strains (Fig. 4.15A-B). This suggests a slight adjustment of relative PS II level or PS I over the incubation period. Con:ΔPsbO:ΔPsbU cells at pH 7.7 were an exception: a decrease in 695 nm fluorescence emission relative to 685 nm emission occurred at 24 h. This might indicate impaired PS II assembly and repair, resulting in accumulation of and fluorescence emission at 685 nm from PS II assembly intermediates, such as RC47. Additionally, low-temperature fluorescence emission via PBS were targeted by 580 nm excitation (Fig. 4.15C-D), with data normalised to the ~645 nm C-phycocyanin emission peak. At pH 7.7, fluorescence emission from the PBS terminal emitter ApcE (685 nm) increased in Con:ΔPsbO:ΔPsbU cells between 2 h and 24 h, and although changes in the pseudorevertant were smaller, some apparent increase in PS I level occurred from 2 h to 24 h. At pH 9.0 fluorescence emission from peaks associated with allophycocyanin (667 nm) from and the ApcE emitter dropped somewhat in both Con:ΔPsbO:ΔPsbU and pseudorevertant cells from 2 h to 24 h. In Con:ΔPsbO:ΔPsbU cells, an apparent increase in PS I level occurred during the incubation period, whereas pseudorevertant PS I levels remained similar. Apparent PS I levels were highest in the pseudorevertant strain at pH 7.7 after 24 h.
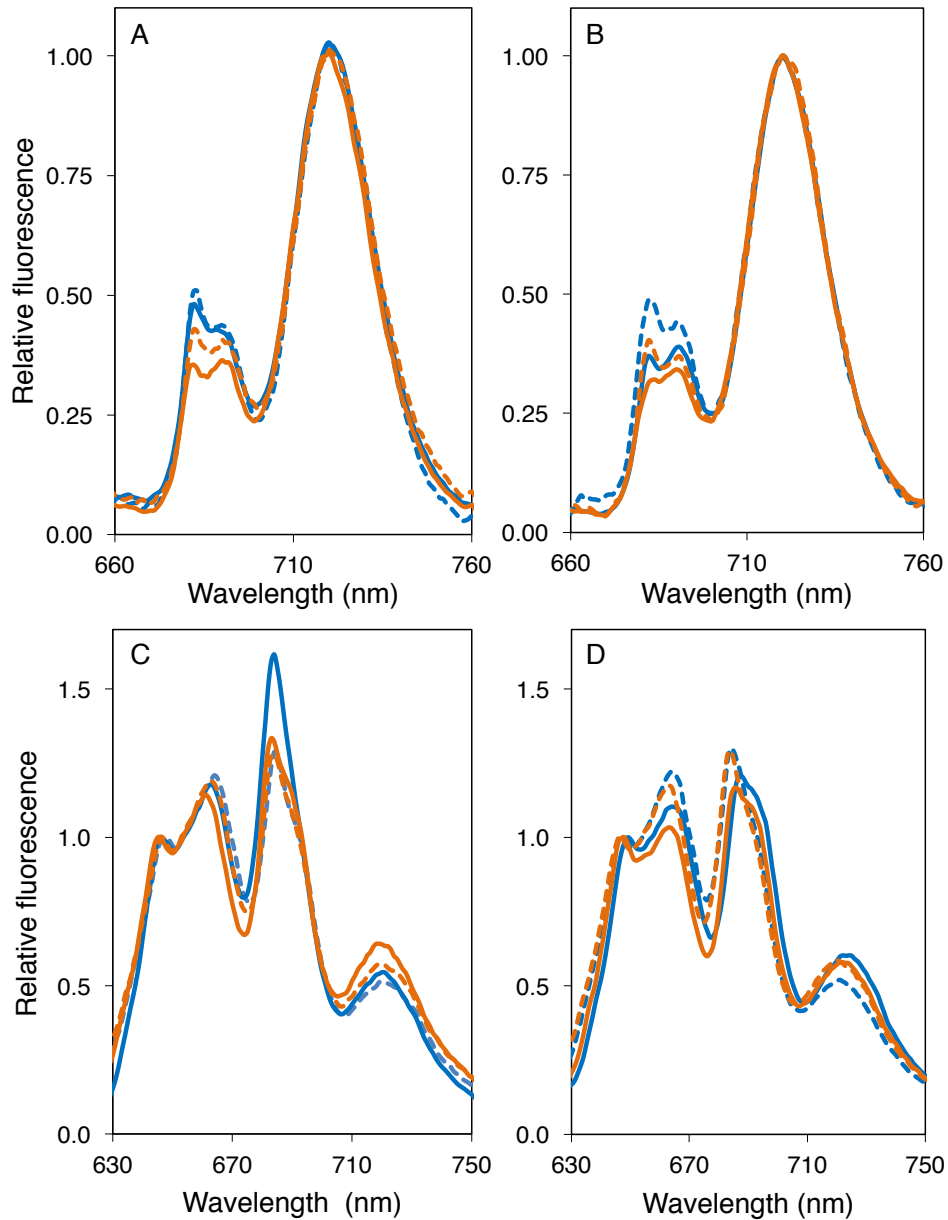
Figure 4.15. Low-temperature fluorescence emission from Con:ΔPsbO:ΔPsbU and pseudorevertant cells incubated for 24 h in photoautotrophic conditions in pH 7.7- (A, C) or pH 9.0-buffered (B, D) BG-11 media (Con:ΔPsbO:ΔPsbU: blue, pseudorevertant: orange). A-B: Fluorescence emission at 440 nm excitation, targeting chlorophyll. C-D: Fluorescence emission at 580 nm excitation, targeting phycobilisomes. Traces represent the mean of 2-4 independent measurements. Dotted lines, fluorescence at 2 h; solid lines, 24 h.

Table 4.2. Thermoluminescence from GT-O1, Con:ΔPsbO:ΔPsbU and pseudorevertant cells. Values of temperature of peak maxima (T_{max}) and peak amplitude (relative, arbitrary units) in the presence of DCMU represent the mean of 2-3 independent measurements ± SEM.

Strain	Q band T_{max} (˚C) (amplitude)	C band T_{max} (˚C) (amplitude)
GT-O1	16.8 ± 0.8 (13420 ± 3688)	54.2 ± 0.7 (3216 ± 499)
Con:ΔPsbO:ΔPsbU	20.9 ± 0.6 (21188 ± 129)	47.9 ± 0.1 (4863 ± 1013)
Pseudorevertant	21.3 ± 0.1 (21653 ± 2368)	48.4 ± 0.4 (6846 ± 47)
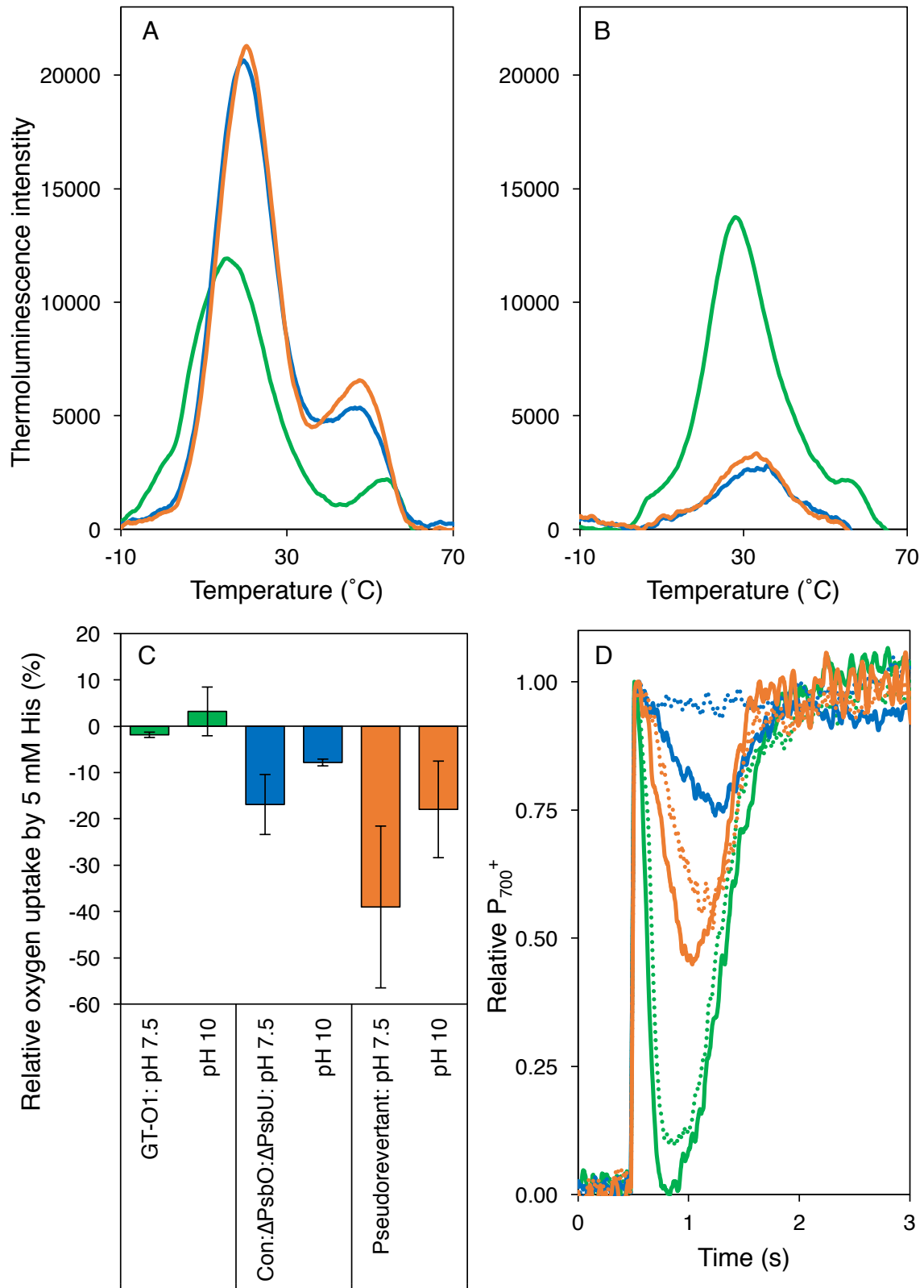
Figure 4.16. Photosynthetic thermoluminescence, oxygen uptake in the presence of histidine (His, His uptake is a proxy for $^1O_2$ production), and P_{700} oxidation in GT-O1, Con:ΔPsbO:ΔPsbU, and pseudorevertant cells (GT-O1: green, Con:ΔPsbO:ΔPsbU: blue, pseudorevertant: orange). A-B: thermoluminescence yield from dark-adapted, mixotrophic-

grown cells assayed in the presence (A) and absence (B) of DCMU. C-D: cells were assayed following 2 h incubation in photoautotrophic conditions in pH 7.5- or pH 10.0-buffered BG-11 media. C: relative oxygen uptake by 5 mM His is a proxy for $^1O_2$ production, due to His-trapping of $^1O_2$. Bars represent the percentage difference in oxygen yield resulting from 5 mM His addition, standardised to the no-His values on each experimental day. D: Relative P_{700}^+ in dark-adapted cells at pH 7.5 (dotted lines) and pH 10.0 (solid lines). Induction of P_{700} oxidation occurs during illumination of cells after 0.5 s. Bars in C (mean, ± SEM) and traces in A, B, & D represent the mean result from 2-3 independent cultures, with 2-3 technical replications per culture, except in D, where only one technical replication was performed.

4.5.3 Comparison of GT-O1, Con:ΔPsbO:ΔPsbU and pseudorevertant cells during 2 h incubation at pH 7.5/pH 10.0

In a pH incubation experiment, GT-O1, Con:ΔPsbO:ΔPsbU and pseudorevertant cells were grown in pH 7.5 and pH 10.0-buffered BG-11 glucose-free media in standard conditions for 2 hours for assessment of $^1O_2$ production, and P_{700} oxidation (indicating electron flow to PS I). Additionally, photosynthetic thermoluminescence in the presence and absence of DCMU was measured in cells raised in permissive pH 7.5 mixotrophic conditions; DCMU occupies the Q_B binding pocket and prevents forward electron transfer from Q_A^-.

Thermoluminescence from photosynthetic membranes (Arnold and Sherwood, 1957) presents the opportunity to investigate charge recombination processes in PS II. Thermoluminescence (TL) is light emission generated by warming irradiated samples, and results from recombination of stable ± charge pairs; warming overcomes activation energy barriers that prevent charge recombination. Freezing samples immediately after illumination minimises recombination and preserves the charge pairs, which allows measurements during progressive warming to reveal different charge pairs in succession by analysis of their temperature-dependent TL bands. TL in PS II typically results from thermally stimulated singlet chlorophylls generated by back reactions in PS II that involve charge recombination via $P_{680}^+Phe^-$ (oxidised RC chlorophyll and reduced Phe; excited P_{680}^* returning to ground state is the TL emitter). In dark-adapted PS II following a single turnover light flash, charge recombination from the $S_2Q_A^-$, $S_2Q_B^-$, and $Y_D^+Q_A^-$ charge pairs generates TL (Sane, 2004; Ducruet and Vass, 2009). In these experiments, TL was measured from cell samples

illuminated with a single-turnover flash at -20°C and heated at 20°C.min⁻¹ from -40°C to 80°C. The photosynthetic TL yield from GT-O1, Con:ΔPsbO:ΔPsbU and pseudorevertant cells revealed minimal TL differences between Con:ΔPsbO:ΔPsbU and pseudorevertant strains; however, these differed markedly from GT-O1 TL (Fig 4.16A-B. In the presence of DCMU, TL was detected from recombination of $S_2Q_A^-$ (so-called 'Q band') at ~20°C, and also from $Y_D^+Q_A^-$ ('C band') at ~50°C. In the absence of DCMU, all strains displayed characteristic 'B' bands (~30 °C) from recombination of $S_2Q_B^-/S_3Q_B^-$ (B_1/B_2 band, referred to collectively as B band hereafter), and a minor contribution from $Y_D^+Q_A^-$ was detectable from GT-O1 only. In the presence of DCMU, Q and C band amplitude was enhanced in Con:ΔPsbO:ΔPsbU and pseudorevertant cells compared to the GT-O1 control (Table 4.2). Fitting of TL curves showed that Q/B and C band amplitudes and peak maxima temperatures (T_{max}) were similar in Con:ΔPsbO:ΔPsbU and pseudorevertant cells, and the T_{max} of Q and C bands in the presence of DCMU was ~4°C higher and ~6 °C lower, respectively, than GT-O1 TL bands. Although fitting of TL curves in the absence of DCMU was impractical due to high signal noise, and low amplitude, it appears that the B-band is upshifted by ~6 °C in Con:ΔPsbO:ΔPsbU and pseudorevertant cells. The increase in B and Q band T_{max} in Con:ΔPsbO:ΔPsbU and pseudorevertant cells likely indicates an increased stability of $S_2Q_B^-/S_2Q_A^-$, requiring greater activation energy to induce charge recombination. In a preliminary experiment (Appendix Fig. A.6). measurement of flash-induced fluorescence decay in the presence of DCMU supported this observation; with increased fluorescence decay times in the presence of DCMU, implying stabilisation of $S_2Q_A^-$. The TL analysis showed a decreased C band T_{max} in Con:ΔPsbO:ΔPsbU and pseudorevertant cells, suggesting destabilised $Y_D^+Q_A^-$ in these mutants compared to the GT-O1 wild type. Generally, the increased amplitude of the Q and +DCMU C band in Con:ΔPsbO:ΔPsbU and pseudorevertant cells indicates an increase in radiative charge recombination pathways (see Chapter One, Sections 1.2.4-1.2.5) in these mutants compared to GT-O1.

PS II-generated $^1O_2$ production results from interaction of ground-state molecular oxygen ($^3O_2$) with triplet chlorophyll generated in aberrant PS II charge recombination. Measurement of $^1O_2$ during oxygen evolution using a Clarke-type electrode can be achieved by addition of histidine (His), which acts as a chemical trap for $^1O_2$ and decreases the electrode signal as oxygen evolved from PS II is converted to $^1O_2$ and trapped by His (Rehman et al., 2013). Following 2 h incubation of GT-O1, Con:ΔPsbO:ΔPsbU, and pseudorevertant cells at pH 7.5 and 10, the percentage reduction in oxygen evolution rate due to the presence of His was calculated (Fig

4.16C). No electron acceptor was used in these measurements. The mean oxygen evolution rate (μmol O_2.(mg chlorophyll).h^{-1}) in the absence of His was: GT-O1, 123 $\pm$ 26 (pH 7.5) and 125 $\pm$ 15 (pH 10.0); Con:ΔPsbO:ΔPsbU, 86 $\pm$ 25 (pH 7.5) and 105 $\pm$ 26 (pH 10.0); and pseudorevertant, 88 $\pm$ 50 (pH 7.5) and 122 $\pm$ 52 (pH 10.0). The reason for the large variation in oxygen evolution in the pseudorevertants strain observed in these measurements is unclear, but could relate to the generally low overall rates (including in GT-O1 cells, see Chapter Three, Section 3.3.3 for comparison), which are presumably due to the lack of artificial electron acceptor. In all three strains, His had a greater effect on oxygen evolution rate at pH 7.5 than 10.0, and was highest in the pseudorevertant cells (39 $\pm$ 17 % reduction in rate at pH 7.5, 18 $\pm$ 10 at pH 10.0), then in Con:ΔPsbO:ΔPsbU cells (17 $\pm$ 6 at pH 7.5, 8 $\pm$ 0.7 at pH 10.0), and lowest (or non-existent) in the GT-O1 wild type (2 $\pm$ 0.6 at pH 7.5, -3 $\pm$ 5 at pH 10.0). The reduction in signal in the presence of His is interpreted to be indicative of the relative production of $^1O_2$. Thus, although $^1O_2$ production may be higher at pH 7.5 than pH 10.0, it appears to be greatest in the pseudorevertant; therefore, production of $^1O_2$ seems unlikely to explain the growth of the pseudorevertant at pH 7.5. It does, however, explain the increased sensitivity of the pseudorevertant to Rose Bengal in another study (Summerfield et al., 2013). However, the lack of a His-mediated effect in the GT-O1 wild type at pH 10.0 is anomalous – it seems likely that some $^1O_2$ would be produced in the assay conditions of ~2.0 $mE.m^{-2}.s^{-1}$ of light, and the low signal observed in this strain at pH 7.5 is much less than the ~10% decline in O_2 yield due to the presence of His seen at pH 7.5 in similar assay conditions in another GT-wild type (Rehman et al., 2013).

Measurement of P_{700} oxidation is a useful tool for investigating relative differences in electron transport reaching PS I. When dark-adapted cells are exposed to actinic light using a Dual-PAM, an increase in the near-infrared absorption signal (A $_{875\,nm}$-A $_{830\,nm}$) occurs, due to rapid reduction of P_{700} (Klughammer and Schreiber, 1994). After ~0.6 s, the signal is quenched by electron flow from PS II (and any CET), reducing P_{700}^+; subsequently, saturation of the electron transport chain occurs and P_{700}^+ accumulates again. Following 2 h incubation at pH 7.5 and 10.0 in GT-O1 cells, there was a relatively small effect of pH on P_{700} oxidation kinetics (Fig. 4.16D); in both pH conditions the signal was almost completely quenched at ~0.6 s and signal maxima was reached again around ~2 s. In GT-O1, Con:ΔPsbO:ΔPsbU and pseudorevertant cells, pH 7.5 reduced the proportion of quenching relative to pH 10.0, and both strains displayed reduced quenching and a more rapid return to maximum P_{700}^+ relative to GT-O1 (~0-25% for Con:ΔPsbO:ΔPsbU, ~40-50% for the pseudorevertant). At pH 7.5, no signal

quenching was observed for Con:ΔPsbO:ΔPsbU, implying a complete lack of electron transport from PS II to PS I in this strain. While electron transport was apparently lower in the pseudorevertant than GT-O1, apparently functional electron transport at pH 7.5 is an interesting explanatory factor for, or result of, the capacity for autotrophic growth of this strain in these pH conditions. In contrast, the lack of electron transport in Con:ΔPsbO:ΔPsbU is in spite of somewhat functional PS II activity at pH 7.5. Low temperature fluorescence shows that PS II is assembled in this strain, TL indicates that charge separation occurs, and oxygen evolution is possible (albeit at a low rate), yet electrons apparently do not reach PS I in this strain.

4.6 Discussion

Assembly of the Con:ΔPsbO:ΔPsbU and pseudorevertant genomes revealed three SNP mutations in genes of the pseudorevertant strain that affect conserved residues in their encoded protein. No mutations affecting genes associated with photosynthesis, or genes known to be involved in pH homeostasis in cyanobacteria (see Chapter One, Section 1.5) were identified. Instead, the candidate mutations for low-pH growth in the pseudorevertant strain appear to affect other cellular processes. The Gly93 to Cys mutation in PmgA seems likely to affect the function of this protein, which bears resemblance to a Ser-Thr kinase and might be an anti-sigma factor (Sakuragi, 2006; De Porcellinis et al., 2016), and which affects the regulation of the CUP component-encoding *nhdF3* and to a lesser extent the HCO_3^- uptake *sbtA* gene (Haimovich-Dayan et al., 2011; Nishijima et al., 2015). The Ala1115 to Val mutation in CheA might be conservative, but could affect the role of this protein in sensing and responding to light (Yoshihara et al., 2000). An Arg54 to Glu mutation in the hypothetical protein Ssr1558 might also be relevant, if its predicted homology to part of a much larger protein recently identified as a Ca^{2+} and/or Mn^{2+}/H^+ antiporter in *A. thaliana* is accurate (Schneider et al., 2016; Wang et al., 2016). However, using a photoautotrophic growth selection top-agar assay, the pseudorevertant mutation in *pmgA* was determined to be the candidate for pH 7.5 growth in this mutant.

In the course of this study, no mutagenesis strategy to introduce the pseudorevertant *pmgA* gene copy into ΔPsbO:ΔPsbU cells (or *vice versa*) was successful. Moreover, it appears that *pmgA* is essential to ΔPsbO:ΔPsbU cells, as multiple, independent mutagenesis strategies failed to yield an ΔPsbO:ΔPsbU:Δ*pmgA* mutant. Interestingly, the transformation of the wild-type substrain GT-O1 with *pmgA* mutations was also problematic, whereas mutagenesis with this gene is reported widely in the literature in other GT wild-type backgrounds. It is possible that genome mutations present or absent in the GT-O1/Con substrain background compared to other GT- substrains explains this result, perhaps by their interaction with *pmgA* or its gene product, but this hypothesis was not tested (see also Chapter 3, Section 3.1). Although some *pmgA* mutants were obtained, *pmgA* deletion or complementation (Control strain) did not affect growth or pH-sensitivity in the strains and conditions tested. No mutagenesis strategy was able to successfully introduce mutations into pseudorevertant cells, raising the possibility that this strain may be non-competent for transformation. If the CheA mutation indeed affects protein function, then type IV pilin biogenesis might be affected, in turn reducing the ability of the

pseudorevertant cells to incorporate foreign DNA into the cell via these pilins (Yoshihara et al., 2000, 2001). This possibility has precedent: the GT-Kazusa strain, with loss of function in PilC, might be non-competent for genetic transformation as a result of altered pilin biosynthesis (Bhaya et al., 2000; Yoshihara et al., 2001).

The failure to independently confirm the result of the top-agar experiment means that this study is unable to conclusively show that the PmgA Gly93 to Cys mutation is responsible for pH 7.5 growth in the pseudorevertant, but some additional evidence was obtained in support of this hypothesis. Loss of *pmgA* was associated with repeated mutations in *ndhF3* in independent cultures in photomixotrophic/1% CO_2 conditions; *pmgA* deletion probably causes some loss of *ndhF3* activity (Nishijima et al., 2015). If, in contrast, the Gly93 to Cys mutation enhances rather than abolishes PmgA function, NdhF3 activity might be enhanced in the pseudorevertant as well. Or, if PmgA is an anti-sigma factor as suggested (Sakuragi, 2006), an alteration in its conformation and loss-of-function due to the Gly93 to Cys mutation might cause de-repression of gene expression in a downstream target, such as NdhF3. Enhanced CUP would be expected to favour growth in pH conditions where equilibrium concentrations of C_i include aqueous CO_2 (generally, pH >8.0, see Chapter One, Section 1.3.2), this overlaps with the optimal *Synechocystis* 6803 growth range from around pH 7.0. Accordingly, enrichment with 3% CO_2 rescued growth of two pH-sensitive PS II mutants, Con:ΔPsbO:ΔPsbU and ΔPsbV:ΔCyanoQ at pH ~7.5, and the loss of pH-sensitivity due to Ci supplementation appears to be a novel observation in PS II mutants. Deletion of *ndhF3* in the latter strain partially eliminated this effect. Growth of Con:ΔPsbO:ΔPsbU cells in ambient CO_2 occurred at pH >8.5, where CUP becomes less relevant compared to HCO_3^- uptake. Subsequently, the link between the pseudorevertant *pmgA* mutation and CUP might be a functional explanation for the growth phenotype of this strain.

Despite numerous studies, the function of PmgA remains enigmatic. Since the initial observation that *pmgA* was essential for mixotrophic growth in *Synechocystis* 6803 (Hihara and Ikeuchi, 1997), a number of studies have investigated its apparently broad role in regulation of growth, carbohydrate storage, and photosystem stoichiometry. In particular, the relationship between *pmgA* and CUP via *ndhF3* appears to be complex. In mixotrophic conditions at ambient CO_2, there might be no link between *pmgA* and CUP, since CO_2 enhancement was strictly required in combination with photomixotrophy to cause altered *nhdF3* regulation in *pmgA* mutants (Haimovich-Dayan et al., 2011). Additionally, the repeated mutation of *nhdF3*

associated with *pmgA* deletion does not appear to affect actual measured rates of CUP (Nishijima et al., 2015), implying that *ndhF3* might not be as important for this function as is currently accepted (e.g. see Price, 2011; Burnap et al., 2015; Orf et al., 2015). However, a Δ*pmgA* mutant was impaired in photomixotrophic growth at pH 7.0 but not pH 8.0 (Sakuragi, 2006), again implicating CUP processes in the role of *pmgA*, since CUP would be more important in the lower pH condition. Other functions ascribed to PmgA include the regulation of PS I in response to high light and mixotrophy; a Δ*pmgA* mutant does not downregulate PS I in high light like the wild-type, and subsequently has a higher chlorophyll production and eventually reaches a somewhat higher culture density over time, similar to the GT-O1:Δ*pmgA* mutant in this study (Hihara et al., 1998; Muramatsu et al., 2009). However, prolonged high light is eventually lethal to this strain, which was displaced by a wild-type strain in mixed culture (Hihara et al., 1998), and was unable to grow in high light when low culture density was maintained by dilution; sub-lethal DCMU addition, mimicking photoinhibition, reversed this effect (Sonoike et al., 2001). Accumulation of glycogen resulting from *pmgA* deletion was also observed in a mutant deficient in a non-coding RNA, PmgR1, which appears to act downstream of *pmgA*; ectopic expression of PmgR1 in a Δ*pmgA* mutant permitted mixotrophic growth (De Porcellinis et al., 2016). Complicating the matter is that studies sometimes appear to find conflicting results following deletion of this gene: maintenance of high levels of PS I under high light was detected by low temperature chlorophyll fluorescence emission (Hihara et al., 1998) and immunoblot of PsaA/B (Muramatsu et al., 2009), but transcript levels of *psaA* and *psaB* decreased in high light in Δ*pmgA* in another study (De Porcellinis et al., 2016). Such differences could arise from undetected mutations in different Δ*pmgA* strains, which apparently are common and occur rapidly in Δ*pmgA* mutants (Haimovich-Dayan et al., 2011; Nishijima et al., 2015); in this study mutagenesis of *pmgA* was problematic as well. PS I function in Δ*pmgA* and Δ*pmgA*:Δ*ndhF3* mutants was similar when P_{700} oxidation was measured, implying a limited role of *ndhF3* in CET, but both strains showed slower P_{700} oxidation kinetics than the wild-type, implying an increased reducing pressure on P_{700} by CET in both mutants (Nishijima et al., 2015).

Linking these broad-ranging observations into a working theory of PmgA function (especially one that might address Con:ΔPsbO:ΔPsbU vs. pseudorevertant pH 7.5 growth) is challenging, and an attempt at a unified hypothesis is given below. One theme is that *pmgA* is essential in conditions where $NADP^+$/NADPH flux would be high; due to added carbon from photomixotrophic conditions or enriched CO_2 especially at pH ~7.0 (where CUP/CA via NDH-

1-MS/NhdF3 and Rubisco activity would both be high), and due to increased photosynthetic activity (in high light). PmgA might thus have a role in preventing redox imbalance due to this flux, perhaps by regulating an alternative electron acceptor in the electron transport chain, such as a respiratory oxidase. When carbon supply is replete (photomixotrophic growth and/or enriched CO_2), the loss of PmgA leads to increased PS I, increased CET, and the accumulation of sugars not being utilised by the oxidase, leading to over-reduction of the electron transport chain, cellular redox imbalance, and death. In this hypothesis, compensatory loss of NdhF3 function in Δ*pmgA* might lead to reduced Calvin-Benson cycle activity and reduced accumulation of sugars, subsequently CET, respiration, and back-pressure on the electron transport chain might be reduced. Testing this theory will be challenging given the propensity of Δ*pmgA* strains to die or mutate in non-permissive conditions. However, observations of ΔPsbO:ΔPsbU mutants in this study to some extent fit the theory: the apparent increase in PS I in pseudorevertant cells after 24 h pH 7.7 incubation, compared to Con:ΔPsbO:ΔPsbU cells, might be further evidence of a loss of PmgA function in the pseudorevertant, and hence an alteration in PS stoichiometry might favour growth of the this mutant at pH ~7.5. In ΔPsbO:ΔPsbU cells with compromised water-splitting and reduced proton gradient across the thylakoid, the activity of a respiratory oxidase regulated by PmgA might be important to generate ΔpH for ATP synthase activity, explaining the inability to delete *pmgA* from ΔPsbO:ΔPsbU strains. In this hypothesis, oxidase activity might be the cause of an apparent lack of electrons reaching Con:ΔPsbO:ΔPsbU PS I at pH ~7.5 (measured by P_{700} oxidation analysis) in spite of PS II activity (albeit limited activity, measured by oxygen evolution) that ought to lead to some electron transport. This would limit NADPH production and Calvin-Benson cycle activity, and prevent growth of ΔPsbO:ΔPsbU cells in ambient CO_2. At pH 10.0, the ΔpH would be naturally enhanced by an increase in pH_{cyt} (Jiang et al., 2013), and less dependent on PS II or oxidase activity. In the pseudorevertant at pH 7.5, with altered *pmgA*, electrons can reach PS I, reducing $NADP^+$, and permitting growth. Altered PS II redox equilibria between Con:ΔPsbO:ΔPsbU and pseudorevertant cells does not appear to be a factor, since TL in PS II and flash-induced fluorescence decay from PS II were similar, and no mutations in the pseudorevertant that directly affect PS II were found. It follows that carbon enrichment in pH-sensitive PS II mutants might bypass the need for CUP to support Calvin-Benson cycle activity, freeing up the limited pool of NADPH in ΔPsbO:ΔPsbU and ΔPsbV:ΔCyanoQ strains, and permitting growth. However, the loss of growth due to *ndhF3* deletion in ΔPsbV:ΔCyanoQ strains is inconsistent with this aspect of the hypothesis, and carbon enrichment might have a much simpler effect on growth in PS II mutants that is

completely unrelated to PmgA. It has been suggested previously that increased Calvin-Benson cycle activity might benefit cells prone to light-induced photodamage (such as PS II mutants) by increasing the sink for electrons in the electron transport chain, enhancing the affinity of electron transport components for PS II-derived electrons that might otherwise produce ROS (Takahashi and Murata, 2005, 2008).

The role of ROS in the pH response of Con:ΔPsbO:ΔPsbU and pseudorevertant cells also appears to be complex, based on the data obtained in this study. Measurements of $^1O_2$ suggested a higher production at pH 7.5 in GT-O1, Con:ΔPsbO:ΔPsbU and pseudorevertant cells compared to pH 10.0, whereas spectrophotometric determination of non-specific ROS indicated it might be higher at pH 9.0 than 7.7 in Con:ΔPsbO:ΔPsbU and pseudorevertant cells. Based on the data presented here, the Con:ΔPsbO:ΔPsbU strain might be producing more overall ROS at the lower pH level, but the pseudorevertant appears to be producing more $^1O_2$, consistent with its increased sensitivity to Rose Bengal than the Con:ΔPsbO:ΔPsbU strain (Summerfield et al., 2013). Interestingly, while the pseudorevertant appears to induce OCP at the transcript level in pH 7.5 conditions (Summerfield et al., 2007), the Con:ΔPsbO:ΔPsbU strain displayed more carotenoid pigments following 24 h pH 7.7 acclimation in this study. Carotenoids quench both excess light energy reaching PS II and also $^1O_2$ (Kirilovsky and Kerfeld, 2016), and thus their accumulation in the Con:ΔPsbO:ΔPsbU strain supports the hypothesis that photoinhibition and ROS at pH 7.5 contribute to, or substantially cause the pH-sensitive response. Other aspects of the Con:ΔPsbO:ΔPsbU pH ~7.5 response observed in this study, such as reduced PS II oxygen evolution activity, impaired PS II assembly and impaired PBS coupling are consistent with a general decline of PS II function in this strain compared to pH ~10.0.

In this study, a number of lines of evidence support the hypothesis that the loss of PsbO and PsbU causes low pH-sensitivity by PS II-independent means, in addition to a possible enhancement of photoinhibition and ROS production. No mutations affecting PS II were identified in the pseudorevertant, instead, a mutation in *pmgA* implicating carbon supply, or electron transport, or cellular redox seems to be responsible for pH 7.5 growth. While PS II assembly and function is certainly compromised in Con:ΔPsbO:ΔPsbU cells at pH 7.5 (Eaton-Rye et al., 2003; Summerfield et al., 2007, 2013), the growth effect of enriched CO_2 would be expected to act on the cell downstream of PS II, and it is a novel finding that this PS II-independent effect rescues the Con:ΔPsbO:ΔPsbU strain. Thus, altered electron transport on

the acceptor side of PS II (affected by CO_2 in Con:ΔPsbO:ΔPsbU, or PmgA in the pseudorevertant) seems to explain the growth phenotype, in spite of the fact that the loss of extrinsic proteins must dramatically affect the PS II donor side as well. These findings suggest that maintenance of electron transport, cellular redox, and probably ΔpH is more difficult at pH 7.5 than pH 10.0, providing a tentative explanation of the pH-sensitivity of some PS II mutants.

Chapter Five: PS II function in PsbV mutants, and mutants with amino acid substitutions in CP47 that potentially affect Y_D and pH-sensitivity

5.1 Function and mutagenesis of the CP47 protein and Y_D in PS II

5.1.1 The role of CP47 and Y_D

In PS II, the chlorophyll-binding core antennae CP47 and CP43 proteins are assembled on the D2 and D1 sides, respectively, of the mature PS II monomer. The proteins are so-called for their assignment as chlorophyll-binding proteins with apparent MW of 47 and 43 kDa, and are sometimes referred to as PS II-B and PS II-C for their encoding genes *psbB* and *psbC*. Both CP47 and CP43, which bind 16 and 13 chlorophylls respectively, are structured with their C- and N- terminal regions on the cytosolic side of the thylakoid membrane (the stroma side in higher plants), and are arranged with six transmembrane helices forming three helical pairs; in addition, a large inter-helical loop, designated loop E in both proteins, extends into the lumen and surrounds the OEC, with CP43 Glu354 on Loop E providing the only direct OEC ligand not contributed by D1. In addition, the nearby CP43 Arg357 is in the OEC second coordination sphere (Ferreira et al., 2004; Eaton-Rye and Putnam-Evans, 2005; Umena et al., 2011). Loop E in CP47 is involved in PsbO binding, and is adjacent to the redox-active residue D2 Tyr160 (Y_D) binding pocket on D2 (Umena et al., 2011; Bricker et al., 2012).

During photosynthesis, the redox-active residue D1 Tyr161 (Y_Z) is almost immediately oxidised (~ns time scale) in the light by P_{680}^+ and rapidly reduced by the OEC (~μs); in contrast, oxidised Y_D^+ is dark-stable for many minutes. Although not involved in water oxidation directly, Y_D is involved in charge-equilibrium with the OEC. Decay of the $S_3/S_2Y_D^+$ state in the dark over ~3-5 mins yields approximately 25% $S_0Y_D^+$/75% $S_1Y_D^+$ PS II centres (Vass and Styring, 1991). With further dark-adaption, Y_D^+ is reduced by an electron from the OEC, yielding a majority of centres in the S_1Y_D state. Evolutionarily speaking, this redox role of Y_D remains somewhat enigmatic. The prevailing theory is twofold: firstly, Y_D appears to be able to oxidise over-reduced OEC centres, and may be important for their assembly; secondly, it is suggested that the proton released from the Y_D radical (which is shared with D2 His189, hereafter His_D) stabilises the positive charge on P_{680}^+, accelerating Y_Z oxidation and confining any damaging charge recombination to the readily-repaired D1 side of PS II (Rutherford et al.,

2004; Styring et al., 2012; Saito et al., 2013). Thus, while Y_D is not essential for PS II activity *in vitro*, it appears to be essential in nature (Styring et al., 2012).

5.1.2 Introduction of point mutations in Loop E

In *Synechocystis* 6803, deletion of Gly351 to Thr365 in Loop E of CP47 produced an obligately heterotrophic strain unable to undergo oxygenic photosynthesis, and this evidence pointed to a role for this region in function and assembly of PS II (Eaton-Rye and Vermaas, 1991). In particular, a conserved Phe-Phe-Glu region (Fig 5.1) was targeted for mutagenesis. A Phe363 to Arg (F363R) point mutant had impaired PS II assembly and function, and was an obligate photoheterotroph in the absence of the extrinsic proteins PsbO or PsbV, whereas an Phe632 to Arg mutant was less severely affected (Clarke and Eaton-Rye, 1999; Eaton-Rye et al., 2003). Glu364 to Gln (E364Q) or Glu364 to Gly substitutions produced a strain similar to wild type, but deletion of PsbV in these strains also appeared to produce an obligate photoheterotroph (Putnam-Evans et al., 1996; Morgan et al., 1998). Deletion of PsbV induced a more severe phenotype in these strains than deletion of PsbO, probably because the CP47 mutation affects PsbO binding anyway (Morgan et al., 1998; Eaton-Rye and Putnam-Evans, 2005; Bricker et al., 2012). Surprisingly, the E364Q:ΔPsbV strain was found to display a similar pH-sensitive phenotype to the ΔPsbO:ΔPsbU mutant; PS II function and assembly were inhibited, and autotrophic growth was not possible at pH 7.5, but pH 10.0 rescued growth (Eaton-Rye et al., 2003). Deletion of CyanoQ from the E364Q:ΔPsbV mutant increased doubling time at pH 10.0 compared to E364Q:ΔPsbV and ΔPsbV:ΔCyanoQ cells, but growth was still possible (Summerfield et al., 2005a).

Accession	Description	Protein sequence alignment
WP_010873685.1	photosystem II CP47 reaction center protein [Synechocystis sp. PCC 6803]	DGIAQEWIGHPIFKDKEGRELEVRRMPNFFETFPVIMTDADGVVRADIPFRR
ABF06657.1	photosystem II CP47 protein [Arthrospira platensis]	DGIAQGWLGHPVFTDAEGRELTVRRLPNFFETFPVILTDADGVIRADVPFRR
AOC54143.1	Photosystem II CP47 protein (PsbB) [Microcystis aeruginosa NIES-2481]	DGIAKSWLGHPVFKDGEGRVLSVRRMPNFFETFPVVLTDSEGIVRADIPFRR
WP_002785360.1	photosystem II chlorophyll-binding protein CP47 [Microcystis aeruginosa]	DGIAKSWLGHPVFKDGEGRVLSVRRMPNFFETFPVVLTDSEGIVRADIPFRR
YP_537004.1	photosystem II 47 kDa protein [Pyropia yezoensis]	DGVAEAWLGHPVFQDKEGRELSVRRMPAFFETFPVILVDKDGIIRADIPFRR
WP_015226093.1	photosystem II chlorophyll-binding protein CP47 [Halothece sp. PCC 7418]	DGLAQAWLGHPVFKDAEGRELTVRRLPNFFETFPVVLEDENGVVRADIPFRR
WP_012409026.1	photosystem II chlorophyll-binding protein CP47 [Nostoc punctiforme]	DGIAQSWQGHAVFKDSEGRELTVRRLPNFFETFPVILTDADGIVRADIPFRR
NP_045849.1	photosystem II 47 kDa protein [Chlorella vulgaris]	DGIAVGWLGHAVFKEKQGNELFVRRMPTFFETFPVVLVDKDGVVRADVPFRR
AAG12343.1	photosystem II CP47 protein [Arabidopsis thaliana]	DGIAVGWLGHPVFRNKEGRELFVRRMPTFFETFPVVLVDGDGIVRADVPFRR
ONM62983.1	Photosystem II CP47 reaction center protein [Zea mays]	DGIAVGWLGHPVFRDKEGRELFVRRMPTFFETFPVVLVDEEGIVRADVPFRR
WP_015188475.1	photosystem II chlorophyll-binding protein CP47 [Gloeocapsa sp. PCC 7428]	NGVALAWLGHPVFQDAEGRELFVRRMPAFFETFPVILTDADGVVRADIPFRR
ACJ50121.1	photosystem II 47 kDa protein [Chlamydomonas reinhardtii]	DGIAVGWLGHASFKDQEGRELFVRRMPTFFETFPVLLLDKDGIVRADVPFRK
WP_011057370.1	photosystem II CP47 reaction center protein [Thermosynechococcus elongatus]	DGIAQAWKGHAVFRNKEGEELFVRRMPAFFESFPVILTDKNGVVKADIPFRR

Figure 5.1. Alignment of the CP47 (PsbB) protein polypeptide sequence from representative cyanobacterial, algal, and higher plant species indicates that the residues Phe363 and Glu364 are conserved throughout these species.

5.1.3 Possible interaction between Glu364 and Y_D

The results discussed above point to a relatively conservative effect of the Glu364 to Gln substitution. However, insights from the 1.9 Å crystal structure of PS II (see also Chapter One, Section 1.7.3) (Umena et al., 2011; Suga et al., 2015) prompted a closer look at this residue, which might be in or near one of several channels from the lumen through the extrinsic proteins to the PS II OEC, RC, and Y_D region (Bricker et al., 2015), and is also involved in H-bonding networks with Y_D. The suggestion that both Glu364 and Phe363 are in a water channel in PS II was made by Bricker et al. (2015) in a study where radiation of isolated PS II was used to determine oxidative modification of water-accessible residues within the PS II complex. Analysis of the PS II structure using MacPyMOL (Fig. 5.2) revealed that Glu364 is within H-bonding distance (~2.8 Å) with Arg294 of D2, which coordinates His_D, the proton recipient from the oxidised Y_D radical (Styring et al., 2012). The hypothesis that Glu364 might be important to H-bonding networks in the Y_D pocket has also been suggested by others (Saito et al., 2013; Sjöholm et al., 2017). Thus, it was hypothesised that a perturbed hydrophobic pocket compounding the absence of PsbV in the obligate photoheterotrophic F363R double mutant might affect Y_D oxidation, altering the dark redox-state of the OEC and resulting in a more deleterious phenotype than in the pH 7.5-sensitive E364Q:ΔPsbV mutant, where the carboxyl group on the substituted Gln might be able to partially contribute to H-bonding with D2 Arg294. Further, it was expected that the mechanism behind the pH-sensitivity of the

E364Q:ΔPsbV strain might therefore be related primarily to an altered PS II redox state, rather than the apparently PS II-independent factors that contribute to pH-sensitivity in the ΔPsbO:ΔPsbU and ΔPsbV:ΔCyanoQ mutants.

Whereas the E364Q & E364Q:ΔPsbV strains have already been characterised in terms of pH-dependent growth, PS II assembly, and oxygen evolution (Putnam-Evans et al., 1996; Morgan et al., 1998; Eaton-Rye et al., 2003; Summerfield et al., 2005a); this investigation used additional methods to probe PS II function and redox state in pH 7.5/mixotrophic & pH 10.0/autotrophic conditions, compared to pH 7.5/autotrophic conditions, which are permissive and non-permissive respectively for growth of the E364Q:ΔPsbV strain. To test the hypothesis that the Glu364 to Gln mutation affects Y_D, analyses of photosynthetic TL, fluorescence induction and decay, and flash oxygen yield were used to probe the function of this mutation in alteration of PS II donor-side redox reactions, compared (depending on the measurement) to that of the F363R mutants, and/or an alternative pH-sensitive PsbV mutant, ΔPsbV:ΔCyanoQ.
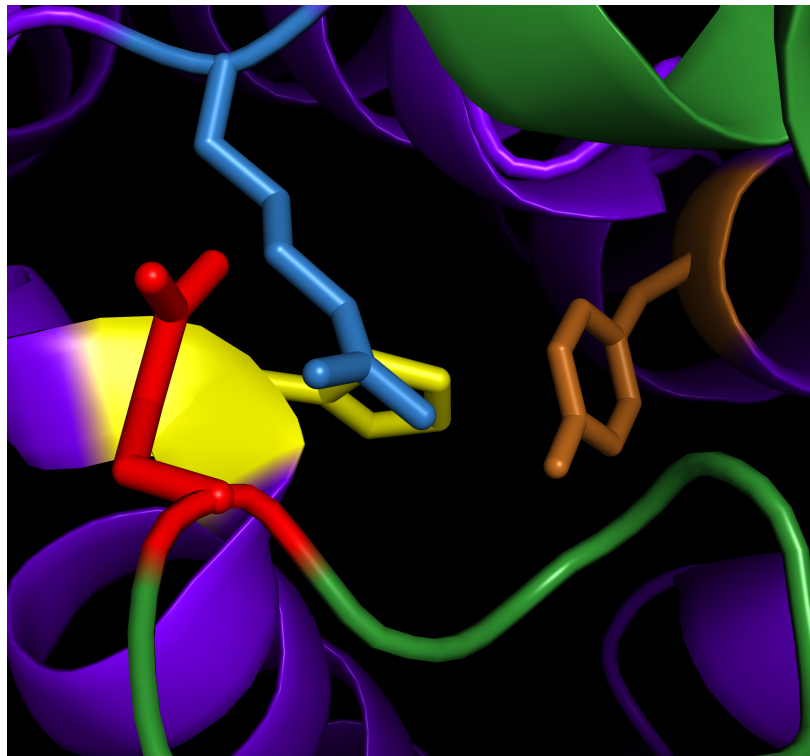
Figure 5.2. The Y_D region of PS II from *T. vulcanus* visualised using PyMOL (Protein Data Base accession 4UB6, Suga et al., 2015). Residues highlighted are CP47 Glu364 (red), D2 Arg294 (blue), Y_D (orange), and His_D (yellow). CP47 and Loop E are depicted in green, and D2 in purple. Other CP47/D2 residue side chains and PS II proteins are omitted for clarity.

5.2 Analysis of CP47 mutants grown in photoheterotrophic conditions

Determinations of the functional properties of PS II were initially carried out in permissive pH 7.5/mixotrophic conditions, since possible changes in electron transfer induced by the Glu364 to Gln mutation would be expected to be more evident due to general improvement in PS II assembly in PS II mutants in such conditions, compared to autotrophic growth.

TL measurements in *Synechocystis* 6803 strains (Fig. 5.3, Table 5.1) in the absence of DCMU showed a general similarity in yield from the B band between GT-O1 and E364Q cells, although the latter strain had increased C band yield, as well as upshifted B band T_{max} and downshifted C band T_{max}; this indicates stabilised $S_2Q_B^-$ and destabilised $Y_D^+Q_A^-$. The ΔPsbV strain had reduced B/C band yield and similar B band T_{max} compared to E364Q, whereas C band T_{max} was similar to the GT-O1 wild type. E364Q:ΔPsbV cells appear to display a compounding effect from both mutations on B band T_{max} and $S_2Q_B^-$ stability, but the effect on the C band was intermediate between the E364Q and ΔPsbV strains. Reduced TL from the F363R mutant was observed compared to GT-O1 cells and the E364Q strain (although the yield from the C-band appeared, with respect to overall TL yield, to be relatively much higher), and TL was barely detectable in the F363R:ΔPsbV mutant. Addition of DCMU increases the midpoint redox potential of the Q_A/Q_A^- pair by ~50 mV (Krieger-Liszkay and Rutherford, 1998), subsequently the $S_2Q_A^-$ pair (Q band) is destabilised and displays a reduced T_{max} in native PS II. TL in the presence of DCMU revealed an exceptional increase in yield from both Q and C bands in the E364Q strain compared to the GT-O1 wild type, and an upshifted Q band/downshifted C band T_{max}; this result was similar to measurements lacking DCMU and indicates a similar effect on both Q_A and Q_B redox potential as a result of this mutation. Increased TL yield in the presence of DCMU allowed improved the resolution of peaks from the E364Q:ΔPsbV and F363R:ΔPsbV strains, which both showed a very high relative C band yield and downshifted T_{max}.
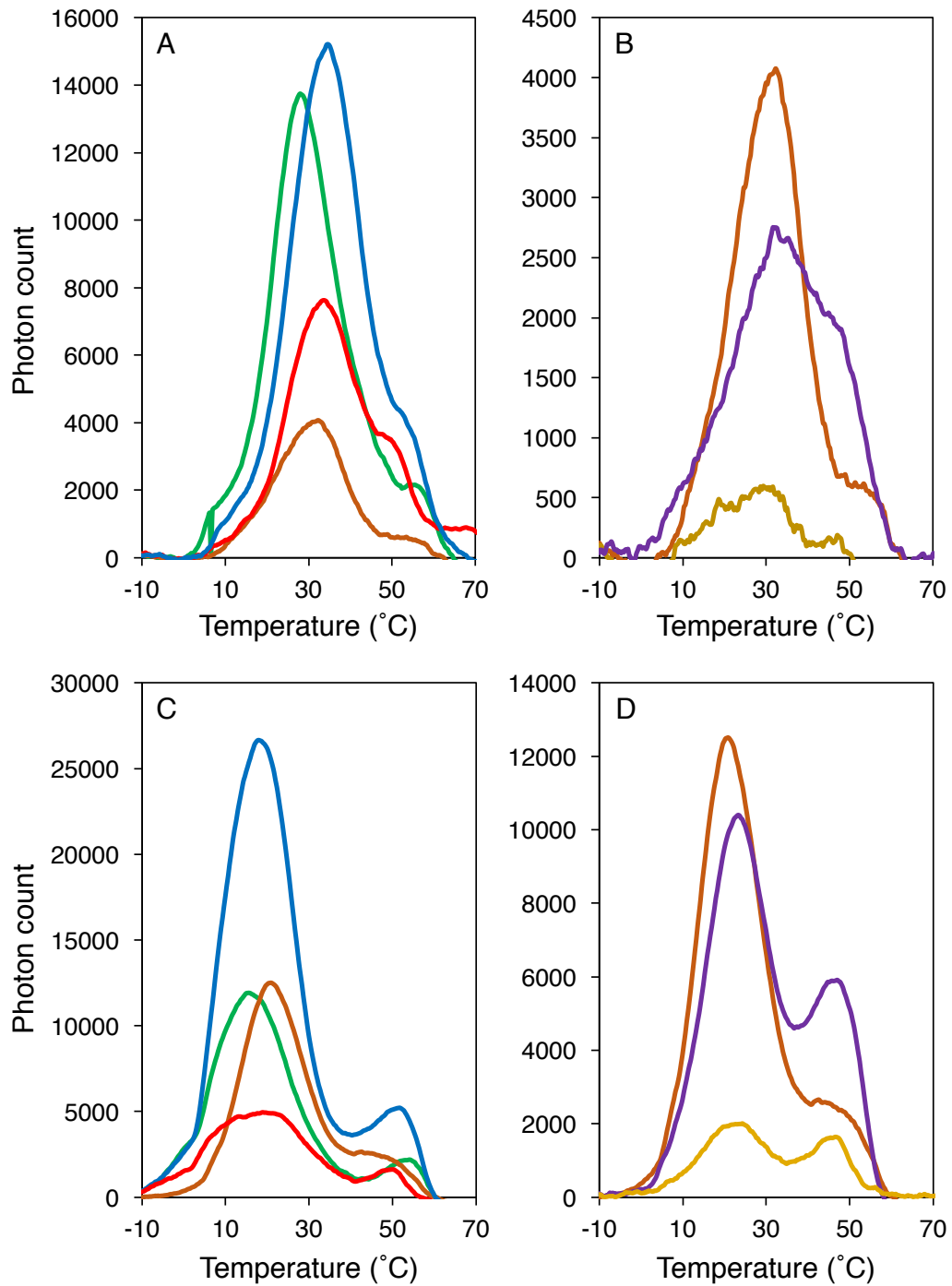
Figure 5.3. Photosynthetic TL from *Synechocystis* 6803 strains grown to mid-late log-phase and assayed in pH 7.5/mixotrophic conditions in the absence (A-B) and presence (C-D) of DCMU. Traces represent the mean photon count from 3-5 independent measurements. A, C: GT-O1 (green), F363R (red), E364Q (blue), and ΔPsbV (orange). B, D: ΔPsbV (orange), F363R:ΔPsbV (yellow), and E364Q:ΔPsbV (purple).

Table 5.1. Temperature of TL peak maxima (T_{max}) and relative peak amplitude of *Synechocystis* 6803 strains assayed in in pH 7.5 mixotrophic conditions, or after 8 h in pH 7.5/pH 10.0 autotrophic conditions (mean ± SEM, *n* = 3-5, of which 2-3 measurements were made by S Kovács). Shaded cells: peaks from <2 replicates could be fitted.

		- DCMU		+ DCMU	
		B band T_{max} (°C)	C band T_{max} (°C)	Q band T_{max} (°C)	C band T_{max} (°C)
Strain	*pH*	(amplitude)	(amplitude)	(amplitude)	(amplitude)
GT-O1	pH 7.5/mixo	29.3 ± 0.3 (15114 ± 327)	57.3 ± 0.1 (2270 ± 85)	16.8 ± 0.8 (13420 ± 3688)	54.2 ± 0.7 (3216 ± 499)
	pH 7.5/auto	32.0 ± 1.0 (9973 ± 1513)	51.2 ± 0.9 (1493 ± 555)	23.4 ± 0.5 (9129 ± 288)	51.6 ± 0.7 (2489 ± 744)
	pH 10.0/auto	32.2 ± 1.7 (7810 ± 682)	56.4 ± 0.8 (1008 ± 294)	20.0 ± 1.7 (9212 ± 461)	52.9 ± 0.4 (4186 ± 319)
E364Q	pH 7.5/mixo	33.8 ± 1.4 (14638 ± 1365)	50.0 ± 1.9 (5767 ± 350)	18.5 ± 1.3 (28467 ± 3106)	51.9 ± 0.6 (5286 ± 1272)
	pH 7.5/auto	30.2 ± 2.4 (16947 ± 439)	50.1 ± 1.3 (4831 ± 553)	21.1 ± 0.7 (31095 ± 4001)	51.1 ± 1.0 (5981 ± 429)
	pH 10.0/auto	29.7 ± 1.7 (22531 ± 1755)	51.0 ± 3.1 (4879 ± 1183)	28.3 ± 3.1 (16716 ± 2717)	53.7 ± 2.7 (7109 ± 2679)
ΔPsbV	pH 7.5/mixo	32.7 ± 0.5 (5122 ± 1048)	57.9 ± 3.0 (1239 ± 394)	22.2 ± 1.4 (11879 ± 4600)	48.2 ± 1.7 (2980 ± 378)
	pH 7.5/auto	30.9 ± 0.6 (2342 ± 655)	-	24.5 ± 2.9 (6060 ± 605)	-
	pH 10.0/auto	-	-	26.9 ± 3.1 (5418 ± 882)	53.0 ± 2.0 (2495 ± 505)
E364Q:ΔPsbV	pH 7.5/mixo	35.5 ± 0.8 (3279 ± 1249)	53.3 ± 0.6 (1499 ± 1073)	25.0 ± 1.5 (10879 ± 2639)	47.1 ± 0.4 (7302 ± 704)
	pH 7.5/auto	33.9 ± 1.3 (2818 ± 1587)	-	26.0 ± 2.3 (16671 ± 9736)	49.7 ± 1.9 (4450 ± 671)
	pH 10.0/auto	-	-	28.1 ± 1.5 (17496 ± 11736)	52.4 ± 3.5 (5593 ± 1417)
ΔPsbV:ΔCyanoQ	pH 7.5/auto	28.4 ± 1.4 (1570 ± 70)	-	25.8 ± 1.4 (4111 ± 441)	47.0 ± 1.0 (2103 ± 56)
	pH 10.0/auto	-	-	30.1 ± 1.5 (4475 ± 825)	52.5 ± 2.4 (2816 ± 65)
F363R	pH 7.5/mixo	-	-	21.5 ± 1.5 (6432 ± 3068)	49.4 ± 0.6 (4257 ± 3443)

Analysis of flash-induced fluorescence decay in these mutants (Fig. 5.4, Tables 5.2-5.3) in the same conditions also indicated altered redox potential of PS II electron transport components in the E364Q and E364Q:ΔPsbV strains, although differences in the latter compared to the GT-O1 wild type appear to be compounded by the effect of the PsbV deletion. Kinetic analysis determined that the half-times ($t_{1/2}$) of the fast phase (electron transfer from Q_A^- to Q_B) and medium phase decay component (Q_A^- to initially unbound Q_B) were not particularly altered in any mutant, although the relative contribution of these components to fluorescence decay was affected in the ΔPsbV mutant. The fast phase decay in the presence of DCMU (reflecting $Y_Z^+(P_{680}^+)Q_A^-$ recombination) was similar between all mutants except the ΔPsbV strain, which displayed a fast phase $t_{1/2}$ roughly double that of other strains. Increased $t_{1/2}$ of the slow-phase decay component in E364Q cells in the absence of DCMU points to stabilised $S_2Q_A^-$, an effect also seen in the presence of DCMU in this stain and in the E364Q:ΔPsbV strain. This effect was less noticeable in the F363R mutant, and low signal to noise ratio in fluorescence decay in the F363R:ΔPsbV strain, likely as a result of reduced PS II assembly, makes it difficult to interpret fluorescence decay results from this strain.

Table 5.2. Kinetics of single-turnover flash-induced chlorophyll fluorescence decay in *Synechocystis* 6803 mutants grown to mid-late log-phase and assayed in pH 7.5/mixotrophic conditions, or incubated for 8 h in pH 7.5/autotrophic or pH 10.0/autotrophic conditions. Fast phase decay occurs due to Q_A^- to Q_B electron transfer in the presence of bound Q_B, medium phase decay represents Q_A^- to Q_B electron transfer where Q_B was not bound, and slow phase decay is due to charge recombination of $S_2Q_A^-/Q_B^-$. Half-times ($t_{1/2}$) and amplitudes (amp) were determined by curve fitting and are the average ($\pm$ SEM) of 3-5 independent measurements (of which 2-3 measurements were made by S Kovács).

Strain	Growth	Fast phase $t_{1/2}$ (µs) [amp (%)]	Medium phase $t_{1/2}$ (ms) [amp (%)]	Slow phase $t_{1/2}$ (s) [amp (%)]
GT-O1	pH 7.5/mixo	244 ± 36 (54 ± 3.9)	1.9 ± 0.3 (28 ± 2.1)	2.4 ± 0.96 (18 ± 2.5)
	pH 7.5/auto	174 ± 17 (50 ± 4.9)	1.5 ± 0.4 (35 ± 5.9)	1.3 ± 0.11 (15 ± 1.8)
	pH 10.0/auto	213 ± 16 (59 ± 1.4)	1.7 ± 0.1 (30 ± 2.5)	4.3 ± 1.28 (11 ± 2.1)
E364Q	pH 7.5/mixo	246 ± 2 (51 ± 2.2)	1.6 ± 0.0 (32 ± 3.3)	3.1 ± 0.75 (17 ± 1.2)
	pH 7.5/auto	253 ± 18 (54 ± 3.8)	2.1 ± 0.2 (31 ± 2.8)	9.5 ± 3.99 (15 ± 2.6)
	pH 10.0/auto	252 ± 20 (49 ± 3.7)	1.9 ± 0.3 (32 ± 2.5)	7.0 ± 3.49 (18 ± 1.8)
ΔPsbV	pH 7.5/mixo	260 ± 19 (68 ± 1.3)	2.5 ± 0.1 (22 ± 0.8)	2.1 ± 0.31 (10 ± 2.1)
	pH 7.5/auto	288 ± 14 (68 ± 3.4)	5.1 ± 2.0 (19 ± 5.2)	7.1 ± 4.82 (12 ± 3.0)
	pH 10.0/auto	259 ± 56 (57 ± 7.8)	4.5 ± 1.6 (24 ± 9.4)	6.1 ± 2.47 (19 ± 7.9)
E364Q:ΔPsbV	pH 7.5/mixo	213 ± 73 (53 ± 5.7)	1.5 ± 0.4 (39 ± 4.6)	2.3 ± 1.34 (8 ± 1.1)
	pH 7.5/auto	216 ± 31 (40 ± 8.7)	1.6 ± 0.5 (36 ± 6.6)	2.5 ± 0.93 (24 ± 7.8)
	pH 10.0/auto	165 ± 21 (46 ± 6.5)	1.3 ± 0.2 (43 ± 9.0)	1.5 ± 0.27 (10 ± 3.6)
F363R	pH 7.5/mixo	244 ± 36 (54 ± 3.9)	1.9 ± 0.3 (28 ± 2.1)	2.4 ± 0.96 (18 ± 2.5)

Table 5.3. Kinetics of single-turnover flash-induced chlorophyll fluorescence decay in *Synechocystis* 6803 mutants grown to mid-late log-phase and assayed in the presence of DCMU in pH 7.5/mixotrophic conditions, or incubated for 8 h in pH 7.5/autotrophic or pH 10.0/autotrophic conditions. Due to occupation of the Q_B site by DCMU, decay primarily occurs due to charge recombination of $S_2Q_A^-$. Half-times ($t_{1/2}$) and amplitudes (amp) were determined by curve fitting and are the average ($\pm$ SEM) of 3-5 independent measurements (of which 2-3 measurements were made by S Kovács).

		Fast phase	*Slow phase*
Strain	*Growth*	$t_{1/2}$ (ms) [amp (%)]	$t_{1/2}$ (s) [amp (%)]
GT-O1	pH 7.5/mixo	0.5 ± 0.1 (1.1 ± 0.2)	0.7 ± 0.07 (99 ± 0.2)
	pH 7.5/auto	2.5 ± 0.9 (2.3 ± 0.4)	0.6 ± 0.04 (98 ± 0.4)
	pH 10.0/auto	1.3 ± 0.3 (3.1 ± 1.1)	0.6 ± 0.04 (97 ± 1.1)
E364Q	pH 7.5/mixo	0.3 ± 0.2 (5.3 ± 2.5)	1.3 ± 0.05 (95 ± 2.5)
	pH 7.5/auto	4.1 ± 2.3 (2.9 ± 1.7)	1.1 ± 0.08 (97 ± 1.7)
	pH 10.0/auto	0.5 ± 0.2 (2.1 ± 0.4)	1.2 ± 0.03 (98 ± 0.4)
ΔPsbV	pH 7.5/mixo	1.2 ± 0.8 (6.0 ± 2.1)	0.8 ± 0.10 (94 ± 2.1)
	pH 7.5/auto	5.3 ± 4.9 (5.2 ± 2.2)	1.0 ± 0.09 (95 ± 2.2)
	pH 10.0/auto	5.1 ± 3.3 (8.9 ± 6.6)	1.0 ± 0.01 (91 ± 6.6)
E364Q:ΔPsbV	pH 7.5/mixo	0.6 ± 0.1 (11.9 ± 8.7)	1.1 ± 0.10 (88 ± 8.7)
	pH 7.5/auto	0.2 ± 0.1 (8.8 ± 2.5)	1.3 ± 0.11 (91 ± 2.1)
	pH 10.0/auto	0.7 ± 0.3 (7.1 ± 2.7)	1.5 ± 0.19 (93 ± 2.7)
F363R	pH 7.5/mixo	0.5 ± 0.1 (1.1 ± 0.2)	0.7 ± 0.07 (99 ± 0.2)
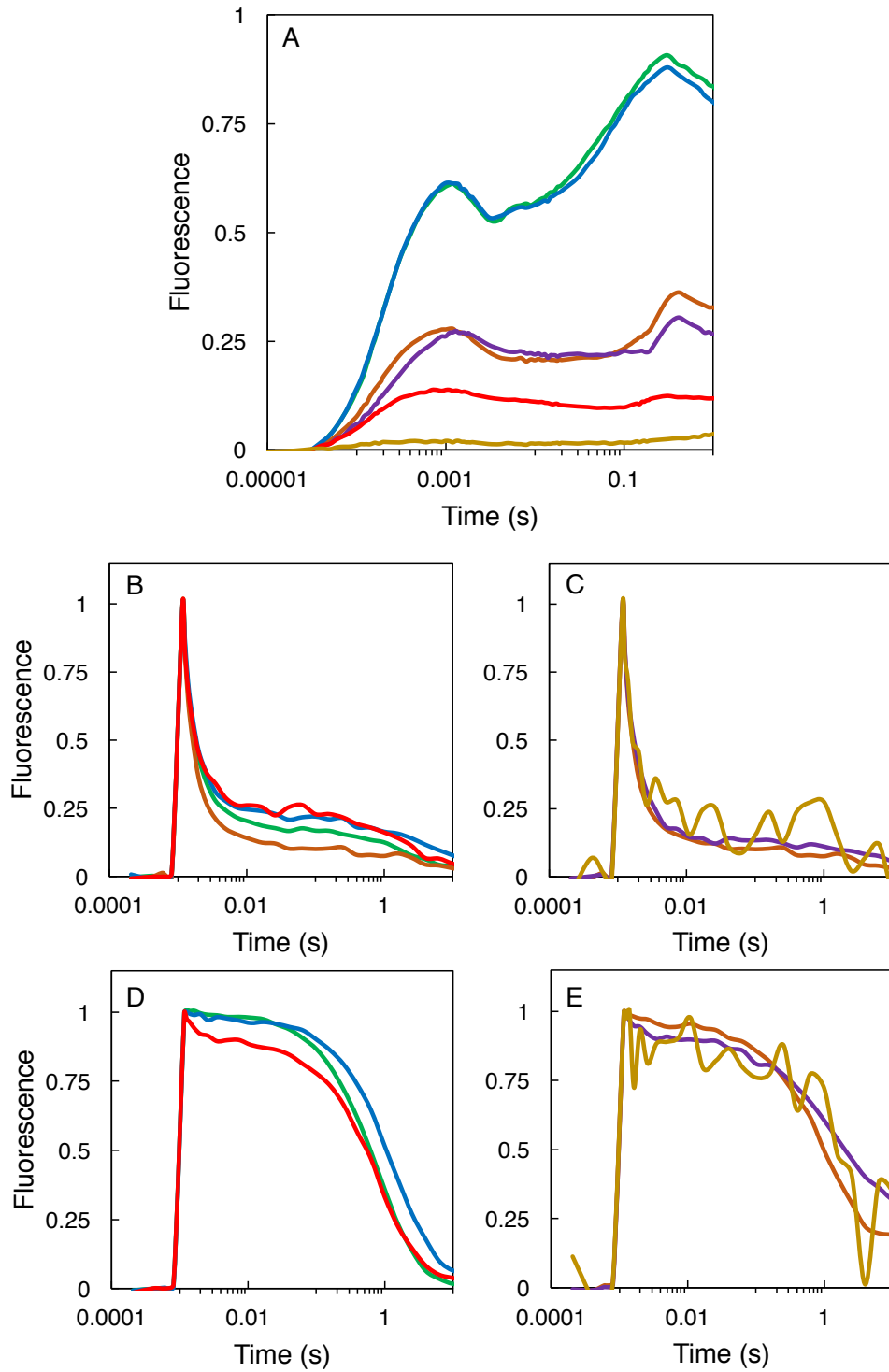
Figure 5.4. Fluorescence induction and flash-induced fluorescence decay from *Synechocystis* 6803 strains assayed in pH 7.5/mixotrophic conditions in the absence (B-C) and presence (D-E) of DCMU. Traces represent the mean from 2-4 measurements. A: Fluorescence induction of GT-O1 (green), F363R (red), E364Q (blue), ΔPsbV (orange), F363R:ΔPsbV (yellow), and E364Q:ΔPsbV (purple). B, D: fluorescence decay in GT-O1 (green), F363R (red), E364Q (blue), and ΔPsbV (orange). C, E: fluorescence decay in ΔPsbV (orange), F363R:ΔPsbV (yellow), and E364Q:ΔPsbV (purple).

Table 5.4. Measurements of variable fluorescence/maximal fluorescence (F_V/F_M) in the absence and presence of DCMU following a single-turnover flash in *Synechocystis* 6803 mutants grown to mid-late log-phase and assayed in pH 7.5/mixotrophic conditions, or incubated for 8 h in pH 7.5/autotrophic or pH 10.0/autotrophic conditions. Values are the mean of 2-4 measurements (of which 2-3 measurements were made by S Kovács).

		- DCMU	+ DCMU
Strain	*Growth*	F_V/F_M	F_V/F_M
GT-O1	pH 7.5/mixo	0.34 ± 0.04	0.36 ± 0.05
	pH 7.5/auto	0.31 ± 0.05	0.40 ± 0.05
	pH 10.0/auto	0.35 ± 0.09	0.43 ± 0.07
E364Q	pH 7.5/mixo	0.33 ± 0.01	0.34 ± 0.01
	pH 7.5/auto	0.29 ± 0.01	0.30 ± 0.02
	pH 10.0/auto	0.35 ± 0.01	0.33 ± 0.00
ΔPsbV	pH 7.5/mixo	0.19 ± 0.04	0.19 ± 0.04
	pH 7.5/auto	0.23 ± 0.02	0.23 ± 0.03
	pH 10.0/auto	0.29 ± 0.07	0.27 ± 0.07
E364Q:ΔPsbV	pH 7.5/mixo	0.17 ± 0.05	0.17 ± 0.05
	pH 7.5/auto	0.08 ± 0.01	0.06 ± 0.01
	pH 10/auto	0.11 ± 0.02	0.09 ± 0.02
ΔPsbV:ΔCyanoQ	pH 7.5/auto	0.16 ± 0.09	0.15 ± 0.11
	pH 10/auto	0.18 ± 0.12	0.15 ± 0.11
F363R	pH 7.5/mixo	0.15 ± 0.06	0.20 ± 0.04

Variable fluorescence yield, determined by F_V/F_M in the absence and presence of DCMU (Table 5.4), is indicative of relative PS II assembly and was similar between GT-O1, and E364Q cells, and between the ΔPsbV mutants; F363R cells had reduced PS II assembly and were more similar to the ΔPsbV mutants. Fluorescence induction measurements, producing the so-called OJIP transient, largely reflected the results above (Fig 5.4), with minimal PS II electron transport evident in the F363R and F363R:ΔPsbV strains. Results were similar between the GT-O1 and E364Q strains, and between the ΔPsbV and E364Q:ΔPsbV strains; sustained electron transfer indicates that OEC activity was possible even in these latter strains lacking PsbV.

Analysis of oxygen yield from single-turnover actinic flashes in dark-adapted cells can be used to determine the function of the OEC, in which single charge-separation events progress the OEC through the S_0-S_4 states (in the Kok cycle). In dark-adapted cells, Y_D remains oxidised over several minutes, and decay of the S-states of the OEC leads to PS II centres of around ~75% $S_1Y_D^+$/~25% $S_0Y_D^+$ (Vass and Styring, 1991). This means that when saturating light flashes are applied to ~5 min dark adapted cells, very little oxygen is produced on flash one (centres predominantly advance S_1 to S_2) and two (S_2 to S_3), but there is a pronounced yield maxima on flash three (with most centres advancing from S_3 to (S_4) to S_0 and releasing oxygen in the unstable (S_4) to S_0 step). Some oxygen release occurs on flash four (from PS II that was initially S_0), and there is little oxygen yield from flash five. Thereafter, accumulated 'double-hits' (two charge separations from one flash), 'misses' (no charge separations from the flash) and charge recombinations in the overall PS II population means that flash yields gradually stabilise. Using a so-called Joliot electrode built in-house, the flash-induced oxygen yield from 5 min dark-adapted cells was determined in the GT-O1 wild-type and the CP47 and ΔPsbV mutant strains (Fig. 5.5). The raw traces of flash oxygen yield show that all mutants lacking PsbV were significantly impaired in flash-oxygen yield, compared to GT-O1 and E364Q cells. Results of a comparison of normalised flash yield showed that both E364Q and E364Q:ΔPsbV cells had an increased 4th flash oxygen yield relative to the 3rd flash, compared to their respective GT-O1 and ΔPsbV backgrounds (Fig. 5.5, Table 5.5). In addition, the 5th flash/4th flash yield was reduced in E364Q cells, indicating that in this mutant, the majority of dark-adapted PS II centres were likely in the S_0 state. No flash-induced oxygen evolution was detected from ΔPsbV:ΔCyanoQ cells in these conditions, indicating an apparently more impaired OEC phenotype than the E364Q:ΔPsbV mutant.

Table 5.5. Ratio of relative flash-induced oxygen yields of *Synechocystis* 6803 strains grown in pH 7.5/mixotrophic conditions. Flash yield ratios (mean ± SEM, $n = 4$) were determined using a normalised first flash value.

	Strain				
Flash ratio	WT GT-O1	E364Q	ΔPsbV	E364Q:ΔPsbV	ΔPsbV:ΔCyanoQ
4th/3rd flash	0.59 ± 0.03	0.67 ± 0.02	0.87 ± 0.06	1.13 ± 0.12	0.49 ± 0.04
5th/4th flash	0.37 ± 0.07	0.23 ± 0.06	0.36 ± 0.10	0.52 ± 0.09	0.52 ± 0.73
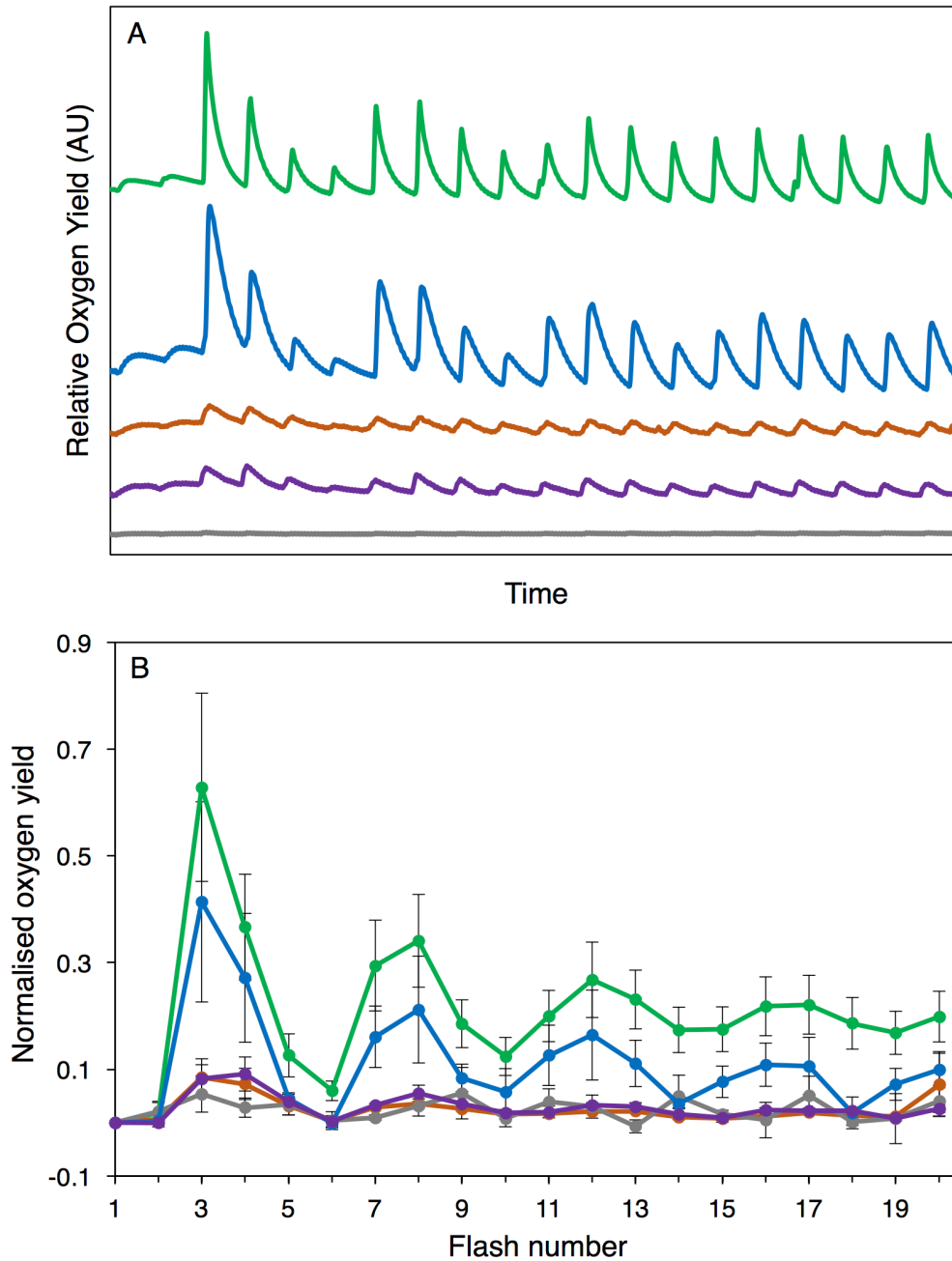
Figure 5.5. Flash-induced oxygen yield from *Synechocystis* 6803 strains grown to mid-late log-phase and assayed following 24 h incubation in pH 7.5/mixotrophic conditions. Oxygen yield is shown as the mean trace (relative, arbitrary units) measured with 20 saturating flashes in dark-adapted cells (A), and the first-flash normalised yield ± SEM (B). Traces represent the mean from 4 independent measurements. GT-O1 (green), E364Q (blue), ΔPsbV (orange), E364Q:ΔPsbV (purple), and ΔPsbV:ΔCyanoQ (grey).

5.3   Analysis of CP47 mutants grown in photoautotrophic conditions

Subsequent to analyses in mixotrophic conditions, PS II function was studied in pH 7.5 and pH 10.0 autotrophic conditions; pH 7.5 conditions are non-permissive for growth and functional PS II assembly in E364Q:ΔPsbV and ΔPsbV:ΔCyanoQ cells, and ΔPsbV cells are also compromised in growth and PS II activity at pH 7.5 compared to pH 10.0 (Eaton-Rye et al., 2003). The impaired autotrophic growth and minimal PS II in the F363R and F363R:ΔPsbV mutants meant that these were generally excluded from autotrophic growth analyses.

TL profiles from all strains indicated a shift in the stability of some PS II charge-pairs due to pH 7.5 autotrophic growth compared to mixotrophic growth at pH 7.5 and autotrophic growth at pH 10.0 (Fig. 5.6, Table 5.1, see also Fig. 5.3). In GT-O1 cells, increased T_{max} from B & C bands as well as Q & C bands in autotrophic conditions (in the absence and presence of DCMU, respectively, following 8 h incubation at pH 7.5) indicates charge stabilisation in PS II compared to mixotrophic conditions. At pH 10.0, greater T_{max} enhancement was observed, except in the Q band. Generally speaking, all PS II mutants showed increased T_{max} of TL bands in autotrophic conditions at pH 7.5 compared to pH 10.0, except B bands, which were somewhat downshifted. It appears that in the absence of DCMU, TL properties between strains were similar between pH 7.5/mixotrophic growth and pH 10.0/autotrophic growth, whereas, in the presence of DCMU, there was a greater similarity between pH 7.5/mixotrophic growth and pH 7.5/autotrophic growth (Fig. 5.3, Fig 5.6). This could reflect the fact that the direct effect of DCMU on the redox potential on PS II electron transfer components (e.g. Q_A/Q_A^-) and TL at pH 7.5 overrides effects due to pH. TL yield from the E364Q mutant was 2-3 times higher than in GT-O1 cells at both pH levels, indicating a large alteration in charge recombination favouring TL pathways. The free-energy required to destabilise B band charge pairs in the E364Q strain was similar at pH 7.5 (similar T_{max}) relative to the GT-O1 wild type, however a noticeable effect was the large increase in Q band T_{max} in E364Q cells between pH 7.5 and pH 10.0 (~+7˚C compared to - ~+3.5˚C in GT-O1), possibly indicative of a substantial decrease in the midpoint redox potential of either Q_A/Q_A^- or the OEC in these conditions. Whereas the C band was upshifted by ~+5˚C at pH 10.0 in GT-O1 cells, it was increased only ~+1˚C in the E364Q mutant, pointing to an altered redox potential of Y_D/Y_D^+ as well. TL yield from ΔPsbV and E364Q:ΔPsbV cells was generally reduced in autotrophic conditions, and curve fitting was more problematic as a result (Table 5.1), but prominent increases in TL yields and T_{max} in the

E364Q:ΔPsbV mutant compared to the ΔPsbV mutant again imply an alteration in charge recombination pathways due to the Glu364 to Gln mutation.
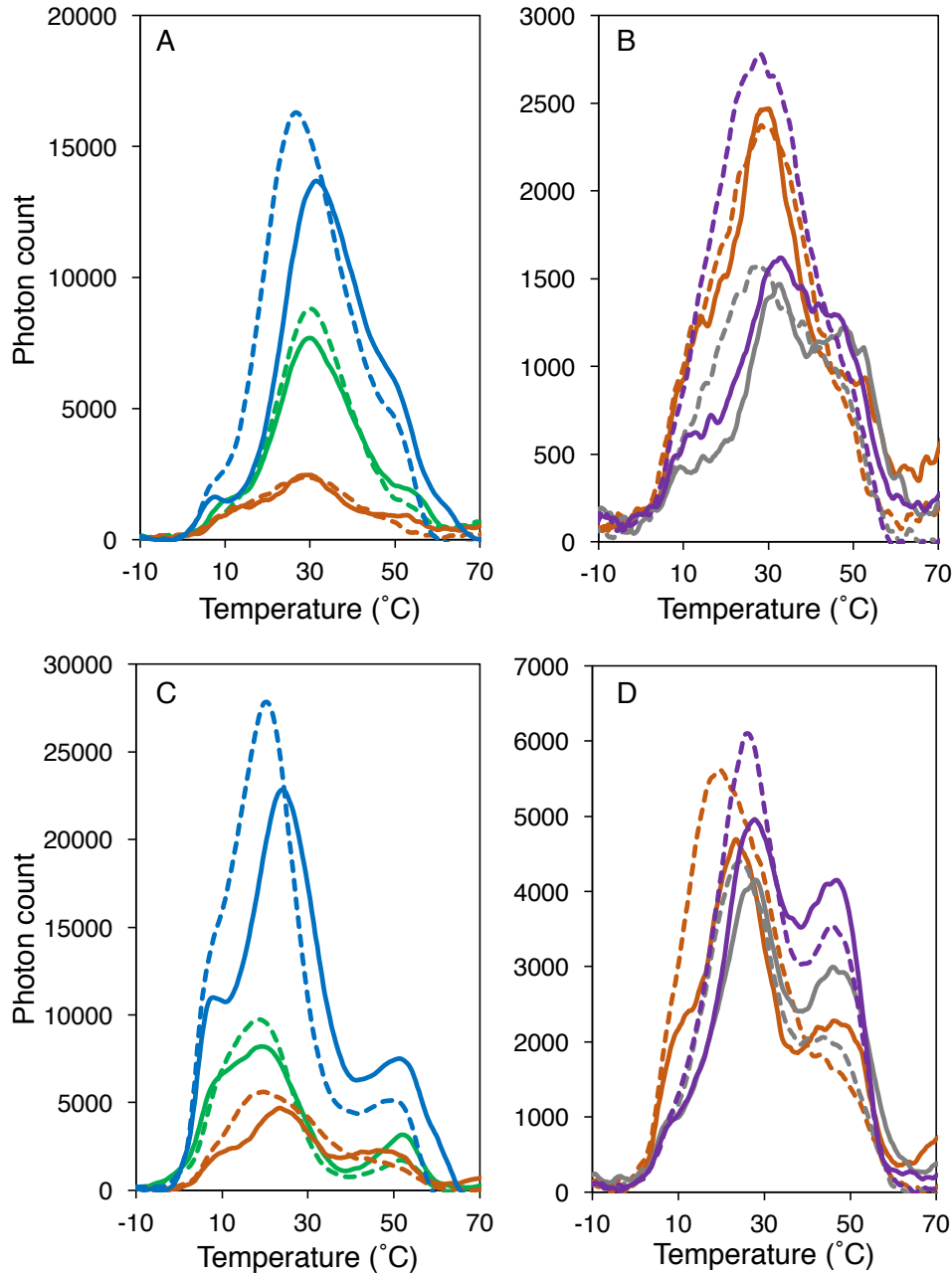
Figure 5.6. Photosynthetic TL from *Synechocystis* 6803 strains grown to mid-late log-phase and incubated for 8 h in pH 7.5/autotrophic or pH 10.0/autotrophic conditions in the absence (A-B) and presence (C-D) of DCMU. Traces represent the mean photon count from 3-5 independent measurements (of which 2-3 measurements were made by S Kovács). A, C: GT-O1 (green), E364Q (blue), and ΔPsbV (orange). B, D: ΔPsbV (orange), E364Q:ΔPsbV (purple), and ΔPsbV:ΔCyanoQ (grey).

Results from TL were generally in agreement with analysis of chlorophyll fluorescence decay kinetics (Fig. 5.7, Tables 5.2-5.3), in which the increased stabilisation of $S_2Q_A^-$ in E364Q cells seen following 8 h at pH 10.0 was accompanied by a dramatic increase in the $t_{1/2}$ of the slow phase fluorescence decay component in the presence and absence of DCMU, relative to the GT-O1 control strain. This effect was also seen at pH 7.5, and although the millisecond (medium) phase decay component was similar in the absence of DCMU (pointing to similar Q_A^- to initially unbound Q_B electron transfer), fast phase decay half-time was generally increased in E364Q cells, especially at pH 7.5, indicating slowed Q_A^- to Q_B electron transfer. In the presence of DCMU, fast phase decay was altered in the E364Q mutant at both pH levels compared to GT-O1 cells. Analysis of the fluorescence decay in ΔPsbV and E364Q:ΔPsbV cells revealed ambiguous results, due to an apparently counter-acting effect of the Glu364 to Gln mutation and the removal of PsbV in the E364Q:ΔPsbV double mutant. Similar to the E364Q mutant, kinetic analyses of the ΔPsbV strain showed an increased slow phase decay $t_{1/2}$ in the absence of DCMU, however the calculated $t_{1/2}$ from the double mutant was more similar to that observed for GT-O1 cells. Although the half-times between the GT-O1 and E364Q:ΔPsbV strains were similar, it is notable that fluorescence did not completely decay in the double mutant, and this effect was more pronounced than in the ΔPsbV strain. In the presence of DCMU, results were similar, with the E364Q:ΔPsbV cells exhibiting half-times closer to those of the GT-O1 strain, but the relative amplitude of slow phase decay in the latter was somewhat reduced, reflecting the delayed return to F_0 in this mutant. In the presence of DCMU, the fluorescence decay observed from E364Q:ΔPsbV cells appeared similar to that of the ΔPsbV:ΔCyanoQ strain, whereas in the absence of DCMU a dramatic decrease in apparent pH 7.5 fast phase decay amplitude and increase in medium phase decay was seen (this could not be satisfactorily modelled kinetically in some experimental replicates and thus kinetic data are not shown). This result does illustrate, however, a general difference between the E364Q:ΔPsbV and ΔPsbV:ΔCyanoQ mutants in spite of their similar pH-sensitive phenotype.

F_V/F_M in the absence and presence of DCMU (Table 5.4), was generally enhanced at pH 10.0 compared to pH 7.5 during 8 h autotrophic growth, indicating increased PS II assembly in this growth condition in all strains. Fluorescence induction measurements also indicated greater variable fluorescence and enhanced election transport at pH 10.0 compared to pH 7.5 (Fig 5.7). Whereas the GT-O1 and E364Q strains were similar at pH 10.0, electron transport was apparently reduced in the mutant at pH 7.5. Deletion of PsbV in the ΔPsbV mutant reduced fluorescence yield; this effect was enhanced by the Glu364 to Gln mutation but was greatest in

the ΔPsbV:ΔCyanoQ mutant. ΔPsbV:ΔCyanoQ cells showed very little variable fluorescence yield, indicating a largely non-functional OEC and/or a lack of PS II assembly.
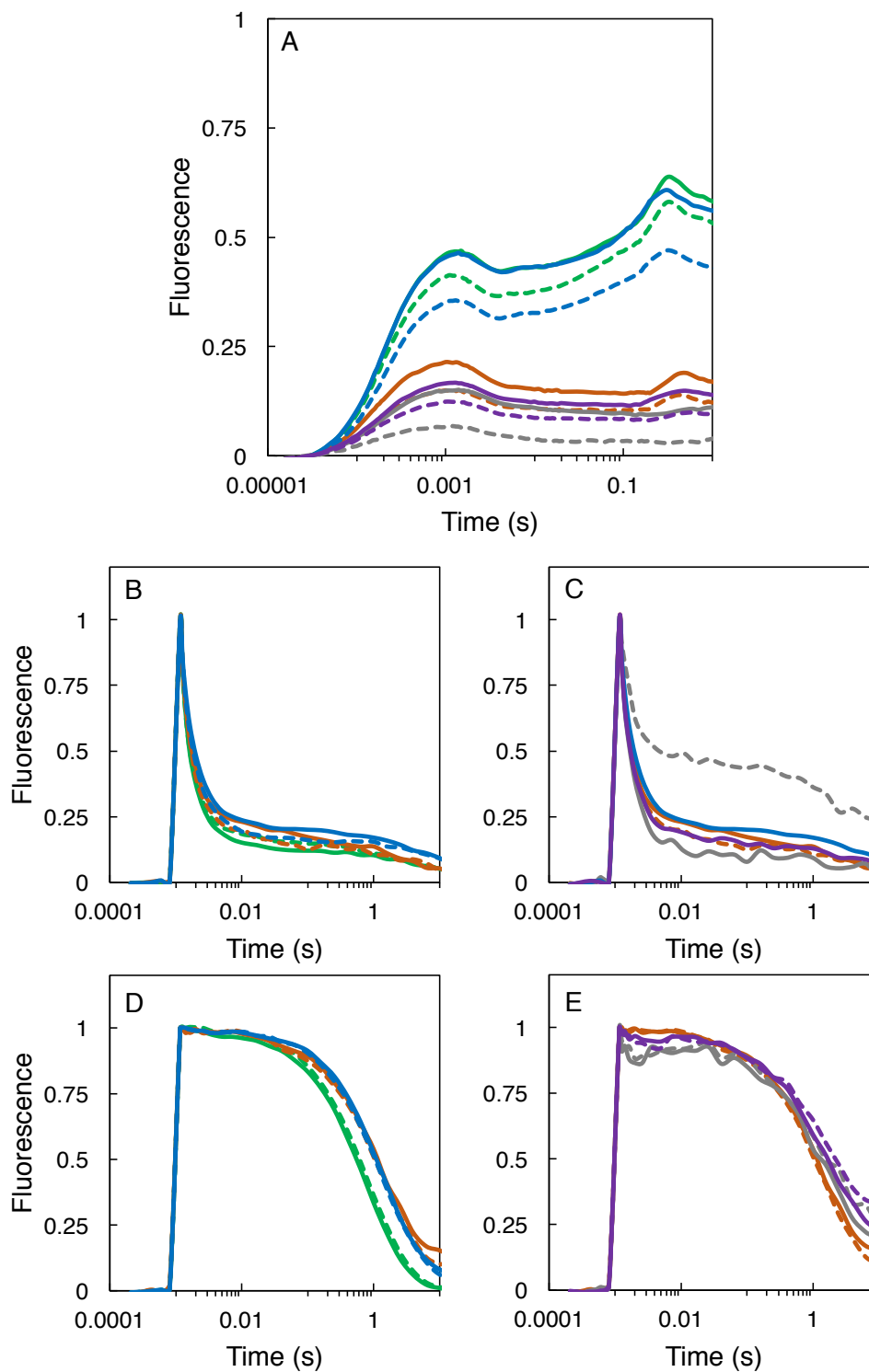
Figure 5.7. Fluorescence induction and flash-induced fluorescence decay from *Synechocystis* 6803 strains incubated for 8 h in pH 7.5/autotrophic (dashed lines) or pH 10.0/autotrophic

(solid lines) conditions. Traces represent the mean from 3-5 measurements (of which 2-4 measurements were made by S Kovács), and measurements took place in the absence (B-C) and presence (D-E) of DCMU. A: Fluorescence induction in GT-O1 (green), E364Q (blue), ΔPsbV (orange), E364Q:ΔPsbV (purple), and ΔPsbV:ΔCyanoQ (grey). B, D: fluorescence decay in GT-O1 (green), E364Q (blue), and ΔPsbV (orange). C, E: fluorescence decay in ΔPsbV (orange), E364Q:ΔPsbV (purple), and ΔPsbV:ΔCyanoQ (grey).

Impaired photoautotrophic growth in strains lacking the PsbV protein meant that flash oxygen yield comparisons were made only in the GT-O1 and E364Q strains in pH 7.5/10.0 autotrophic conditions. Measurements were made following 24 h incubation in this case, to emphasise the effects of pH on flash yield. As in the case of mixotrophic growth, flash oxygen yields were somewhat reduced in the E364Q mutant compared to GT-O1 cells (Fig. 5.8), in particular at pH 10.0. Whereas the 4th flash/3rd flash yield from the GT-O1 strain was similar between pH levels (Table 5.6), the yield was reduced compared to GT-O1 at pH 7.5, and increased at pH 10.0 in the E364Q strain. This effect was somewhat variable, but the far more striking reduction in 5th flash/4th flash yield in E364Q cells (oxygen yield was negligible on flash five) again provides some evidence of a tendency towards an increased population of the dark-S_0 state in the E364Q mutant, rather than S_1 – but, experimental variability means that this interpretation might require further investigation.
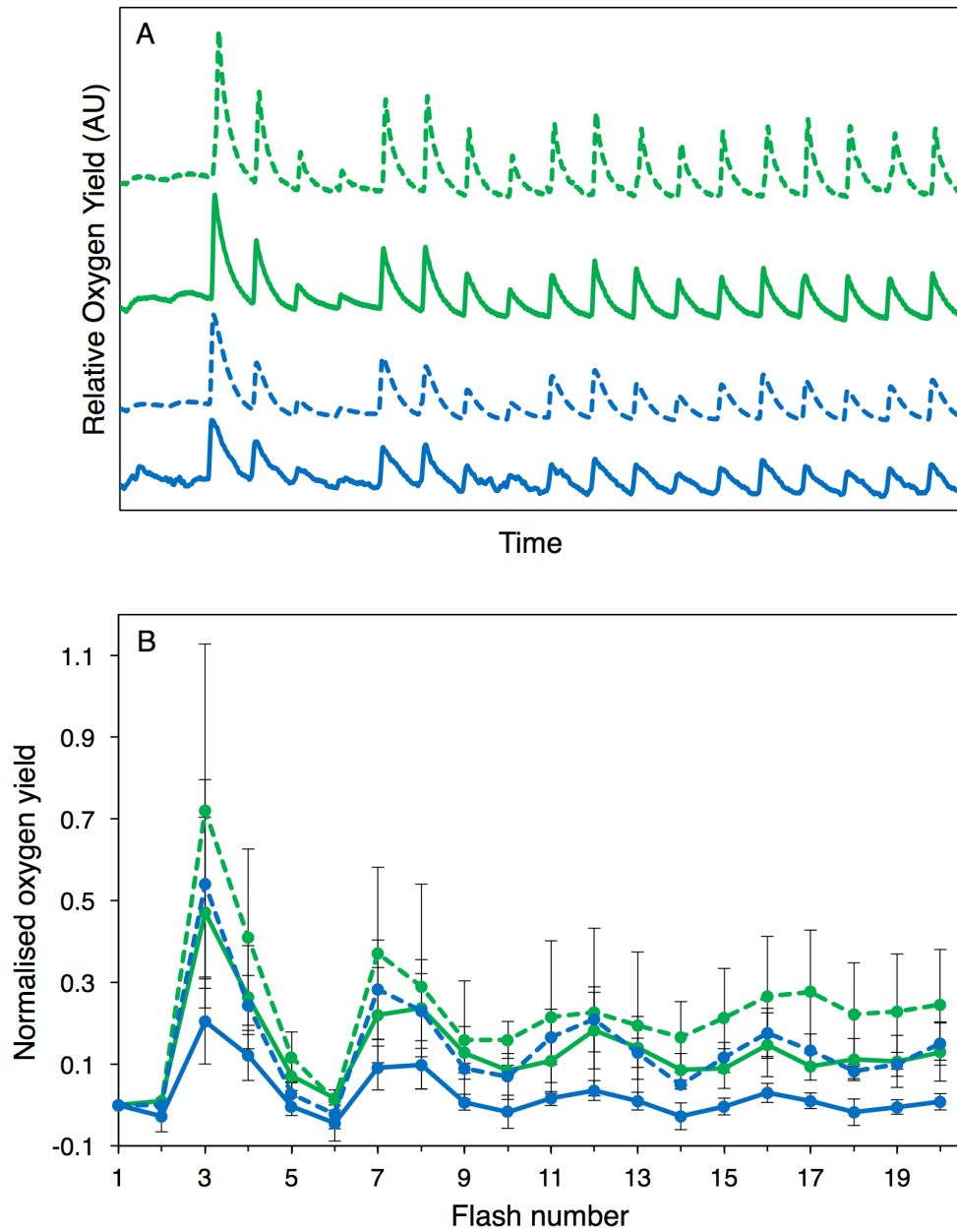
Figure 5.8. Flash-induced oxygen yield from GT-O1 and E364Q cells grown to mid-late log-phase and incubated for 24 h in pH 7.5/autotrophic (dashed lines) or pH 10.0/autotrophic (solid lines) conditions. Oxygen yield is shown as the mean trace (relative, arbitrary units) measured with 20 saturating flashes in dark-adapted cells (A), and the first-flash normalised yield ± SEM (B). Traces represent the mean from 3 independent measurements. GT-O1 (green), and CP47 E364Q (blue).

Table 5.6. Ratio of relative flash-induced oxygen yields of GT-O1 and E364Q strains grown in autotrophic pH 7.5 and pH 10.0 conditions for 24 h. Flash yield ratios (mean ± SEM, $n = 3$) were determined using a normalised first flash value.

	WT GT-O1		E364Q	
Flash ratio	pH 7.5	pH 10	pH 7.5	pH 10
4th/3rd flash	0.57 ± 0.03	0.56 ± 0.01	0.45 ± 0.08	0.59 ± 0.11
5th/4th flash	0.28 ± 0.01	0.27 ± 0.01	0.11 ± 0.14	0.03 ± 0.22

One possible explanation for the observed altered flash oxygen yield in E364Q cells on a per-chlorophyll basis might be a change in the ratio of PS II to PS I in mixotrophic vs. autotrophic conditions, or between pH levels. Determination of low-temperature chlorophyll fluorescence with 440 nm excitation wavelength, targeting chlorophyll, suggested this was not the case, with only a slight variation in PS II levels detected between pH 7.5 and 10.0 in autotrophic conditions (Fig. 5.9), and between pH 7.5 autotrophic and mixotrophic conditions (low temperature fluorescence in mixotrophic conditions is shown in Appendix Fig. A.6). Generally, pH 10.0 resulted in slightly reduced PS II fluorescence levels in GT-O1 and E364Q, and in particular, reduced 685 nm emission from the strains lacking the PsbV protein, implying a reduction in unassembled PS II centres in these conditions. With 580 nm excitation wavelength (Fig. 5.10), PBS fluorescence was reduced at pH 10.0, indicating improved accessory pigment coupling in these conditions. In particular, significant emission from the PBS terminal emitter was detected in the double mutants in which PsbV had been removed, but this effect was quenched substantially in pH 10.0 conditions. Minimal differences were detected between the GT-O1 and E364Q strains, and although fluorescence yield was altered in E364Q:ΔPsbV cells compared to the ΔPsbV strain, it was similar to that of the ΔPsbV:ΔCyanoQ mutant and might reflect similarly altered PS II assembly arising from double mutations involving the PS II extrinsic protein domains.
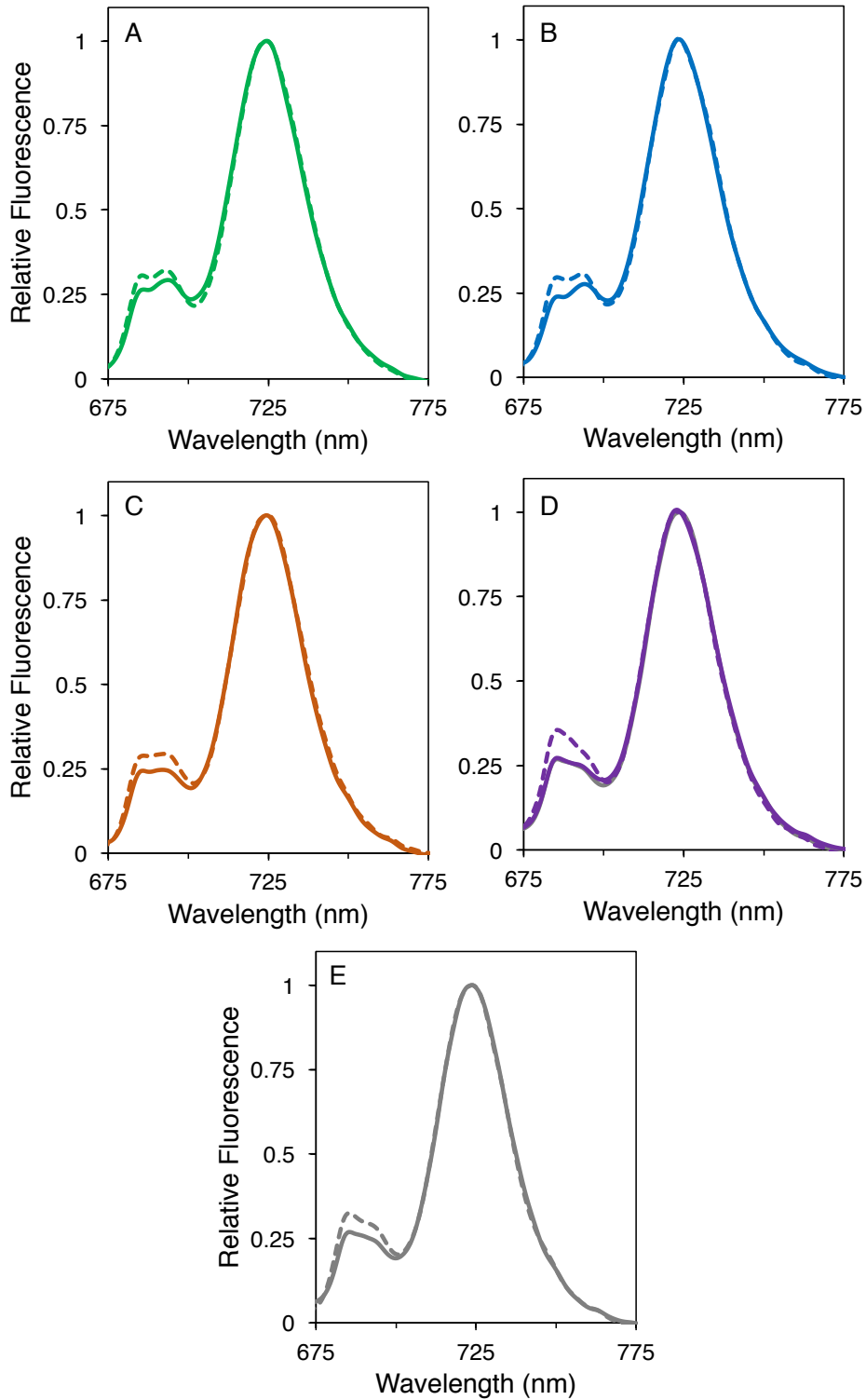
Figure 5.9. Low-temperature fluorescence emission of *Synechocystis* 6803 strains with 440 nm excitation wavelength, targeting chlorophyll. Cells were grown to mid-late log phase and incubated for 24 h in pH 7.5/autotrophic (dashed lines) or pH 10.0/autotrophic (solid lines) conditions. Traces represent the mean of 3-4 independent measurements and are normalised to the ~725 nm PS I fluorescence emission maxima. A, GT-O1; B, E364Q; C, ΔPsbV; D, E364Q:ΔPsbV; E, ΔPsbV:ΔCyanoQ.
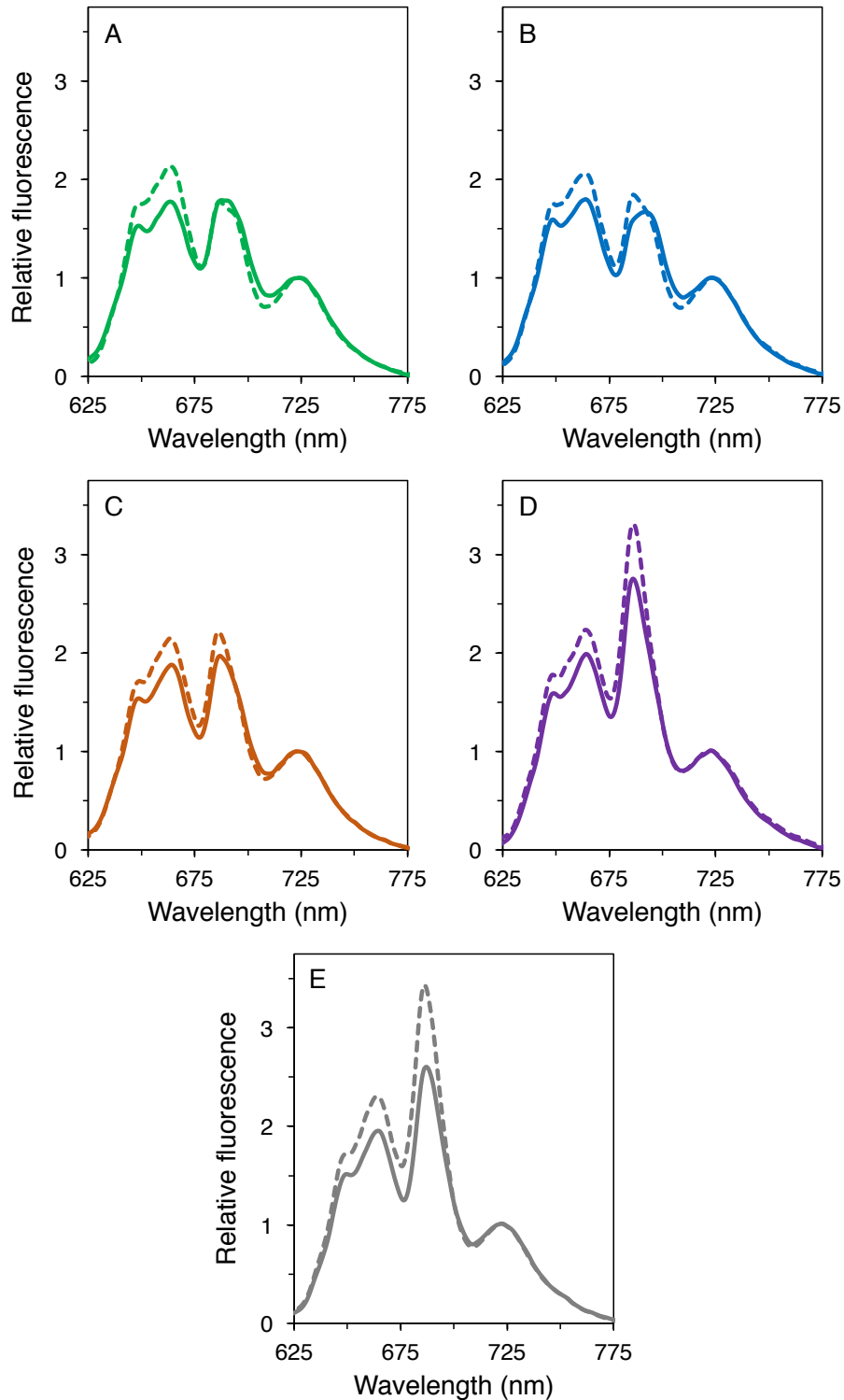
Figure 5.10. Low-temperature fluorescence emission of *Synechocystis* 6803 strains with 580 nm excitation wavelength, targeting PBS. Cells were grown to mid-late log phase and incubated for 24 h in pH 7.5/autotrophic (dashed lines) or pH 10.0/autotrophic (solid lines) conditions. Traces represent the mean of 3-4 independent measurements and are normalised to the ~725 nm PS I fluorescence emission maxima. A, GT-O1; B, E364Q; C, ΔPsbV; D, E364Q:ΔPsbV; E, ΔPsbV:ΔCyanoQ.

The net effect of PS II function in terms of LEF can be inferred from analysis of P_{700} oxidation kinetics (Fig. 5.11), although CET can contribute to this as well. When P_{700} oxidation was induced in dark adapted cells at pH 7.5 vs pH 10.0, a clear effect of pH 10.0 in enhancing electron transport to PS I was observed, with greater and generally more rapid quenching of P_{700}^+ after ~0.5 s. P_{700}^+ in E364Q cells was apparently quenched slightly more rapidly than in the GT-O1 strain, and deletion of PsbV both slowed and reduced the ability of electron transport to reduce P_{700}^+. This effect was greater in the double mutants, with the somewhat surprising result that electron transport to PS I was apparently greater in ΔPsbV:ΔCyanoQ cells than in E364Q:ΔPsbV cells, despite the indication from room temperature fluorescence data, and flash-oxygen yield (albeit in mixotrophic conditions), that PS II function might be relatively better in the latter strain.
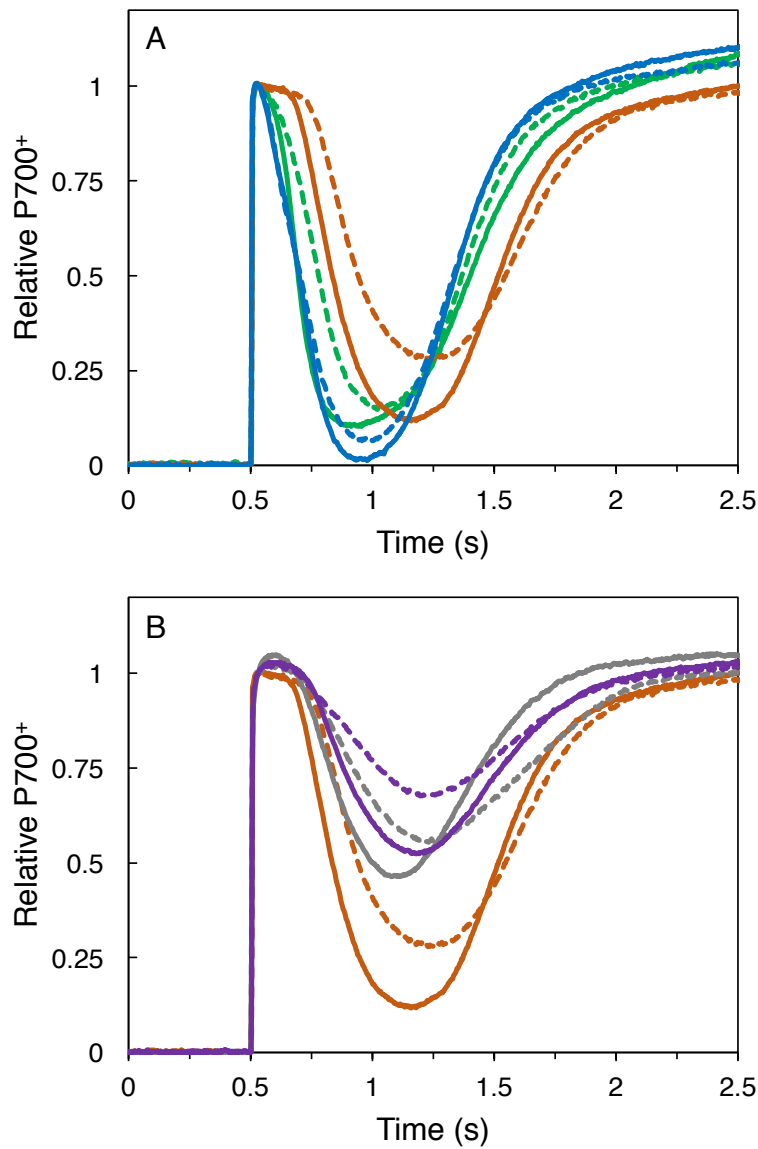
Figure 5.11. Relative P_{700}^+ in dark-adapted *Synechocystis* 6803 strains grown to mid-late log phase and incubated for 24 h in pH 7.5/autotrophic (dashed lines) or pH 10.0/autotrophic (solid lines) conditions. Induction of P_{700} oxidation occurs during actinic illumination of cells after 0.5 s. Traces represent the mean result from 3-4 independent measurements (of which 2-3 measurements were made by S Kovács). A: GT-O1 (green), E364Q (blue), and ΔPsbV (orange). B: ΔPsbV (orange), E364Q:ΔPsbV (purple), and ΔPsbV:ΔCyanoQ (grey).

5.4 Discussion

Previous studies of loop E in CP47 identified that perturbations in residues now known to be located adjacent to Y_D based on the 1.9 Å PS II crystal structure (Umena et al., 2011; Suga et al., 2015) were important for PS II assembly and function, but an Glu364 to Gln substitution in CP47 appeared to produce a minor phenotype (Eaton-Rye and Vermaas, 1991; Putnam-Evans et al., 1996; Morgan et al., 1998). Although this amino acid substitution did not substantially affect growth and PS II-dependent oxygen evolution in those studies, this work shows that changes in the redox potential of electron carriers in PS II and alterations in charge recombination result from this mutation. In addition, the redox state of PS II was found to vary between photoautotrophic and photomixotrophic conditions, and between pH 7.5 and pH 10.0. These effects were more pronounced in pH-sensitive mutants and the E364Q mutant than in the wild-type GT-O1. However, TL in the GT-O1 wild-type was affected by pH, suggesting that alteration of external pH is able to affect the electron transport processes embedded within PS II. In TL measurements, addition of DCMU, which directly affects redox state of the Q_A/Q_A^- couple (Krieger-Liszkay and Rutherford, 1998), resulted in generally enhanced TL yields in mutant cells (the GT-O1 strain was much less affected in terms of TL yield), and in particular the TL yield from the C band, reflecting $Y_D^+Q_A^-$ charge stabilisation.

In the E364Q and E364Q:ΔPsbV strains, the results of the experiments in this study suggest a greater likelihood of charge recombination via P_{680}^*, possibly due to a shift in redox balance between Q_A/Q_A^- and/or Y_D/Y_D^+. The TL yield data obtained in this study suggests that far greater charge recombination between Y_D^+ and Q_A^- occurs in the E364Q and E364Q:ΔPsbV cells than in the wild-type cells or ΔPsbV strain, and therefore that the population of Y_D^+ is increased by the Glu364 to Gln substitution. If Y_D is more oxidised in dark-adapted E364Q and E364Q:ΔPsbV cells, the electrostatic change in this region might influence the positive charge on P_{680}^+ following illumination, which could be destabilised as a result (Rutherford et al., 2004; Styring et al., 2012). This could increase the likelihood of the charge recombination leading to the formation of chlorophyll triplets and $^1O_2$ production (Cser and Vass, 2007; Fufezan et al., 2007). However, a preliminary experiment using the His-trapping method of Rehman et al. (2013) did not find differences in $^1O_2$ production between GT-O1 and E364Q cells at pH 7.5 or pH 10.0 (data not shown). Nevertheless, a less readily oxidised Y_D would also increase the energy gap between Y_D^+ and Q_A^-, an interpretation supported by the increase in $Y_D^+Q_A^-$ stabilisation in E364Q cells compared to that observed in the GT-O1 wild-type. This result is

indicated by enhanced C band TL from the mutant in all conditions tested and particularly at pH 10.0, and also by an inability of flash-induced fluorescence from E364Q and E364Q:ΔPsbV cells to decay over ~10 s compared to the GT-O1 control. The striking increase in TL yield in the E364Q mutant overall reflects a far greater probability that P_{680}^* is repopulated during charge recombination and that the efficiency of non-radiative charge recombination is reduced (Cser and Vass, 2007). In particular, the high TL from B/Q bands in E364Q compared to GT-O1 points to redox shifts between the OEC and the quinone electron acceptors (increased $S_2Q_B^-$/$S_2Q_A^-$ stabilisation) that is presumably being caused by the perturbation near Y_D. The fact that the TL peak temperatures shifted in E364Q cells in both the presence and absence of DCMU points to a change on the donor side of PS II rather than an alteration in Q_A or Q_B (Vass and Govindjee, 1996). Autotrophic conditions at pH 7.5 caused the greatest enhancement in B/Q band yield in this strain, and this redox alteration could be an explanatory factor in the pH-sensitivity of the E364Q:ΔPsbV double mutant.

The TL profile from the ΔPsbV mutant studied here, with reduced yield and elevated B/Q T_{max} bands relative to wild type, is similar to that reported previously in the *Synechocystis* 6803 ΔPsbV mutant (Shen et al., 1995, 1998). In ΔPsbV cells, dark adaption periods cause rapid deactivation of the Mn_4CaO_5 complex (Shen et al., 1995); therefore, as both TL and flash-oxygen yield are dependent on functional S-state transitions in the OEC, it is unsurprising that the all mutants lacking PsbV in this study display reduced TL and flash-oxygen yield. Yet, a number of results obtained here suggest that the phenotype of the E364Q:ΔPsbV strain shows traits that are somewhat different from a simply compounding effect of the two PS II mutations. For example, modelled fluorescence decay kinetics were more similar between E364Q:ΔPsbV and GT-O1 cells than between the E364Q:ΔPsbV and ΔPsbV strains, and B & Q band TL yields in autotrophic conditions were similar between the E364Q:ΔPsbV and ΔPsbV mutants, whereas in E364Q and GT-O1 cells TL yields were strikingly different. To a certain extent, this might reflect reduced PS II assembly in the double mutant, indicated by room-temperature fluorescence yield and F_V/F_M in this study, and in prior studies (Eaton-Rye et al., 2003). Thus, while TL B & Q band yields were similar or slightly lower in E364Q:ΔPsbV cells compared to the ΔPsbV strain, they might still indicate a shift in the double mutant towards charge recombination via P_{680}^*, potentially producing chlorophyll triplets and $^1O_2$. The most striking effect in the double mutant is on the C band TL yields, which were much higher in most conditions and indicate that the main site of redox shift due to the Glu364 to Gln mutation is changes in the redox potential of Y_D/Y_D^+. In addition, the F363R and F363R:ΔPsbV mutants

showed a similar pattern, but results were more severe in terms of altered TL and impaired fluorescence decay, which is consistent with the severe growth impairments and reduced PS II levels in this strain. The large modification of C band TL in the F363R mutants strongly supports the interpretation that changes in the environment of Y_D appear to affect the Y_D/Y_D^+ redox potential in the CP 47 Loop E mutants studied here.

It is of note that the E364Q:ΔPsbV mutant and ΔPsbV:ΔCyanoQ mutant appear very different in a number of respects, some of which appear counter-intuitive. For example, there was no detected flash oxygen yield from ΔPsbV:ΔCyanoQ cells, yet oxygen evolution in this strain was similar to the rates observed in the E364Q:ΔPsbV strain (Summerfield et al., 2005a), and in this study electron transport to P_{700}^+ in the ΔPsbV:ΔCyanoQ mutant was enhanced relative to the situation in the E364Q:ΔPsbV strain. However, the ΔPsbV:ΔCyanoQ strain showed increased low temperature fluorescence upon excitation at 580 nm in pH 7.5 conditions compared to the E364Q:ΔPsbV strain, which indicates greater pigment decoupling from PS II in the former strain. Yet, the impairment of fluorescence decay following a single-turnover actinic flash from E364Q:ΔPsbV cells in the presence of DCMU exceeded that observed in the ΔPsbV:ΔCyanoQ mutant. However, in the absence of DCMU the ΔPsbV:ΔCyanoQ strain appeared to be most severely affected compared to the GT-O1 control, especially at pH 7.5. It seems reasonable to conclude, based on these somewhat conflicting data, that the deletion of CyanoQ induces very different functional changes in PS II compared to the Glu364 to Gln substitution. Therefore, the mechanism of pH-sensitivity in the E364Q:ΔPsbV strain might differ as well. However, whether exogenous factors affecting CCM activity (such as enriched CO_2) or ROS might affect the pH 7.5 response of the E364Q:ΔPsbV strain was not tested in this study.

Other aspects of photosynthesis investigated in this study support a consistently harmful effect of pH 7.5 growth conditions relative to pH 10.0 on PS II mutant strains, similar to the patterns observed in the ΔPsbO:ΔPsbU mutants (see Chapter Four). Generally, altered low-temperature fluorescence emission indicating impaired PS II assembly and reduced PBS binding, reduced electron transfer quenching of P_{700}^+, reduced fluorescence yield during fluorescence induction, and altered (generally slowed) chlorophyll decay kinetics was observed compared to pH 10.0. These effects were limited in the *Synechocystis* 6803 wild type used here, reflecting its apparent insensitivity to pH in terms of growth and PS II activity reported in other studies (Eaton-Rye et al., 2003; Summerfield et al., 2005a).

As well as generalised effects on growth, pH manipulations in these experiments are likely to have directly affected TL, and OEC and Y_D function, depending on the extent of the cellular pH homeostatic response. Many studies have analysed TL and Y_D function in terms of their pH-dependency (e.g. Rutherford et al., 1984; Vass and Styring, 1991), but these have generally used isolated thylakoids from higher plants; isolated thylakoids are probably less buffered against pH change than intact *Synechocystis* 6803 cells, which display a relatively small increase in pH_{cyt} from ~6.8 to ~7.2 when pH_{ext} is increased from ~8.0 to ~10.0 respectively (Jiang et al., 2013). Altered PS II function, a primary source of protons for pH homeostasis, would reduce the capacity for pH-control in PS II mutants compared to the apparently well-buffered wild type. However, in *Synechocystis* 6803, mixotrophic conditions can somewhat increase internal pH (Ryu et al., 2004). Altered pH homeostasis might explain discrepancies seen in the E364Q mutant in the apparent dark S_0/S_1 ratios (indicated by $4^{th}/3^{rd}$ flash oxygen yield) between mixotrophic and autotrophic conditions; pH affects the stability and efficiency of S-state transitions in the OEC with a tendency towards decreased activity in acidic (<6.0) and alkaline (>8.0) pH ranges (Najafpour et al., 2016). One possible effect of the Glu364 to Gln mutation on the redox potential of PS II components and pH-sensitivity could be an alteration in the dark state of the OEC. For example, a tendency towards slow S_3 decay in the dark would yield PS II centres in dark S_2 state rather than S_1, wherein one flash in TL measurements would yield $S_3Q_B^-$, which emits TL at roughly double the yield of $S_2Q_A^-$ (Rutherford et al., 1984); this could explain the large enhancement in TL yield in E364Q cells. However, flash oxygen yield data indicate that this is not likely to be the case. A dark S_2 state would result in peak flash oxygen yield on flash two, yet this was consistently seen on flash three and flash four in the E364Q strain with little oxygen yield from flash one or two, suggesting a mixed S_0/S_1 dark state. The S_0/S_1 ratios of the GT-O1 wild type were unaffected by autotrophy/mixotrophy, or by pH 7.5/pH 10.0 changes, but results with the E364Q strain were variable between the three conditions tested. Likewise, TL appeared to vary more strongly in E364Q cells than in the GT-O1 control between growth conditions. In fact, the flash oxygen yield data obtained here suggest that the Glu364 to Gln mutation results in PS II centres with a tendency towards S_0, leading to a relatively enhanced 4th flash yield in permissive growth conditions ($4^{th}/3^{rd}$ flash yield: GT-O1 < E364Q < ΔPsbV < E364Q:ΔPsbV). Deletion of PsbV in *T. elongatus* also resulted in an increase in dark S_0 state in another study, prompting the suggestion that PsbV binding might also affect Y_D oxidation (Kirilovsky et al., 2004); this would imply a twofold effect on Y_D in the E364Q:ΔPsbV mutant.

Whereas isolated thylakoids show a relatively stable TL B band T_{max} from pH ~7.5 to ~10.0, the Q band T_{max} increases significantly (Vass and Inoue, 1986). However, in this study, wild-type GT-O1 B band T_{max} values were stable between autotrophic pH 7.5 and pH 10.0 conditions, and Q band T_{max} values decreased; we can conclude that pH-buffering in wild-type cells counteracted the effects of pH on TL seen in isolated thylakoids. In contrast, the T_{max} of the B band in E364Q cells was stable, but the T_{max} of the Q band increased markedly; this could imply an alteration in internal pH in the mutant cells, causing TL changes more similar to that in isolated thylakoids. If this is the case, increased pH_{cyt} in E364Q cells at pH 10.0 would result in more rapid electron transfer from Y_D to the OEC during illumination and from the OEC to Y_D^+ in the dark (Vass and Styring, 1991; Styring et al., 2012). This could represent a functional explanation for growth of the E364Q:ΔPsbV mutant in pH 10.0, where the directly pH-altered redox properties of Y_D are sufficient to counteract perturbations caused by the mutation in the H-bonding network of Y_D/Glu364. These perturbations are likely to affect the deprotonation of His_D, which affects the oxidation rate of Y_D by the OEC (Vass and Styring, 1991; Saito et al., 2013; Sjöholm et al., 2017). Thus, the coordination environment of His_D, which includes Glu364, is directly relevant to the Y_D oxidation rate. This interpretation is supported by the apparent changes in redox equilibria for specific steps associated with the turnover of the S-states and electron transfer between Q_A and Q_B in the E364Q mutant. The loss of PsbV appears to have altered the accessibility of the OEC to reductants in the lumen (Shen et al., 1998; Kirilovsky et al., 2004; Bricker et al., 2012), but the E364Q mutation might impair the oxidation of the OEC by Y_D, and it is therefore unsurprising that the E364Q:ΔPsbV double mutant shows a complicated phenotype with respect to the apparent redox state of PS II electron carriers compared to the E364Q and ΔPsbV mutants.

The analysis of the conservative Glu364 to Gln mutation and its apparent effect on PS II redox equilibria is consistent with a number of prevailing theories of Y_D function. Alterations in the stability of $S_2Q_B^-/S_2Q_A^-$ and $Y_D^+Q_A^-$ charge pairs in the E364Q strain point to changes in the capacity of Y_D to maintain charge equilibrium with the OEC, potentially because the coordination environment around the proton recipient critical for Y_D oxidation, His_D, is affected by altered conformation in the vicinity of D2 Arg294 in the E364Q mutant. This results in altered fluorescence decay (following a single turnover flash) and flash oxygen yield, with a tendency towards a dark S_0 state. However, impaired growth of E364Q:ΔPsbV cells at pH 7.5 occurs in conditions of 24 h light, so the dark-redox state of Y_D and any aberrant charge

recombination in the dark might well be irrelevant to the mechanism of pH-sensitivity in the E364Q:ΔPsbV strain. What is more likely is that putative redox shifts in the E364Q strains affect electron transport and charge recombination, particularly when the PS II acceptor side is already reduced, during periods of illumination. The large increase in TL indicates greater charge recombination via $P_{680}*$, but in illuminated conditions, the proposed ability of Y_D to relieve acceptor side electron pressure and to increase the potential for Y_Z oxidation and restrict PS II damage to the D1 side of PS II (Rutherford et al., 2004; Styring et al., 2012) might be altered in the E364Q strains. However, at pH 10.0, the enhanced internal pH promotes Y_D oxidation, and might mitigate this effect. Overall, these data suggest a role of the extrinsic Loop E domain in maintaining a proper redox state around Y_D. Perturbations in the conserved Phe-Phe-Glu region of CP 47 thus affect redox equilibria in PS II, even in strains which appear to grow normally; removal of PsbV and subsequently increased exposure of the OEC to the reductive environment of the lumen impairs growth and results in obligately photoheterotrophic or pH-sensitive strains.

Chapter Six: General discussion and conclusions

6.1 Genome mutation and phenotypic variation in optimal growth conditions

The first part of this study involved the assembly of the genome sequence of two wild-type substrains of *Synechocystis* 6803, GT-O1 and GT-O2, and a long-term culturing experiment was used to trace the fate of a novel genomic mutation that arose in GT-O1. Analysis of the physiology of the GT-O1 substrain was made in comparison to the internationally studied PCC-Moscow substrain, as well as the GT-Kazusa substrain, from which the original genome sequence of *Synechocystis* 6803 was determined (Kaneko et al., 1995, 1996). This study has identified a significant number of novel mutations in the *Synechocystis* 6803 wild types GT-O1 and GT-O2, some of which are likely to affect gene function, which have arisen during routine laboratory culture conditions. In particular, the mutations in GT-O2, such as the apparent loss of function of ChlH and Hik8 point to a process of genetic selection based on the conditions experienced during long-term culturing: resources apparently diverted from chlorophyll biosynthesis and day/night detection might favour optimal growth in GT-O2. In the course of this study, a culture of GT-O1 obtained a homozygous insertion in *slr0856*, which might give rise to a new, functional ISY*100*-type transposase ORF. Both GT-O2 and the wild-type GT-W display reduced chlorophyll biosynthesis (Crawford et al., 2016; Tichý et al., 2016), and it is noteworthy that the genome mutation leading to this phenotype in GT-W was flanked by ISY*100*-type transposase genes, raising the possibility that its phenotype arose from ISY*100* transposition in a process similar to that detected in GT-O1. The data presented in this study revealed small differences in physiological traits between the PCC-Moscow and GT-Kazusa substrains compared to the GT-O1 substrain. Whereas growth rate was similar, cells from the GT-O1 substrain are smaller than PCC-Moscow and GT-Kazusa cells. The overall similarities in most respects between PCC-Moscow and GT-Kazusa cells revealed by this study imply that the reduced cell size is a GT-O-specific or GT-Vermaas-specific phenotype.

Although the genetic instability of cyanobacteria has been highlighted (Jones, 2014), baseline comparisons between wild-type GT-O1, GT-Kazusa and PCC-Moscow substrains of *Synechocystis* 6803 in this study showed minimal phenotypic variation. This is in spite of several unique mutations per strain, which have been summarised in an up-to-date family tree of the *Synechocystis* 6803 wild types for which genome information could be obtained (Fig.

6.1). A version of this figure was presented in Ikeuchi and Tabata (2001) and has been updated sporadically by researchers upon publication of their own lab's wild-type genome sequence, in particular by Trautmann et. al (2012), based simply on the presence or absence of certain SNPs and indels in the strains that underwent re-sequencing. The wild-type mutations in GT-O2 and GT-W (Crawford et al., 2016; Tichý et al., 2016) suggest that in conditions of long term culturing, *Synechocystis* 6803 shows a tendency to undergo genomic mutations that affect photosynthesis and probably reflect optimisation of growth strategy. Such a tendency can be avoided in laboratory contexts by appropriate culture technique (such as the frequent refreshment of lab cultures from frozen cell stocks, rather than reliance on continuously cultured of strains), but it might be impractical to avoid genomic drift in large-scale bioreactor cultures such as those used for bioenergy. In other model micoorganisms, such as *Chlamydomonas reinhardtii* (Gallaher et al., 2015) and *Chlorella vulgaris* (Müller et al., 2005), similar genetic drift has also been observed; and even laboratory culture stocks of higher plants such as *A. thaliana* and *Zea may*s are apparently affected by contamination, heterotrophy, or mutation (Bergelson et al., 2016). In *Synechocystis* 6803, short generation times and rapid domination of cultures by more successful strains (within days, e.g. Hihara et al., 1998) make whole genome resequencing an imperative and useful tool not only to validate the wild-type background in use, but also to reveal interesting phenotypes associated with spontaneous mutants (Hihara and Ikeuchi, 1997; Crawford et al., 2016; Tichý et al., 2016); these tools might inform our understanding of photosynthetic processes and natural selection.
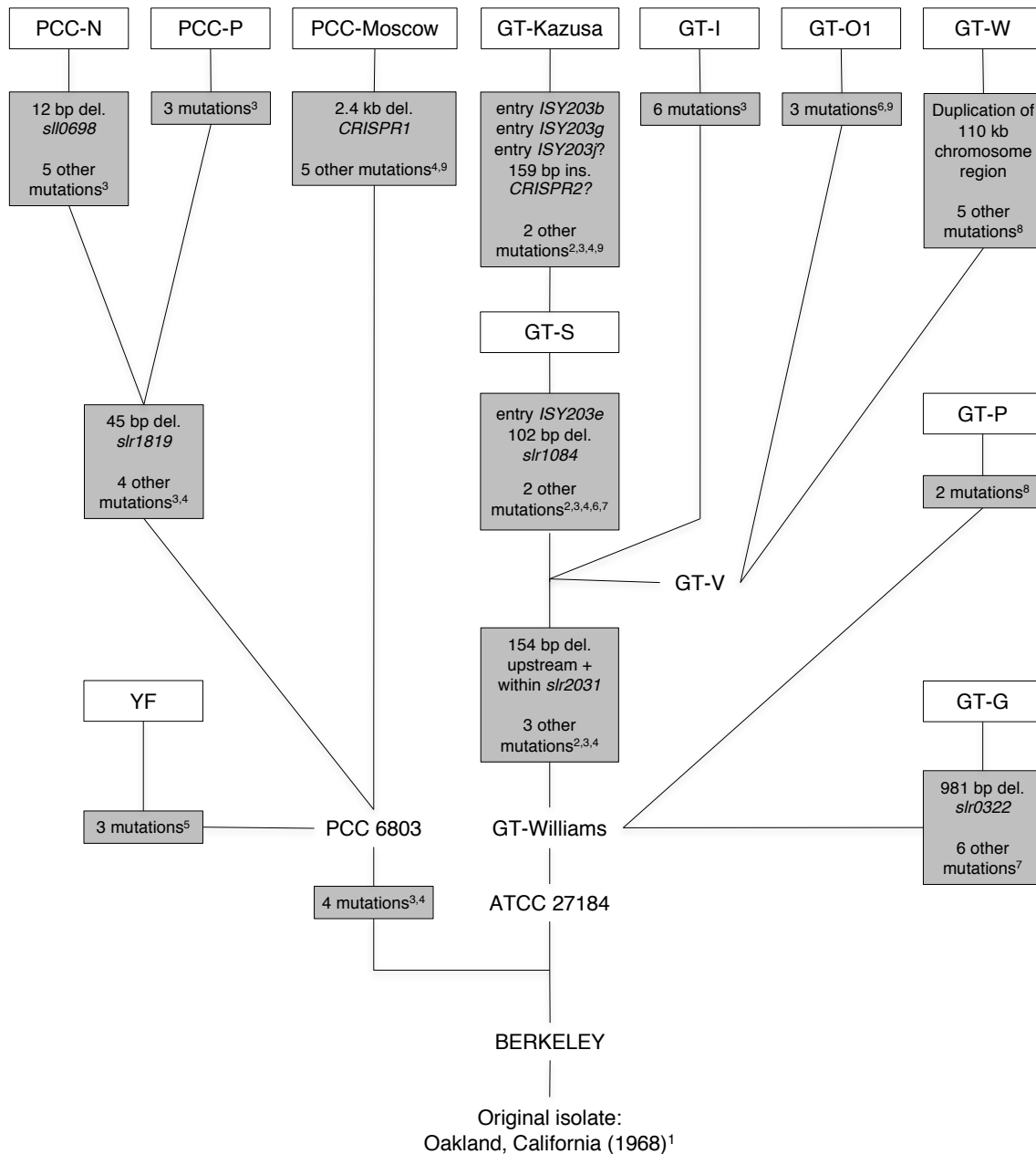
Figure 6.1. Graphical representation of the divergence of *Synechocystis* sp. PCC 6803 substrains into the motile PCC-lineage and non-motile GT-lineage. Large indels (>10 bp) and the number of known substrain-specific SNPs and <10 bp indels are included on their known branch point. Sequenced substrains are depicted in solid boxes. The position of the YF strain and the GT-V substrain (for Prof. WFJ Vermaas) is speculative, as is the position of the ISY*203j* and *CRISPR2* insertions, which might have occurred prior to the isolation of the GT-I or GT-S strains. This figure was modified after Trautmann et al. (2012). The substrain GT-O2 has been omitted for clarity. Letters in superscript: [1]Stanier et al. (1971), [2]Tajima et al. (2011), [3]Kanesaki et al. (2012), [4]Trautmann et al. (2012), [5]Aoki et al. (2012), [6]Morris et al. (2014), [7]Ding et al. (2015), [8]Tichý et al. (2016), [9]Morris et al. (2017).

6.2 Genome mutation and pH response in pH-sensitive PS II mutants deficient in extrinsic proteins

The second part of this study investigated genomic and physiological differences between a pH 7.5-sensitive ΔPsbO:ΔPsbU PS II mutant, and a pseudorevertant strain capable of pH 7.5 autotrophic growth. The pseudorevertant was found to carry three specific mutations that affect conserved residues in the proteins PmgA, CheA and Ssr1558, and results of a top-agar experiment suggested that the apparent Gly93 to Cys mutation in PmgA is the candidate for restoration of growth at pH 7.5. However, in the course of this study, no mutagenesis strategy to introduce the pseudorevertant *pmgA* gene copy into ΔPsbO:ΔPsbU cells (or *vice versa*) was successful. Additionally, *pmgA* appears to be essential to ΔPsbO:ΔPsbU cells, and it was not possible to assess the effect of *pmgA* deletion in this mutant.

In addition to a general reduction in PS II activity, an alteration in levels of ROS production (seen in this study), or sensitivity to ROS (Summerfield et al., 2013), due to reduced pH seems likely to contribute to the pH-sensitivity of ΔPsbO:ΔPsbU mutants. Based on the data presented here, the Con:ΔPsbO:ΔPsbU strain might be producing more overall ROS at ~pH 7.5 compared to pH 9.0/10 or compared to the pseudorevertant, but the pseudorevertant appears to be producing more $^1O_2$ specifically. Thus, the absolute production of ROS is not necessarily a straightforward explanation for low pH-growth of the pseudorevertant. If the Gly93 to Cys mutation in PmgA affects the function of this protein (which bears resemblance to a Ser-Thr kinase and might be an anti-sigma factor) it is possible that perturbed gene regulation, affecting carbon uptake, is able to rescue growth of the pseudorevertant strain. This interpretation is supported by the capacity for pH ~7.5 growth of the Con:ΔPsbO:ΔPsbU and ΔPsbV:ΔCyanoQ strains in enriched CO_2, and a reduction of growth in enriched CO_2 in the ΔPsbV:ΔCyanoQ:ΔNdhF3 mutant. The growth effect of enriched CO_2 would be expected to act on the cell downstream of PS II, and it is a novel finding that this potentially PS II-independent effect rescues the Con:ΔPsbO:ΔPsbU strain. Thus, altered electron transport on the acceptor side of PS II and/or downstream of electron transport chain (affected by PmgA in the pseudorevertant or CO_2 in Con:ΔPsbO:ΔPsbU) seems to explain the growth phenotype, in spite of the fact that the loss of extrinsic proteins must dramatically affect the PS II donor side as well. These findings suggest that maintenance of electron transport, carbon uptake, and probably ΔpH is more difficult at pH 7.5 than pH 10.0, providing a tentative explanation of the pH-sensitivity of some PS II mutants.

6.3   PS II redox equilibria and the pH response of CP47 and PsbV mutants

The final part of this study addressed the possibility that perturbations in the redox state of PS II arise from mutations in the vicinity of Y_D, and that these perturbations might be enhanced by low pH growth. In E364Q and E364Q:ΔPsbV, the results of the experiments in this study suggest a greater likelihood of charge recombination via $P_{680}*$ due to a shift in redox balance between Y_D/Y_D^+, and the efficiency of non-radiative charge recombination is reduced in these strains. The data obtained in this study suggests that charge recombination between Y_D^+ and Q_A^- is more likely in the E364Q and E364Q:ΔPsbV cells than in the wild-type cells or ΔPsbV strain, and therefore that the population of Y_D^+ is increased by the Glu364 to Gln substitution. It appears that Y_D perturbations are the main site of redox shift in the CP47 Loop E mutants studied here: one possible effect of the Glu364 to Gln mutation on the redox equilibria of PS II electron transport components and pH-sensitivity could be due to an alteration in the dark state of the OEC. If this is the case, increased pH_{cyt} in E364Q at pH 10.0 would result in more rapid electron transfer from Y_D to the OEC during illumination and from the OEC to Y_D^+ in the dark (Vass and Styring, 1991; Styring et al., 2012). This could represent a functional explanation for growth of the E364Q:ΔPsbV mutant in pH 10.0, where the directly pH-altered redox properties of Y_D are sufficient to counteract perturbations caused by the mutation in the H-bonding network of Y_D/Glu364. Overall, these data suggest to a role of the extrinsic Loop E domain in maintaining a proper redox state around Y_D. Additionally, TL in the GT-O1 wild-type was affected by pH, suggesting that alteration of external pH is able to affect the electron transport processes embedded within PS II, despite the physical separation of the OEC from the external environment by the thylakoid and cytoplasmic membranes, as well as the peptidoglycan cell wall.

6.4   Future perspectives and unanswered questions

The findings in Chapter Three that phenotypic variation was relatively limited between GT-O1, GT-Kazusa and PCC-Moscow does not rule out the possibility that they may vary substantially in their utility as representative wild-type substrains of *Synechocystis* 6803. In particular, their capacity for growth and photosynthesis in stressful growth conditions was not tested, nor was the impact of introducing analogous mutations. It appears that certain wild-type backgrounds might display variable responses to stressors (e.g. solvents, see Jones, 2014), and variable phenotypes upon deletion of the same gene, such as *pmgA*; deletion of this gene was impractical in GT-O1 compared with another GT-substrain (Hihara and Ikeuchi, 1997). In

addition, the observation of mutations potentially affecting ISY*100* was not functionally categorised, and the co-occurrence of ISY*100* mutations in a culture of GT-O1 and GT-W might be a coincidence.

The suggestion in Chapter Four that a PmgA Gly93 to Cys mutation rescues growth of the Con:ΔPsbO:ΔPsbU strain at pH 7.5 was not conclusively resolved in this study, due to the inability to fully segregate a ΔPsbO:ΔPsbU:ΔPmgA mutant and/or introduce the G93C-encoding gene copy into this strain; thus future mutagenesis experiments might be warranted. The PmgA protein appears widely in the *Synechocystis* 6803 literature but has not been analysed in terms of protein structure, and its role remains unclear. Even if the PmgA mutation contributes to the pH 7.5 growth of the pseudorevertant strain, an Arg54 to Glu mutation in the hypothetical protein Ssr1558 might also be relevant, if its predicted homology to a recently identified Ca^{2+} and/or Mn^{2+}/H^+ antiporter in *A. thaliana* is accurate. But, this possibility was not investigated in this study, as only the pseudorevertant *pmgA* rescued Con:ΔPsbO:ΔPsbU growth in a top agar experiment. Furthermore, some genome mutations in GT-O1 were undetected by genome assembly, and had to be analysed by PCR; therefore, the possibility exists that a large indel was undetected during pseudorevertant genome assembly and that this affects low-pH growth. This possibility has precedent; an ISY*203*-type insertion event in the GT-Kazusa strain interrupts the *hik32* gene, with an unknown impact on *hik32*-mediated stress responses.

The differences between the ΔPsbV:ΔCyanoQ mutant and the E364Q:ΔPsbV mutant in Chapter Five prompted the suggestion that the mechanism behind the pH-sensitivity of the two mutants might vary. However, whether enriched CO_2 might affect the pH 7.5 response of the E364Q:ΔPsbV strain was not tested in this study, and thus it is unknown whether CO_2 enhancement represents a universal strategy for obtaining photoautotrophic growth from pH-sensitive PS II mutants. In addition, the perturbations in OEC activity and redox equilibria in the E364Q mutants could be further extended by additional but similar experiments to those employed here, such as TL analysis in the presence of multiple light flashes (to further investigate the dark S-states of PS II in these mutants), or investigation of the kinetics and rates of flash-oxygen release using the Joliot-type electrode.

A

pH 7.5: In the ΔPsbO:ΔPsbU mutant, PS II-specific ROS causes photoinhibition and prevents D1 repair; reduced proton efflux from the OEC reduces the trans-thylakoid ΔpH, and in turn, ATP synthase activity is low

B

pH 10.0: ROS production is reduced, and upregulated ROS antioxidant mechanisms allow D1 repair; ΔpH is enhanced as a direct result of enhanced environmental pH, as well as greater OEC activity; ATP synthase activity is increased

C

pH 7.5 + 3% CO_2: Rubisco activity in the carboxysome is increased, requiring NADPH; an increased electron sink enhances photosynthetic electron transfer and ROS production is decreased

Overleaf: Figure 6.2. Proposed model of pH effects on a ΔPsbO:ΔPsbU strain of *Synechocystis* 6803 at pH 7.5 (A), green background; pH 10.0 (B), blue background; and pH 7.5 with 3% CO_2 (C), green background. The ΔPsbO:ΔPsbU strain was chosen for illustrative purposes only; we would expect a similar response from other pH 7.5-sensitive strains, such as ΔPsbV:ΔCyanoQ. (A) At pH 7.5, ROS formation from an impaired OEC prevents PS II repair, causing photoinhibition and reducing PS II levels. Additionally, reduced delivery of protons to the thylakoid lumen results in low pH and insufficient ATP synthase activity (alternatively, growth may be retarded via sensing of the reduced ΔpH [not shown]). (B) At pH 10.0, however, upregulation of oxidative stress response genes induces the synthesis of antioxidant defence compounds, allowing PS II repair and photoautotrophic growth. Increased environmental pH naturally enhances ΔpH, increasing ATP synthase activity (or activating other pH-dependent processes that promote photoautotrophic growth [not shown]). (C) With 3% CO_2, enhanced Rubisco activity in the carboxysome requires NADPH, drawing electrons from PS II that would otherwise lead to excess ROS production and photoinhibition. The internal pH values indicated are based on those determined for wild-type cells by Belkin et al. (1987) and Jiang et al. (2013), and might be different in PS II mutants.

A working theory for the pH response of PS II mutants was presented in Morris et al. (2016) but remains tentative at the conclusion of this study (Fig. 6.2). In this theory, a number of factors were postulated to explain the pH-sensitivity of PS II extrinsic protein mutants, from production of ROS, to the loss of ΔpH to drive ATP synthase, to impaired PS II repair; but, only the former was directly addressed in this study. The experiments employed here to detect production of ROS during photosynthesis did not establish a clear link between low-pH growth and ROS production, but did provide some support for this theory. More $^1O_2$ was produced in all strains at pH 7.5 compared to pH 10.0, and more ROS was produced in non-growth-permissive pH 7.7 conditions in the Con:ΔPsbO:ΔPsbU strain. However, the pseudorevertant, which is autotrophic at both pH levels, appeared to produce more $^1O_2$ during photosynthesis at both pH levels than the Con:ΔPsbO:ΔPsbU mutant. Furthermore, the effect of enriched CO_2 on PS II mutants was suggested in this model to have a role in preventing photoinhibition by promoting Calvin-Benson cycle activity, enhancing the electron sink from PS II. However, the rescue of PS II mutant growth by enriched CO_2 could be counteracted by mutagenesis of *ndhF3*, despite the fact that 3% CO_2 should saturate Rubisco independently of CUP activity

(Zhang et al., 2004). Possibly, altered cellular NADPH supply or proton pumping across the thylakoid membrane (both affected by NdhF3) explains the rescue of ΔPsbO:ΔPsbU growth, rather than effects on electron transport downstream of PS II. However, it is clear from the results of this study that increased pH promotes a general improvement in PS II activity, electron transport and growth, and it is suggested that direct effects of pH 10.0 on PS II redox equilibria might ameliorate the effect of the Glu364 to Gln mutation and provide a functional mechanism for growth of the E364Q strain. Nevertheless, OEC activity in this strain was different to that of GT-O1 at pH 10.0 in terms of TL, flash oxygen yield and fluorescence decay, and it remains unresolved whether the enhancement of TL-inducing charge recombination pathways in the E364Q:ΔPsbV mutant affects $^{1}O_2$ production; but TL was high at both pH 7.5 and pH 10.0 and thus ROS seems unlikely to be an explanatory factor in pH-dependent growth of this mutant.

6.5 Final conclusion

This study sought to investigate the capacity for *Synechocystis* 6803 to undergo genome mutation in two model systems: the response of wild-type cells to ideal growth conditions, and the response of PS II mutants to stressful pH 7.5 conditions. In addition, aspects of the pH 7.5 response of PS II mutants were investigated. It was found that wild-type substrains of *Synechocystis* 6803 are prone to genomic mutation, especially during long term culturing, but that the functional effects of these mutations are limited in some wild-type substrains currently in use. Genomic mutation in a ΔPsbO:ΔPsbU substrain carrying deletions in PS II extrinsic proteins showed that PS II-independent processes affect the capacity for growth, but in an E364Q:ΔPsbV mutant, the direct effects of pH on the redox equilibria of PS II electron transport components such as Y_D might be explanatory factors for growth. These findings support the idea that the extrinsic proteins of PS II, while not absolutely necessary for PS II function, are important for maintenance of PS II redox equilibria and protection of the OEC, but exogenous factors (such as added glucose or CO_2) can improve cellular function in their absence. The rates of genomic mutation and responses to pH are directly relevant to the culture conditions in bioreactors, where long-term culturing of *Synechocystis* 6803 or similar species is currently a prospect for bioenergy production. Maintenance of pH conditions appropriate to the cyanobacterial strains used, and recognition of the capacity for genomic mutation will prove useful in maintenance of bioreactor cultures with desired traits, avoiding undetected genetic drift, and potentially reduced culture growth or productivity.

References

Akai, M., Onai, K., Kusano, M., Sato, M., Redestig, H., Toyooka, K., Morishita, M., Miyake, H., Hazama, A., Checchetto, V., Szabo, I., Matsuoka, K., Saito, K., Yasui, M., Ishiura, M., and Uozumi, N. (2011). Plasma membrane aquaporin AqpZ protein is essential for glucose metabolism during photomixotrophic growth of *Synechocystis* sp. PCC 6803. *Journal of Biological Chemistry* 286, 25224–25235.

Allahverdiyeva, Y., Mustila, H., Ermakova, M., Bersanini, L., Richaud, P., Ajlani, G., Battchikova, N., Cournac, L., and Aro, E.-M. (2013). Flavodiiron proteins Flv1 and Flv3 enable cyanobacterial growth and photosynthesis under fluctuating light. *Proceedings of the National Academy of Sciences of the United States of America'* 110, 4111–4116.

Altschul, S. F., Gish, W., Miller, W., Myers, E. W., and Lipman, D. J. (1990). Basic local alignment search tool. *Journal of Molecular Biology* 215, 403–410.

Alvarenga, D. O., Fiore, M. F., and Varani, A. M. (2017). A metagenomic approach to cyanobacterial genomics. *Frontiers in Microbiology* 8, 1–16.

Anderson, S. L., and McIntosh, L. (1991). Light-activated heterotrophic growth of the cyanobacterium *Synechocystis* sp. strain PCC 6803: a blue-light-requiring process. *Journal of Bacteriology* 173, 2761–2767.

Aoki, R., Takeda, T., Omata, T., Ihara, K., and Fujita, Y. (2012). MarR-type transcriptional regulator ChlR activates expression of tetrapyrrole biosynthesis genes in response to low-oxygen conditions in cyanobacteria. *Journal of Biological Chemistry* 287, 13500–13507.

Arnold, W., and Sherwood, H. K. (1957). Are chloroplasts semiconductors? *Proceedings of the National Academy of Sciences of the United States of America* 43, 105–114.

Barber, J. (2016). Photosystem II : the water splitting enzyme of photosynthesis and the origin of oxygen in our atmosphere. *Quarterly Reviews of Biophysics* 49, 1–21.

Battchikova, N., Eisenhut, M., and Aro, E.-M. (2011). Cyanobacterial NDH-1 complexes: Novel insights and remaining puzzles. *Biochimica et Biophysica Acta - Bioenergetics* 1807, 935–944.

Beck, C., Knoop, H., and Steuer, R. (2017). Modules of co-occurrence in the cyanobacterial pan-genome. *bioRxiv*, 1–32.

Becking, L. G. M. B., Kaplan, I. R., and Moore, D. (1960). Limits of the natural environment in terms of pH and oxidation-reduction potentials. *The Journal of Geology* 68, 243–284.

Belkin, S., and Boussiba, S. (1991). Resistance of *Spirulina platensis* to ammonia at high pH values. *Plant and Cell Physiology* 32, 953–958.

Belkin, S., Mehlhorn, R. J., and Packer, L. (1987). Proton gradients in intact cyanobacteria. *Plant Physiology* 84, 25–30.

Belkin, S., and Packer, L. (1988). Determination of pH gradients in intact cyanobacteria by electron

spin resonance spectroscopy. *Methods in Enzymology* 167, 677–685.

Bergelson, J., Buckler, E. S., Ecker, J. R., Nordborg, M., and Weigel, D. (2016). A proposal regarding best practices for validating the identity of genetic stocks and the effects of genetic variants. *The Plant Cell* 28, 606–609.

Berry, S., Fischer, J. H., Kruip, J., Hauser, M., and Wildner, G. F. (2005). Monitoring cytosolic pH of carboxysome-deficient cells of *Synechocystis* sp. PCC 6803 using fluorescence analysis. *Plant Biology* 7, 342–347.

Bersanini, L., Allahverdiyeva, Y., Battchikova, N., Heinz, S., Lespinasse, M., Ruohisto, E., Mustila, H., Nickelsen, J., Vass, I., and Aro, E. M. (2017). Dissecting the photoprotective mechanism encoded by the *flv4-2* operon: a distinct contribution of Sll0218 in photosystem II stabilization. *Plant Cell and Environment* 40, 378–389.

Bhaya, D., Bianco, N. R., Bryant, D., and Grossman, A. (2000). Type IV pilus biogenesis and motility in the cyanobacterium *Synechocystis* sp. PCC 6803. *Molecular Microbiology* 37, 941–951.

Billini, M., Stamatakis, K., and Sophianopoulou, V. (2008). Two members of a network of putative Na^+/H^+ antiporters are involved in salt and pH tolerance of the freshwater cyanobacterium *Synechococcus elongatus*. *Journal of Bacteriology* 190, 6318–6329.

Bilwes, A. M., Alex, L. A., Crane, B. R., and Simon, M. I. (1999). Structure of CheA, a signal-transducing histidine kinase. *Cell* 96, 131–141.

Birnboim, H. C., and Doly, J. (1979). A rapid alkaline extraction procedure for screening recombinant plasmid DNA. *Nucleic Acids Research* 7, 1513–1523.

Blanco-Rivero, A., Leganes, F., Fernandez-Valiente, E., Calle, P., and Fernandez-Pinas, F. (2005). *mrpA*, a gene with roles in resistance to Na^+ and adaptation to alkaline pH in the cyanobacterium *Anabaena* sp. PCC 7120. *Microbiology* 151, 1671–1682.

Blanco-Rivero, A., Leganés, F., Fernández-Valiente, E., and Fernández-Piñas, F. (2009). *mrpA* (*all1838*), a gene involved in alkali and Na^+ sensitivity, may also have a role in energy metabolism in the cyanobacterium *Anabaena* sp. strain PCC 7120. *Journal of Plant Physiology* 166, 1488–1496.

Bricker, T. M., Mummadisetti, M. P., and Frankel, L. K. (2015). Recent advances in the use of mass spectrometry to examine structure/function relationships in photosystem II. *Journal of Photochemistry and Photobiology B: Biology* 152, 227–246.

Bricker, T. M., Roose, J. L., Fagerlund, R. D., Frankel, L. K., and Eaton-Rye, J. J. (2012). The extrinsic proteins of Photosystem II. *Biochimica et Biophysica Acta - Bioenergetics* 1817, 121–142.

Brock, T. D. (1973). Lower pH limit for the existence of blue-green algae: evolutionary and ecological implications. *Science* 179, 480–483.

Burnap, R. L., Hagemann, M. A., and Kaplan, A. (2015). Regulation of CO_2 concentrating mechanism in cyanobacteria. *Life* 5, 348–371.

Burnap, R. L., Nambudiri, R., and Holland, S. (2013). Regulation of the carbon-concentrating

mechanism in the cyanobacterium *Synechocystis* sp. PCC 6803 in response to changing light intensity and inorganic carbon availability. *Photosynthesis Research* 118, 115–124.

Burnap, R. L., and Sherman, L. A. (1991). Deletion mutagenesis in *Synechocystis* sp. PCC 6803 indicates that the Mn-stabilizing protein of Photosystem II is not essential for oxygen evolution. *Biochemistry* 30, 440–446.

Burut-Archanai, S., Eaton-Rye, J., and Incharoensakdi, A. (2011). Na$^+$-stimulated phosphate uptake system in *Synechocystis* sp. PCC 6803 with Pst1 as a main transporter. *BMC Microbiology* 11, 225.

Cassier-Chauvat, C., Poncelet, M., and Chauvat, F. (1997). Three insertion sequences from the cyanobacterium *Synechocystis* sp. PCC 6803 support the occurrence of horizontal DNA transfer among bacteria. *Gene* 195, 257–266.

Castielli, O., De la Cerda, B., Navarro, J. A., Hervas, M., and De la Rosa, M. A. (2009). Proteomic analyses of the response of cyanobacteria to different stress conditions. *FEBS Letters* 583, 1753–1758.

Checchetto, V., Segalla, A., Allorent, G., La Rocca, N., Leanza, L., Giacometti, G. M., Uozumi, N., Finazzi, G., Bergantino, E., and Szabo, I. (2012). Thylakoid potassium channel is required for efficient photosynthesis in cyanobacteria. *Proceedings of the National Academy of Sciences of the United States of America* 109, 11043–11048.

Checchetto, V., Teardo, E., Carraretto, L., Formentin, E., Bergantino, E., Giacometti, G. M., and Szabo, I. (2013). Regulation of photosynthesis by ion channels in cyanobacteria and higher plants. *Biophysical Chemistry* 182, 51–57.

Clarke, S. M., and Eaton-Rye, J. J. (1999). Mutation of Phe-363 in the Photosystem II protein CP47 impairs photoautotrophic growth, alters the chloride requirement, and prevents photosynthesis in the absence of either PSII-O or PSII-V in *Synechocystis* sp. PCC 6803. *Biochemistry* 38, 2707–2715.

Cody, M. L. (1965). A general theory of clutch size. *Evolution* 20, 174–184.

Commet, A., Boswell, N., Yocum, C. F., and Popelka, H. (2012). pH optimum of the Photosystem II H$_2$O oxidation reaction: effects of PsbO, the manganese-stabilizing protein, Cl$^-$ retention, and deprotonation of a component required for O$_2$ evolution activity. *Biochemistry* 51, 3808–3818.

Cormann, K. U., Bartsch, M., Rögner, M., and Nowaczyk, M. M. (2014). Localization of the CyanoP binding site on Photosystem II by surface plasmon resonance spectroscopy. *Frontiers in Plant Science* 5, 1–10.

Crawford, T. S. (2015). The role of *psbA1* in *Synechocystis* sp. PCC 6803 under low-oxygen conditions.

Crawford, T. S., Eaton-Rye, J. J., and Summerfield, T. C. (2016). Mutation of Gly195 of the ChlH subunit of Mg-chelatase reduces chlorophyll and further disrupts PS II assembly in a Ycf48-deficient strain of *Synechocystis* sp. PCC 6803. *Frontiers in Plant Science* 7, 1–11.

Cser, K., and Vass, I. (2007). Radiative and non-radiative charge recombination pathways in

References

Photosystem II studied by thermoluminescence and chlorophyll fluorescence in the cyanobacterium *Synechocystis* 6803. *Biochimica et Biophysica Acta - Bioenergetics* 1767, 233–243.

Daley, S. M., Kappell, A. D., Carrick, M. J., and Burnap, R. L. (2012). Regulation of the cyanobacterial CO_2-concentrating mechanism involves internal sensing of $NADP^+$ and α-ketogutarate levels by transcription factor CcmR. *PLoS One* 7, e41286.

Darmon, E., and Leach, D. R. F. (2014). Bacterial genome instability. *Microbiology and Molecular Biology Reviews* 78, 1–39.

Dasgupta, J., Ananyev, G. M., and Dismukes, G. C. (2008). Photoassembly of the water-oxidizing complex in Photosystem II. *Coordination Chemistry Reviews* 252, 347–360.

Deák, Z., Sass, L., Kiss, É., and Vass, I. (2014). Characterization of wave phenomena in the relaxation of flash-induced chlorophyll fluorescence yield in cyanobacteria. *Biochimica et Biophysica Acta - Bioenergetics* 1837, 1522–1532.

Ding, Q., Chen, G., Wang, Y., and Wei, D. (2015). Identification of specific variations in a non-motile strain of cyanobacterium *Synechocystis* sp. PCC 6803 originated from ATCC 27184 by whole genome resequencing. *International Journal of Molecular Sciences* 16, 24081–24093.

Ding, X., Matsumoto, T., Gena, P., Liu, C., Pellegrini-Calace, M., Zhong, S., Sun, X., Zhu, Y., Katsuhara, M., Iwasaki, I., Kitagawa, Y., and Calamita, G. (2013). Water and CO_2 permeability of SsAqpZ, the cyanobacterium *Synechococcus* sp. PCC 7942 aquaporin. *Biological Cell* 105, 118–128.

Dobakova, M., Sobotka, R., Tichy, M., and Komenda, J. (2008). Psb28 protein is involved in the biogenesis of the Photosystem II inner antenna CP47 (PsbB) in the cyanobacterium *Synechocystis* sp. PCC 6803. *Plant Physiology* 149, 1076–1086.

Doney, S. C., Fabry, V. J., Feely, R. A., and Kleypas, J. A. (2009). Ocean acidification: the other CO_2 problem. *Annual Review of Marine Science* 1, 169–192.

Doolittle, W. F., and Sapienza, C. (1980). Selfish genes, the phenotype paradigm and genome evolution. *Nature* 284, 601–603.

Drews, G. (2011). "The evolution of cyanobacteria and photosynthesis," in *Bioenergetic Processes of Cyanobacteria*, eds. G. A. Peschek et al. (Springer), 265–284.

Ducruet, J. M., and Vass, I. (2009). Thermoluminescence: experimental. *Photosynthesis Research* 101, 195–204.

Dvořák, P., Casamatta, D. A., Hašler, P., Jahodářová, E., Norwich, A. R., and Poulíčková, A. (2017). "Diversity of the cyanobacteria," in *Modern Topics in the Phototrophic Prokaryotes*, ed. P. C. Hallenbeck (Springer), 3–46.

Eaton-Rye, J. J. (2011). "Construction of gene interruptions and gene deletions in the cyanobacterium *Synechocystis* sp. strain PCC 6803," in *Photosynthesis Research Protocols*, ed. R. Carpentier (Springer), 295–312.

References

Eaton-Rye, J. J., and Putnam-Evans, C. (2005). "The CP47 and CP43 core antenna components," in *Photosystem II: The Light-Driven Water:Plastoquinone Oxidoreductase*, eds. T. J. Wydrzynski et al. (Springer), 45–70.

Eaton-Rye, J. J., Shand, J. A., and Nicoll, W. S. (2003). pH-dependent photoautotrophic growth of specific photosystem II mutants lacking lumenal extrinsic polypeptides in *Synechocystis* PCC 6803. *FEBS Letters* 543, 148–153.

Eaton-Rye, J. J., and Vermaas, W. F. J. (1991). Oligonucleotide-directed mutagenesis of *psbB*, the gene encoding CP47, employing a deletion mutant strain of the cyanobacterium *Synechocystis* sp. PCC 6803. *Plant Molecular Biology* 17, 1165–1177.

Elanskaya, I. V, Karandashova, I. V, Bogachev, A. V, and Hagemann, M. (2002). Functional analysis of the Na^+/H^+ antiporter encoding genes of the cyanobacterium *Synechocystis* PCC 6803. *Biochemistry (Moscow)* 67, 432–440.

Emlyn-Jones, D., Ashby, M. K., and Mullineaux, C. W. (1999). A gene required for the regulation of photosynthetic light harvesting in the cyanobacterium *Synechocystis* 6803. *Molecular Microbiology* 33, 1050–1058.

Espie, G. S., and Kimber, M. S. (2011). Carboxysomes: cyanobacterial RubisCO comes in small packages. *Photosynthesis Research* 109, 7–20.

Feng, X., and Colloms, S. D. (2007). In vitro transposition of IS*Y100*, a bacterial insertion sequence belonging to the Tc*1*/*mariner* family. *Molecular Microbiology* 65, 1432–1443.

Ferreira, K. N., Iverson, T. M., Maghlaoui, K., Barber, J., and Iwata, S. (2004). Architecture of the photosynthetic oxygen-evolving complex. *Science* 303, 1831–1838.

Fischer, W. W., Hemp, J., and Johnson, J. E. (2016). Evolution of oxygenic photosynthesis. *Annual Review of Earth and Planetary Sciences* 44, 647–683.

Fleischmann, R., Adams, M., White, O., Clayton, R., Kirkness, E., Kerlavage, A., Bult, C., Tomb, J., Dougherty, B., Merrick, J., and Al., E. (1995). Whole-genome random sequencing and assembly of *Haemophilus influenzae* Rd. *Science* 269, 496–512.

Folea, I. M., Zhang, P., Aro, E. M., and Boekema, E. J. (2008). Domain organization of photosystem II in membranes of the cyanobacterium *Synechocystis* PCC 6803 investigated by electron microscopy. *FEBS Letters* 582, 1749–1754.

Fork, D. C., and Mohanty, P. (1986). "Fluorescence and other characteristics of blue-green algae (cyanobacteria), red algae, and cryptomonads," in *Light Emission by Plants and Bacteria*, eds. Govindjee et al. (Academic Press), 451–496.

Fufezan, C., Gross, C. M., Sjödin, M., Rutherford, A. W., Krieger-Liszkay, A., and Kirilovsky, D. (2007). Influence of the redox potential of the primary quinone electron acceptor on photoinhibition in photosystem II. *Journal of Biological Chemistry* 282, 12492–12502.

Fujisawa, T., Narikawa, R., Maeda, S. I., Watanabe, S., Kanesaki, Y., Kobayashi, K., Nomata, J., Hanaoka, M., Watanabe, M., Ehira, S., Suzuki, E., Awai, K., and Nakamura, Y. (2017).

References

CyanoBase: A large-scale update on its 20th anniversary. *Nucleic Acids Research* 45, 551–554.

Gallaher, S. D., Fitz-Gibbon, S. T., Glaesener, A. G., Pellegrini, M., and Merchant, S. S. (2015). *Chlamydomonas* genome resource for laboratory strains reveals a mosaic of sequence variation, identifies true strain histories, and enables strain-specific studies. *The Plant Cell* 27, 2335–2352.

Grigorieva, G., and Shestakov, S. (1982). Transformation in the cyanobacterium *Synechocystis* sp. 6803. *FEMS Microbiology Letters* 13, 367–370.

Gunnelius, L., Tuominen, I., Rantamaki, S., Pollari, M., Ruotsalainen, V., Tyystjärvi, E., and Tyystjärvi, T. (2010). SigC sigma factor is involved in acclimation to low inorganic carbon at high temperature in *Synechocystis* sp. PCC 6803. *Microbiology* 156, 220–229.

Hagemann, M. (2011). Molecular biology of cyanobacterial salt acclimation. *FEMS Microbiology Reviews* 35, 87–123.

Haimovich-Dayan, M., Kahlon, S., Hihara, Y., Hagemann, M., Ogawa, T., Ohad, I., Lieman-Hurwitz, J., and Kaplan, A. (2011). Cross-talk between photomixotrophic growth and CO_2-concentrating mechanism in *Synechocystis* sp. strain PCC 6803. *Environmental Microbiology* 13, 1767–1777.

Hamada, A., Hibino, T., Nakamura, T., and Takabe, T. (2001). Na^+/H^+ antiporter from *Synechocystis* species PCC 6803, homologous to SOS1, contains an aspartic residue and long c-terminal tail important for the carrier activity. *Plant Physiology* 125, 437–446.

Hanahan, D. (1983). Studies on transformation of *Escherichia coli* with plasmids. *Journal of Molecular Biology* 166, 557–580.

Havaux, M., Guedeney, G., Hagemann, M., Yeremenko, N., Matthijs, H. C. P., and Jeanjean, R. (2005). The chlorophyll-binding protein IsiA is inducible by high light and protects the cyanobacterium *Synechocystis* PCC 6803 from photooxidative stress. *FEBS Letters* 579, 2289–2293.

Heinz, S., Liauw, P., Nickelsen, J., and Nowaczyk, M. (2015). Analysis of photosystem II biogenesis in cyanobacteria. *Biochimica et Biophysica Acta*.

Hess, W. R. (2011). Cyanobacterial genomics for ecology and biotechnology. *Current Opinion in Microbiology* 14, 608–614.

Hihara, Y. (2001). DNA microarray analysis of cyanobacterial gene expression during acclimation to high light. *The Plant Cell* 13, 793–806.

Hihara, Y., and Ikeuchi, M. (1997). Mutation in a novel gene required for photomixotrophic growth leads to enhanced photoautotrophic growth of *Synechocystis* sp. PCC 6803. *Photosynthesis Research* 53, 243–252.

Hihara, Y., Sonoike, K., and Ikeuchi, M. (1998). A novel gene, *pmgA*, specifically regulates photosystem stoichiometry in the cyanobacterium *Synechocystis* species PCC 6803 in response to high light. *Plant Physiology* 117, 1205–1216.

Ho, S. N., Hunt, H. D., Horton, R. M., Pullen, J. K., and Pease, L. R. (1989). Site-directed mutagenesis by overlap extension using the polymerase chain reaction. *Gene* 77, 51–59.

Hohmann-Marriott, M. F., and Blankenship, R. E. (2011). Evolution of photosynthesis. *Annual Review*

of Plant Biology 62, 515–548.

Ifuku, K. (2015). Localization and functional characterization of the extrinsic subunits of photosystem II: an update. *Bioscience, Biotechnology, and Biochemistry* 79, 1223–1231.

Ifuku, K., and Noguchi, T. (2016). Structural coupling of extrinsic proteins with the oxygen-evolving center in Photosystem II. *Frontiers in Plant Science* 7, 1–11.

Ikeuchi, M., and Tabata, S. (2001). *Synechocystis* sp. PCC 6803 – a useful tool in the study of the genetics of cyanobacteria. *Photosynthesis Research* 70, 73–83.

Inaba, M., Sakamoto, A., and Murata, N. (2001). Functional expression in *Escherichia coli* of low-affinity and high-affinity Na$^+$(Li$^+$)/H$^+$ antiporters of *Synechocystis*. *Journal of Bacteriology* 183, 1376–1384.

Inoue, H., Nojima, H., and Okayama, H. (1990). High efficiency transformation of *Escherichia coli* with plasmids. *Gene* 96, 23–28.

Jackson, S. A. (2012). Structure and function of the extrinsic lipoproteins of Photosystem II in *Synechocystis* sp. PCC 6803.

Jackson, S. A., and Eaton-Rye, J. J. (2015). Characterization of a *Synechocystis* sp. PCC 6803 double mutant lacking the CyanoP and Ycf48 proteins of Photosystem II. *Photosynthesis Research* 124, 217–229.

Jensen, P. E., Gibson, L. C. D., Henningsen, K. W., and Hunter, C. N. (1996). Expression of the *chlI*, *chlD*, and *chlH* genes from the cyanobacterium *Synechocystis* PCC 6803 in *Escherichia coli* and demonstration that the three cognate proteins are required for magnesium-protoporphyrin chelatase activi. *Journal of Biological Chemistry* 271, 16662–16667.

Jensen, S. I., Steunou, A. S., Bhaya, D., Kuhl, M., and Grossman, A. R. (2011). In situ dynamics of O$_2$, pH and cyanobacterial transcripts associated with CCM, photosynthesis and detoxification of ROS. *The ISME Journal* 5, 317–328.

Jiang, H. B., Cheng, H. M., Gao, K. S., and Qiu, B. S. (2013). Inactivation of Ca^{2+}/H$^+$ exchanger in *Synechocystis* sp. strain PCC 6803 promotes cyanobacterial calcification by upregulating CO$_2$-concentrating mechanisms. *Applied and Environmental Microbiology* 79, 4048–4055.

Joliot, P., and Joliot, A. (1968). A polarographic method for detection of oxygen production and reduction of Hill reagent by isolated chloroplasts. *Biochimica et Biophysica Acta - Bioenergetics* 153, 625–634.

Jones, P. R. (2014). Genetic instability in cyanobacteria - an elephant in the room? *Frontiers in Bioengineering and Biotechnology* 2, 1–5.

Joshua, S., and Mullineaux, C. W. (2005). The *rpaC* gene product regulates phycobilisome-photosystem II interaction in cyanobacteria. *Biochimica et Biophysica Acta - Bioenergetics* 1709, 58–68.

Kaczmarzyk, D., and Fulda, M. (2010). Fatty acid activation in cyanobacteria mediated by acyl-acyl carrier protein synthetase enables fatty acid recycling. *Plant Physiology* 152, 1598–1610.

References

Kahlon, S., Beeri, K., Ohkawa, H., Hihara, Y., Murik, O., Suzuki, I., Ogawa, T., and Kaplan, A. (2006). A putative sensor kinase, Hik31, is involved in the response of *Synechocystis* sp. strain PCC 6803 to the presence of glucose. *Microbiology* 152, 647–655.

Kale, R., Hebert, A. E., Frankel, L. K., Sallans, L., Bricker, T. M., and Pospíšil, P. (2017). Amino acid oxidation of the D1 and D2 proteins by oxygen radicals during photoinhibition of Photosystem II. *Proceedings of the National Academy of Sciences of the United States of America* 114, 2988–2993.

Kallas, T. (2012). "Cytochrome b_6f complex at the heart of energy transduction and redox signalling," in *Photosynthesis: Plastid Biology, Energy Conversion, and Carbon Assimilation*, eds. J. J. Eaton-Rye et al. (Springer), 501–560.

Kallas, T., and Castenholz, R. W. (1982). Internal pH and ATP-ADP pools in the cyanobacterium *Synechococcus* sp. during exposure to growth-inhibiting low pH. *Journal of Bacteriology* 149, 229–236.

Kamei, A., Yuasa, T., Orikawa, K., Geng, X., and Ikeuchi, M. (2001). A eukaryotic-type protein kinase SpkA is required for the normal motility of the unicellular cyanobacterium, *Synechocystis* sp. PCC 6803. *Journal of Bacteriology* 183, 1505–1510.

Kaneko, T., Nakamura, Y., Sasamoto, S., Watanabe, A., Kohara, M., Matsumoto, M., Shimpo, S., Yamada, M., and Tabata, S. (2003). Structural analysis of four large plasmids harboring in a unicellular cyanobacterium, *Synechocystis* sp. PCC 6803. *DNA Research* 10, 221–228.

Kaneko, T., Sato, S., Kotani, H., Tanaka, A., Asamizu, E., Nakamura, Y., Miyajima, N., Hirosawa, M., Sugiura, M., Sasamoto, S., Kimura, T., Hosouchi, T., Matsuno, A., Muraki, A., Nakazaki, N., Naruo, K., Okumura, S., Shimpo, S., Takeuchi, C., Wada, T., Watanabe, A., Yamada, M., Yasuda, M., and Tabata, S. (1996). Sequence analysis of the genome of the unicellular cyanobacterium *Synechocystis* sp. strain PCC 6803. II. Sequence determination of the entire genome and assignment of potential protein-coding regions. *DNA Research* 3, 109–136.

Kaneko, T., and Tabata, S. (1997). Complete genome structure of the unicellular cyanobacterium *Synechocystis* sp. PCC 6803. *Plant and Cell Physiology* 38, 1171–1176.

Kaneko, T., Tanaka, A., Sato, S., Kotani, H., Sazuka, T., Miyajima, N., Sugiura, M., and Tabata, S. (1995). Sequence analysis of the genome of the unicellular cyanobacterium *Synechocystis* sp. strain PCC 6803. I. Sequence features in the 1 Mb region from map positions 64% to 92% of the genome. *DNA Research* 2, 153–166.

Kanesaki, Y., Shiwa, Y., Tajima, N., Suzuki, M., Watanabe, S., Sato, N., Ikeuchi, M., and Yoshikawa, H. (2012). Identification of substrain-specific mutations by massively parallel whole-genome resequencing of *Synechocystis* sp. PCC 6803. *DNA Research* 19, 67–79.

Katoh, A., Lee, K. S., Fukuzawa, H., Ohyama, K., and Ogawa, T. (1996a). *cemA* homologue essential to CO_2 transport in the cyanobacterium *Synechocystis* PCC 6803. *Proceedings of the National Academy of Sciences of the United States of America* 93, 4006–4010.

References

Katoh, A., Sonoda, M., Katoh, H., and Ogawa, T. (1996b). Absence of light-induced proton extrusion in a *cotA*-less mutant of *Synechocystis* sp. strain PCC 6803. *Journal of Bacteriology* 178, 5452–5455.

Kerfeld, C. A., Kerfeld, C. A., Sawaya, M. R., Tanaka, S., Nguyen, C. V, Phillips, M., Beeby, M., and Yeates, T. O. (2005). Protein structures forming the shell of primitive bacterial organelles. *Science* 309, 936–938.

Kirilovsky, D., and Kerfeld, C. A. (2016). Cyanobacterial photoprotection by the orange carotenoid protein. *Nature Plants* 2, 1–7.

Kirilovsky, D., Roncel, M., Boussac, A., Wilson, A., Zurita, J. L., Ducruet, J.-M., Bottin, H., Sugiura, M., Ortega, J. M., and Rutherford, A. W. (2004). Cytochrome c_{550} in the cyanobacterium *Thermosynechococcus elongatus*: study of redox mutants. *Journal of Biological Chemistry* 279, 52869–52880.

Klughammer, B., Sültemeyer, D., Badger, M. R., and Price, G. D. (1999). The involvement of NAD(P)H dehydrogenase subunits, NdhD3 and NdhF3, in high- affinity CO_2 uptake in *Synechococcus* sp. PCC 7002 gives evidence for multiple NDH- 1 complexes with specific roles in cyanobacteria. *Molecular Microbiology* 32, 1305–1315.

Klughammer, C., and Schreiber, U. (1994). An improved method, using saturating light-pulses, for the determination of Photosystem-I quantum yield via P_{700}^{+}-absorbancy changes at 830 nm. *Planta* 192, 261–268.

Kobayashi, K., Endo, K., and Wada, H. (2016). Multiple impacts of loss of plastidic phosphatidylglycerol biosynthesis on photosynthesis during seedling growth of *Arabidopsis*. *Frontiers in Plant Science* 7, 1–12.

Kopf, M., Klahn, S., Pade, N. A., Weingartner, C., Hagemann, M. A., Voss, B., Hess, W. R., Klähn, S., Pade, N. A., Weingärtner, C., Hagemann, M. A., Voß, B., Hess, W. R., Klahn, S., Pade, N. A., Weingartner, C., Hagemann, M. A., Voss, B., Hess, W. R., Voß, R. N., Pade, N. A., Weinga, C. H., Hagemann, M. A., and Jo, B. (2014a). Comparative genome analysis of the closely related *Synechocystis* strains PCC 6714 and PCC 6803. *DNA Research* 21, 1–12.

Kopf, M., Klähn, S., Scholz, I., Matthiessen, J. K. F., Hess, W. R., Voß, B., Pade, N., Weingärtner, C., Hagemann, M., Voß, B., and Hess, W. R. (2014b). Comparative genome analysis of the closely related *Synechocystis* strains PCC 6714 and PCC 6803. *DNA Research* 21, 527–539.

Koropatkin, N. M., Koppenaal, D. W., Pakrasi, H. B., and Smith, T. J. (2007). The structure of a cyanobacterial bicarbonate transport protein, CmpA. *Journal of Biological Chemistry* 282, 2606–2614.

Kotani, H., Kaneko, T., Matsubayashi, T., Sato, S., Sugiura, M., and Tabata, S. (1994). A physical map of the genome of a unicellular cyanobacterium *Synechocystis* sp. strain PCC 6803. *DNA Research* 1, 303–307.

Krieger-Liszkay, A., and Rutherford, A. W. (1998). Influence of herbicide binding on the redox

potential of the quinone acceptor in Photosystem II: relevance to photodamage and phytotoxicity. *Biochemistry* 37, 17339–17344.

Krulwich, T. A., Sachs, G., and Padan, E. (2011). Molecular aspects of bacterial pH sensing and homeostasis. *Nature Reviews Microbiology* 9, 330–343.

Kupriyanova, E. V, Sinetova, M. A., Cho, S. M., Park, Y. I., Los, D. A., and Pronina, N. A. (2013). CO_2-concentrating mechanism in cyanobacterial photosynthesis: organization, physiological role, and evolutionary origin. *Photosynthesis Research* 117, 133–146.

Kurian, D., Phadwal, K., and Mäenpää, P. (2006). Proteomic characterization of acid stress response in *Synechocystis* sp. PCC 6803. *Proteomics* 6, 3614–3624.

Labarre, J., Chauvat, F., and Thuriaux, P. (1989). Insertional mutagenesis by random cloning of antibiotic resistance genes into the genome of the cyanobacterium *Synechocystis* strain PCC 6803. *Journal of Bacteriology* 171, 3449–3457.

Lea-Smith, D. J., Bombelli, P., Vasudevan, R., and Howe, C. J. (2016). Photosynthetic, respiratory and extracellular electron transport pathways in cyanobacteria. *Biochimica et Biophysica Acta - Bioenergetics* 1857, 247–255.

Li, H., and Durbin, R. (2009). Fast and accurate short read alignment with Burrows-Wheeler transform. *Bioinformatics* 25, 1754–1760.

Li, H., Handsaker, B., Wysoker, A., Fennell, T., Ruan, J., Homer, N., Marth, G., Abecasis, G., and Durbin, R. (2009). The Sequence Alignment/Map format and SAMtools. *Bioinformatics* 25, 2078–2079.

Li, Y., Rao, N., Yang, F., Zhang, Y., Yang, Y., Liu, H., Guo, F., and Huang, J. (2014). Biocomputational construction of a gene network under acid stress in *Synechocystis* sp. PCC 6803. *Research in Microbiology* 165, 420–428.

Liberton, M., Howard Berg, R., Heuser, J., Roth, R., and Pakrasi, H. B. (2006). Ultrastructure of the membrane systems in the unicellular cyanobacterium *Synechocystis* sp. strain PCC 6803. *Protoplasma* 227, 129–138.

Lin, S., Haas, S., Zemojtel, T., Xiao, P., Vingron, M., and Li, R. (2011). Genome-wide comparison of cyanobacterial transposable elements, potential genetic diversity indicators. *Gene* 473, 139–149.

Linke, K., and Ho, F. M. (2014). Water in Photosystem II: structural, functional and mechanistic considerations. *Biochimica et Biophysica Acta - Bioenergetics* 1837, 14–32.

Liu, H., Zhang, H., Weisz, D. A., Vidavsky, I., Gross, M. L., and Pakrasi, H. B. (2014). MS-based cross-linking analysis reveals the location of the PsbQ protein in cyanobacterial photosystem II. *Proceedings of the National Academy of Sciences of the United States of America* 111, 4638–4643.

Lopez-Archilla, A. I., Moreira, D., Lopez-Garcia, P., and Guerrero, C. (2004). Phytoplankton diversity and cyanobacterial dominance in a hypereutrophic shallow lake with biologically produced alkaline pH. *Extremophiles* 8, 109–115.

References

Lorch, S., Capponi, S., Pieront, F., and Bondar, A.-N. (2015). Dynamic carboxylate/water networks on the surface of the PsbO subunit of Photosystem II. *The Journal of Physical Chemistry B* 119, 12172–12181.

Lyons, T. W., Reinhard, C. T., and Planavsky, N. J. (2014). The rise of oxygen in Earth's early ocean and atmosphere. *Nature* 506, 307–315.

Ma, W., and Mi, H. (2008). Effect of exogenous glucose on the expression and activity of NADPH dehydrogenase complexes in the cyanobacterium *Synechocystis* sp. strain PCC 6803. *Plant Physiology and Biochemistry* 46, 775–779.

Mabbitt, P. D., Wilbanks, S. M., and Eaton-Rye, J. J. (2014). Structure and function of the hydrophilic Photosystem II assembly proteins: Psb27, Psb28 and Ycf48. *Plant Physiology and Biochemistry* 81, 96–107.

MacKinney, G. (1941). Absorption of light by chlorophyll solutions. *Journal of Biological Chemistry* 140, 315–322.

Maestri, O., and Joset, F. (2000). Regulation by external pH and stationary growth phase of the acetolactate synthase from *Synechocystis* PCC 6803. *Molecular Microbiology* 37, 828–838.

Mangan, N. M., Flamholz, A., Hood, R. D., Milo, R., and Savage, D. F. (2016). pH determines the energetic efficiency of the cyanobacterial CO_2 concentrating mechanism. *Proceedings of the National Academy of Sciences of the United States of America* 113, E5354–E5362.

Matsuda, N., Kobayashi, H., Katoh, H., Ogawa, T., Futatsugi, L., Nakamura, T., Bakker, E. P., and Uozumi, N. (2004). Na^+-dependent K^+ uptake Ktr system from the cyanobacterium *Synechocystis* sp. PCC 6803 and its role in the early phases of cell adaptation to hyperosmotic shock. *Journal of Biological Chemistry* 279, 54952–54962.

Matsuhashi, A., Tahara, H., Ito, Y., Uchiyama, J., Ogawa, S., and Ohta, H. (2015). Slr2019, lipid A transporter homolog, is essential for acidic tolerance in *Synechocystis* sp. PCC 6803. *Photosynthesis Research* 125, 267–277.

McGinn, P. J., Price, G. D., Maleszka, R., and Badger, M. R. (2003). Inorganic carbon limitation and light control the expression of transcripts related to the CO_2-concentrating mechanism in the cyanobacterium *Synechocystis* sp. strain PCC 6803. *Plant Physiology* 132, 218–229.

van de Meene, A. M. L., Hohmann-Marriott, M. F., Vermaas, W. F. J., and Roberson, R. W. (2006). The three-dimensional structure of the cyanobacterium *Synechocystis* sp. PCC 6803. *Archives of Microbiology* 184, 259–270.

van de Meene, A. M. L., Sharp, W. P., McDaniel, J. H., Friedrich, H., Vermaas, W. F. J., and Roberson, R. W. (2012). Gross morphological changes in thylakoid membrane structure are associated with Photosystem I deletion in *Synechocystis* sp. PCC 6803. *Biochimica et Biophysica Acta - Bioenergetics* 1818, 1427–34.

Menon, B. B., Heinhorst, S., Shively, J. M., and Cannon, G. C. (2010). The carboxysome shell is permeable to protons. *Journal of Bacteriology* 192, 5881–5886.

References

Minda, R., Ramchandani, J., Joshi, V. P., and Bhattacharjee, S. K. (2005). A homozygous *recA* mutant of *Synechocystis* PCC 6803: construction strategy and characteristics eliciting a novel RecA independent UVC resistance in dark. *Molecular Genetics and Genomics* 274, 616–624.

Mitschke, J., Georg, J., Scholz, I., Sharma, C. M., Dienst, D., Bantscheffa, J., Voß, B., Steglich, C., Wilde, A., Vogel, J., and Hess, W. R. (2011). An experimentally anchored map of transcriptional start sites in the model cyanobacterium *Synechocystis* sp. PCC 6803. *Proceedings of the National Academy of Sciences of the United States of America* 108, 1–33.

Mizuno, T., Kaneko, T., and Tabata, S. (1996). Compilation of all genes encoding bacterial two-component signal transducers in the genome of the cyanobacterium, *Synechocystis* sp. strain PCC 6803. *DNA Research* 3, 407–414.

Mohanta, T. K., Pudake, R. N., and Bae, H. (2017). Genome-wide identification of major protein families of cyanobacteria and genomic insight into the circadian rhythm. *European Journal of Phycology* 52, 149–165.

Mohapatra, P. K., Schubert, H., and Schiewer, U. (1996). Short term toxicity effect of dimethoate on transthylakoid pH gradient of intact *Synechocystis* sp. PCC 6803 cells. *Bulletin of Environmental Contamination Toxicology* 57, 722–728.

Morgan, T. R., Shand, J. a., Clarke, S. M., and Eaton-Rye, J. J. (1998). Specific requirements for cytochrome c_{550} and the manganese-stabilizing protein in photoautotrophic strains of *Synechocystis* sp. PCC 6803 with mutations in the domain Gly-351 to Thr-436 of the chlorophyll-binding protein CP47. *Biochemistry* 37, 14437–14449.

Morris, J. N., Crawford, T. S., Jeffs, A., Stockwell, P. A., Eaton-Rye, J. J., and Summerfield, T. C. (2014). Whole genome re-sequencing of two "wild-type" strains of the model cyanobacterium *Synechocystis* sp. PCC 6803. *New Zealand Journal of Botany* 52, 36–47.

Morris, J. N., Eaton-Rye, J. J., and Summerfield, T. C. (2016). Environmental pH and the requirement for the extrinsic proteins of Photosystem II in the function of cyanobacterial photosynthesis. *Frontiers in Plant Science* 7, 1–8.

Morris, J. N., Eaton-Rye, J. J., and Summerfield, T. C. (2017). Phenotypic variation in wild-type substrains of the model cyanobacterium *Synechocystis* sp. PCC 6803. *New Zealand Journal of Botany* 55, 25–35.

Mulkidjanian, A. Y., Koonin, E. V., Makarova, K. S., Mekhedov, S. L., Sorokin, A., Wolf, Y. I., Dufresne, A., Partensky, F., Burd, H., Kaznadzey, D., Haselkorn, R., and Galperin, M. Y. (2006). The cyanobacterial genome core and the origin of photosynthesis. *Proceedings of the National Academy of Sciences of the United States of America* 103, 13126–13131.

Müller, J., Friedl, T., Hepperle, D., Lorenz, M., and Day, J. G. (2005). Distinction between multiple isolates of *Chlorella vulgaris* (Chlorophyta, Trebouxiophyceae) and testing for conspecificity using amplified fragment length polymorphism and ITS rDNA sequences. *Journal of Phycology* 41, 1236–1247.

References

Mullineaux, C. W. (2008). Phycobilisome-reaction centre interaction in cyanobacteria. *Photosynthesis Research* 95, 175–182.

Mullineaux, C. W. (2014). Electron transport and light-harvesting switches in cyanobacteria. *Frontiers in Plant Science* 5, 1–6.

Mullineaux, C. W., and Emlyn-Jones, D. (2005). State transitions: An example of acclimation to low-light stress. *Journal of Experimental Botany* 56, 389–393.

Mulo, P., Sakurai, I., and Aro, E. M. (2012). Strategies for *psbA* gene expression in cyanobacteria, green algae and higher plants: from transcription to PSII repair. *Biochimica et Biophysica Acta - Bioenergetics* 1817, 247–257.

Muramatsu, M., and Hihara, Y. (2012). Acclimation to high-light conditions in cyanobacteria: from gene expression to physiological responses. *Journal of Plant Research* 125, 11–39.

Muramatsu, M., Sonoike, K., and Hihara, Y. (2009). Mechanism of downregulation of photosystem I content under high-light conditions in the cyanobacterium *Synechocystis* sp. PCC 6803. *Microbiology* 155, 989–996.

Murata, N., Allakhverdiev, S. I., and Nishiyama, Y. (2012). The mechanism of photoinhibition in vivo: re-evaluation of the roles of catalase, α-tocopherol, non-photochemical quenching, and electron transport. *Biochimica et Biophysica Acta - Bioenergetics* 1817, 1127–1133.

Murata, N., and Satoh, K. (1986). "Absorption and fluorescence emission by intact cells, chloroplasts, and chlorophyll–protein complexes," in *Light Emission by Plants and Bacteria*, eds. Govindjee et al. (New York: Academic Press), 137–159.

Murata, N., and Suzuki, I. (2006). Exploitation of genomic sequences in a systematic analysis to access how cyanobacteria sense environmental stress. *Journal of Experimental Botany* 57, 235–247.

Murata, N., Takahashi, S., Nishiyama, Y., and Allakhverdiev, S. I. (2007). Photoinhibition of photosystem II under environmental stress. *Biochimica et Biophysica Acta (BBA) - Bioenergetics* 1767, 414–421.

Nagarajan, S., Srivastava, S., and Sherman, L. A. (2014). Essential role of the plasmid *hik31* operon in regulating central metabolism in the dark in *Synechocystis* sp. PCC 6803. *Molecular Microbiology* 91, 79–97.

Najafpour, M. M., Renger, G., Moghaddam, A. N., Aro, E.-M., Carpentier, R., Nishihara, H., Eaton-Rye, J. J., Shen, J.-R., and Allakhverdiev, S. I. (2016). Manganese compounds as water-oxidizing catalysts: from the natural water-oxidizing complex to nanosized manganese oxide structures. *Chemical Reviews*.

Nelson, N., and Junge, W. (2015). Structure and energy transfer in photosystems of oxygenic photosynthesis. *Annual Review of Biochemistry* 84, 659–683.

Nevo, R., Charuvi, D., Shimoni, E., Schwarz, R., Kaplan, A., Ohad, I., and Reich, Z. (2007). Thylakoid membrane perforations and connectivity enable intracellular traffic in cyanobacteria. *The EMBO Journal* 26, 1467–1473.

References

Nguyen, B. T., and Rittmann, B. E. (2016). Effects of inorganic carbon and pH on growth kinetics of *Synechocystis* sp. PCC 6803. *Algal Research* 19, 363–369.

Nickelsen, J., and Rengstl, B. (2013). Photosystem II assembly: from cyanobacteria to plants. *Annual Review of Plant Biology* 64, 609–635.

Nishijima, Y., Kanesaki, Y., Yoshikawa, H., Ogawa, T., Sonoike, K., Nishiyama, Y., and Hihara, Y. (2015). Analysis of spontaneous suppressor mutants from the photomixotrophically grown *pmgA*-disrupted mutant in the cyanobacterium *Synechocystis* sp. PCC 6803. *Photosynthesis Research* 126, 465–475.

Nishimura, T., Takahashi, Y., Yamaguchi, O., Suzuki, H., Maeda, S. I., and Omata, T. (2008). Mechanism of low CO_2-induced activation of the *cmp* bicarbonate transporter operon by a LysR family protein in the cyanobacterium *Synechococcus elongatus* strain PCC 7942. *Molecular Microbiology* 68, 98–109.

Nixon, P. J., Michoux, F., Yu, J., Boehm, M., and Komenda, J. (2010). Recent advances in understanding the assembly and repair of photosystem II. *Annals of Botany* 106, 1–16.

Ohkawa, H., Pakrasi, H. B., and Ogawa, T. (2000a). Two types of functionally distinct NAD(P)H dehydrogenases in *Synechocystis* strain PCC 6803. *Journal of Biological Chemistry* 275, 31630–31634.

Ohkawa, H., Price, G. D., and Badger, M. R. (2000b). Mutation of *ndh* genes leads to inhibition of CO_2-uptake rather than HCO_3^- uptake in *Synechocystis* sp. strain PCC 6803. *Journal of Bacteriology* 182, 2591–2596.

Ohkawa, H., Sonoda, M., Katoh, H., and Ogawa, T. (1998). The use of mutants in the analysis of the CO_2-concentrating mechanism in cyanobacteria. *Canadian Journal of Botany* 76, 1035–1042.

Ohta, H., Shibata, Y., Haseyama, Y., Yoshino, Y., Suzuki, T., Kagasawa, T., Kamei, A., Ikeuchi, M., and Enami, I. (2005). Identification of genes expressed in response to acid stress in *Synechocystis* sp. PCC 6803 using DNA microarrays. *Photosynthesis Research* 84, 225–230.

Okamoto, S., Ikeuchi, M., Ohmori, M., and Primer, P. (1999). Experimental analysis of recently transposed insertion sequences in the cyanobacterium *Synechocystis* sp. PCC 6803. *DNA Research* 6, 265–73.

Omata, T., Price, G. D., Badger, M. R., Okamura, M., Gohta, S., and Ogawa, T. (1999). Identification of an ATP-binding cassette transporter involved in bicarbonate uptake in the cyanobacterium *Synechococcus* sp. strain PCC 7942. *Proceedings of the National Academy of Sciences of the United States of America* 96, 13571–13576.

Orf, I., Klähn, S., Schwarz, D., Frank, M., Hess, W. R., Hagemann, M., and Kopka, J. (2015). Integrated analysis of engineered carbon limitation in a quadruple CO_2/HCO_3^- uptake mutant of *Synechocystis* sp. PCC 6803. *Plant Physiology* 169, 1787–1806.

Padan, E., Bibi, E., Ito, M., and Krulwich, T. A. (2005). Alkaline pH homeostasis in bacteria: new insights. *Biochimica et Biophysica Acta – Biomembranes* 1717, 67–88.

References

De Porcellinis, A. J., Klähn, S., Rosgaard, L., Kirsch, R., Gutekunst, K., Georg, J., Hess, W. R., and Sakuragi, Y. (2016). The non-coding RNA Ncr0700/PmgR1 is required for photomixotrophic growth and the regulation of glycogen accumulation in the cyanobacterium *Synechocystis* sp. PCC 6803. *Plant and Cell Physiology* 57, 2091–2103.

Price, C. W. (2000). "Protective function and regulation of the general stress response in Bacillus subtilis and related Gram-positive bacteria," in *Bacterial Stress Response*, eds. G. Storz and R. Hengge-Aronis (ASM Press,).

Price, G. D. (2011). Inorganic carbon transporters of the cyanobacterial CO_2 concentrating mechanism. *Photosynthesis Research* 109, 47–57.

Price, G. D., Badger, M. R., Woodger, F. J., and Long, B. M. (2008). Advances in understanding the cyanobacterial CO_2-concentrating-mechanism (CCM): functional components, C_i transporters, diversity, genetic regulation and prospects for engineering into plants. *Journal of Experimental Botany* 59, 1441–1461.

Price, G. D., Shelden, M. C., and Howitt, S. M. (2011). Membrane topology of the cyanobacterial bicarbonate transporter, SbtA, and identification of potential regulatory loops. *Molecular Membrane Biology* 28, 265–275.

Price, G. D., Woodger, F. J., Badger, M. R., Howitt, S. M., and Tucker, L. (2004). Identification of a SulP-type bicarbonate transporter in marine cyanobacteria. *Proceedings of the National Academy of Sciences of the United States of America* 101, 18228–18233.

Putnam-Evans, C., Wu, J., and Bricker, T. M. (1996). Site-directed mutagenesis of the CP47 protein of photosystem II: alteration of conserved charged residues which lie within lethal deletions of the large extrinsic loop E. *Plant Molecular Biology* 32, 1191–1195.

Rae, B. D., Long, B. M., Badger, M. R., and Price, G. D. (2013). Functions, compositions, and evolution of the two types of carboxysomes: polyhedral microcompartments that facilitate CO_2 fixation in cyanobacteria and some proteobacteria. *Microbiology and Molecular Biology Reviews* 77, 357–379.

Rast, A., Heinz, S., and Nickelsen, J. (2015). Biogenesis of thylakoid membranes. *Biochimica et Biophysica Acta - Biomembranes* 1847, 821–30.

Raven, J. A. (2012). "Carbon," in *Ecology of Cyanobacteria II*, ed. B. A. Whitton (Springer), 443–460.

Raven, J. A., and Beardall, J. (2016). The ins and outs of CO_2. *Journal of Experimental Botany* 67, 1–13.

Raven, J. A., Beardall, J., and Giordano, M. (2014). Energy costs of carbon dioxide concentrating mechanisms in aquatic organisms. *Photosynthesis Research* 121, 111–124.

Rehman, A. U., Cser, K., Sass, L., and Vass, I. (2013). Characterization of singlet oxygen production and its involvement in photodamage of Photosystem II in the cyanobacterium *Synechocystis* PCC 6803 by histidine-mediated chemical trapping. *Biochimica et Biophysica Acta - Bioenergetics* 1827, 689–698.

References

Ren, Q., Shi, M., Chen, L., Wang, J., Zhang, W., Menglaing, S., Chen, L., Wang, J., and Zhang, W. (2014). Integrated proteomic and metabolomic characterization of a novel two-component response regulator Slr1909 involved in acid tolerance in *Synechocystis* sp. PCC 6803. *Journal of Proteomics* 109, 76–89.

Renger, G., and Hanssum, B. (2009). Oxygen detection in biological systems. *Photosynthesis Research* 102, 487–498.

Rippka, R., Deruelles, J., Waterbury, J. B., Herdman, M., and Stanier, R. Y. (1979). Generic assignments, strain histories and properties of pure cultures of cyanobacteria. *Journal of General Microbiology* 111, 1–61.

Roose, J. L., Frankel, L. K., Mummadisetti, M. P., and Bricker, T. M. (2016). The extrinsic proteins of photosystem II: update. *Planta* 243, 889–908.

Ruffing, A. M., and Kallas, T. (2016). Editorial: Cyanobacteria: the green *E. coli*. *Frontiers in Bioengineering and Biotechnology* 4, 1–2.

Rühle, T., and Leister, D. (2016). Photosystem II assembly from scratch. *Frontiers in Plant Science* 6, 1–5.

Rutherford, A. W., Boussac, A., and Faller, P. (2004). The stable tyrosyl radical in Photosystem II: Why D? *Biochimica et Biophysica Acta - Bioenergetics* 1655, 222–230.

Rutherford, A. W., Renger, G., Koike, H., and Inoue, Y. (1984). Thermoluminescence as a probe of photosystem II. The redox and protonation states of the secondary acceptor quinone and the O_2-evolving enzyme. *Biochimica et Biophysica Acta - Bioenergetics* 767, 548–556.

Ryu, J. Y., Song, J. Y., Lee, J. M., Jeong, S. W., Chow, W. S., Choi, S. B., Pogson, B. J., and Park, Y. I. (2004). Glucose-induced expression of carotenoid biosynthesis genes in the dark is mediated by cytosolic pH in the cyanobacterium *Synechocystis* sp. PCC 6803. *Journal of Biological Chemistry* 279, 25320–25325.

Saito, K., Rutherford, A. W., and Ishikita, H. (2013). Mechanism of tyrosine D oxidation in Photosystem II. *Proceedings of the National Academy of Sciences of the United States of America* 110, 7690–7695.

Sakashita, N., Watanabe, H. C., Ikeda, T., and Ishikita, H. (2017). Structurally conserved channels in cyanobacterial and plant photosystem II. *Photosynthesis Research* 133, 75–85.

Sakuragi, Y. (2006). α-Tocopherol plays a role in photosynthesis and macronutrient homeostasis of the cyanobacterium *Synechocystis* sp. PCC 6803 that is independent of its antioxidant function. *Plant Physiology* 141, 508–521.

Sane, P. V (2004). "Thermoluminescence," in *Photosynthesis Research Protocols*, ed. R. Carpentier (Totowa, NJ: Humana Press), 229–248.

Schneider, A., Steinberger, I., Herdean, A., Morper, A., Rühle, T., Labs, M., Gandini, C., Flugge, U. I., Geimer, S., Spetea Wiklund, C., Leister, D., Eisenhut, M., Kurz, S., Weber, A. P. M., Schmidt, S. B., Husted, S., and Hoecker, N. (2016). The evolutionarily conserved protein

References

PHOTOSYNTHESIS AFFECTED MUTANT71 is required for efficient manganese uptake at the thylakoid membrane in *Arabidopsis*. *The Plant Cell* 28, 892–910.

Scholz, I., Lange, S. J., Hein, S., Hess, W. R., and Backofen, R. (2013). CRISPR-Cas systems in the cyanobacterium *Synechocystis* sp. PCC 6803 exhibit distinct processing pathways involving at least two Cas6 and a Cmr2 protein. *PLoS One* 8, e56470.

Schopf, J. W. (2012). "The Fossil Record of Cyanobacteria," in *Ecology of Cyanobacteria II*, ed. B. A. Whitton (Dordrecht: Springer Netherlands), 15–36.

Shen, G., Boussiba, S., and Vermaas, W. F. (1993). *Synechocystis* sp. PCC 6803 strains lacking photosystem I and phycobilisome function. *The Plant Cell* 5, 1853–1863.

Shen, J.-R. (2015). The structure of photosystem II and the mechanism of water oxidation in photosynthesis. *Annual Review of Plant Biology* 66, 23–48.

Shen, J.-R., Burnap, R. L., and Inoue, Y. (1995). An independent role of cytochrome c_{550} in cyanobacterial photosystem II as revealed by double-deletion mutagenesis of the *psbO* and *psbV* genes in *Synechocystis* sp. PCC 6803. *Biochemistry* 34, 12661–12668.

Shen, J.-R., Qian, M., Inoue, Y., and Burnap, R. L. (1998). Functional characterization of *Synechocystis* sp. PCC 6803 Δ*psbU* and Δ*psbV* mutants reveals important roles of cytochrome c_{550} in cyanobacterial oxygen evolution. *Biochemistry* 37, 1551–1558.

Shibata, M., Katoh, H., Sonoda, M., Ohkawa, H., Shimoyama, M., Fukuzawa, H., Kaplan, A., and Ogawa, T. (2002). Genes essential to sodium-dependent bicarbonate transport in cyanobacteria: Function and phylogenetic analysis. *Journal of Biological Chemistry* 277, 18658–18664.

Shibata, M., Ohkawa, H., Kaneko, T., Fukuzawa, H., Tabata, S., Kaplan, A., and Ogawa, T. (2001). Distinct constitutive and low-CO_2-induced CO_2 uptake systems in cyanobacteria: Genes involved and their phylogenetic relationship with homologous genes in other organisms. *Proceedings of the National Academy of Sciences of the United States of America* 98, 11789–11794.

Shin, B. J., Oh, J., Kang, S., Chung, Y. H., Park, Y. M., Kim, Y. H., Kim, S., Bhak, J., and Choi, J. S. (2008). Cyanobacterial hybrid kinase Sll0043 regulates phototaxis by suppressing pilin and twitching motility protein. *Journal of Microbiology* 46, 300–308.

Siguier, P., Gourbeyre, E., and Chandler, M. (2014). Bacterial insertion sequences: their genomic impact and diversity. *FEMS Microbiology Reviews* 38, 865–891.

Simm, S., Keller, M., Selymesi, M., and Schleiff, E. (2015). The composition of the global and feature specific cyanobacterial core-genomes. *Frontiers in Microbiology* 6, 1–21.

Singh, A. K., and Sherman, L. A. (2005). Pleiotropic effect of a histidine kinase on carbohydrate metabolism in *Synechocystis* sp. strain PCC 6803 and its requirement for heterotrophic growth. *Journal of Bacteriology* 187, 2368–2376.

Sjöholm, J., Ho, F., Ahmadova, N., Brinkert, K., Hammarström, L., Mamedov, F., and Styring, S. (2017). The protonation state around $Tyr_D/Tyr_D^{\bullet}$ in photosystem II is reflected in its biphasic oxidation kinetics. *Biochimica et Biophysica Acta - Bioenergetics* 1858, 147–155.

References

So, A. K. C., Kassam, A., and Espie, G. S. (1998). Na^+-dependent HCO_3^- transport in the cyanobacterium *Synechocystis* PCC 6803. *Canadian Journal of Botany* 76, 1084–1091.

Sonoda, M., Katoh, H., Vermaas, W., Schmetterer, G., and Ogawa, T. (1998). Photosynthetic electron transport involved in PxcA-dependent proton extrusion in *Synechocystis* sp. strain PCC 6803: Effect of *pxcA* inactivation on CO_2, HCO_3^-, and NO_3^- uptake. *Journal of Bacteriology* 180, 3799–3803.

Sonoike, K., Hihara, Y., and Ikeuchi, M. (2001). Physiological significance of the regulation of photosystem stoichiometry upon high light acclimation of *Synechocystis* sp. PCC 6803. *Plant and Cell Physiology* 42, 379–384.

Soo, R. M., Hemp, J., Parks, D. H., Fischer, W. W., and Hugenholtz, P. (2017). On the origins of oxygenic photosynthesis and aerobic respiration in cyanobacteria. *Science* 355, 1436–1440.

Stal, L. J. (2012). "Cyanobacterial mats and stromatolites," in *Ecology of Cyanobacteria II*, ed. B. A. Whitton (Springer), 65–125.

Stanier, R. Y., and Cohen-Bazire, G. (1977). Phototrophic prokaryotes: the cyanobacteria. *Annual Review of Microbiology* 31, 225–274.

Stanier, R. Y., Kunisawa, R., Mandel, M., and Cohen-Bazire, G. (1971). Purification and properties of unicellular blue-green algae (order Chroococcales). *Bacteriological Reviews* 35, 171–205.

Steinberg, C. E. W., Schäfer, H., and Beisker, W. (1998). Do acid-tolerant cyanobacteria exist? *Acta Hydrochimica et Hydrobiologica* 26, 13–19.

Stumm, W., and Morgan, J. J. (2012). *Aquatic Chemistry: Chemical equilibria and rates in natural waters*. John Wiley & Sons.

Styring, S., Sjöholm, J., and Mamedov, F. (2012). Two tyrosines that changed the world: Interfacing the oxidizing power of photochemistry to water splitting in photosystem II. *Biochimica et Biophysica Acta - Bioenergetics* 1817, 76–87.

Suga, M., Akita, F., Hirata, K., Ueno, G., Murakami, H., Nakajima, Y., Shimizu, T., Yamashita, K., Yamamoto, M., Ago, H., and Shen, J.-R. (2015). Native structure of photosystem II at 1.95 Å resolution viewed by femtosecond X-ray pulses. *Nature* 517, 99–103.

Summerfield, T. C., Crawford, T. S., Young, R. D., Chua, J. P., Macdonald, R. L., Sherman, L. A., and Eaton-Rye, J. J. (2013). Environmental pH affects photoautotrophic growth of *Synechocystis* sp. PCC 6803 strains carrying mutations in the lumenal proteins of PS II. *Plant and Cell Physiology* 54, 859–874.

Summerfield, T. C., Eaton-Rye, J. J., and Sherman, L. A. (2007). Global gene expression of a ΔPsbOΔPsbU mutant and a spontaneous revertant in the cyanobacterium *Synechocystis* sp. strain PCC 6803. *Photosynthesis Research* 94, 265–274.

Summerfield, T. C., Shand, J. A., Bentley, F. K., and Eaton-Rye, J. J. (2005a). PsbQ (Sll1638) in *Synechocystis* sp. PCC 6803 is required for Photosystem II activity in specific mutants and in nutrient-limiting conditions. *Biochemistry* 44, 805–815.

References

Summerfield, T. C., and Sherman, L. A. (2008). Global transcriptional response of the alkali-tolerant cyanobacterium *Synechocystis* sp. strain PCC 6803 to a pH 10 environment. *Applied Environmental Microbiology* 74, 5276–5284.

Summerfield, T. C., Winter, R. T., and Eaton-Rye, J. J. (2005b). Investigation of a requirement for the PsbP-like protein in *Synechocystis* sp. PCC 6803. *Photosynthesis Research* 84, 263–268.

Tahara, H., Matsuhashi, A., Uchiyama, J., Ogawa, S., and Ohta, H. (2015). Sll0751 and Sll1041 are involved in acid stress tolerance in *Synechocystis* sp. PCC 6803. *Photosynthesis Research* 125, 233–242.

Tahara, H., Uchiyama, J., Yoshihara, T., Matsumoto, K., and Ohta, H. (2012). Role of Slr1045 in environmental stress tolerance and lipid transport in the cyanobacterium *Synechocystis* sp. PCC 6803. *Biochimica et Biophysica Acta* 1817, 1360–1366.

Tajima, N., Sato, S., Maruyama, F., Kaneko, T., Sasaki, N. V, Kurokawa, K., Ohta, H., Kanesaki, Y., Yoshikawa, H., Tabata, S., Ikeuchi, M., and Sato, N. (2011). Genomic structure of the cyanobacterium *Synechocystis* sp. PCC 6803 strain GT-S. *DNA Research* 18, 393–399.

Takahashi, H., Uchimiya, H., and Hihara, Y. (2008). Difference in metabolite levels between photoautotrophic and photomixotrophic cultures of *Synechocystis* sp. PCC 6803 examined by capillary electrophoresis electrospray ionization mass spectrometry. *Journal of Experimental Botany* 59, 3009–3018.

Takahashi, S., and Badger, M. R. (2011). Photoprotection in plants: a new light on photosystem II damage. *Trends in Plant Science* 16, 53–60.

Takahashi, S., and Murata, N. (2005). Interruption of the Calvin cycle inhibits the repair of Photosystem II from photodamage. *Biochimica et Biophysica Acta - Bioenergetics* 1708, 352–361.

Takahashi, S., and Murata, N. (2008). How do environmental stresses accelerate photoinhibition? *Trends in Plant Science* 13, 178–82.

Tchernov, D., Helman, Y., Keren, N., Luz, B., Ohad, I., Reinhold, L., Ogawa, T., and Kaplan, A. (2001). Passive entry of CO_2 and its energy-dependent intracellular conversion to HCO_3^- in cyanobacteria are driven by a Photosystem I-generated $\Delta\mu H^+$. *Journal of Biological Chemistry* 276, 23450–23455.

Teuber, M., Rogner, M., and Berry, S. (2001). Fluorescent probes for non-invasive bioenergetic studies of whole cyanobacterial cells. *Biochimica et Biophysica Acta - Bioenergetics* 1506, 31–46.

Thornton, L. E., Ohkawa, H., Roose, J. L., Kashino, Y., Keren, N., and Pakrasi, H. B. (2004). Homologs of plant PsbP and PsbQ proteins are necessary for regulation of Photosystem II activity in the cyanobacterium *Synechocystis* 6803. *The Plant Cell* 16, 2164–2175.

Tichý, M., Bečková, M., Kopečná, J., Noda, J., Sobotka, R., and Komenda, J. (2016). Strain of *Synechocystis* PCC 6803 with aberrant assembly of Photosystem II contains tandem duplication of a large chromosomal region. *Frontiers in Plant Science* 7, 1–10.

Tomo, T., Kusakabe, H., Nagao, R., Ito, H., Tanaka, A., Akimoto, S., Mimuro, M., and Okazaki, S.

(2012). Luminescence of singlet oxygen in photosystem II complexes isolated from cyanobacterium *Synechocystis* sp. PCC 6803 containing monovinyl or divinyl chlorophyll *a*. *Biochimica et Biophysica Acta - Bioenergetics* 1817, 1299–1305.

Trautmann, D., Voss, B., Wilde, A., Al-Babili, S., and Hess, W. R. (2012). Microevolution in cyanobacteria: re-sequencing a motile substrain of *Synechocystis* sp. PCC 6803. *DNA Research* 19, 435–448.

Tsunekawa, K., Shijuku, T., Hayashimoto, M., Kojima, Y., Onai, K., Morishita, M., Ishiura, M., Kuroda, T., Nakamura, T., Kobayashi, H., Sato, M., Toyooka, K., Matsuoka, K., Omata, T., and Uozumi, N. (2009). Identification and characterization of the Na^+/H^+ antiporter NhaS3 from the thylakoid membrane of *Synechocystis* sp. PCC 6803. *Journal of Biological Chemistry* 284, 16513–16521.

Turner, D. R., Whitfield, M., and Dickson, A. G. (1981). The equilibrium speciation of dissolved components in freshwater and sea water at 25°C and 1 atm pressure. *Geochimica et Cosmochimica Acta* 45, 855–881.

Tyystjärvi, E. (2013). Photoinhibition of Photosystem II. *International Review of Cell and Molecular Biology* 300, 243–303.

Tyystjärvi, T., Huokko, T., Rantamäki, S., and Tyystjärvi, E. (2013). Impact of different group 2 sigma factors on light use efficiency and high salt stress in the cyanobacterium *Synechocystis* sp. PCC 6803. *PLoS ONE* 8, e63020.

Uchiyama, J., Asakura, R., Kimura, M., Moriyama, A., Tahara, H., Kobayashi, Y., Kubo, Y., Yoshihara, T., and Ohta, H. (2012). Slr0967 and Sll0939 induced by the SphR response regulator in *Synechocystis* sp. PCC 6803 are essential for growth under acid stress conditions. *Biochimica et Biophysica Acta - Bioenergetics* 1817, 1270–1276.

Uchiyama, J., Asakura, R., Moriyama, A., Kubo, Y., Shibata, Y., Yoshino, Y., Tahara, H., Matsuhashi, A., Sato, S., Nakamura, Y., Tabata, S., and Ohta, H. (2014). Sll0939 is induced by Slr0967 in the cyanobacterium *Synechocystis* sp. PCC 6803 and is essential for growth under various stress conditions. *Plant Physiology and Biochemistry* 81, 36–43.

Uchiyama, J., Kanesaki, Y., Iwata, N., Asakura, R., Funamizu, K., Tasaki, R., Agatsuma, M., Tahara, H., Matsuhashi, A., Yoshikawa, H., Ogawa, S., and Ohta, H. (2015). Genomic analysis of parallel-evolved cyanobacterium *Synechocystis* sp. PCC 6803 under acid stress. *Photosynthesis Research* 125, 243–254.

Umena, Y., Kawakami, K., Shen, J. R., and Kamiya, N. (2011). Crystal structure of oxygen-evolving photosystem II at a resolution of 1.9 Å. *Nature* 473, 55–60.

Urasaki, A., Sekine, Y., and Ohtsubo, E. (2002). Transposition of cyanobacterium insertion element IS*Y100* in *Escherichia coli*. *Journal of Bacteriology* 184, 5104–5112.

Vandecraen, J., Chandler, M., Aertsen, A., and Van Houdt, R. (2017). The impact of insertion sequences on bacterial genome plasticity and adaptability. *Critical Reviews in Microbiology* 43, 709–730.

References

Vass, I. (2012). Molecular mechanisms of photodamage in the Photosystem II complex. *Biochimica et Biophysica Acta - Bioenergetics* 1817, 209–217.

Vass, I., and Cser, K. (2009). Janus-faced charge recombinations in photosystem II photoinhibition. *Trends in Plant Science* 14, 200–205.

Vass, I., and Govindjee (1996). Thermoluminescence from the photosynthetic apparatus. *Photosynthesis Research* 48, 117–126.

Vass, I., Horvath, G., Herczeg, T., and Demeter, S. (1981). Photosynthetic energy conservation investigated by thermoluminescence. *Biochimica et Biophysica Acta - Bioenergetics* 634, 140–152.

Vass, I., and Inoue, Y. (1986). pH dependent stabilization of $S_2Q_A^-$ and $S_2Q_B^-$ charge pairs studied by thermoluminescence. *Photosynthesis Research* 10, 431–436.

Vass, I., Kirilovsky, D., and Etienne, A. L. (1999). UV-B radiation-induced donor- and acceptor-side modifications of photosystem II in the cyanobacterium *Synechocystis* sp. PCC 6803. *Biochemistry* 38, 12786–94.

Vass, I., and Styring, S. (1991). pH-Dependent charge equilibria between tyrosine-$_D$ and the S states in photosystem II. Estimation of relative midpoint redox potentials. *Biochemistry* 30, 830–839.

Vermaas, W. F. J., Charit, J., and Eggers, B. (1990). "System for site-directed mutagenesis in the *psbD1/C* operon of *Synechocystis* sp. PCC 6803," in *Current Research in Photosynthesis*, ed. M. Baltscheffsky (Dordrecht: Kluwer Academic Publishers), 231–238.

Vinyard, D. J., Ananyev, G. M., Dismukes, C. G., and Charles Dismukes, G. (2013). Photosystem II: the reaction center of oxygenic photosynthesis. *Annual Review of Biochemistry* 82, 577–606.

Vinyard, D. J., and Brudvig, G. W. (2017). Progress toward a molecular mechanism of water oxidation in Photosystem II. *Annual Review of Physical Chemistry* 68, 101–116.

Vogt, L., Vinyard, D. J., Khan, S., and Brudvig, G. W. (2015). Oxygen-evolving complex of Photosystem II: an analysis of second-shell residues and hydrogen-bonding networks. *Current Opinion in Chemical Biology* 25, 152–158.

Waditee, R., Hossain, G. S., Tanaka, Y., Nakamura, T., Shikata, M., Takano, J., Takabe, T., and Takabe, T. (2004). Isolation and functional characterization of Ca^{2+}/H^+ antiporters from cyanobacteria. *Journal of Biological Chemistry* 279, 4330–4338.

Waditee, R., Tanaka, Y., and Takabe, T. (2006). "Na^+/H^+ antiporters in plants and cyanobacteria," in *Abiotic Stress Tolerance in Plants*, eds. A. Rai and T. Takabe (Springer Netherlands), 163–175.

Wang, C., Xu, W., Jin, H., Zhang, T., Lai, J., Zhou, X., Zhang, S., Liu, S., Duan, X., Wang, H., Peng, C., and Yang, C. (2016). A putative chloroplast-localized Ca^{2+}/H^+ antiporter CCHA1 is involved in calcium and pH homeostasis and required for PSII function in *Arabidopsis*. *Molecular Plant* 9, 1183–1196.

Wang, H.-L., Postier, B. L., and Burnap, R. L. (2002). Polymerase chain reaction-based mutageneses identify key transporters belonging to multigene families involved in Na^+ and pH homeostasis of

Synechocystis sp. PCC 6803. *Molecular Microbiology* 44, 1493–1506.

Wang, H. L., Postier, B. L., and Burnap, R. L. (2004). Alterations in global patterns of gene expression in *Synechocystis* sp. PCC 6803 in response to inorganic carbon limitation and the inactivation of *ndhR*, a LysR family regulator. *Journal of Biological Chemistry* 279, 5739–5751.

Watanabe, M., and Ikeuchi, M. (2013). Phycobilisome: architecture of a light-harvesting supercomplex. *Photosynthesis Research* 116, 265–276.

Wetzel, R. (2001). *Limnology - Lake and River Ecosystems*. Academic Press.

Whitton, B. A., and Potts, M. (2012). "Introduction to the Cyanobacteria," in *Ecology of Cyanobacteria II: Their Diversity in Space and Time*, ed. B. A. Whitton, 1–13.

Wijffels, R. H., Kruse, O., and Hellingwerf, K. J. (2013). Potential of industrial biotechnology with cyanobacteria and eukaryotic microalgae. *Current Opinion in Biotechnology* 24, 405–413.

Williams, J. G. K. (1988). Construction of specific mutations in Photosystem II photosynthetic reaction center by genetic engineering methods in *Synechocystis* 6803. *Methods in Enzymology* 167, 766–778.

Xu, M., Bernát, G., Singh, A., Mi, H., Rögner, M., Pakrasi, H. B., and Ogawa, T. (2008). Properties of mutants of *Synechocystis* sp. strain PCC 6803 lacking inorganic carbon sequestration systems. *Plant and Cell Physiology* 49, 1672–1677.

Xu, W., and McFadden, B. a (1997). Sequence analysis of plasmid pCC5.2 from cyanobacterium *Synechocystis* PCC 6803 that replicates by a rolling circle mechanism. *Plasmid* 37, 95–104.

Xu, W., and Wang, Y. (2017). "Function and Structure of Cyanobacterial Photosystem I," in *Photosynthesis: Structures, Mechanisms, and Applications*, eds. H. J. M. Hou et al. (Springer International Publishing), 111–168.

Yamori, W., and Shikanai, T. (2016). Physiological functions of cyclic electron transport around Photosystem I in sustaining photosynthesis and plant growth. *Annual Review of Plant Biology* 67, 81–106.

Yang, X., and McFadden, B. A. (1993). A small plasmid, pCA2.4, from the cyanobacterium *Synechocystis* sp. strain PCC 6803 encodes a Rep protein and replicates by a rolling circle mechanism. *Journal of Bacteriology* 175, 3981–3991.

Yang, X., and McFadden, B. A. (1994). The complete DNA sequence and replication analysis of the plasmid pCB2.4 from the cyanobacterium *Synechocystis* PCC 6803. *Plasmid* 31, 131–137.

Yao, L., Cengic, I., Anfelt, J., and Hudson, E. P. (2016). Multiple gene repression in cyanobacteria using CRISPRi. *Synthetic Biology* 5, 207–212.

Yoshihara, S., Geng, X. X., Okamoto, S., Yura, K., Murata, T., Go, M., Ohmori, M., and Ikeuchi, M. (2001). Mutational analysis of genes involved in pilus structure, motility and transformation competency in the unicellular motile cyanobacterium *Synechocystis* sp. PCC 6803. *Plant and Cell Physiology* 42, 63–73.

Yoshihara, S., Suzuki, F., Fujita, H., Geng, X. X., and Ikeuchi, M. (2000). Novel putative photoreceptor

and regulatory genes required for the positive phototactic movement of the unicellular motile cyanobacterium *Synechocystis* sp. PCC 6803. *Plant and Cell Physiology* 41, 1299–1304.

Zhang, L.-F., Yang, H.-M., Cui, S.-X., Hu, J., Wang, J., Kuang, T.-Y., Norling, B., and Huang, F. (2009a). Proteomic analysis of plasma membranes of cyanobacterium *Synechocystis* sp. strain PCC 6803 in response to high pH stress. *Journal of Proteome Research* 8, 2892–2902.

Zhang, P., Allahverdiyeva, Y., Eisenhut, M., and Aro, E.-M. (2009b). Flavodiiron proteins in oxygenic photosynthetic organisms: photoprotection of Photosystem II by Flv2 and Flv4 in *Synechocystis* sp. PCC 6803. *PLoS ONE* 4, e5331.

Zhang, P., Battchikova, N., Jansen, T., Appel, J., Ogawa, T., and Aro, E.-M. (2004). Expression and functional roles of the two distinct NDH-1 complexes and the carbon acquisition complex NdhD3/NdhF3/CupA/Sll1735 in *Synechocystis* sp. PCC 6803. *The Plant Cell* 16, 3326–3340.

Zhang, X., Chen, G., Qin, C., Wang, Y., and Wei, D. (2012). Slr0643, an S2P homologue, is essential for acid acclimation in the cyanobacterium *Synechocystis* sp. PCC 6803. *Microbiology* 158, 2765–2780.

Zhu, T., Hou, S., Lu, X., and Hess, W. R. (2017). Draft genome sequences of nine cyanobacterial strains from diverse habitats. *Genome Announcements* 5, e01676-16.

Zouni, A., Witt, H.-T., Kern, J., Fromme, P., Krauss, N., Saenger, W., and Orth, P. (2001). Crystal structure of photosystem II from *Synechococcus elongatus* at 3.8 Å resolution. *Nature* 409, 739–743.

Appendices

A.1 Significant contribution of others to this work

| Experiment or analysis	Description of work	Contribution of others
Chapter Three and Four: Genome sequencing for GT-O1, GT-O2, Con:ΔPsbO:ΔPsbU and pseudorevertant strains	Extraction of genomic DNA, library construction, sequencing	Not carried out by the author. This work was undertaken by JA Daniels (Dept. of Biochemistry) and NZ Genomics Ltd. prior to the commencement of this study.
Chapter Three: Genome assembly of GT-O1 and GT-O2	Genome assembly of sequencing data using the software BWA and SAMtools	Carried out by PA Stockwell. The author carried out a more substantial analysis using alternative software (CLC), and the results were compared and pooled. Data interpretation for BWA/SAMtools output was carried out by the author.
Chapter Five: photomixotrophic experiments carried out at BRC Szeged	P_{700} oxidation measurements, room-temperature chlorophyll fluorescence and thermoluminescence measurements	Experiments were designed and carried out by the author with assistance, particularly during simultaneous measurements, from S Kovács (BRC Szeged), who assisted with the operation of equipment for P_{700} oxidation, fluorescence, and thermoluminescence measurements. Machine settings for these instruments were determined by I Vass (BRC Szeged) or S Kovács. All data analysis was carried out by the author.
Chapter Five: pH 7.5/10 photoautotrophic experiments carried out at BRC Szeged	P_{700} oxidation measurements, room-temperature chlorophyll fluorescence and thermoluminescence measurements	Experiments were designed by the author and an initial experiment was carried out with assistance, particularly during simultaneous measurements, from S Kovács, who assisted with the operation of equipment for P_{700} oxidation, fluorescence, and thermoluminescence measurements. S Kovács then repeated 2-3 independent replications of the same experiment where cells were incubated at pH 7.5/10 for 8 hrs, and their P_{700} oxidation, thermoluminescence, fluorescence decay and induction was determined. All data analysis was carried out by the author.

A.2 Supplementary data, Chapter Two
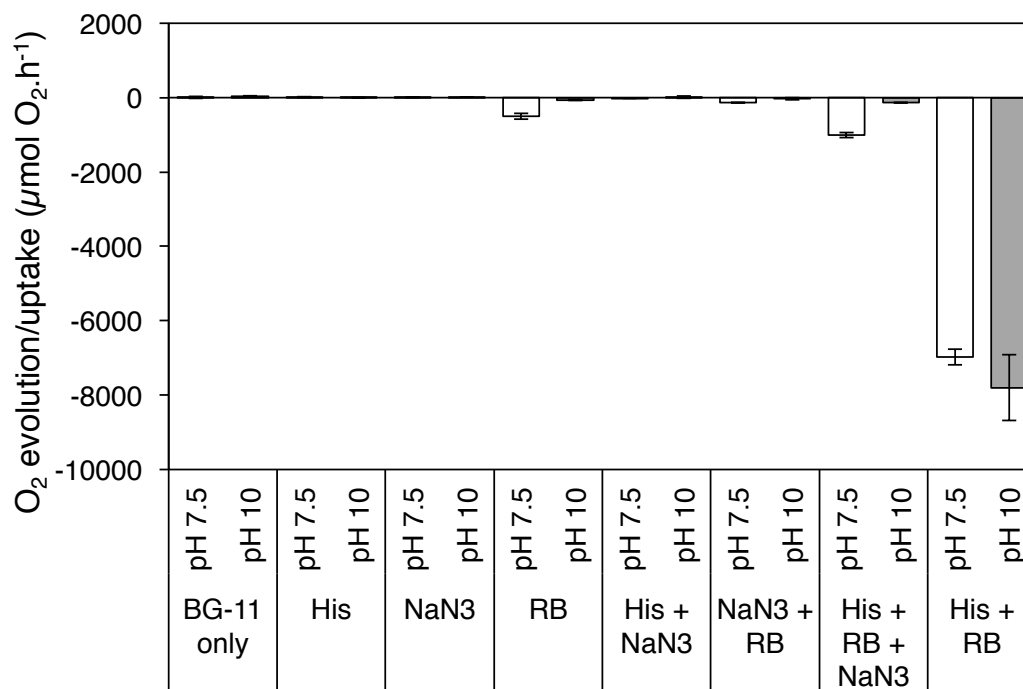
Figure A.1. Validation of the histidine-trapping method for the detection of $^1O_2$ (Rehman et al., 2013) in cell-free pH-7.5 and pH-10.0 buffered media. BG-11 media was illuminated in the presence of the $^1O_2$-sensitiser 1 μM Rose Bengal (RB), the $^1O_2$ trap 5 mM histidine (His), and the $^1O_2$ quencher NaN$_3$. Bars represent the mean of 2-4 measurements ± SEM.
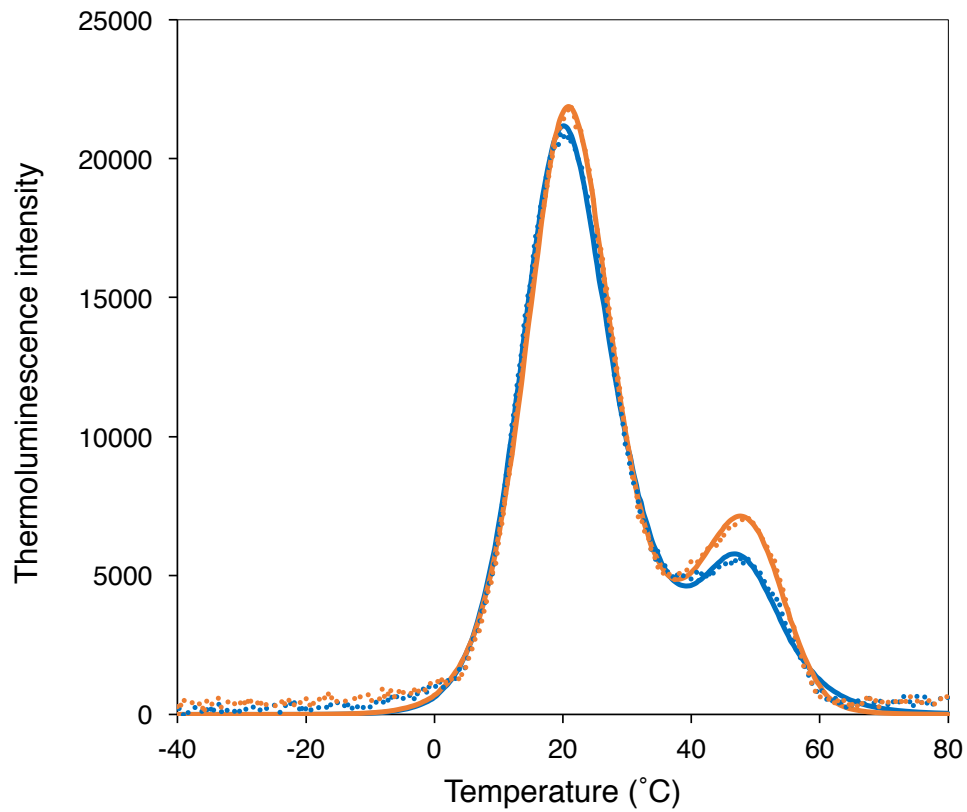
Figure A.2. Validation of the thermoluminescence curve-fitting method for determination of peak T_{max} and amplitude, by comparison of fitted (solid lines) and unfitted (dotted lines) thermoluminescence curves from a representative data set. Curves represent the mean of fitted and unfitted data for the Con:ΔPsbO:ΔPsbU and pseudorevertant strains, in the presence of DCMU.

A.3 Supplementary data, Chapter Three
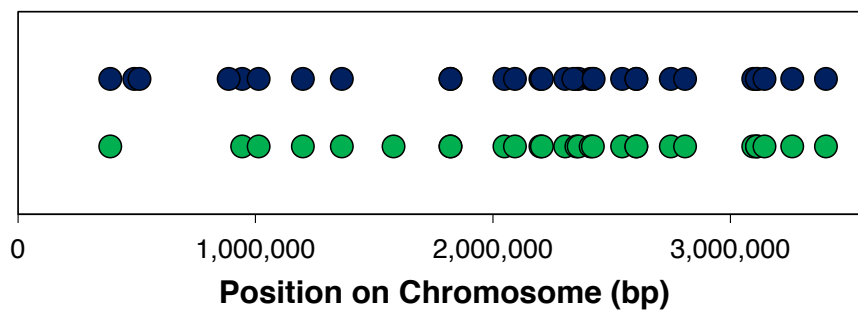
Figure A.3. Map depicting the chromosome position of SNPs, indels and database errors in the genomic sequence of the *Synechocystis* 6803 substrains GT-O1 and GT-O2 compared to the GT-Kazusa reference sequence. GT-O1 – green; GT-O2 – blue.

A.4 Supplementary data, Chapter Four
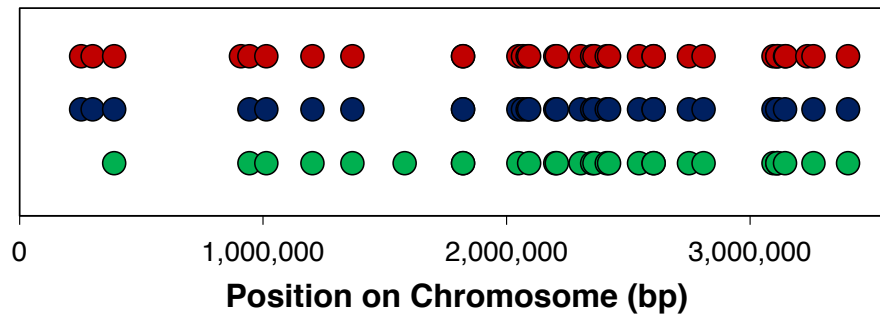
Figure A.4. Map depicting the chromosome position of SNPs, indels and database errors in the genomic sequence of the *Synechocystis* 6803 substrains GT-O1, Con:ΔPsbO:ΔPsbU, and pseudorevertant compared to the GT-Kazusa reference sequence. GT-O1 – green; Con:ΔPsbO:ΔPsbU – blue; pseudorevertant – red.
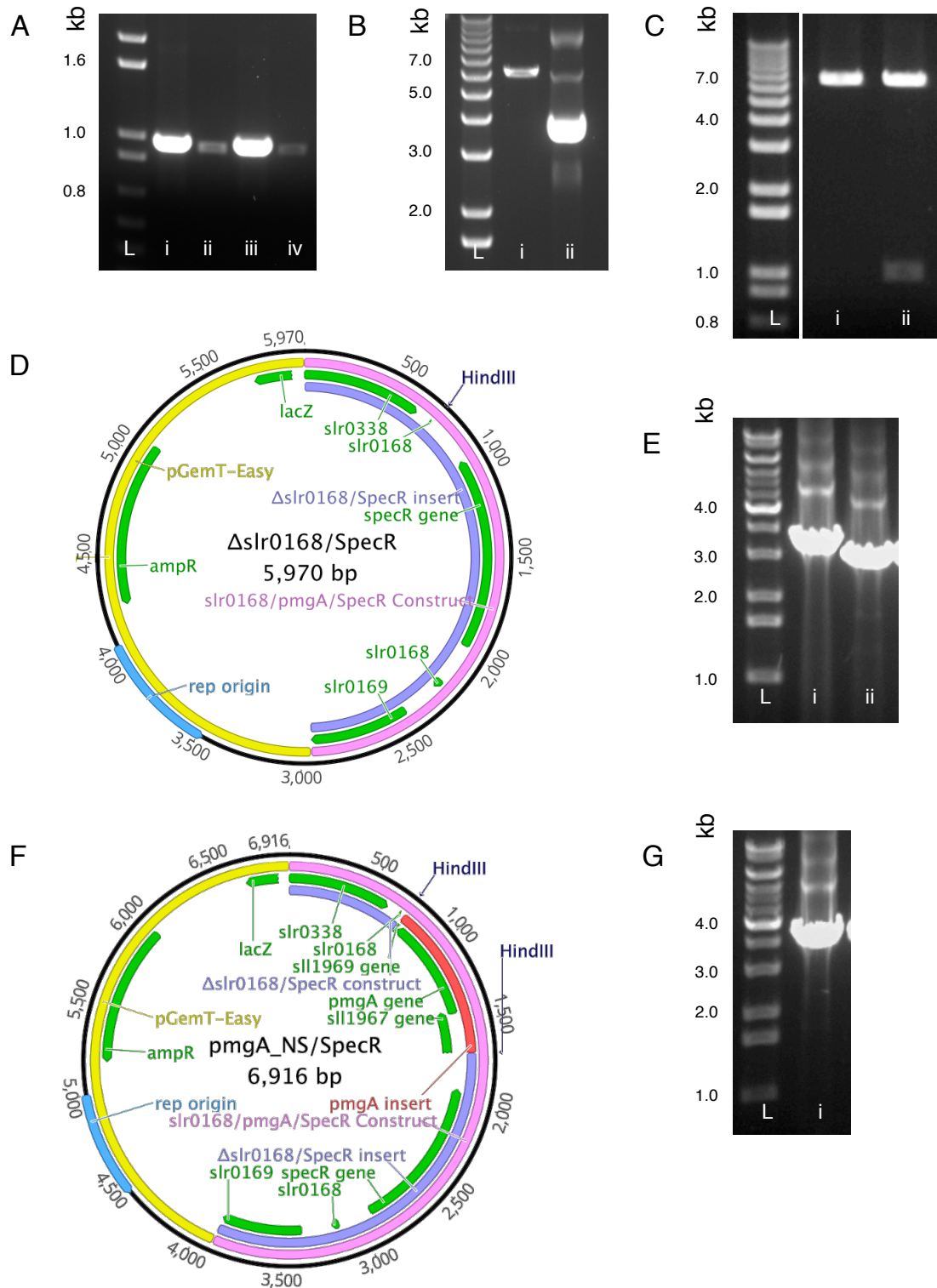
Figure A.5. Construction of a *pmgA* neutral site (NS) plasmid from a pΔ*slr0168*/Spec^R plasmid for introduction into *Synechocystis* 6803. A: amplification of *pmgA* in the GT-O1 wild-type and the pseudorevertant (i and iii), and their respective HindIII digestion products (ii and iv). B: HindIII digestion of the Δ*slr0168* plasmid (i), and undigested plasmid (ii). C: HindIII digestion of the pΔ*slr0168* plasmid (i), and pΔ*slr0168* plasmid containing a successfully ligated

GT-O1 *pmgA* insert (from A, ii) to yield the final *pmgA* NS/Spec[R] plasmid (ii). D: map of pΔ*slr0168*/Spec[R] plasmid. E: PCR amplification of the *slr0168* gene region from a GT-O1:Δ*slr0168*/Spec[R] transformant (i) and GT-O1 (ii), showing the predicted insert band size (3.4 kb) and wild-type band size respectively (3.0 kB). F: map of Δ*pmgA* NS/Spec[R] plasmid. G: PCR amplification of the *slr0168* gene region from a GT-O1:Δ*pmgA* NS/Spec[R] transformant (i), showing the predicted insert band size (3.9 kb). (In A-C, L = 1 kb[+] DNA ladder; and in E & G, L = KAPA Universal DNA Ladder; both were used to estimate amplicon sizes).
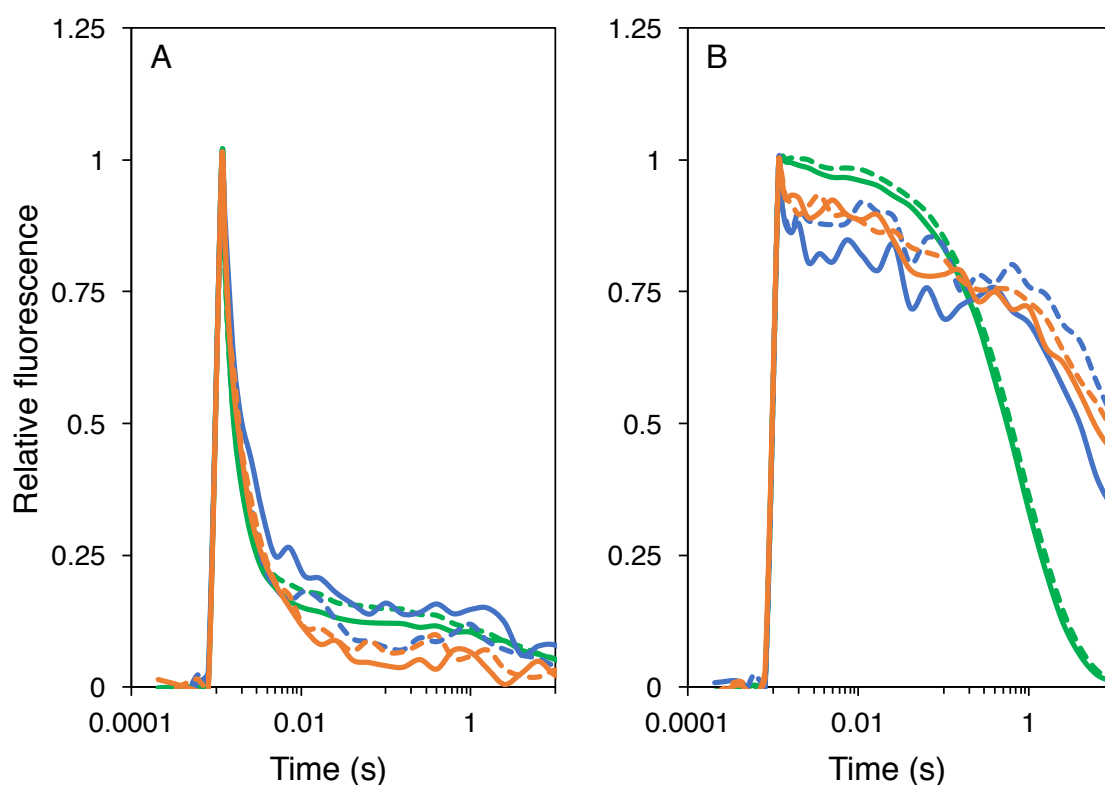
Figure A.6. Flash-induced fluorescence decay in the GT-O1, Con:ΔPsbO:ΔPsbU, and pseudorevertant cells, in the absence (A) and presence (B) of 1 μM DCMU (GT-O1: green, Con:ΔPsbO:ΔPsbU: blue, pseudorevertant: orange). Cells were assayed following 2 h incubation in photoautotrophic conditions in pH 7.5- or pH 10.0-buffered BG-11 media. Traces represent the mean signal from a preliminary experiment, $n = 2$.
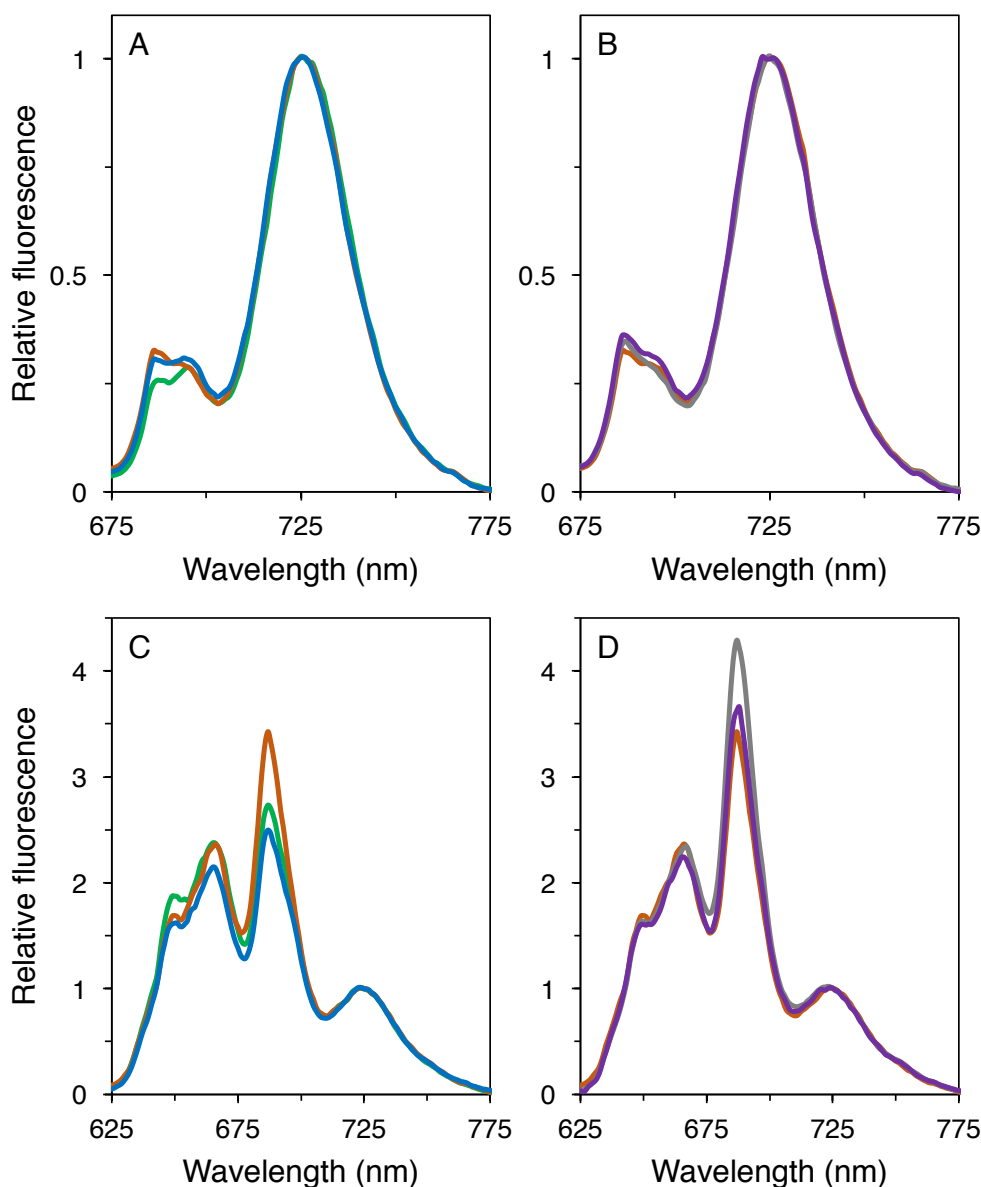
A.5 Supplementary data, Chapter Five

Figure A.7. Low temperature fluorescence of *Synechocystis* 6803 mutants grown to mid-late log phase and assayed in pH 7.5/mixotrophic conditions. Fluorescence was determined with 440 nm excitation wavelength (A-B) and 580 nm excitation (C-D); traces represent the mean of 3-4 independent measurements and are normalised to the ~725 nm PS I fluorescence emission maxima. A, C: GT-O1 (green), E364Q (blue), ΔPsbV (orange). B, D: ΔPsbV (orange), E364Q:ΔPsbV (purple), and ΔPsbV:ΔCyanoQ (grey).

A.6 Morris et al., (2014) cover page

Taylor & Francis
Taylor & Francis Group

RESEARCH ARTICLE

Whole genome re-sequencing of two 'wild-type' strains of the model cyanobacterium *Synechocystis* sp. PCC 6803

JN Morris[a], TS Crawford[a,b], A Jeffs[b,c], PA Stockwell[b], JJ Eaton-Rye[b] and TC Summerfield[a]*

[a]*Department of Botany, University of Otago, Dunedin, New Zealand;* [b]*Department of Biochemistry, University of Otago, Dunedin, New Zealand;* [c]*Otago Genomics, University of Otago, Dunedin, New Zealand*

The photoautotrophic cyanobacterium *Synechocystis* sp. PCC 6803 is a widely used model in genomic research and was the first photosynthetic organism to have its entire genome sequenced. Here, we report the genome sequence for two glucose-tolerant laboratory 'wild-type' strains, GT-O1 and GT-O2, in use at the University of Otago. Using high-throughput genome sequencing techniques and subsequent Sanger sequencing of detected variants, we have identified ten de novo mutations in the two strains, of which six are unique to GT-O2 cells. The presence of these unique mutations highlights the need to know the genomic background of the parent strain when constructing mutants in *Synechocystis* sp. PCC 6803 strains.

Keywords: cyanobacteria; genome mapping; single nucleotide polymorphism; *Synechocystis* sp. PCC 6803; whole-genome re-sequencing

Introduction

Autotrophic, prokaryotic cyanobacteria are widely used as model organisms for research into the evolution, genetics and biochemistry of photosynthesis, as they are believed to be ancestral to plant plastids. Among cyanobacteria, the freshwater species *Synechocystis* sp. PCC 6803 (hereafter *Synechocystis* 6803) was the first to have its entire genome sequenced (Kaneko et al. 1995, 1996). The early availability of the full genome sequence, the ability of this organism to switch between photoautotrophic and heterotrophic growth and its capacity to readily incorporate exogenous DNA via double-homologous recombination means that *Synechocystis* 6803 is widely used throughout the world for functional genomic, proteomic and transcriptomic studies of photosynthesis, metabolism and environmental adaptation (Grigorieva & Shestakov 1982; Williams 1988; Vermaas 1998).

The ancestry of the main strains of *Synechocystis* 6803 has been previously described (Ikeuchi &

Tabata 2001; Trautmann et al. 2012). Briefly, the original 'Berkeley strain' was isolated from freshwater in California (Stanier et al. 1971). The original strain was deposited in the Pasteur Culture Collection (PCC 6803 strain) and the American Type Culture Collection (ATCC 27184 strain). In 1988, Dr JGK Williams isolated a glucose-tolerant (GT) strain from ATCC 27184 cells (Williams 1988; Ikeuchi & Tabata 2001). The Williams GT strain was subsequently passed on to the Kazusa DNA Research Institute, Japan, and GT-Kazusa was derived from this strain. The sequences of the 3.5 Mb chromosome and major plasmids (0.4 Mb total) of GT-Kazusa *Synechocystis* 6803 were reported in 1995–1996 and 2003, respectively (Kaneko et al. 1995, 1996, 2003). The GT-O1 strain in use at the University of Otago was a gift from Dr WFJ Vermaas (Arizona State University) and was also derived from the original Williams GT strain; it was brought to New Zealand in 1994.

Recently, errors have been reported in the published genomic sequence of the GT-Kazusa

---

*Corresponding author. Email: tina.summerfield@otago.ac.nz

A.7 Morris et al., (2016) cover page

Environmental pH and the Requirement for the Extrinsic Proteins of Photosystem II in the Function of Cyanobacterial Photosynthesis

Jaz N. Morris[1], Julian J. Eaton-Rye[2] and Tina C. Summerfield[1]*

[1] *Department of Botany, University of Otago, Dunedin, New Zealand,* [2] *Department of Biochemistry, University of Otago, Dunedin, New Zealand*

In one of the final stages of cyanobacterial Photosystem II (PS II) assembly, binding of up to four extrinsic proteins to PS II stabilizes the oxygen-evolving complex (OEC). Growth of cyanobacterial mutants deficient in certain combinations of these thylakoid-lumen-associated polypeptides is sensitive to changes in environmental pH, despite the physical separation of the membrane-embedded PS II complex from the external environment. In this perspective we discuss the effect of environmental pH on OEC function and photoautotrophic growth in cyanobacteria with reference to pH-sensitive PS II mutants lacking extrinsic proteins. We consider the possibilities that, compared to pH 10.0, pH 7.5 increases susceptibility to PS II-generated reactive oxygen species (ROS) causing photoinhibition and reducing PS II assembly in some mutants, and that perturbations to channels in the lumenal regions of PS II might alter the accessibility of water to the active site as well as egress of oxygen and protons to the thylakoid lumen. Reduced levels of PS II in these mutants, and reduced OEC activity arising from the disruption of substrate/product channels, could reduce the *trans*-thylakoid pH gradient (ΔpH), leading to the impairment of photosynthesis. Growth of some PS II mutants at pH 7.5 can be rescued by elevating CO_2 levels, suggesting that the pH-sensitive phenotype might primarily be an indirect result of back-pressure in the electron transport chain that results in heightened production of ROS by the impaired photosystem.

Keywords: assembly, extrinsic proteins, oxygen-evolving complex, pH, photosystem II, reactive oxygen species, thylakoid lumen

INTRODUCTION

Photosystem II (PS II) is a thylakoid membrane-bound protein complex that functions as a water-plastoquinone oxidoreductase in oxygenic phototrophs (Vinyard et al., 2013). In cyanobacteria, the mature PS II monomer contains at least 17 membrane-spanning subunits, of which seven are essential for PS II function, as well as up to four extrinsic, thylakoid-lumen-associated subunits (PsbO, PsbU, PsbV, and possibly CyanoQ), which are necessary for maximal rates of oxygen evolution (Shen, 2015; Heinz et al., 2016; Roose et al., 2016). The PS II extrinsic proteins, along with the lumenal domains of the intrinsic reaction center proteins D1 and D2 and the adjacent

A.8 Morris et al., (2017) cover page

Taylor & Francis
Taylor & Francis Group

RESEARCH ARTICLE

Phenotypic variation in wild-type substrains of the model cyanobacterium *Synechocystis* sp. PCC 6803

J. N. Morris[a], J. J. Eaton-Rye[b] and T. C. Summerfield[a]

[a]Department of Botany, University of Otago, Dunedin, New Zealand; [b]Department of Biochemistry, University of Otago, Dunedin, New Zealand

ABSTRACT

Genome re-sequencing has revealed numerous genetic differences between wild-type substrains of the model cyanobacterium *Synechocystis* sp. PCC 6803 held in laboratories around the world. These substrains can be divided into the motile PCC-lineage and non-motile GT-lineage, and frequently display unique genetic mutations that result in residue changes in proteins associated with environmental sensing, gene regulation, cellular transport and photosynthesis. However, despite these findings, phenotypic variation between wild-type substrains does not appear to have been widely reported. In this study, we compared the growth and physiology of three wild-type substrains of *Synechocystis* sp. PCC 6803, the GT-Kazusa substrain (the source of the original genome sequence for this cyanobacterium), the widely studied PCC-Moscow substrain, and the GT-O1 substrain, in use in our laboratory. We found similarity between all three substrains in terms of growth rate, oxygen evolution and total chlorophyll levels. Although differences in cell size, whole-cell absorption and 77 K fluorescence were observed, the wild-type substrains analysed here are comparable under standard laboratory conditions.

Introduction

It has been 20 years since the genome sequence of the cyanobacterium *Synechocystis* sp. PCC 6803 (hereafter *Synechocystis* 6803) was first reported (Kaneko et al. 1995, 1996, 2003), and in that time this strain has been used extensively as a model organism for the study of photosynthesis, environmental sensing and stress response (Vermaas 1998; Ikeuchi & Tabata 2001; Kopf et al. 2014). *Synechocystis* 6803 is naturally transformable with exogenous DNA via double-homologous recombination, and the ability of this organism to grow on glucose means that otherwise essential genes encoding products involved in photosynthesis can be interrupted using genetic modification techniques (Grigorieva & Shestakov 1982; Williams 1988; Vermaas 1998; Eaton-Rye 2011).

Two distinct lineages of *Synechocystis* 6803 have been identified, based on the loss of motility in the GT (glucose tolerant) group arising from a 1 bp insertion in the *spkA*